INFORMATION TO USERS

This manuscript has been reproduced from the microfilm master. UMI films the text directly from the original or copy submitted. Thus, some thesis and dissertation copies are in typewriter face, while others may be from any type of computer printer.

The quality of this reproduction is dependent upon the quality of the copy submitted. Broken or indistinct print, colored or poor quality illustrations and photographs, print bleedthrough, substandard margins, and improper alignment can adversely affect reproduction.

In the unlikely event that the author did not send UMI a complete manuscript and there are missing pages, these will be noted. Also, if unauthorized copyright material had to be removed, a note will indicate the deletion.

Oversize materials (e.g., maps, drawings, charts) are reproduced by sectioning the original, beginning at the upper left-hand corner and continuing from left to right in equal sections with small overlaps. Each original is also photographed in one exposure and is included in reduced form at the back of the book.

Photographs included in the original manuscript have been reproduced xerographically in this copy. Higher quality 6" x 9" black and white photographic prints are available for any photographs or illustrations appearing in this copy for an additional charge. Contact UMI directly to order.

UMI

University Microfilms International
A Bell & Howell Information Company
300 North Zeeb Road, Ann Arbor, MI 48106-1346 USA
313/761-4700 800/521-0600

Order Number 9325100

Fluorescence spectroscopy of human nonmalignant and malignant cells and tissues

Glassman, Wenling Sha, Ph.D.

City University of New York, 1993

U·M·I
300 N. Zeeb Rd.
Ann Arbor, MI 48106

FLUORESCENCE SPECTROSCOPY OF HUMAN NONMALIGNANT AND MALIGNANT CELLS AND TISSUES

by

WENLING SHA GLASSMAN

A dissertation submitted to the Graduate Faculty in physics in partial fulfillment of the requirements for the degree of Doctor of Philosophy, The City University of New York

1993

This manuscript has been read and accepted by the Graduate Faculty in Physics in satisfaction of the dissertation requirement for the degree of Doctor of Philosophy.

3/29/93
Date

R.R. Alfano
Chair of Examining Committee

3/30/93
Date

Executive Officer

Mark Steinberg

Roger Donsinville

Daniel Akins

Ping Ho

Joel Gersten

Supervisory Committee

THE CITY UNIVERSITY OF NEW YORK

ABSTRACT

FLUORESCENCE SPECTROSCOPY FROM HUMAN NONMALIGNANT AND MALIGNANT CELLS AND TISSUES

by

Wenling Sha Glassman

Advisor: Professor **Robert R. Alfano,** Distinguished Professor of Science and Engineering.

This thesis explores steady state and time resolved fluorescence spectroscopy from human malignant and non-malignant cells and tissues. The focus of these studies are the analysis of the excitation spectra, emission spectra, and decay time based on the contribution from several key intrinsic fluorophors: NAD(P)H, flavins, tryptophan, elastin and collagen that exist in different amounts in the human tissues and cells. The comparison between the spectra from malignant and non-malignant cells and tissues gives information on the changes that occurs from non-malignancy to malignancy in the cells and tissues. The spectra of tissues and cells are also compared to help in understanding what fluorophors are responsible for fluorescence spectral differences between the malignant and non-malignant tissues

and cells.

The results in this thesis show that the spectral differences between the normal and cancerous tissues and cells exist in various wavelength ranges. The experimental data from GYN tissues have shown with over 95% of the sensitivity and specificity to separate malignant from non-malignant tissues using 300nm excitation. The 340nm band, which is mostly in response to intrinsic fluorophor (amino acid tryptophan), from malignant tissues were relatively higher then that from the non-malignant tissues. This might have been caused by the higher concentration of free tryptophan in the malignant tumor when compared to that of the normal tissue. This has been found in medical clinical study. The experimental data in this thesis also show that the fluorescence intensities around 450nm -- 460nm, which are mostly due to the intrinsic fluorophor coenzyme NADH, from both malignant cells in vitro and tissues in vitro are relatively higher than from non-malignant cells in vitro and tissues in vitro. These findings are reinforced by the faster decay time of the NADH fluorescence from normal cells in vitro than from neoplasm cells in vitro. Thus, the NADH in the mitochondria might be bound less tight in the malignant cells then that in the non-malignant cells because of metabolism changes from non-malignance to malignance.

This thesis contributes to the new field of "mediphotonics" in life science.

Preface

Recently, fluorescence spectroscopy, an optical physics phenomenon, has been applied to the medical field as a new potential tool for diagnosing diseases. Extensive studies have shown the possibilities of diagnosis of human breast cancer, human colonic dysplasia, atherosclerotic plaque, etc. The purpose of this thesis is to extend the fluorescence spectroscopy study to the gynecological (GYN) neoplasm as well as into cell level in the wavelength range from 300nm to 700nm.

The focus of this thesis is on the laser or light induced fluorescence (LIF) spectral differences between GYN tissues in the malignant and in the non-malignant states. This thesis concentrates on the LIF spectral differences between the malignant and non-malignant cells. Studies have been performed on the numbers of important intrinsic fluorophors, in order to understand their contributions to the spectra of malignant and non-malignant tissues and cells. The joint study of spectroscopies of the tissues and cells gives basic understanding of the spectroscopic changes that are the result of the complicated composition of the tissue.

In this thesis, I have tried to analyze the complicated fluorescence spectra of the tissues and cells and their changes. Based on the physical principle of the fluorescence

and the biochemical properties of the tissues and cell, I have discussed the possible relationships between the changes of the fluorescence spectra and the changes of the tissues from normal to malignant. This thesis should give an understanding of the fluorescence (emission, excitation and time resolved) spectral structures of the malignant and non-malignant tissues and cells in the 300nm to 600nm wavelength range.

This thesis is organized into seven chapters.

The first chapter consists of three independent sections. In the first section, I will introduce the background and past history of research in laser or light induced fluorescence (LIF) spectroscopies in application of medical diagnosis. In the second section, I will describe the composition of the tissue and the cell and remark some of the known differences between the two which might affect their optical properties. In the third section, I will introduce key intrinsic fluorophors, describing their functions in the cells and tissues and their fluorescence properties.

In the second chapter, I will review aspects of the physics of fluorescence from a theoretical perspective. I will describe and discuss the physical model of the time-resolved and steady state fluorescence spectra.

In the third chapter, I describe the experimental methods: the measurement setups, instruments, and techniques used in this research. The description will include the technique of steady-state laser induced fluorescence emission

spectra, lamp based steady-state light induced excitation and emission spectra, and ultra-fast picosecond laser pulse generated time resolved fluorescence decay.

In the fourth chapter, I present the fluorescence spectra studies on the cultured human breast normal and cancerous cell lines. I also present the excitation and emission spectra in the various wavelength range which correspond to various intrinsic fluorophors. The time resolved fluorescence decay spectra are also presented. Spectral comparison and analysis is also made between normal and cancerous cell lines.

In the fifth chapter, I present the fluorescence spectra studies on the human gynecological malignant and non-malignant tissues. I present the excitation and emission spectra in the various wavelength range which are the results of various intrinsic fluorophors. The spectral comparison and analysis are made between malignant and non-malignant tissues.

In the sixth chapter, I will present some conclusions reached from my research that the relatively stronger 340nm fluorescence band in the malignant GYN tissues and the relatively stronger 460nm band in both malignant GYN tissues and breast cells are the best selection for diagnostic purposes because they represent important biochemical changes that occur when tissues and cells become malignant.

In the last chapter, I will discuss some remaining questions which have not been studied in this thesis. Directions for future research will be suggested.

To My Son and Husband

Adam Sha Glassman

Michael Glassman

With All My Love and Hope

ACKNOWLEDGEMENTS

First of all, I sincerely thank my parents for their many sacrifices and great support to my education and my dreams throughout my life. Their love, encouragement, and unlimited help have always been given me strength in facing the challenges and difficulties of my life. I would also like to thank my husband for his understanding, encouragement and help; and my parents in law for their help during this highly pressured time.

I would especially like to sincerely thank Prof. R.R. Alfano for suggesting this thesis problem and his patient guidance and rigorous training. His professional knowledge, positive attitude and deep sense of caring have been the greatest help in the preparation of this thesis.

I would also like to take this chance to express my deep appreciation to all the members in IUSL, especially to Prof. P.Ho, Prof. R. Dosinville, Megan Gibbs, Joan Brijlall, H.Liu, C.G.Tang, and Dr. Ockman. I thank the members of the Physics Department for their help. I thank Prof. N.P. Chang who brought me into this program, and Prof. Baumel for his understanding and support. I would like to thank Dr. M. Kamiyama, a biomedical researcher, who first taught me the tissue culturing technique and certain biomedical lab technologies.

I would like to sincerely thank Dr. C. Lubicz, (MD) specialist in gynecology and oncology who collaborated with us in research work on the malignant and non-malignant tissues and provided us with the tissues and pathological reports. I would also like to thank Prof. M. Steinberg of biochemistry department: in his laboratory I cultured and prepared my cell samples, for his very helpful guidance and instruction.

I would like to thank CUNY for support from the organized research funds through IUSL. The last year of my Ph.D thesis has been supported by the special fellowship raised by the Physics Department in the name of Michael Rukin Scholarship for medical physics research.

TABLE OF CONTENTS

List of Tables

Chapter 1.

Chapter 4.

Lists of Figures

Chapter 1.

Appendix II.

Appendix III.

Chapter 1. Introduction

Section A. Historical background

The use of the laser or light induced fluorescence (LIF) spectroscopy in the diagnosis of disease is a new, novel and promising method for the medical field. Over the years, nuclei radiation, X-ray and pathology tests have played an important role in the detection of tumors as well as certain treatments. Histological testing is a complicated and time consuming process. Nuclear and X-ray radiation are usually used in medicine, but it is commonly known now that nuclear and X-ray radiation have inherent potential dangers for both patients and doctors. Recently, the potential for X-ray to cause cancer has recently been realized in research.[1] These potential problems may be the result of high energy carried by the radiation. Due to the lower energy carried by single radiation particles, the use of UV and visible light may be a better alternative technique for diagnosis. Over the years, lasers have been used in surgery and other surface treatments like ablation. The use of the light for detecting and diagnosing is just beginning.

Fluorescence is an old, effective tool to study the

physical and chemical processes of the molecular basis. One of the major advantages of the LIF technique is that the fluorescence spectrum contains a great deal of information about the microscopic world. Since fluorophors are sensitive to the changes in the local environment, fluorescence measurements can give information about underlying molecular conformation, binding sites, solvent interactions, degree of flexibility, intermolecular distances, and diffusion coefficient of macromolecule. Fluorescence spectroscopy can reveal the physical and chemical changes from fluorophors. Over years, fluorescence stains are used as probes to study where substances can be used effectively and efficiently. In the medical field, for example, using fluorescence from NADH, fluorescence can localize the cerebral ischemia regions in the rat brain (Welsh, etc., 1977)[2]. Over the years, the hematoporphyrin derivative (HpD) has been found to be tumor-localized and to be an effective fluorescence photosensitizer in the photodynamic therapy for treatment of a variety of solid malignant tumors (Dougherty et al., 1978;[3] Kessel and Dougherty, 1983;[4] Kessel, 1984;[5] Andreoni and Cubeddu, 1984[6]). On the other hand, intrinsic fluorophors are the chromophores which play a role in the biological system. They are a natural probe whose fluorescence signal may reveal the native physical and chemical changes without any external disturbances.

Professor Alfano's research group was the first to start using the native LIF spectroscopies from various tissues for diagnostic purposes. In 1981, Alfano and Yao were the first to use this method in the detection of the carious regions of teeth[7,8]. This LIF technique was later successfully extended by Alfano's group to distinguish normal and tumor in rat tissues (1984)[9]. The technique was extended even further when it distinguished human breast and lung normal and neoplasm tissues (1987)[10]. The light source used was the 488nm, 514nm and 457nm lines from CW argon laser and the observed spectral wavelength region were between 500nm to 700nm. The statistical rate of success was around 86%.[11] Subsequently, the excitation spectra[11](Alfano, et. al., 1989), the emission spectra excited with picosecond pulse laser with wavelength 351nm (Tang et al., 1989)[12] and the time resolved fluorescence decay spectra excited with picosecond pulse laser with wavelength 527nm (Tang et al., 1989)[13] from human breast normal and cancerous tissues was investigated. In 1991, Alfano's group was again successful in the use of the LIF technique to distinguish malignant and non-malignant human breast tissues by using UV light source at 300nm to excite and observe the spectral range 320nm to 580nm (Alfano, et al., 1991)[14]. The reported rate of success was over 95%. This work was later on extended to study malignant and non-malignant gynecological tract by myself for this thesis (Glassman, 1992)[15]. The rate of success was again

reported to be very high, with a statistics over 95%. In addition, the fluorescence spectra from GYN malignant and non-malignant tract over the range 340nm to 600nm excited with wavelength 320nm were also investigated.[15] The time resolved fluorescence kinetics from malignant and non-malignant human breast tissues excited with UV femotosecond laser pulse of 310nm were also studied (Pradhan, et al., 1992)[16].

In addition, Alfano's group started to use the IR fourier Transform Raman Spectroscopy to study its uses in separating cancerous tissues from benign tissues. They successfully distinguished malignant and non-malignant human breast tissues (Alfano et al., 1991)[17]. Later they distinguished normal and atherosclerotic human aorta (Liu, et al., 1991)[18,19], and did extensive study of malignant and non-malignant GYN tissues (Liu et al, 1993)[20].

The time resolved fluorescence spectra from normal and atherosclerotic human aorta has also been studied (Pradhan, et al., 1992)[21]. Most recently, I have studied the LIF spectroscopy from the cultured malignant and non-malignant human cells. It has been observed that the intrinsic fluorophor NADH in the cells contribute to the fluorescence spectra differently between the normal and neoplasia cells in both steady state and time resolved decay spectra.[22]

Feld's group at MIT focused on using LIF spectroscopy to diagnose the fibrous arterial atherosclerosis (Kittrell, et al., 1985).[23] This study has been extended to the UV

wavelength range (Baraga et al., 1989).[24] The time resolved fluorescence decay spectra from normal and plaque aorta has also been studied with excitation wavelength 320nm picosecond laser (Park, et al., 1990).[25] The MIT group also worked on the gastrointestinal tissue diagnosis by LIF technique. In 1990, they first reported the results by using the endoscopy to study the colonic tissues in vivo (Cothren et al., 1990)[26]. They then reported the study results of colonic tissues in vitro by using the excitation emission matrix method (Richards-Kortum et al., 1991)[27] and extended the method to bladder tissues (Rava et al., 1991)[28].

Deckelbaum's group at Yale University School of Medicine has also used the LIF technique successfully to distinguish atherosclerotic plaque from the normal aorta (Deckelbaum et al., 1987)[29]. They used a continuous-wave helium-cadmium laser at wavelength 325nm to excite and optical fiber to deliver the excitation laser and collect the fluorescence. The study was done on 91 normal and 91 atherosclerotic specimens. The overall classification accuracy was 95%.[30] They extended their work to study rabbit normal and atherosclerotic arteries in vivo (Deckelbaum et al., 1988)[31]. They also did an interesting study on the fluorescence spectra from human skin in vivo (Leffell et al., 1988).[32] The results showed that LIF can be a potential marker of the photoaging of the skin. In 1990, they also published a study showing LIF spectroscopy of human colonic Mucosa (Kapadia et

al., 1990)[33]. With 325nm excitation, their results gave 100% satisfaction over the 34 normal specimens and 16 adenomatous polyps and 94% accuracy for classifying the hyperplastic polyps (nonadenomatous) as normal mucosa.

In 1992, Harvard Medical School has also reported their LIF study results on colonic tissues in vivo and in vitro (Schomacker, et al).[47,48] They used the UV light source (wavelength 337nm) to induce the fluorescence spectra, and observed the predominant change between normal and hyperplastic or adenomatous polyps is a decrease in the collagen fluorescence. With their analysis method, the success rate for distinguishing between hyperplastic and adenomatous polyps was reported over 77% to 86%. These rates are greater than evaluating polyps based on visual assessment and are nearly comparable to the clinical pathologists' assessment of colonic polyps. The report has point out that their LIF technique has the potential to achieve the predictive value by the senior pathologists at the gold standard level.

Research groups outside the United States were also using the LIF technique in the medical field. The Chinese research group at Fudan University was the first to recognize that the fluorescence peaks at 630nm and 690nm from internal porphyrin compounds, which are native to the tissue can be used to diagnose tumors (Yang YL,1987)[34]. They used the Xe ion laser with 365nm and observed the spectra range around 500nm to

700nm range. They studied both tissues in vitro and tissues in vivo cases in the oral cavity, esophagus, and stomach. They reported 89% accuracy from 100 oral tumor cases.

Most recently, a study result obtained by a study group (Konig K. et al.) at the Institute for Laser Technology in Medicine in Germany has pointed out that some bacteria at the carious regions are synthesized fluorescent porphyrins.[35] These porphyrins can be helpful for early detection of the carious range. One should point out that the result from the Chinese group (stated above) may actually be caused by porphyrins from those bacteria at the malignant range in the oral cavity and stomach.

The research group at Lund Institute of Technology, Sweden has also done research on the fluorescence from HpD in normal and malignant tissues.[36, 37, 38, 39]. They did extensive work investigating the fluorescence spectroscopy from various rodent tissues and human skin tumor samples (Andersson et al., 1991)[40], and especially from the human aorta (Andersson et al., 1987[41], 1992 [42]).

In Germany, Lohmann also found that the native fluorescence can be used to diagnose diseases. He first studied the fluorescence of plasma from patients with acute leukemia (Lohmann, et al., 1988)[43]. Then, he studied the fluorescence from the dysplasia and invasive carcinomas in the human cervix uteri in vitro (Lohmann, et al., 1989)[44,45], and the human skin with malignant melanomas and nevi in vitro

(Lohmann, et al., 1989)[46]. He used the wavelength 365nm from Hg lamp to excite the tissues and observed the fluorescence intensity around 465nm from invasive dysplastic tissue (at the edge of the tumor), which is several fold higher than the intensity from the normal site of the tissue. However, he also observed that the fluorescence intensity from the core of the tumor was much weaker than that from the normal site. The study has been done under the microscopy and compared with histological examination with HE staining.

The brief list of the historical development in this field is presented in the Table 1.1.

Table 1.1 List of the historical development of LIF fluorescence spectroscopy diagnosis techniques.

Authors	Year	Tissue Type	Wavelength (nm)	Statistics % / Total*	Note
Alfano, et al.[7]	1981	Human Tooth (caries)	488	~	
Alfano, et al.[9]	1984	Rat cancer in tissues	488	~	
Kittrell, et al.[23]	1985	Human arota fibrous & atherosclerosis		~	
Alfano, et al.[10,11]	1987	Human Breast & lang cancer	488	87% / 15 N 88% / 16 C	
Yong YL, et al.[34]	1987	Human beccal carcinoma	365	89% / 100	
Deckelbum, et al.[29,30]	1987	Human Atherosclerotic aorta	325	~	
Deckelbum, et al.[31]	1988	Rabbit Atherosclerotic aorta	325		in vivo
Leffell, et al.[32]	1988	Human skin for photo-ageing	325	100% / 28 in three groups	

O'Brien, et al.	1989	Human aorta (perforation, fatty plaque, white atheromatous plaque)	337	100% / 21	
Tang, et al.	1989	Human breast cancer	527 pulse	~	Time Resolved
Young, et al.[13]	1990	aortic plaque	320 pulse	100% /16 normal, 10 calcified & 10 non-calcified	Time resolved
Kapadia, et al.[23]	1990	Human colonic Mucosa (adenomatous polyps, hyperplastic)	325	100% / 34 N 100% / 16A.P. 94% / 16 H.P.	
Cothren, et al.[26]	1990	Human gastrointestinal tissues (adenomas, hyperplastic polyps)	370	100% / 31A.P. 97% / 4H.P. 94% / 32 N	in vivo
Richards-Kortum et al.[27]	1991	Human colonic Dysplasia	EEM	95% / 26	
Rava, et al.[28]	1991	Human colon % bladder dysplasia	EEM	~	

Alfano, et al.[14]	1991	Human breast maligmancy	300	95% / 19 M 100% / 20 B&N	
Pradhan, et al.[21]	1991	Human atherosclerotic arteries	310 pluse	100% / 6 fibrous 83% / 12 other	Time-resolved
Pradhan, et al.[16]	1991	Human breast malignancy	310 pluse		Time-resolved
Glassman, et al.[15]	1992	Human gynecologic malignancy	300 & 320	100% / 10 N 95% / 18 M	
Schomacker[47,48]	1992	Human colon	337	80% to 86%	in vivo

* Note: **% / Total** means the rate of success / number of tested samples. In the table, terms is defined as follows:
N --- Normal tissue, C --- Cancerous tissue,
B --- Benign tissue, M --- Malignant tissue,
A.P. --- adenomatous polyps,
H.P. --- hyperplastic polyps.

Section B. Histology of tissues and cells

Tissues are the general building block of body parts. The fundamental tissues of the body are blood, bone, muscle, cartilage, fat, and nerve. Tissue is basically a gathering of cells supported by the fibrous protein matrix. The cells are individual units, each type carrying different tasks within the body. For example there are muscle cells, sensory cells, nerve cells, flagellated cells, etc. A type of tissue can be a mixture of different types of cells that have been arranged in a particular fashion, forming an organ system. The fibrous proteins are for bonding cells in positions; they also give support to the tissues. In between the cells there is also tissue fluid. Tissue fluid is plasma which contains organic and non-organic substances including ions, gases sugars, vitamins, hormones, amino acid, etc. which are necessary supplements for the biological system. The tissue fluids originate from the blood capillaries, which are spread through the tissue. Many of the substances of blood plasma are filtered through the thin vessel walls into spaces between the tissue cells; this becomes the tissue fluid which allows the blood and the cells to exchange substances. The tissue fluid is further modified by the activities of the tissue cells. The tissue fluid maintains a balance through a second transport vessel, the lymphatic system, which deals with the excess. In between the cells, the lipids can also

build up and become strong.[49]

Neoplasm tumors occur when there is any abnormal or unusual increase in the number of cells in the tissue. This is due to certain abnormalities within the involved cells. Neoplasms are commonly divided into the two ill-defined, overlapping categories of benign and malignancy. Malignant tumors are commonly called cancer. The hallmark of these cancerous tumors is the propensity of its cells to metastasize (i.e., to spread via the blood stream, to distant sites in the body). Benign tumors are differentiated from cancerous tumors in the low possibility of their metastasizing. Under the view of the microscopic examination of the histopathology, the benign tumor tends to grow from a central point of origin, compressing surrounding structures and thus producing a well defined capsule containing the spheroid or ovoid tumor mass. In contrast the malignant tumors are often poorly demarcated and individual neoplastic cells can be seen infiltrating the surrounding normal tissue. It is important for one to keep in mind that many neoplasms gradually become more malignant during the neoplastic progression.[50]

Studies of tumor vasculature and oxygenation have revealed that the periphery of an invading cancer shows prolific capacity for growth while parts of the tumor which become separated from the capillary blood supply by more than 169 um become necrotic. It has been demonstrated that the growth fraction of a given tumor is inversely related to the

tumor mass (i.e., small tumors have high growth fractions and a high rate of DNA synthesis while large tumors have a diminished growth fraction). The well vascularized periphery of a tumor has an increased rate of DNA synthesis compared to the hypoxic core.[51]

The cell is the basic unit of the organic function. The structure of a "typical" cell is shown on Figure 1.1. It basically contains: cell membrane, mitochondria, cytoplasm, endoplasmic reticulum, Golgi body, and nucleus (including the nuclear membrane and nucleolus).[52] All the parts serve individual purposes, but they are closely related to each other and affect each other.

The cell membrane provides the exterior boundary of the cell. It also serves for communications between the cells. Malignant cell membranes appear to be carrying an extra charge, which causes malignant cells to repel each other.[50]

The mitochondria convert the chemical energy of carbohydrates $(CH_2O)_n$ and fats into energy forms which the rest of the cell can use when needed. It is the power house of the cell. Many enzyme proteins are at work in the mitochondria.

The endoplasmic reticulum and Golgi body are concerned with the synthesis and packaging of the macromolecule needed for cellular structure and function. The cytoplasm seems to show an absence of structure as fluid; a considerable portion of the total cellular constituents (such as vitamin, protein, ...) apparently occurs free in it.

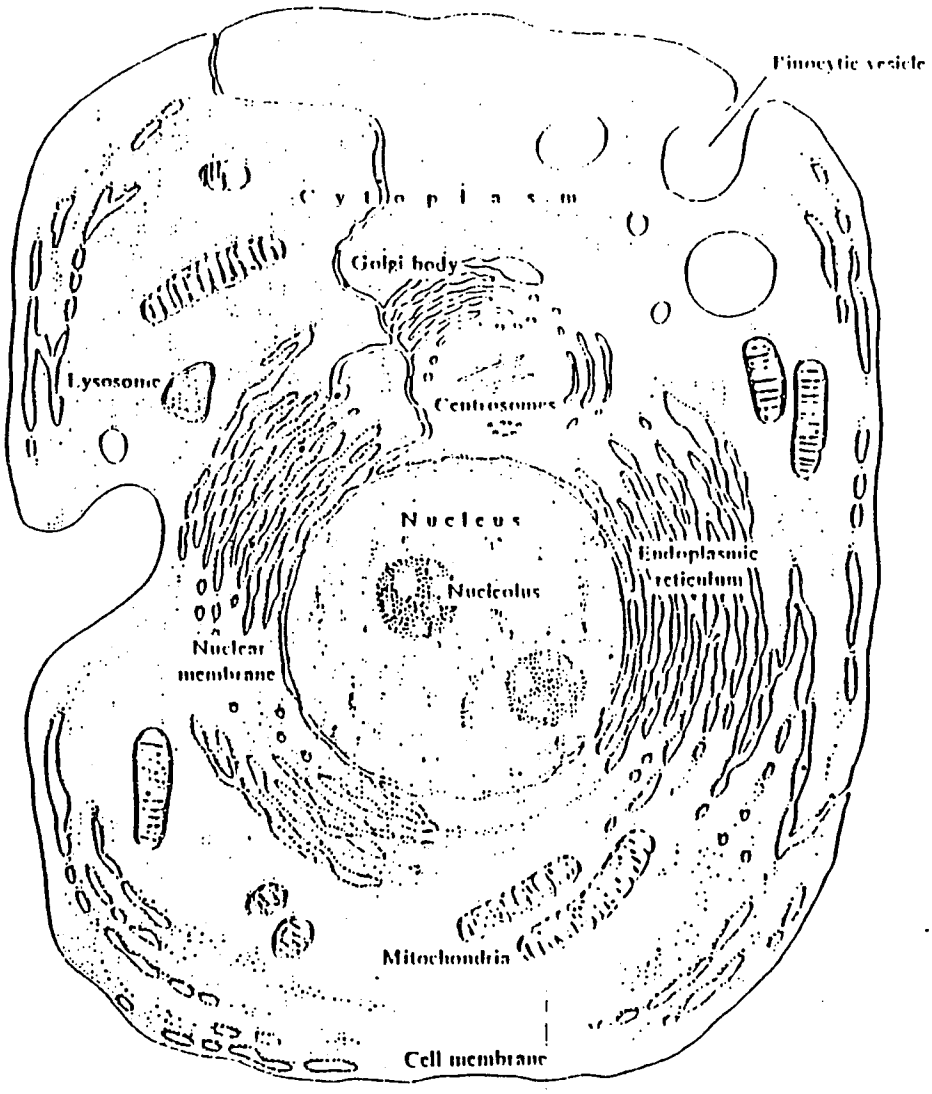

Figure 1.1 A "Typical" cell diagram based on what is seen in electric graphs. --From J. Brachet: Sci. Am., 205: 3 (1961).

The nucleus is separated from the cytoplasm by the nuclear membrane. Most of the DNA (> 95%) is found in the nucleus. The nucleoli is distinct from the other parts of the nucleus by its density, it is also particularly rich in RNA.

It is known that cancer is caused by genetic change. This means that DNA is changed in the cancer disease cell. This affects RNA and some enzyme proteins because all parts of cell have to work under a unique system.

Several important differences should be noticed in this study concerning the conformation between the tissues and cells when comparing the spectra between the two. First, there is hemoglobin in the native tissues and very little in the cells. Hemoglobin absorbs light intensively in the UV and visible range. Its absorption spectra contains a strong band at 440nm and two small bands at 540nm and 570nm (Figure 1.2)[53]. This absorption will modify the fluorescence spectrum from tissues. Secondly, tissues usually contain much more collagen and elastin because they mostly form the extracellular matrices which help bind cells into tissues. The cells contain only some collagen and elastin in the various cellular membrane. Finally, the cultured cells were not grown in the exact same conditions as cells in the human body, so the relative ratio of the concentration of each type of molecular structure may be different.

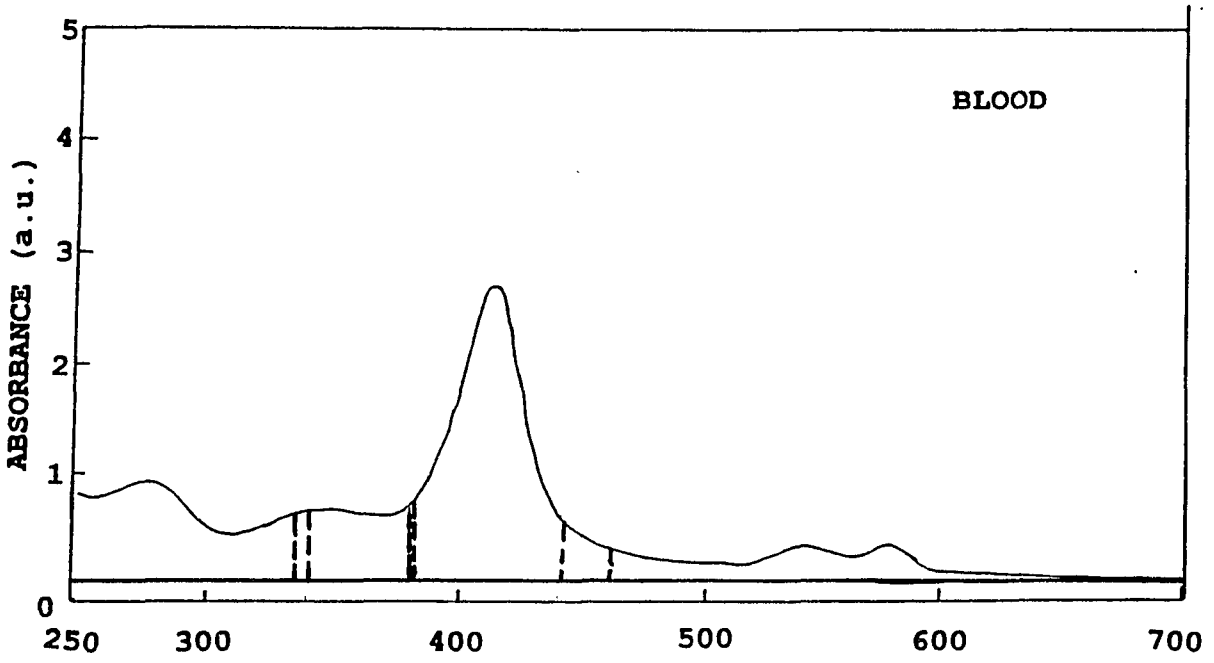

$\alpha(340nm)/\alpha_{max}=0.24$ $\alpha(440nm)/\alpha_{max}=0.24$

$\alpha(383nm)/\alpha_{max}=0.28$ $\alpha(460nm)/\alpha_{max}=0.11$

$\alpha(335nm)/\alpha_{max}=0.21$ $\alpha(380nm)/\alpha_{max}=0.25$

Figure. 1.2 Absorption spectrum of the blood.

The gynecological tissues I have studied are from the uterus, cervix, and ovary. (see Figure 1.3 and 1.4) The tissues from the uterus can sometimes be separated into endometrium and myometrium. Endometrium is the inside layer of the uterus. Myometrium is the muscle layer (outside the endometrium) of the uterus.

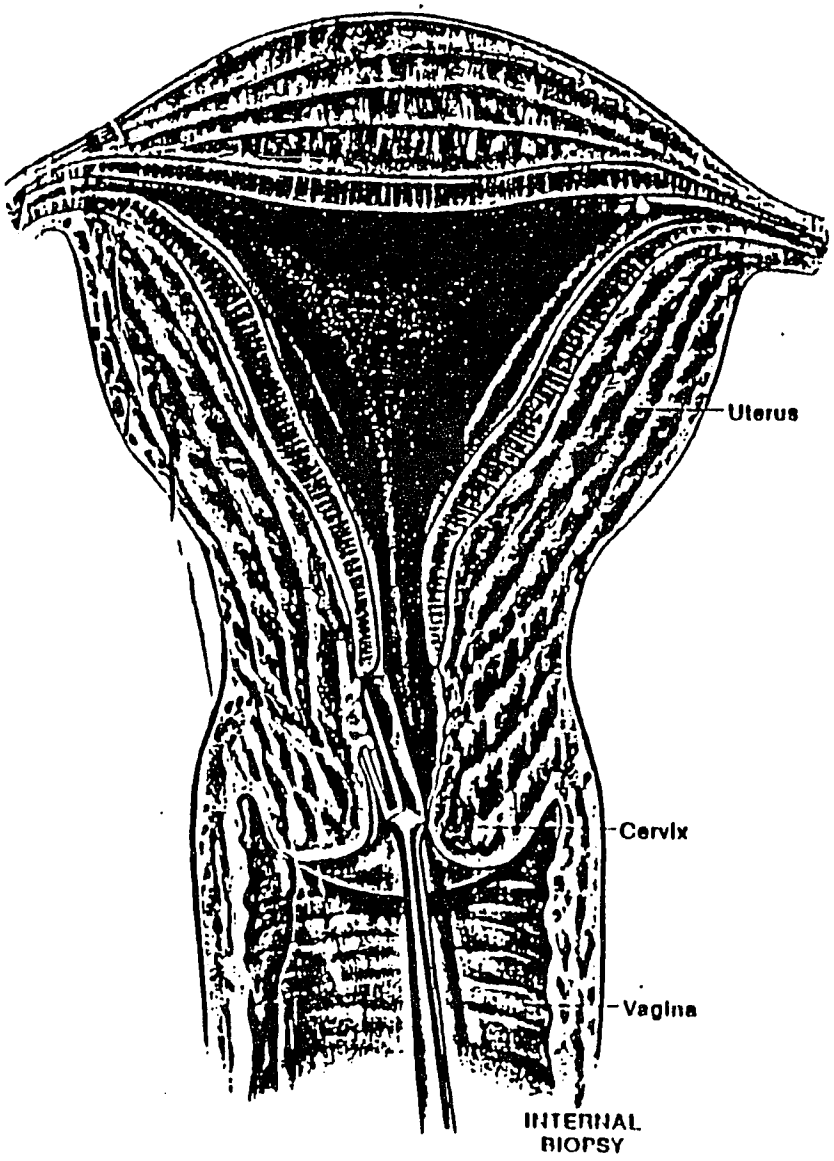

Figure 1.3 Diagram of location of the endometrium, myometrium, cervix tissues.

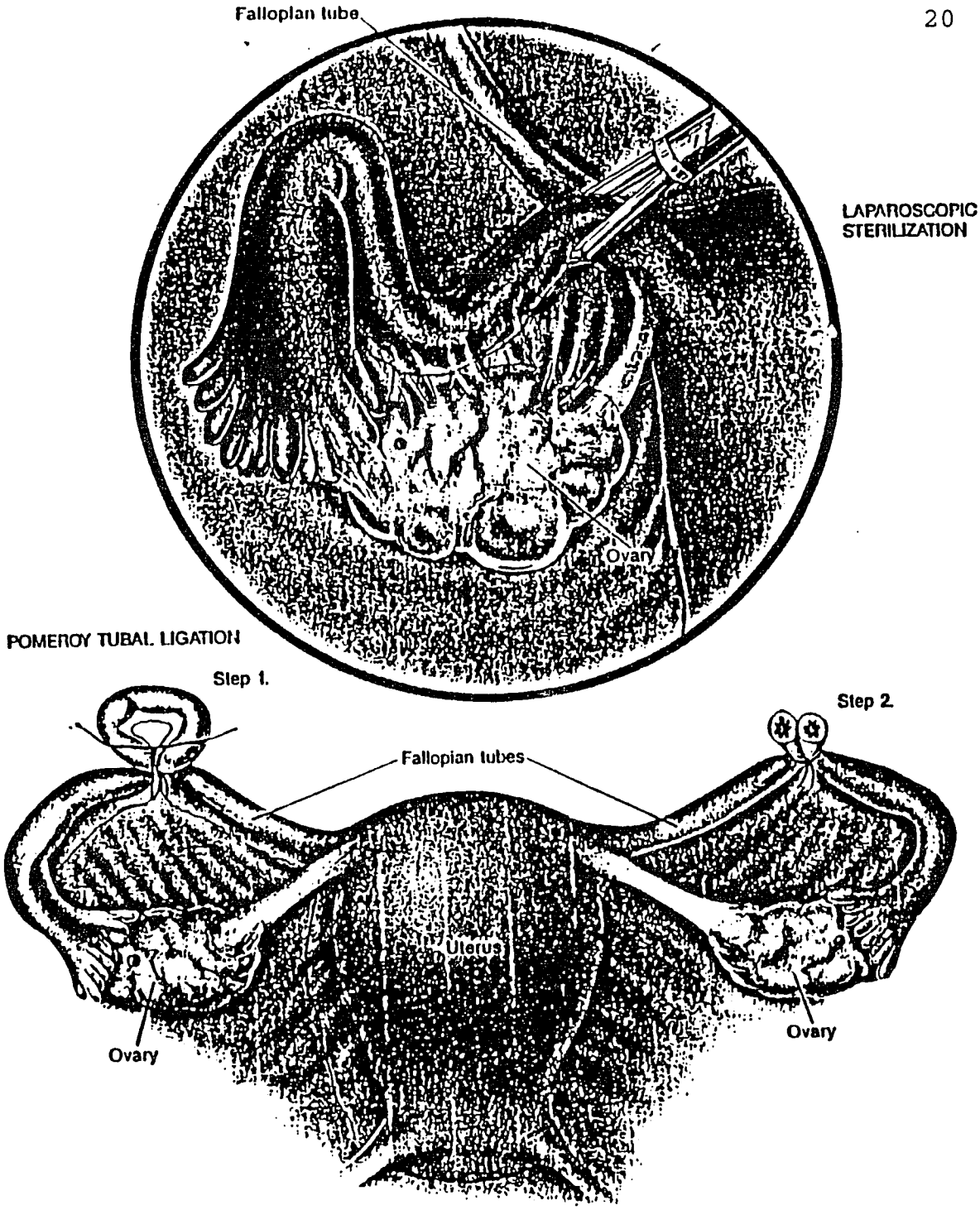

Figure 1.4 Diagram of the location of the ovary tissue.

Section C. Intrinsic fluorophors in human cells and tissues and their fluorescence properties.

Four decades ago, scientists found that tissues and cells emit fluorescence. Since then a number of studies have been done to probe what molecules are responsible for the fluorescence[54,55]. Quite a bit of research has also been done on the fluorescence properties of various molecular groups[56]. A number of biological molecules have been found to have fluorescence in various wavelength ranges: for example, trysine, tryptophan, NADH, t-RNA, and their fluorescence properties have been heavily studied[57].

The research presented in this thesis is involved with the wavelength range from 300nm to 700nm. There are several important intrinsic fluorophors in the native tissues and cells which have fluorescence in this wavelength range. These are tryptophan, collagen, elastin, NAD(P)H, flavins, and some other weaker fluorophors. The fluorescence properties and biochemical functions of these intrinsic fluorophors will be described in the following paragraphs.

The free amino acid **tryptophan** gives rise to a very strong fluorescence peak at 350nm and has a weak absorption band maximum at 275nm and a strong absorption band maximum at 215nm (Figure 1.5)[56]. The fluorescence efficiency is 0.2 and

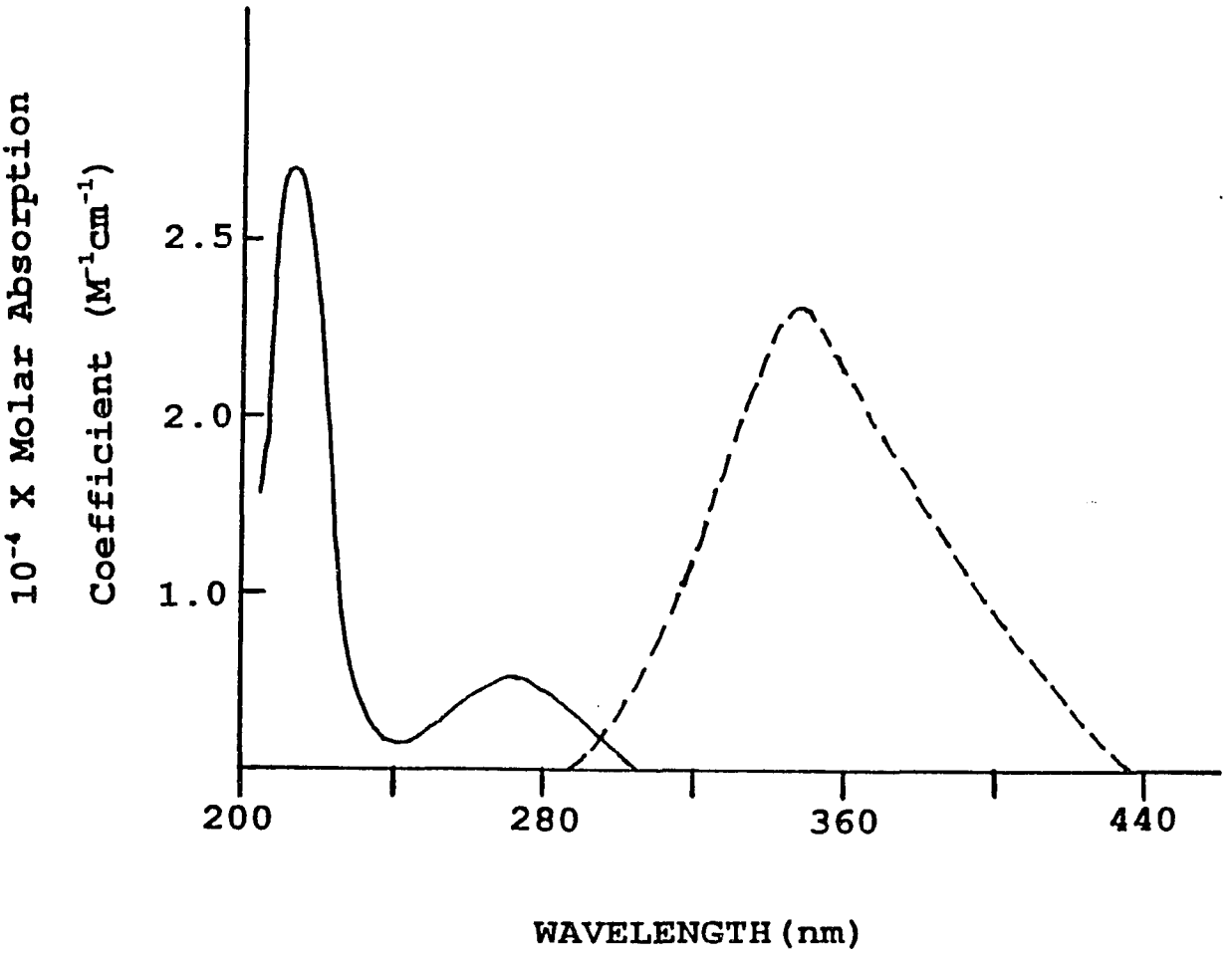

Figure. 1.5 Absorption and fluorescence spectrum of Tryptophan. Solid line: molar absorption coefficient as a function of wavelength. Dashed line: emission spectrum in the arbitrary units. --From: Freifelder, David; **Physical Biochemistry**, Second Ed.

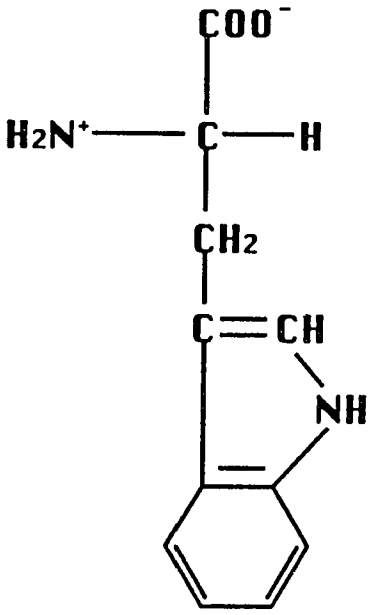

Figure 1.6 The molecular structure of the tryptophan.

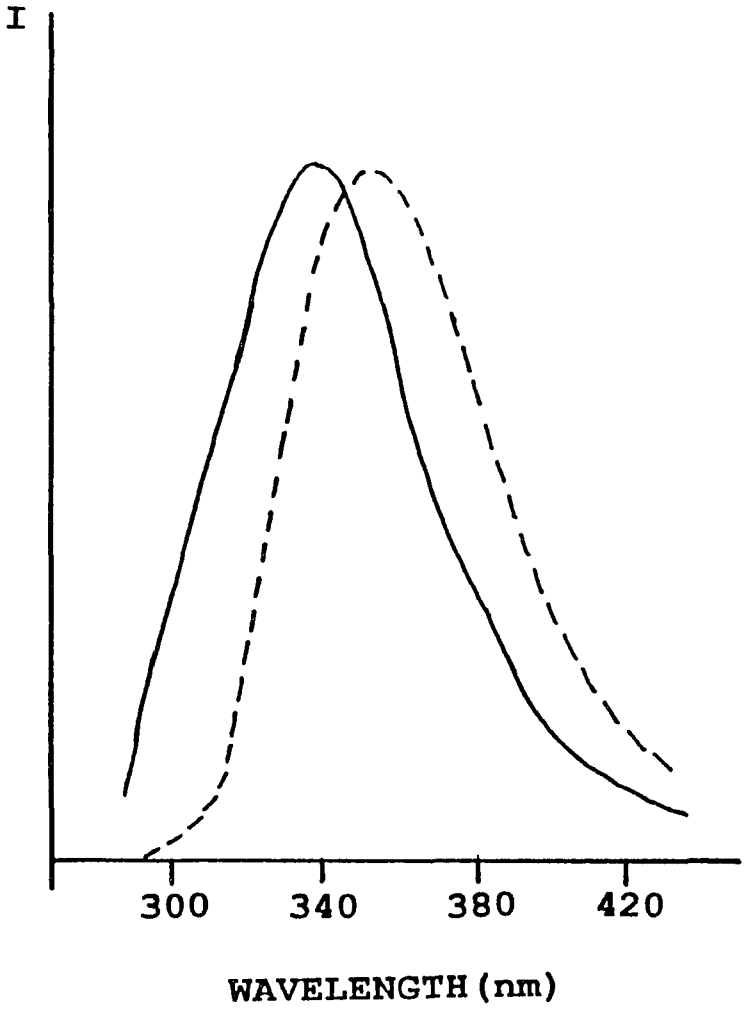

Figure 1.7 Normalized fluorescence emission spectra of the human serum albumin (solid line), Tryptophan alone (dashed line). Note that, except for a spectral shift, the spectrum of the protein closely resembles that of pure tryptophan. [After J. W. Longworth, in Excited States of Proteins and Nucleic Acids. ed. R. F. Steiner and I. Weinryb (New York: Plenum Press, 1971).]

the fluorescence decay time is 2.6ns.[57] Tryptophan's molecular structure is shown in Figure 1.6. Tryptophan is a basic biological building block in the forming of proteins. Together with other amino acids, they connect in different sequences in the different proteins. In these different proteins, or the same type of protein from different species, tryptophan may have residue in different locations in the sequence.[58] When the tryptophan is bound in the protein, its fluorescence spectrum will be blue shifted to maximum at 340nm (Figure 1.7).[59,57] With the different residue in the different proteins, the fluorescence properties of the tryptophan vary from protein to protein in both fluorescence efficiency and fluorescence kinetics.[60] The fluorescence decays with multi-decay times. For example, the tryptophans in myoglobin have fluorescence decay times as 14ps, 106ps and 2680ps.[60] That is why tryptophan is a useful optical probe of the protein structure.

Collagen gives rise to the fluorescence maximum around 380nm when the excitation wavelength is 320nm (Figure 1.8) and about the same but lower intensity when the excitation wavelength is 300nm (Figure 1.9). The fluorescence peaks will be slightly shifted to 390nm when the excitation wavelength is 351nm (Figure 1.10). The measured excitation spectrum of collagen are shown in Figure 1.11 and Figure 1.12 when the emission wavelength is 380nm and 460nm, respectively. The excitation peak maximum is located at 340nm and 345nm. All

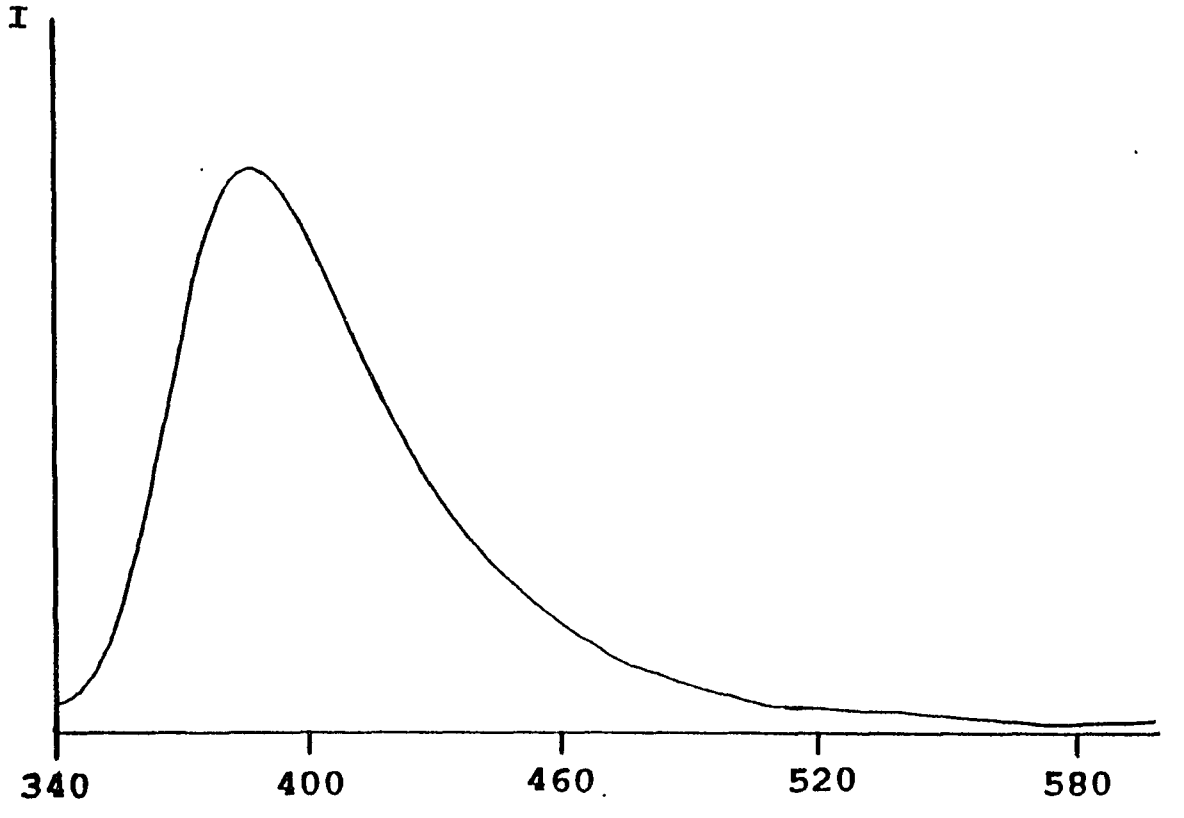

Figure 1.8 Fluorescence spectrum of collagen when the excitation wavelength is 320nm. The intensity is in arbitrary units. The sample was studied in the solid, non-solubilized state.

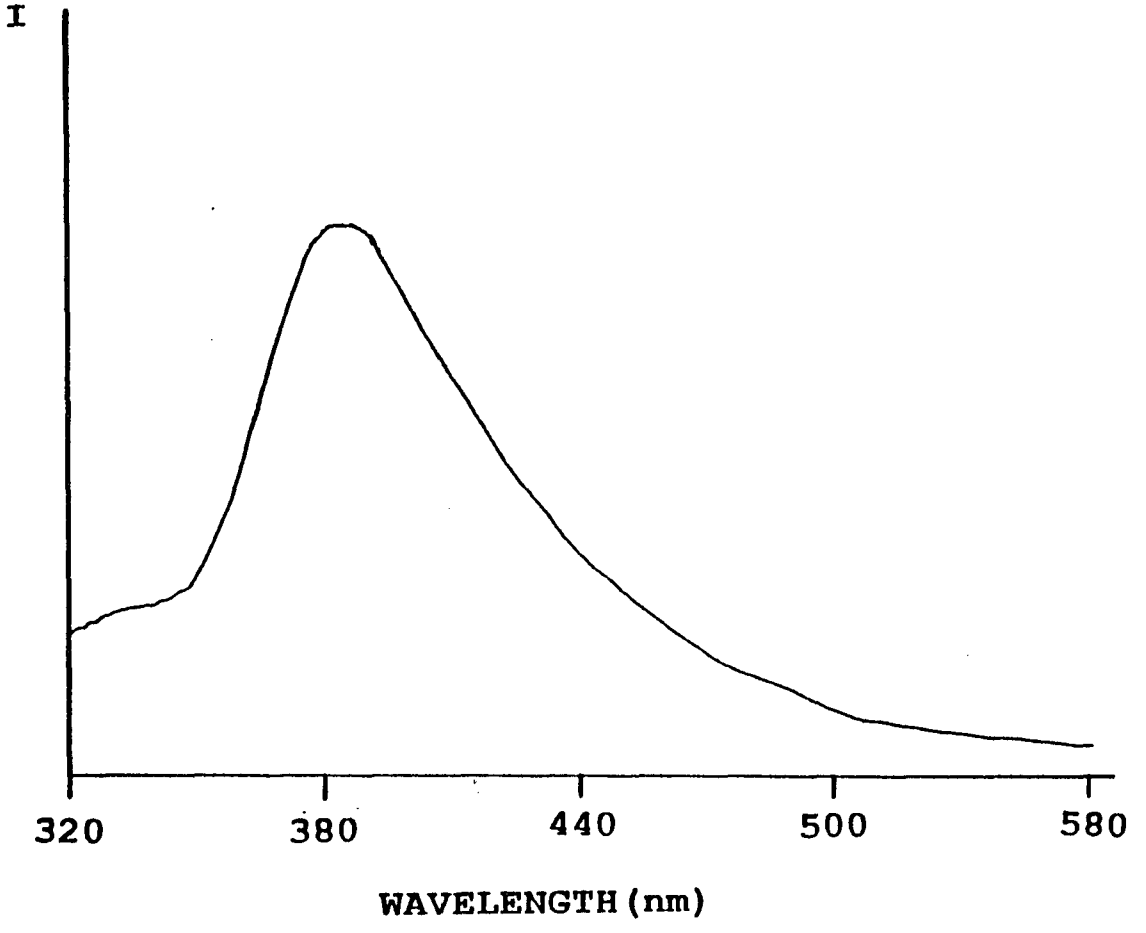

Figure 1.9 Fluorescence spectrum of collagen when the excitation wavelength is 300nm. The intensity is in arbitrary units. The sample was studied in the solid, non-solubilized state.

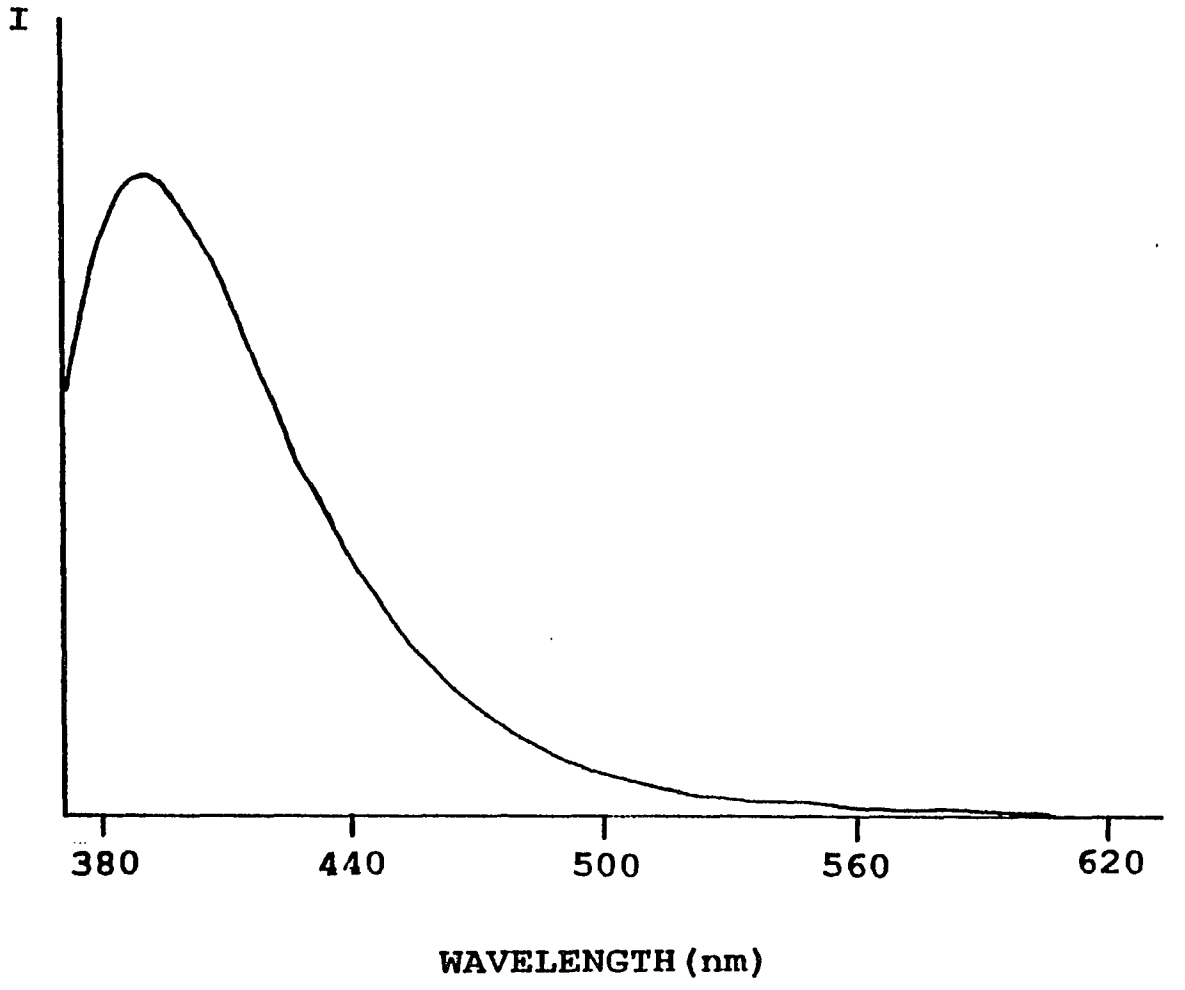

Figure 1.10 Fluorescence spectrum of collagen when the excitation wavelength is 351nm. The intensity is in arbitrary units. The sample was studied in the solid, non-solubilized state.

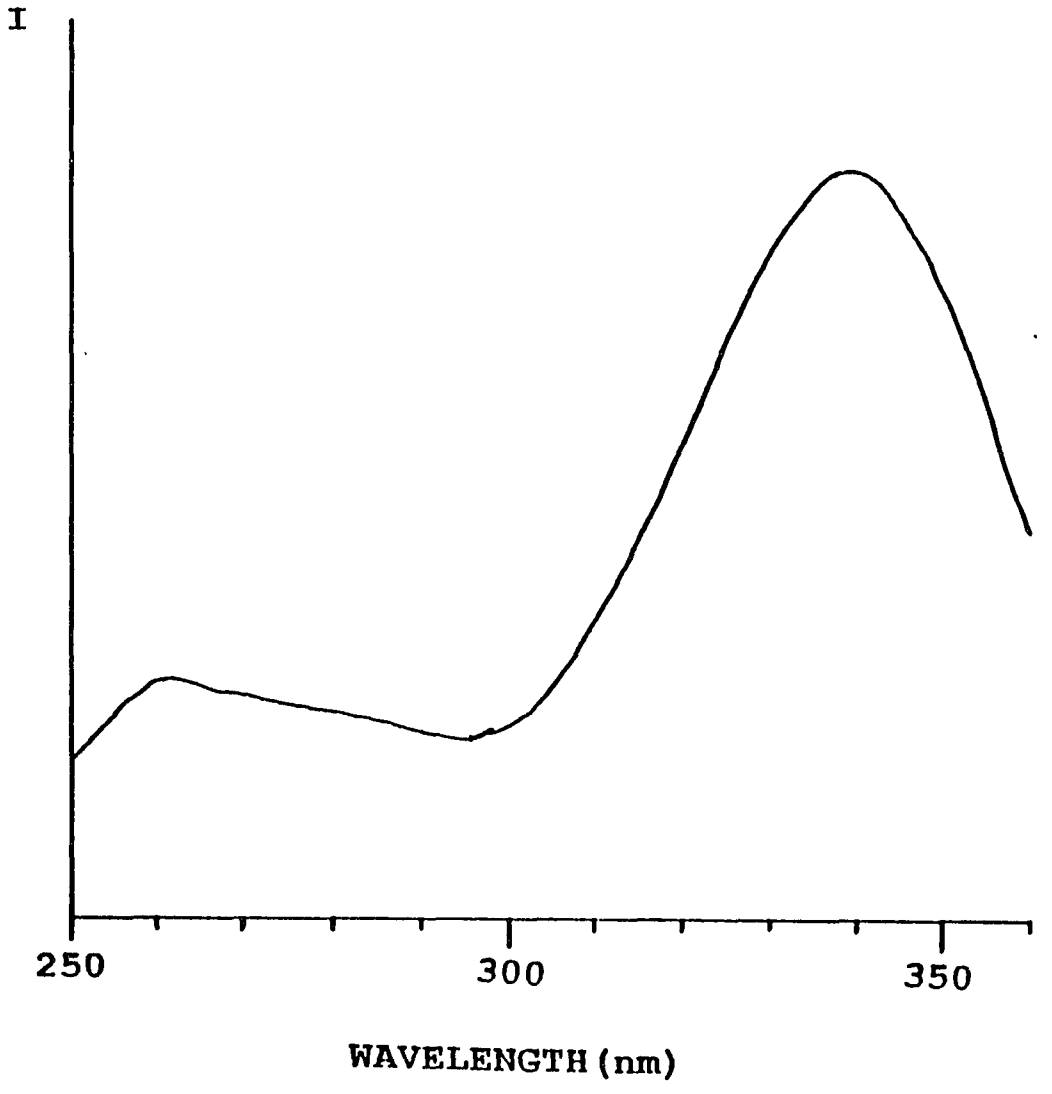

Figure 1.11 Fluorescence excitation spectrum of collagen when the emission wavelength is 380nm. The intensity is in the arbitrary unit. The sample was studied in the solid, non-solubilized state.

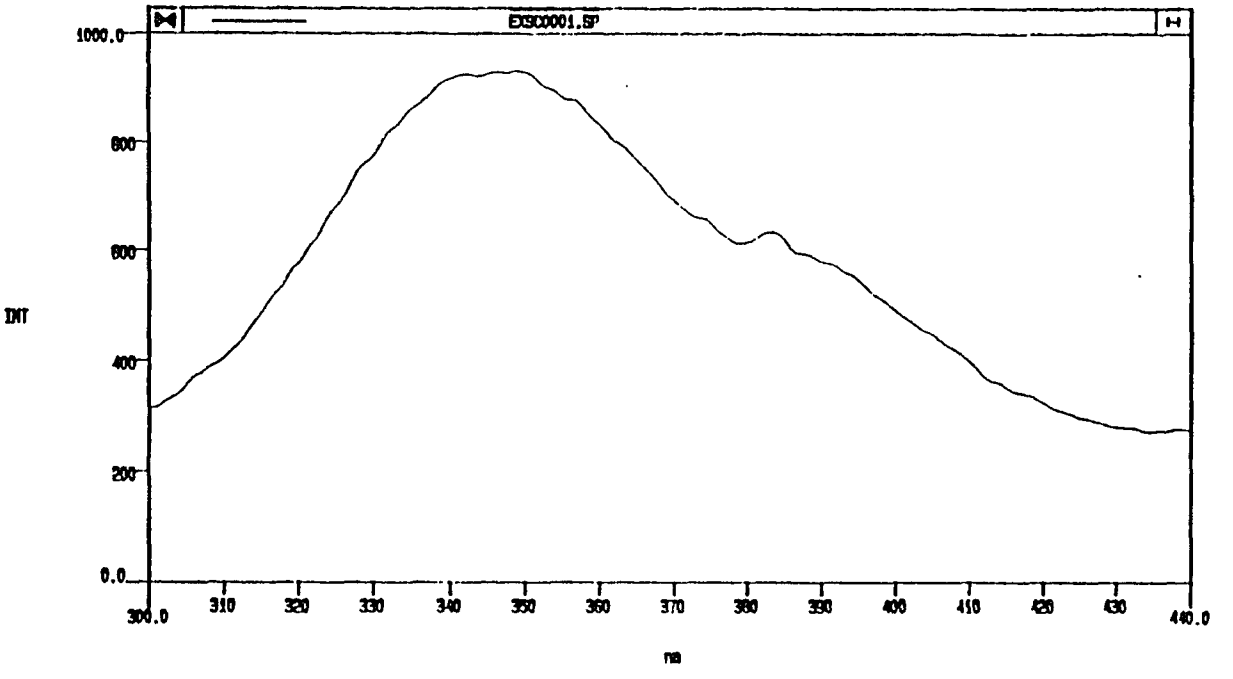

Figure 1.12 Fluorescence excitation spectrum of collagen when the emission wavelength is 460nm. The intensity is in arbitrary units. The sample was studied in the solid, non-solubilized state.

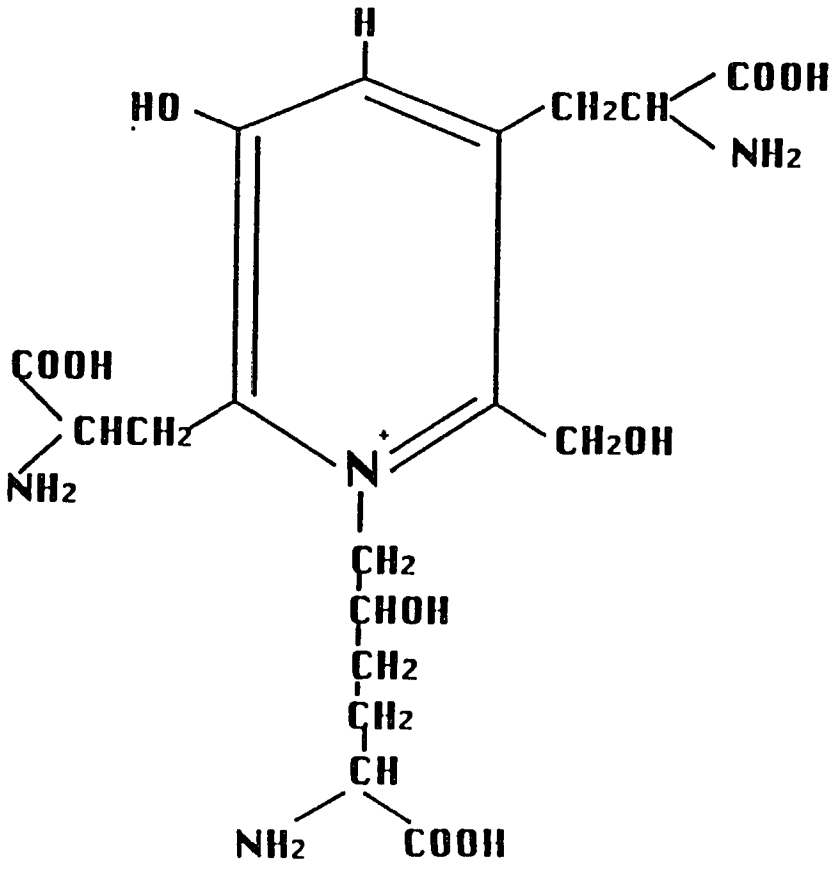

Figure 1.13 The possible molecular structure of "pyridinoline". [After Fujimoto, D., Akiba, k., Nakamura, N., in **Biochemical and Biophysical research communications**, 1977]

the above spectra of collagen were measured on LS-50 (Perkin Elmer, see Chap. 4.2 for detail). The collagen (from Sigma Co.) is measured in the solid, non-solubilized state. The possible fluorophor which unites in the collagen is "Pyridinoline"[61]. It is cross-linked in collagen. The predicted molecular structures of the "Pyridinoline" is shown on Figure 1.13. Collagen is a major fibrous protein of connective tissue.[58] Its biological function will be stated together with elastin in the next paragraph.

Elastin gives fluorescence spectra with a maximum at wavelength 400nm when the excitation wavelength is 325nm[32] or 320nm (Figure 1.14 and 1.15). Our measurements show that it gives fluorescence maximum at wavelength 415nm to 420nm when the excitation wavelength is 300nm or 351nm (Figure 1.16 and 1.17). Its excitation spectrum are shown in the Figure 1.18 when the excitation wavelength is 420nm. The peak of the excitation spectrum is at 355nm. The peak of the excitation spectra shifts to 385nm when the emission wavelength is at 460nm (see Figure 1.19). All the above spectra of the elastin (from Sigma Co.) were also measured on LS-50 (Perkin Elmer, see Chap. 4.2 for detail). Figure 1.14. was measuered by another group. The possible fluorophor is desmosine, whose fluorescence spectrum is also shown in Figure 1.14[32]. Desmosine is one of the amino acids which only exists in elastin[58]. It is cross-linked in elastin[58]. The molecular structures of the desmosine are shown on Fig. 1.20[58].

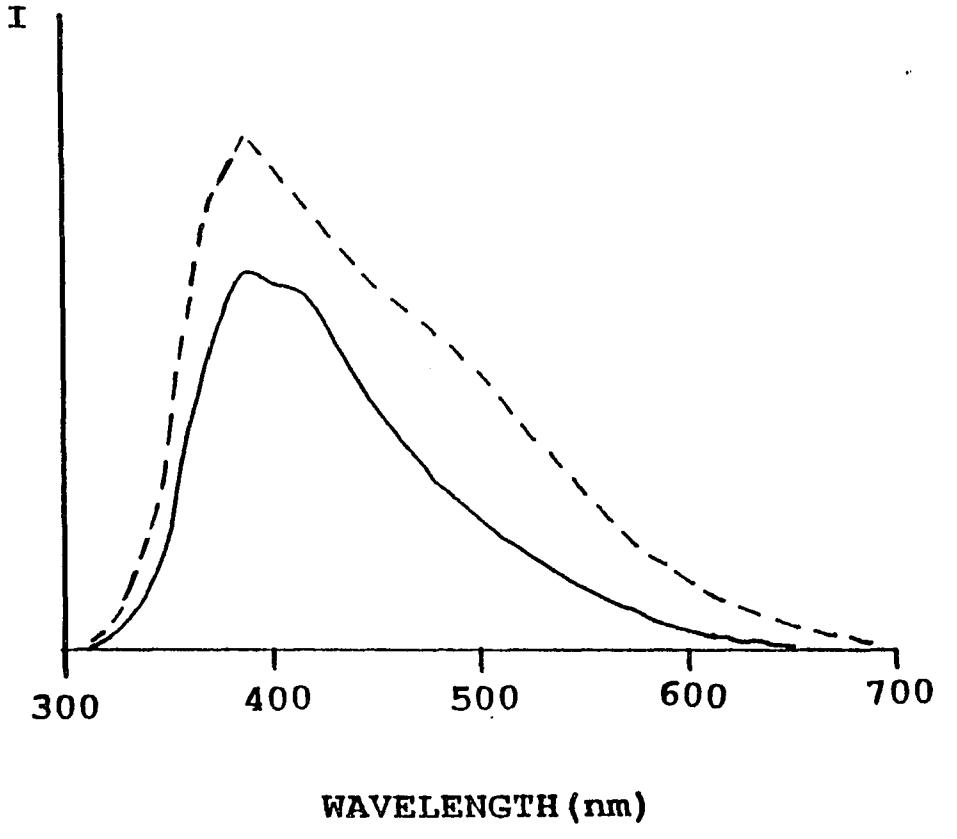

Figure 1.14 Fluorescence spectrum of elastin (solid line) and desmosine (dashed line) when the excitation wavelength is 325nm. The intensity is in arbitrary units. The sample was studied in the solid, non-solubilized state. (After: D.J. Lefell, etc., in Arch. Dermatol. **vol. 124** [32])

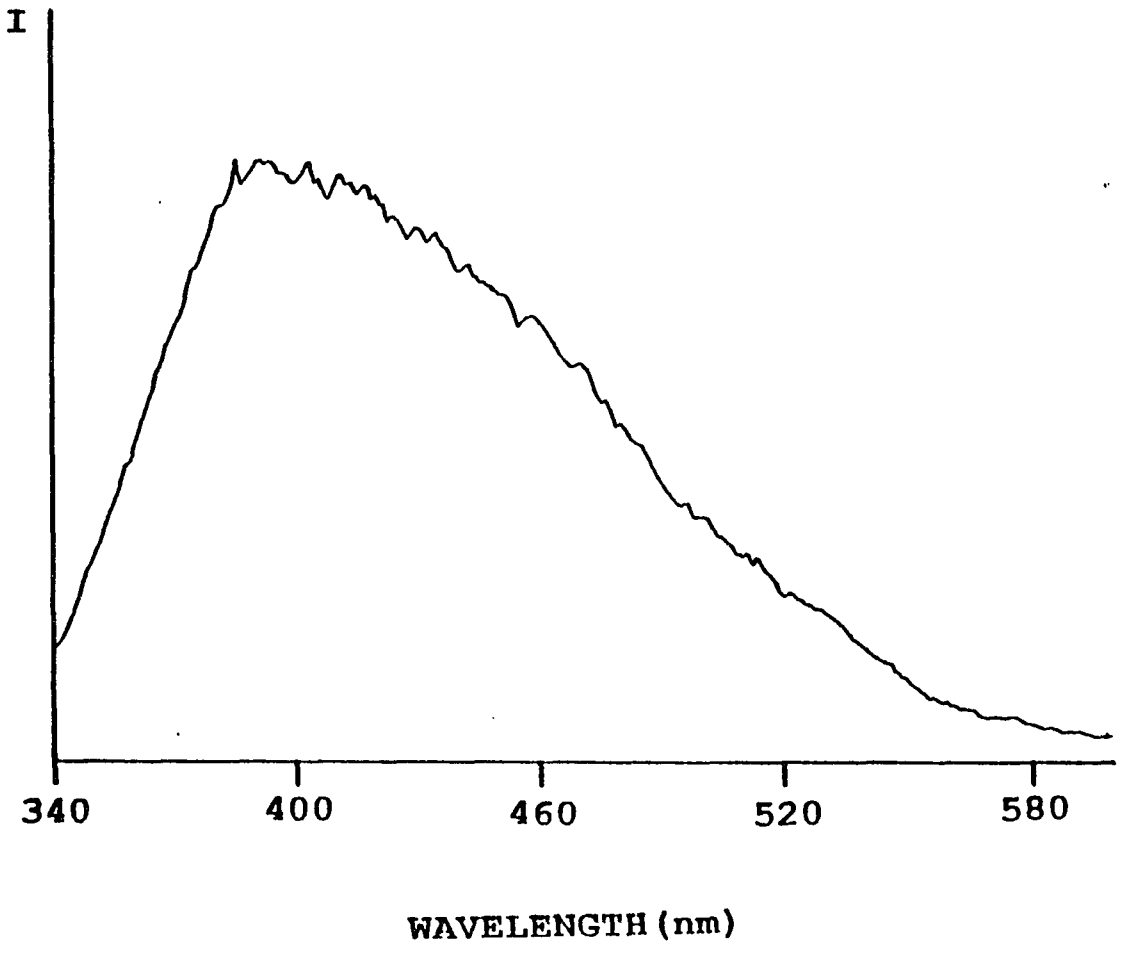

Figure 1.15 Fluorescence spectrum of elastin when the excitation wavelength is 320nm. The intensity is in arbitrary units. The sample was studied in the solid, non-solubilized state.

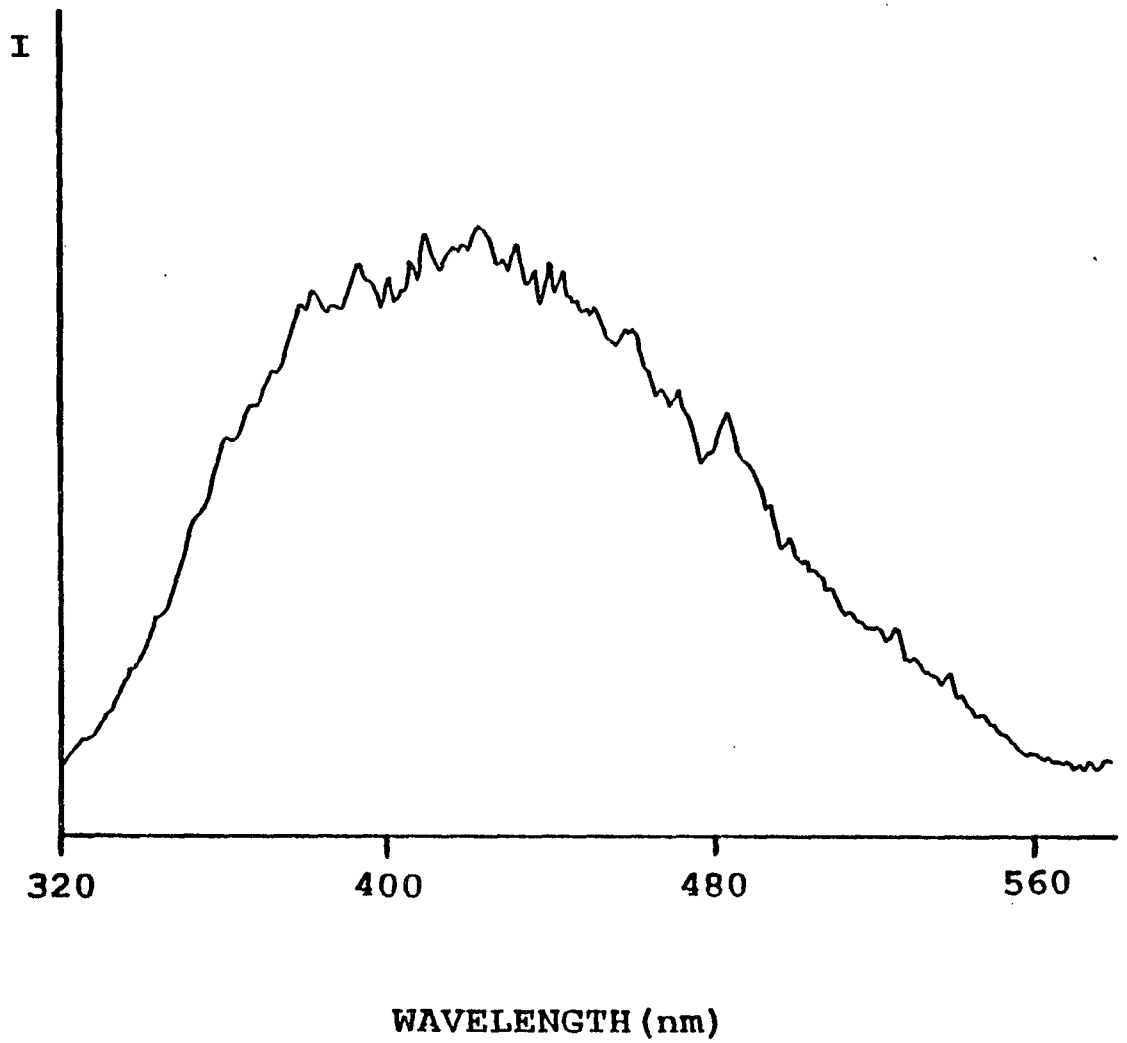

Figure 1.16 Fluorescence spectrum of elastin when the excitation wavelength is 300nm. The intensity is in arbitrary units. The sample was studied in the solid, non-solubilized state.

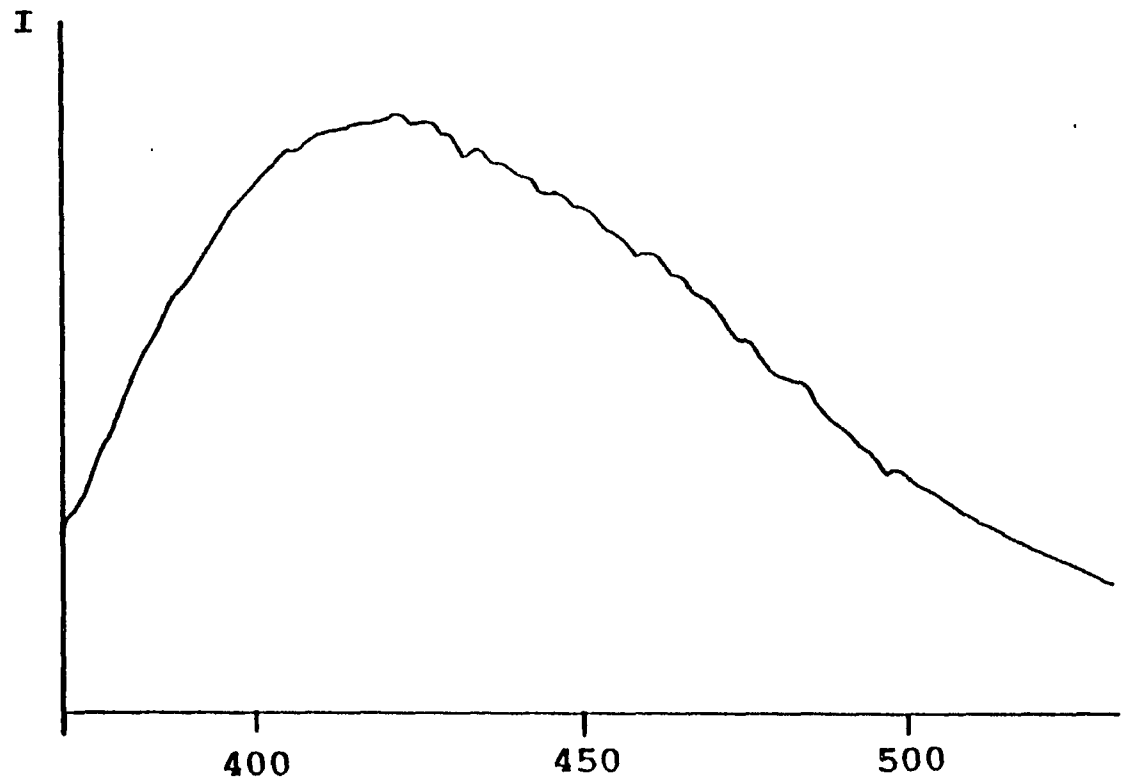

Figure 1.17 Fluorescence spectrum of elastin when the excitation wavelength is 351nm. The intensity is in arbitrary units. The sample was studied in the solid, non-solubilized state.

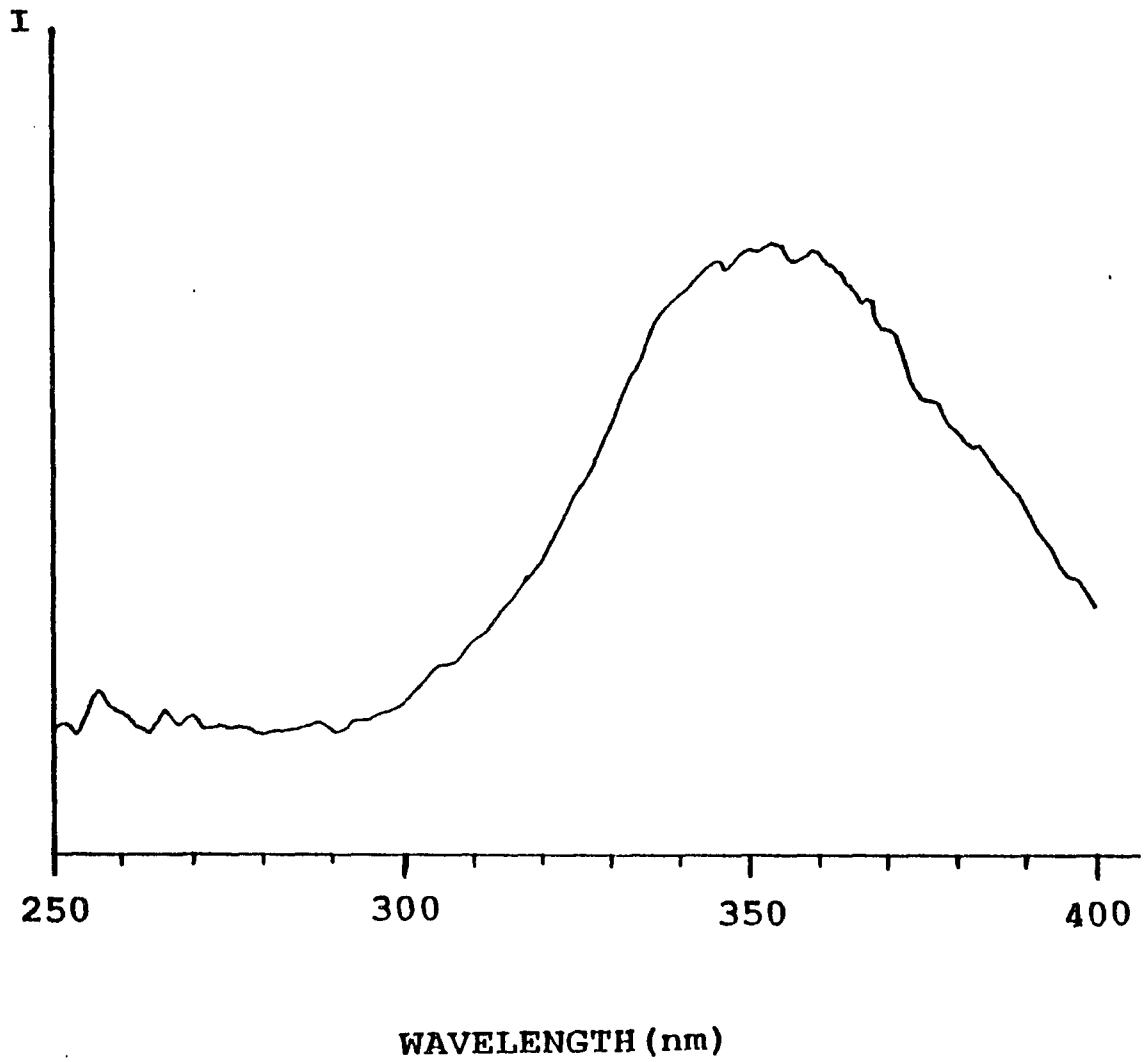

Figure 1.18 Fluorescence excitation spectrum of elastin when the emission wavelength is 420nm. The intensity is in arbitrary units. The sample was studied in the solid, non-solubilized state.

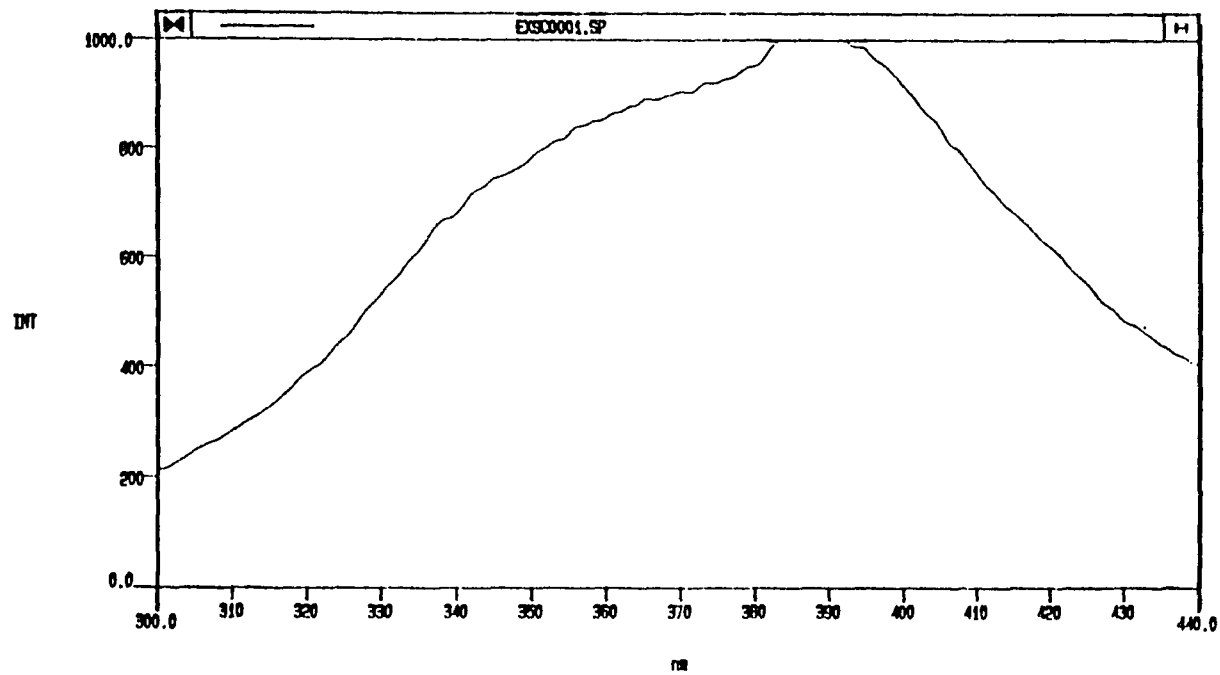

Figure 1.19 Fluorescence excitation spectrum of elastin when the emission wavelength is 460nm. The intensity is in arbitrary units. The sample was studied in the solid, non-solubilized state.

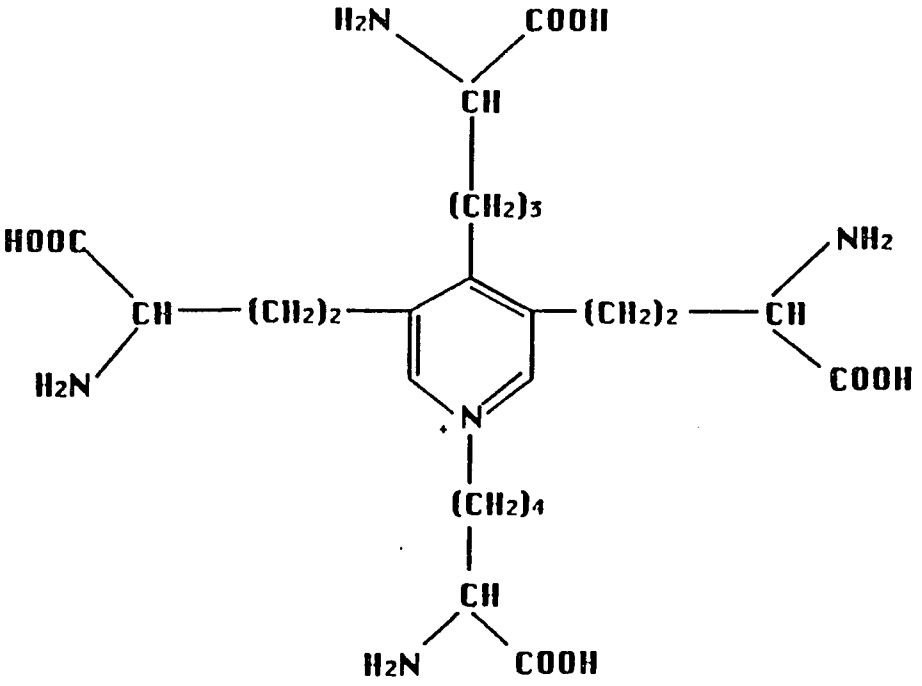

Figure 1.20 The molecular structure of desmosine [From Lehninger, Albert L., Principle of Biochemistry, third printing, Worth Publishers, Inc. (1984)]

Collagen and elastin are the major fibrous proteins of connective tissues.[58] The connective tissue consists of the extracellular structural and supportive elements of the body. It forms the matrix of bones, enveloping blood vessels. It forms an important structural layer under the skin, help bind cells together into tissues, and forms the extracellular ground substance between cells. Collagen and elastin occur together in most connective tissues but vary in their proportions. For example, the collagen makes up 6% of the weight of the total human uterus, while elastin only makes up 1%.[62] On the other hand, the collagen and elastin are about equal in the lung and artery tissues[63]. The collagen fibril do not stretch whereas elastin fibrils are elastic. The collagen is especially rich in tissues like tendons, bones, skin fibers, and blood vessels. Elastin is rich in elastic tissues like ligaments and the elastic connective tissue layer of large arteries. The fibrous proteins take up to one half or more of the total body proteins while collagen takes nearly one third of the total body proteins (that is about 19% of the human body)[58].

Reduced form of nicotinamide adenine dinucleotide (**NADH**) and reduced form of nicotinamide adenine dinucleotide phosphate (**NADPH**) fluoresce with maximum at 460nm (Figure 1.21)[59] and absorb with maximum at 260nm and 340nm (Figure 1.22)[64]. NAD(P)H occurs either in the oxidized or [$NAD(P)^+$] or in reduced form (NAD(P)H). $NAD(P)^+$ does not absorb around

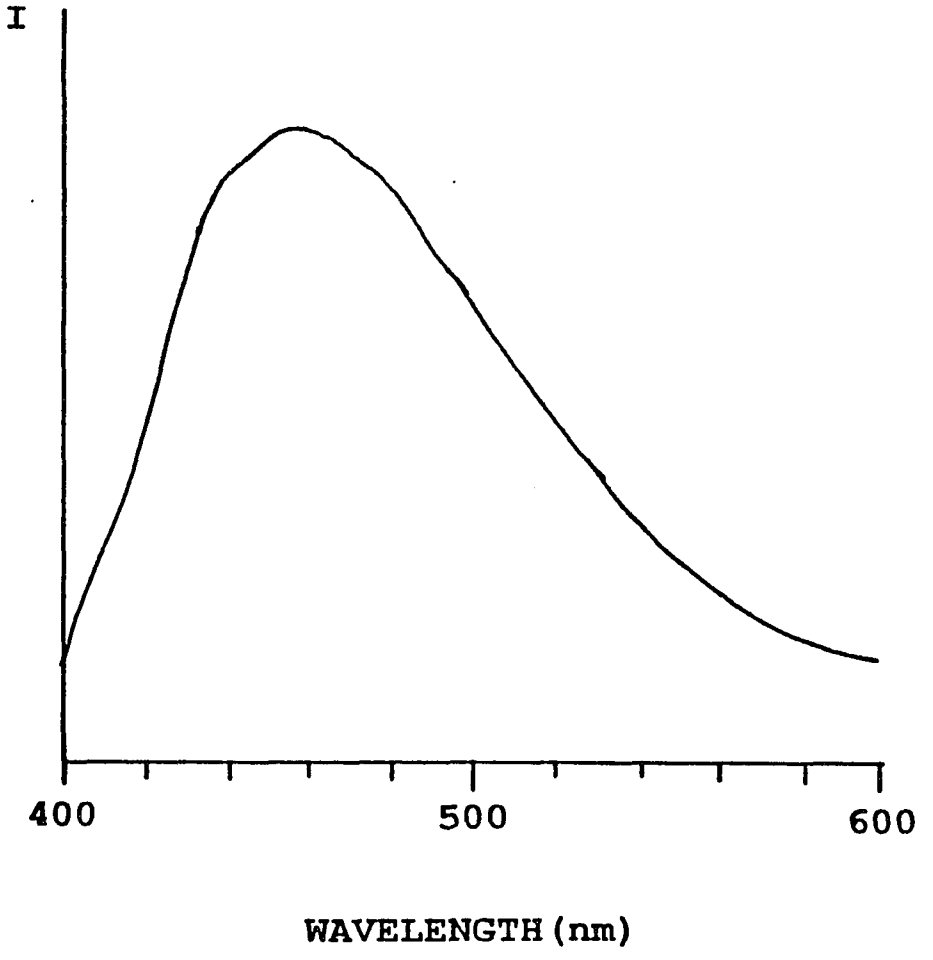

Figure 1.21. Fluorescence emission spectrum of NADH [From Undenfriend, Sidney Fluorescence Assay in biology and Medicine Vol.I, Academic Press, New York (1962)]

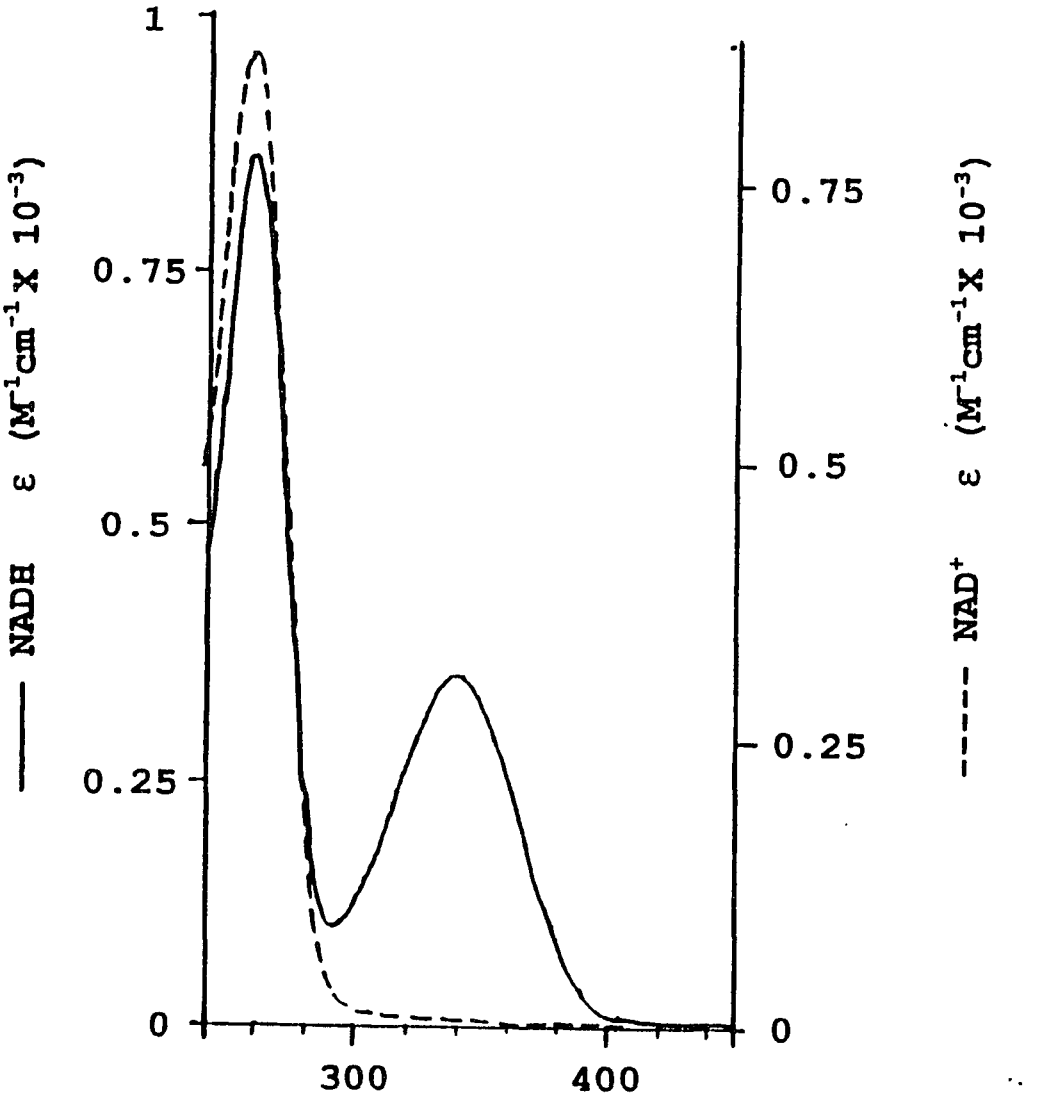

Figure 1.22. The absorption spectra of NADH (reduced form, in solid line) and NAD^+ (oxidized form, in dashed line). [From Lehninger, Albert L., Principle of Biochemistry, Second printing, Worth publishers, Inc.]

340nm efficiently (see Figure 1.22).[64] NADPH fluorescent much less efficiently then the NADH.[65] It is also known that the binding of the NADH will cause the spectral blue shift from 460nm to 450nm when compared to the spectrum of the free NADH. The fluorescence efficiency of the free NADH is 0.04.[57] The lifetime of the fluorescence of free NADH is about 0.4ns[57].

NADH is an important coenzyme in the biological system. Coenzymes are complex organic molecules which are required by certain enzymes for activity. As functional units of the cell metabolism , these enzymes act in well structured sequences and are able to catalyze many step wise reactions (i.e., in the hundreds), which lead to nutrient molecules being degraded, the production of cell macromolecule from simple precursors, and the conservation and transformation of chemical energy. A special class, called regulatory enzymes, participates in the metabolism. These regulatory enzymes are special because they are able to sense the different metabolic signals and change their catalytic rates accordingly. The coordinated action of the enzyme systems allows the many different metabolic activities which sustain life to act together. Inheritable genetic disorders (for example, cancer) may have a deficiency, or even a total absence, of one or more of these enzymes in the tissues. Therefore, the ability to measure certain enzyme activity in the blood plasma and/or the tissue takes on great significance in the diagnosis of

cancer.[58] The coenzymes will either be bonded to the enzymes in a loose and transient fashion, or in a tight and permanent fashion.[58]

NAD is mostly found in the mitochondria. It plays an important role in the electron transport in the oxidative phosphorylation. As mentioned before, it can exist in two forms: oxidized and reduced. The molecular structures of the oxidized form $NAD(P)^+$ and reduced form NAD(P)H are shown on Figure 1.23 and Figure 1.24. The nicotinamide component of NAD serves as the transient intermediate carrier of a hydride ion that is enzymatically removed from a substrate molecule (consider it as A) by the action of certain dehydrogenase. NAD^+ accepts two electrons and one proton to become NADH.

$$AH_2 \xrightarrow{\text{oxidation}} A + 2e^- + 2H^+$$

$$NAD_+ + 2e^- + H^+ \xrightarrow{\text{reduction}} NADH$$

Overall, it shows as

$$AH_2 + NAD^+ \longrightarrow A + NADH + H^+$$

The reduced NAD (NADH) then can transfer the electron to other compounds, thereby effecting another oxidation-reduction reaction. An example is the oxygen in aerobic respiration

$$NADH \xrightarrow{\text{oxidation}} NAD^+ + 2e^- + H^+$$

$$1/2\ O_2 + 2H^+ + 2e^- \longrightarrow H_2O$$

Overall,

$$NADH + 1/2\ O_2 + H^+ \longrightarrow NAD^+ + H_2O$$

NADH is in the higher energy level than NAD^+. The free energy of oxidation of NADH is used to form most of the

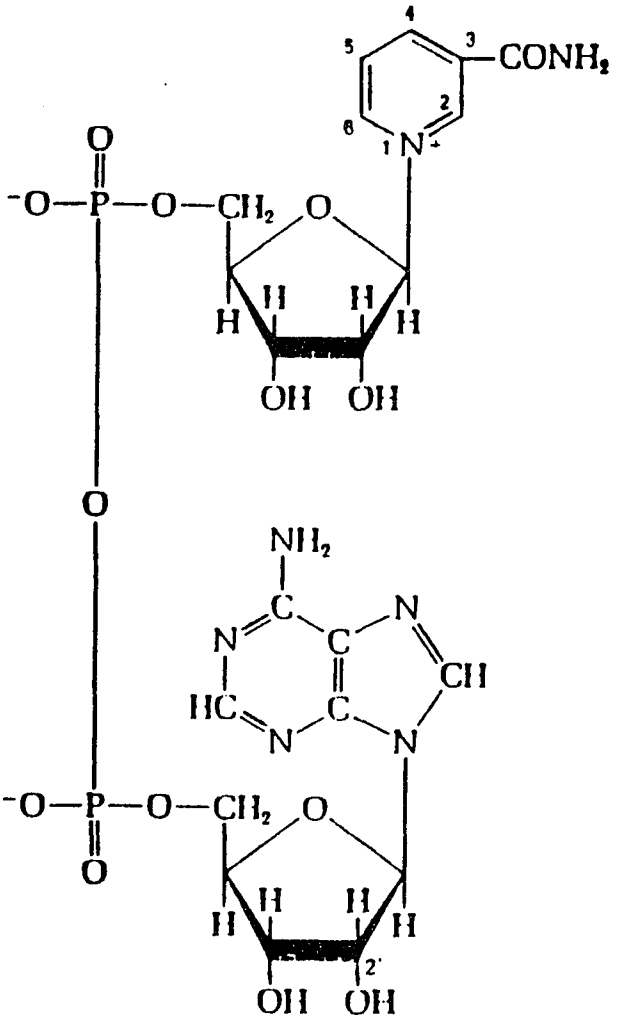

Figure 1.23. Molecular structure of NADH [From Lehninger, Albert L., Principle of Biochemistry, Second printing, Worth publishers, Inc.]

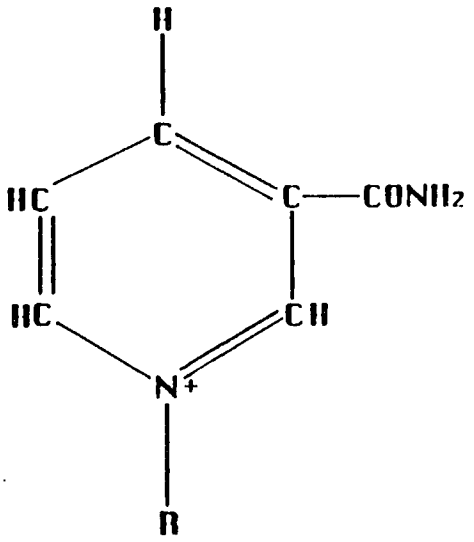

NAD +

OXIDIZED FORM

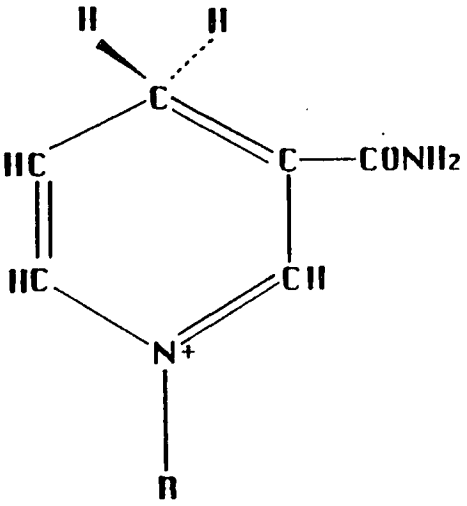

NADH

REDUCED FORM

Figure 1.24. Molecular structure change of the oxidized form and reduced form of the NAD [From Lehninger, Albert L., Principle of Biochemistry, Second printing, Worth publishers, Inc.]

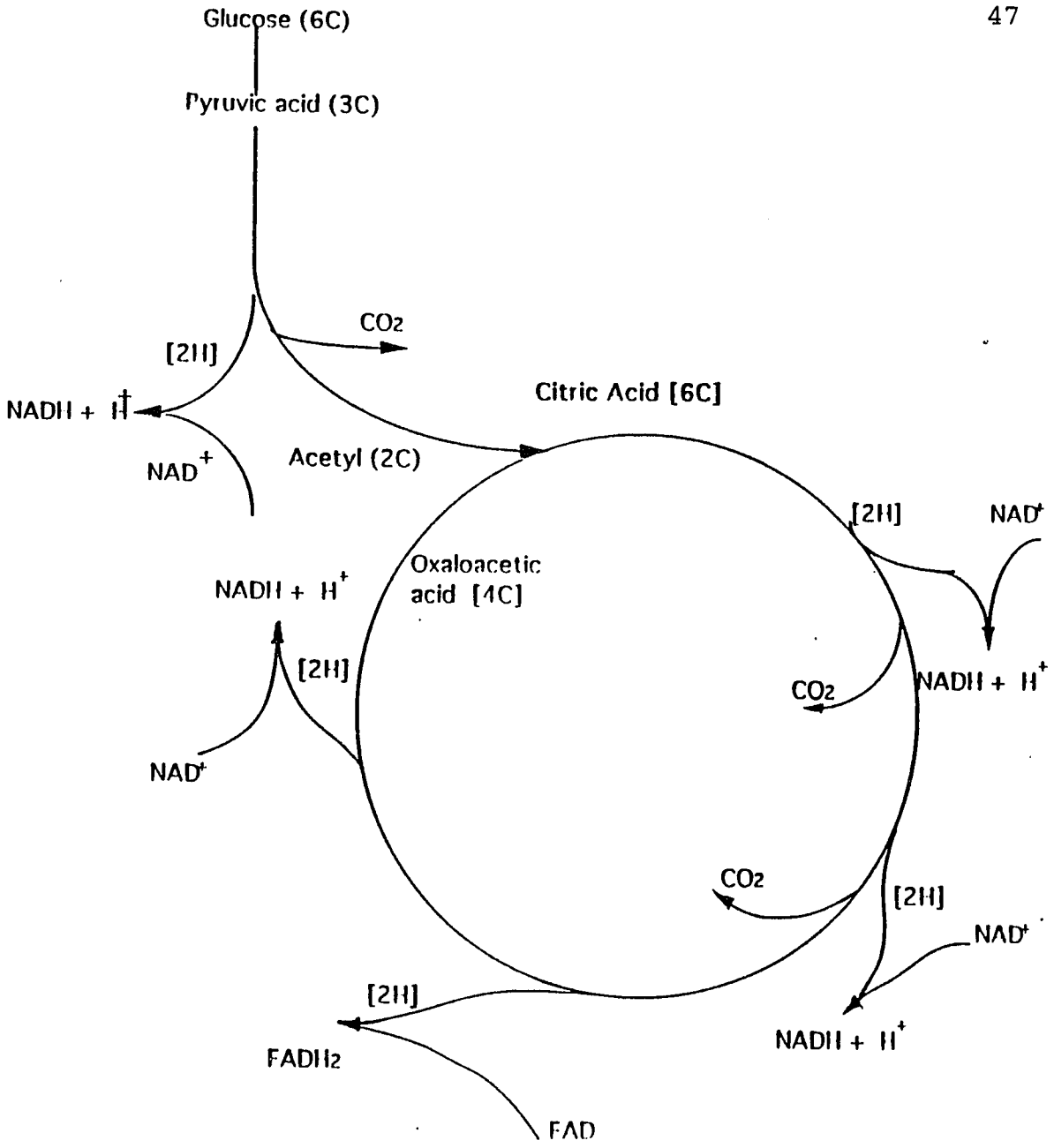

Figure 1.25 Diagram of the citric acid cycle.

ATP from ADP in the cell. ATP represents the energy currency of the cell, and is the form in which metabolic energy is supplied to do the work of the cell. The overall process of aerobic respiration is the oxidation of glucose by oxygen as

$$C_6H_{12}O_6 + 6O_2 \text{ ------> } 6CO_2 + 6H_2O + \text{energy}$$

In the process, the glucose molecules are first broken down only partially, yielding two molecular of pyruvic acid with 3C. The pyruvic acid enters the mitochondria, where it is first converted to a 2C acetyl group; the acetyl group then combines with a molecule of oxaloacetic acid (with 4C) to form citric acid. This is the starting of the citric acid cycle (see Figure 1.25) . This cycle results in the oxidation of the citric acid, converts it to $2CO_2$ and back to oxaloacetic acid again. In the oxidation cycle, electrons and protons have been transferred to NAD and FAD (see next paragraph), so three of NAD^+ and one of FAD become three of NADH and one of $FADH_2$. Therefore the energy originally in the glucose is transferred to NADH and $FADH_2$ and then transferred to ATP.[66]

Flavins' (riboflavin, FMN, FAD) fluorescence spectrum and absorption spectrum are shown in Figure 1.26 and Figure 1.27 respectively. The maximum of the fluorescence is around 520nm and the maximum of the absorption is around 450nm and 375nm and two more peaks at shorter wavelength[55]. Studies have also shown that the fluorescence decay time of the free FAD (flavin adenine dinucleotide) has two components, 200ps and 3ns.[67,68] The intensity of the 200ps component is weak under

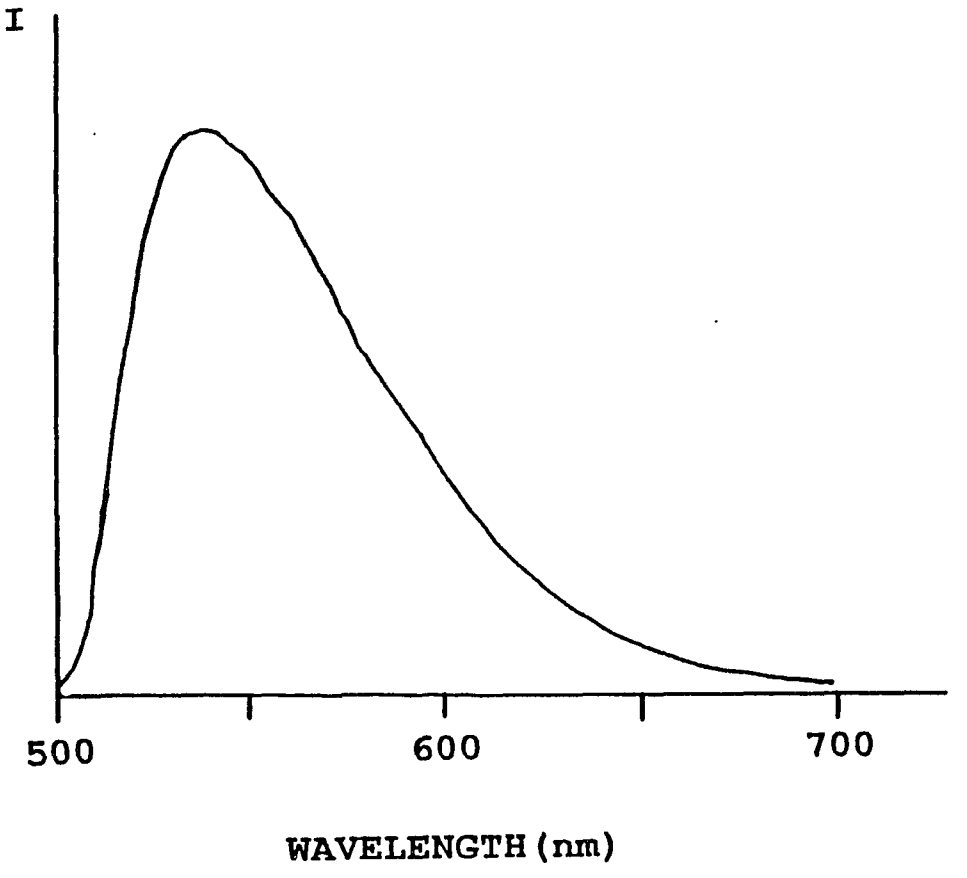

Figure 1.26 Fluorescence emission spectrum of flavins (FAD, FMN, and riboflavin) [From Benson, R.C., Meyer, R.A., Zaruba, M.E. and McKhann, G.M., The Journal of Histochemistry and Cytochemistry, 1971]

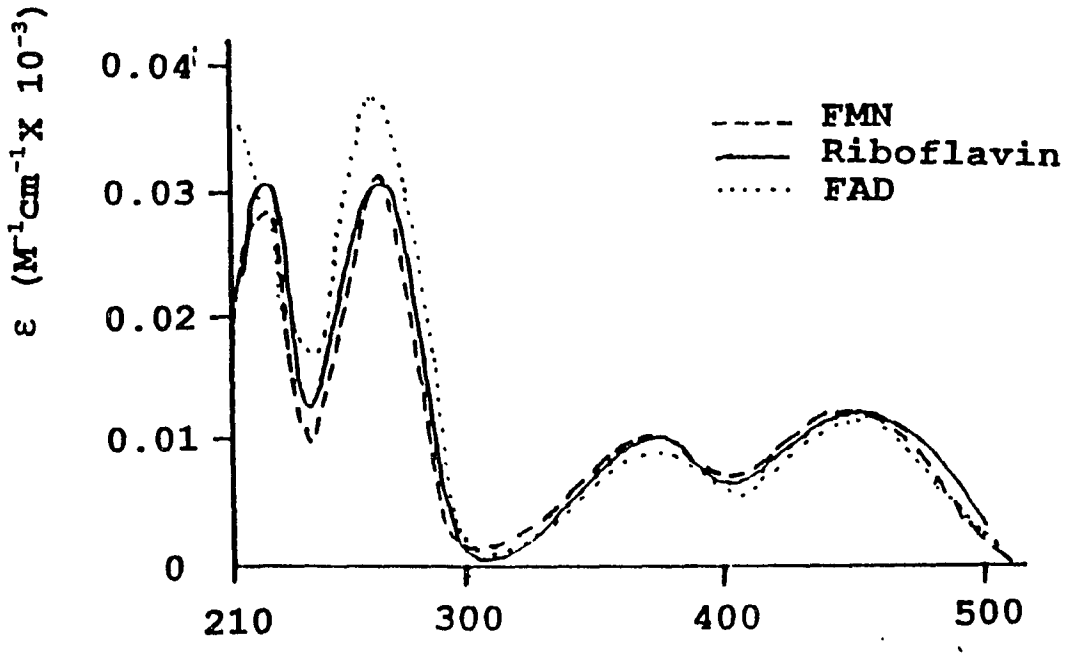

Figure 1.27 Absorption spectra of flavins in pH 7.0 [Undenfriend, Siney. Fluorescence Assay in biology and Medicine, Vol. I, Academic Press: New York.]

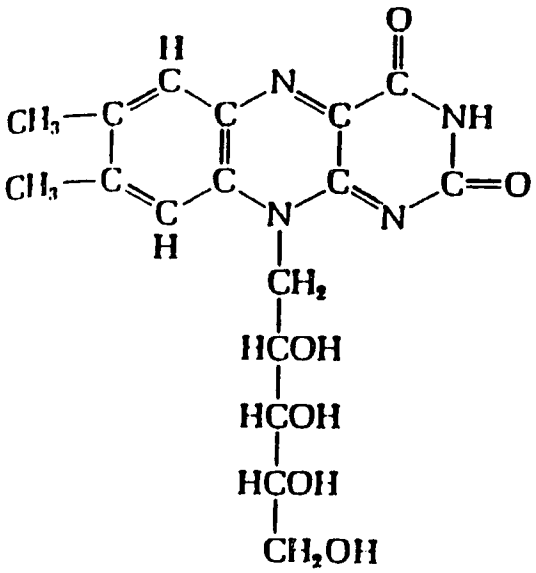

Figure 1.28. Molecular structure of riboflavin.

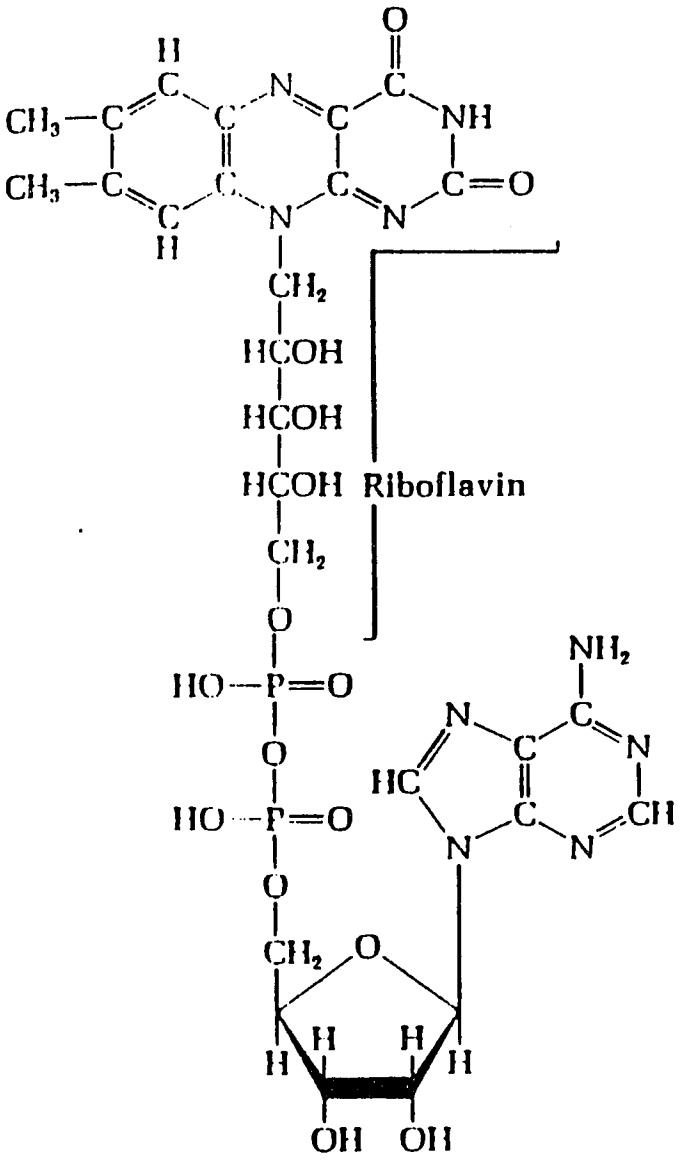

Figure 1.29. Molecular structure of FAD.

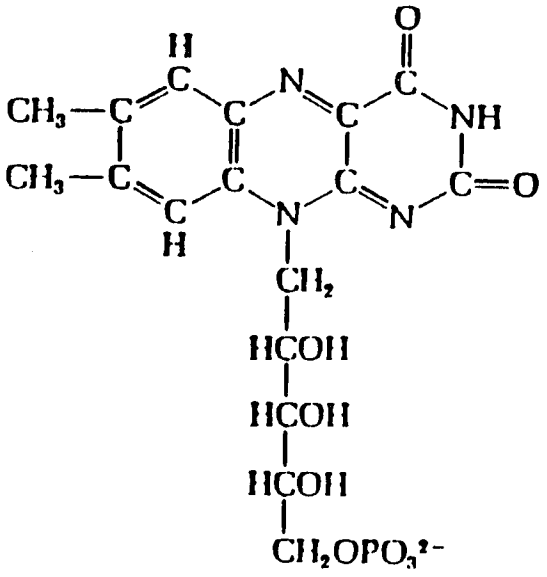

Figure 1.30. Molecular structure of FMN.

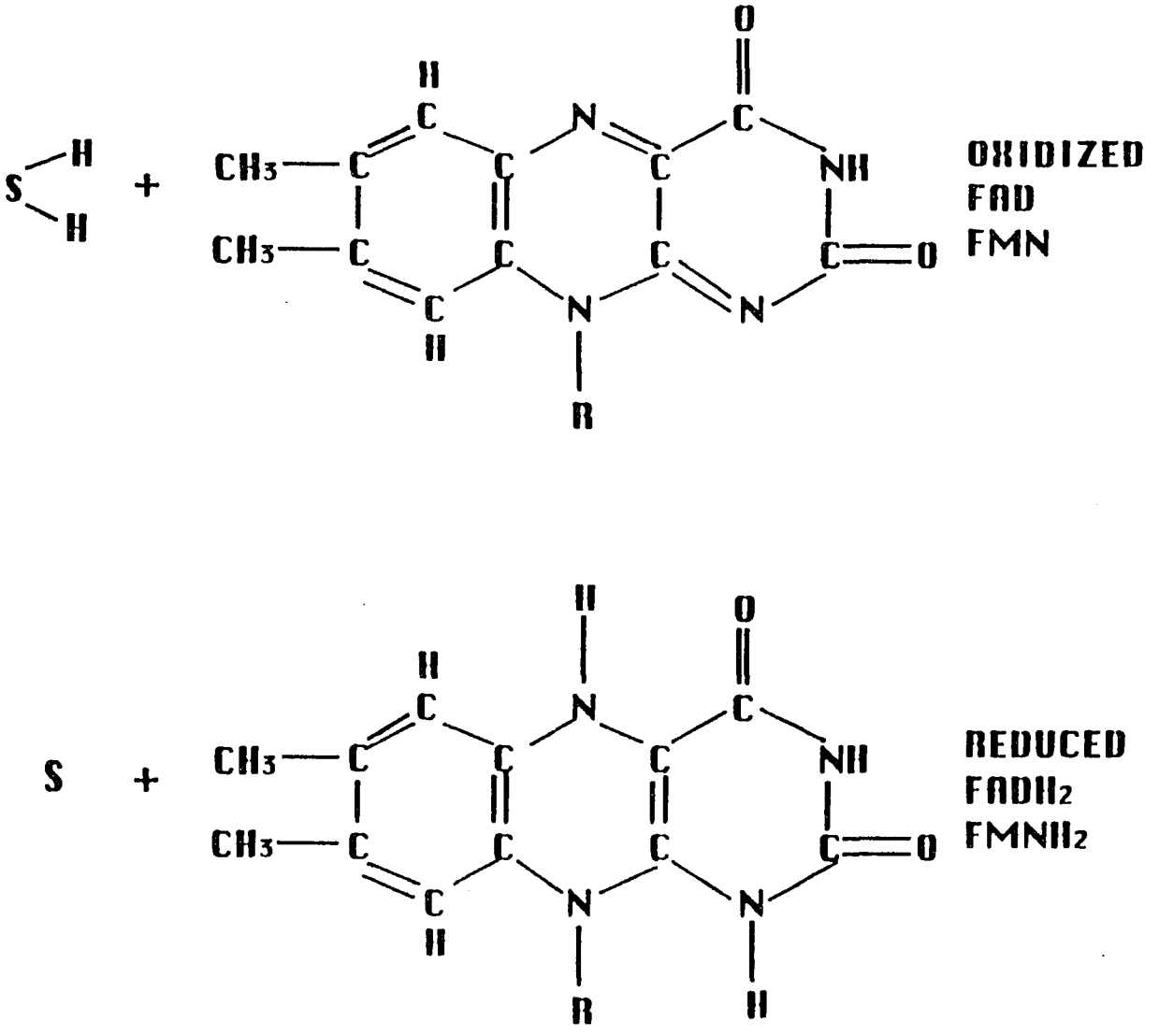

Figure 1.31 The molecular structure changes between oxidized form and reduced form of the flavins.

the room temperature and increases when the temperature decreases.[68] FMN (flavin mononucleotide) has the fluorescence decay time around 4.5ns.[68] Riboflavin (vitamin B_2) is a component of these two closely related coenzymes, FMN and FAD. The molecular structure of the Riboflavin, FAD and FMN are shown on Figure 1.28, 1.29, 1.30 respectively.

Flavins play an important role in redox metabolism in the cell. FAD and FMN are mostly found in the mitochondria. They function as tightly bound prosthetic groups of a class of dehydrogenase known as flavoproteins or flavin dehydrogenase. In the reactions catalyzed by these enzymes the isoalloxazine ring of the flavin nucleotidase serves as a transient carrier of a pair of hydrogen atoms removed from the subtract molecule.

$$AH_2 + FAD(FMN) \longrightarrow A + FAD(FMN)H_2$$

$$FAD(FMN)H_2 + 1/2\ O_2 \longrightarrow FAD(FMN) + H_2O$$

For example: FAD in citric acid cycle of the aerobic respiration (see last paragraph) and FMN in the NADH dehydrogenase.[58,66]

$$2NADH + FMN \longrightarrow NAD^+ + FMNH_2 + e$$

It is known that the absorption peak at 450nm disappears when the flavins are in the reduced state[64]. The molecular structure changes between oxidized state are shown on Figure 1.31.

This thesis studies the fluorescence in cells and tissues mostly arising from these intrinsic fluorophors. One may

probe certain different conformational states involved with these fluorophors between non-malignant and malignant cells and tissues by using different pump wavelengths. The overall view of the emission and absorption spectra of these fluorophors are presented in the Figure 1.32 and Figure 1.33. Their known parameters which are related to fluorescence properities: quantum effeiciency; decay times; decay components ratio are listed on the Table 1.2.

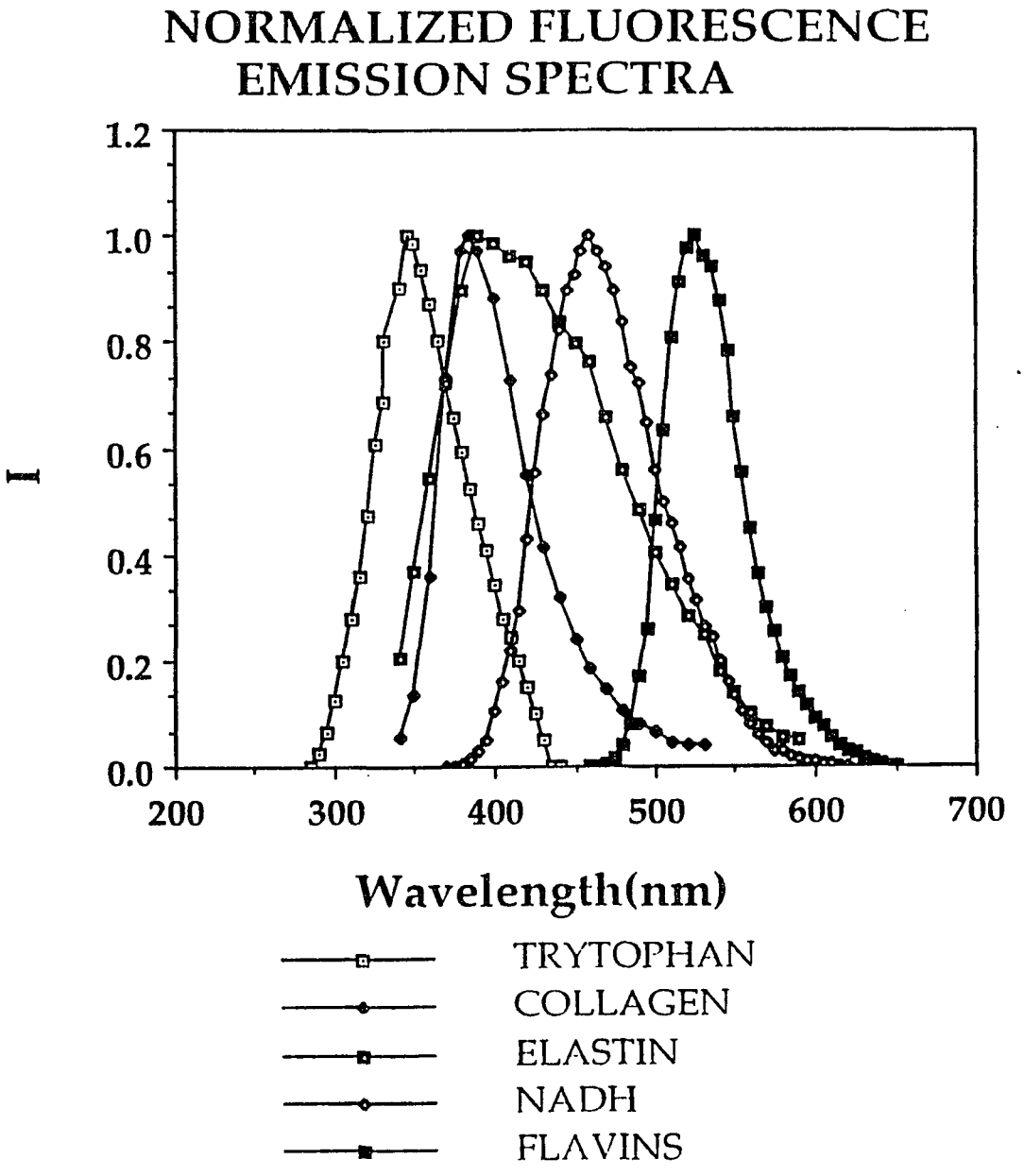

Figure 1.32 The overall view of the normalized emission spectra from various fluorophors.

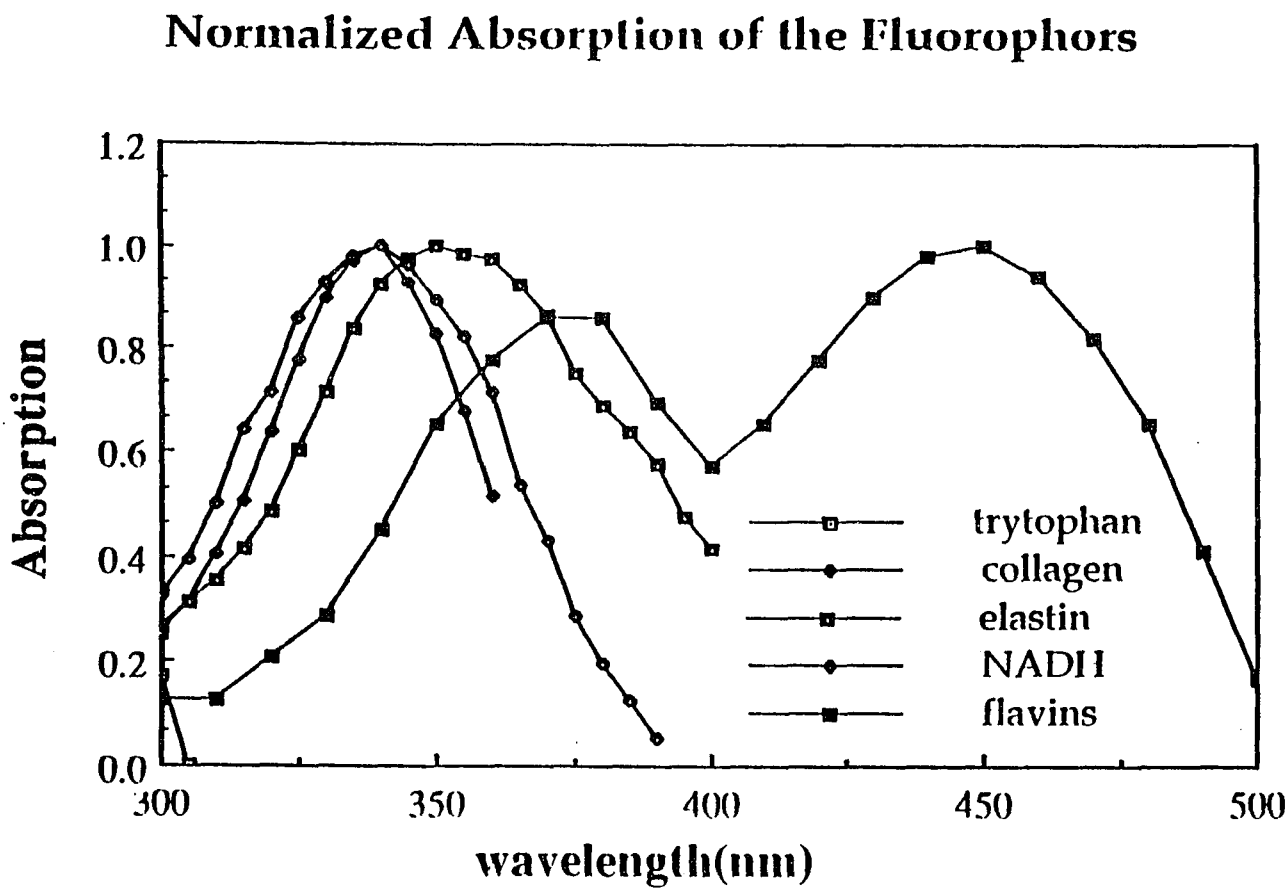

Figure 1.33 The overall view of the normalized absorption spectra from various fluorophors.

Table 1.2 List of the parameters of the fluorescence properties of various fluorophors.

Fluorophor	Fluorescence decay times*			Quantum efficiency ϕ_F
	τ_f (ps)	τ_s (ns)	A_f/A_s	
Tryptophan (in H_2O) [57]	-	2.6	-	0.2
Elastin (in H_2O, but non-solubilized) [81]	47	2.1	0.56	-
Collagen (in H_2O, but non-solubilized) [81]	76	3.5	0.59	-
NADH (in H_2O) [57]	400	-	-	0.04
FAD (in H_2O) [67]	200	3	0.33	-
FMN (in H_2O) [67]	-	4.5	-	-
Riboflavin	-	-	-	-

* τ_f is the fast decay time, τ_s is the slow decay time, and A_f/A_s is the ratio of the intensities between the fast and slow components.

Chapter 2. Physics Model of Fluorescence

This chapter will discuss the main frame of the physics models of the fluorescence spectroscopy. This will lead us to understand what physics information has been presented in the spectroscopy. This idea will be fulfilled with details in the later chapters (Chapter 4 and Chapter 5) when I am dealing with specific samples and wavelength ranges.

Luminescence is the emission of photons from electronically excited states. This photon emission, related to the transition of the molecular in the singlet excited state back to singlet ground state, is called **fluorescence.** The life time of this photon emission is usually in the time range of picosecond to nanosecond. The photon emission is called phosphorescence when a transition is from a triplet excitation state to singlet ground state. Since this trasition is quantum mechanically "forbidden", the magnitude of the phosphorescence is much smaller and the life-time of it is much slower (in ms and s range) than those of fluorescence. The substances which display significant fluorescence generally possess delocalized electrons formally present in conjugated double bonds[70] such as all the fluorophors I had mentioned in section C of chapter 1.

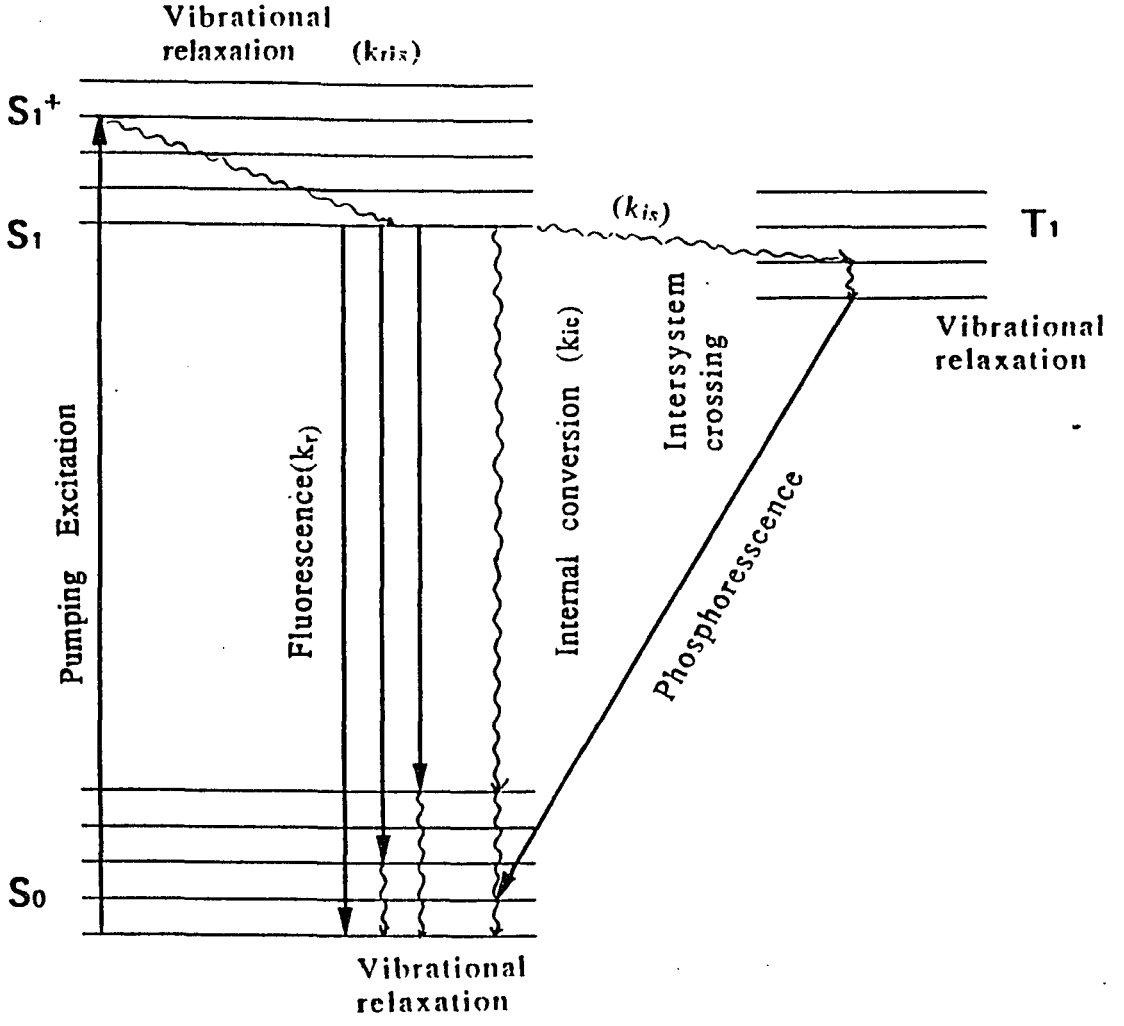

Figure 2.1 Diagram of energy level of organic molecule.

The quantum mechanical process of luminescence can be simply illustrated on the energy level diagram as shown on Figure 2.1. Assume that S_o is the ground state; S_1^+ is the first singlet excitation state; S_1 is the storage level of the first singlet excitation state; and T_1 is the first triplet excitation state of a organic molecular. A pump pulse with total energy of E and wavelength of λ will excite the molecular to singlet excitation level of S_1^+. The molecular usually will relax to the lowest level of the singlet excitation state, the storage level of S_1 through the vibrational relaxation with the rate of k_{rlx}. This vibrational relaxation usually happens in the few picosecond range which means k_{rlx} is usually very large. From this storage level S_1, the molecular can be deexcited by emitting the fluorescence (suppose the radiative rate is k_r) or through some other non-radiative process (suppose the total non-radiative rate is k_{nr}). Those non-radiative processes can include internal conversion (suppose the rate as k_{ic}) in which the energy is delivered away through the vibration or rotation of the molecular so the molecular relax to ground state; intersystem crossing (suppose the rate as k_{is}) in which the molecular undergo conversion to the first triplet state T_1; and quenching (suppose rate as $k_q(Q)$) in which the molecular energy is delivered to other molecular or particulars. It is obvious that,

$$k_{nr} = k_{ic} + k_{is} + k_q(Q) \qquad (2.1)$$

The time profile of the pump laser pulse power usually in Gaussian distribution which can be expressed as

$$P(t) = P_0 \exp(-t^2 / \tau^2) \qquad (2.2)$$
$$= (E/\sqrt{\pi}\tau) \exp(-t^2 / \tau^2)$$

and energy

$$E = \int_{-\infty}^{\infty} P(t)\, dt = P_0\sqrt{\pi}\tau$$

where τ is the a half of the pulse's time width.

Suppose the absorption coefficient of the substance is ε, According to the Beer's law:

$$I=I_0\, e^{-2.303\varepsilon cl} = I_0\, e^{-\alpha l} ,$$

here, c is the concentration of the molecules, and l is the penetration depth in the sample. Taking the first order expansion, the proportion of the excitation light has been absorbed is:

$$\beta = (I_0 - I)/I_0 = 2.303\varepsilon cl = \alpha l.$$

Then the excited numbers of molecules per second is $\beta P(t)/h\nu$ by the pumping pulse. The population of the molecules in the excitation state S_1^+ is

$$dN(S_1^+) / dt = \beta\, P(t)/h\nu - k_{rlx}\, N(S_1^+) \qquad (2.3)$$

and the population of the molecules in the storage level S_1 is

$$dN(S_1) / dt = k_{rlx}\, N(S_1^+) - (k_r + k_{nr})\, N(S_1) \qquad (2.4)$$

Here, $N(S_1^+)$ and $N(S_1)$ present the population of the molecule at, S_1^+ and S_1 states at time t, respectively.

Let

$$k_F = k_r + k_{nr} \qquad (2.5)$$

to present the total decay rate of the S_1 state. Solving the

equation (2.3), we have:

$$N(S_1^+) = e^{-k_{rlx}t} \left[\int_{-\infty}^{t} (\beta/h\nu)\, P(\theta)\, e^{k_{rlx}\theta}\, d\theta \right]$$

$$= e^{-k_{rlx}t} \left\{ (\beta P_0/h\nu) \int_{-\infty}^{t} \exp[-(\theta/\tau - k_{rlx}\tau/2)^2 + (k_{rlx}/2)^2]\, d\theta \right\}$$

$$= (\beta P_0/h\nu)\, e^{-k_{rlx}t} \exp[(k_{rlx}\tau/2)^2] \int_{-\infty}^{t} \exp[-(\theta/\tau - k_{rlx}\tau/2)^2]\, d\theta$$

The solution of the equation (2.3) is:

$$N(S_1^+) = (\beta\sqrt{\pi}\tau P_0/h\nu)\, e^{-k_{rlx}t} \exp[(k_{rlx}\tau/2)^2] * \Phi\,[\sqrt{2}\,(\theta/\tau - k_{rlx}\tau/2)]$$

$$= (\beta E/h\nu)\, e^{-k_{rlx}t} \exp[(k_{rlx}\tau/2)^2] * \Phi\,[\sqrt{2}\,(t/\tau - k_{rlx}\tau/2)] \qquad (2.6)$$

where the $\Phi(x)$ is the cumulative normal distribution function defined as

$$\Phi(x) = \int_{-\infty}^{t} 1/\sqrt{2\pi} \exp(-u^2/2)\, du \quad . \qquad (2.7)$$

The solution for equation (2.4) is:

$$N(S_1) = e^{-k_r t} \left[\int_{-\infty}^{t} k_{rlx} N(S_1^+)\, e^{k_r\theta}\, d\theta \right]$$

$$= (\beta k_{rlx} E/h\nu) \exp[(k_{rlx}\tau/2)^2]\, e^{-k_r t} * \left\{ \int_{-\infty}^{t} \Phi[\,2(\theta/\tau - k_{rlx}\tau/2)]\, e^{-(k_{rlx} - k_F)\theta}\, d\theta \right\} \qquad (2.8)$$

In the case of the excitation pulse being very short (as $1/\tau >> k_F$) and the vibrational relaxation being much faster then the radiative and non-radiative decay from the storage level (as $k_{rlx} >> k_F$), the integral term in the formula (2.8) will be close to a constant after a very short time. This is because both $\Phi(x)$ and $\exp(-x)$ have significant values only in a very narrow area close to point 0 when x is small. Suppose this short time is t', then the population of the molecular at

the storage level can be decreasing as a single exponential function after t′. During that short time ($t < t'$), the sharp increasing of the cumulative normal distribution function will contribute to the $N(S_1)$ significantly so that the population at S_1 will be increasing.

For a clearer look at the physical process, one can assume the pump pulse time duration is very short, so the molecules have been excited to the excitation state S_1^+ at once at the time t=0. Using a delta function to express the time profile of the pumping pulse as:

$$P(t) = E\,\delta(t) \quad . \tag{2.9}$$

and

$$E = \int_{-\infty}^{\infty} P(t)\,dt = E \quad .$$

Then the solution for Equation (2.3) will be

$$N(S_1^+) = e^{-k_{rlx}t}\left[\int_{-\infty}^{t} (\beta/h\nu)\,P(\theta)\,e^{k_{rlx}\theta}\,d\theta\right]$$

$$= (\beta E/h\nu)\,e^{-k_{rlx}t} \quad , \tag{2.10}$$

when $t \geq 0$. At t=0, $N(S_1^+) = \beta E/h\nu$.

The solution for Equation (2.4) will be

$$N(S_1) = e^{-k_r t}\left[\int_0^t k_{rlx} N(S_1^+)\,e^{k_r\theta}\,d\theta\right]$$

$$= (\beta k_{rlx} E/h\nu)\,e^{-k_r t}\left[\int_0^t e^{-k_{rlx}\theta} e^{k_r\theta}\,d\theta\right]$$

$$= [\beta k_{rlx} E/h\nu (k_{rlx} - k_F)]\,e^{-k_r t}\left[1 - e^{-k_{rlx}t} e^{k_r t}\right]$$

$$= [\beta k_{rlx} E/h\nu (k_{rlx} - k_F)]\,\{e^{-k_r t} - e^{-k_{rlx}t}\}. \tag{2.11}$$

The observed number of photons emitting as fluorescence per second, F, shall be directed proportionally to the emission photon number and that is proportional to the population of

the molecular at the storage level of the first singlet excitation state S_1 and the radiation decay rate of the molecular, which will be

$$F(t) = k_r N(S_1). \qquad (2.12)$$

In the above very short light pulse pumping case, the observed fluorescence decay time profile will be:

$$F(t)=k_r [\beta k_{rlx}E/h\nu(k_{rlx} - k_F)] \{e^{-k_rt} - e^{-k_{rlx}t}\} . \qquad (2.13a)$$

As we keep in mind the assumption of $k_F << k_{rlx}$, one can plot the time profile of this function with $k_F = 0.05\ ps^{-1}$ and $k_{rlx} = 1\ ps^{-1}$ (Figure 2.2). This gives τ_F=20ps and τ_{rlx}=1ps. From the figure, one can clearly see the rise of the population at the beginning which caused by the relaxation decay from S_1^+ to $S_{1\ (k}$rlx), and the decay of the population at the later time is due to the radiation and non-radiation processes (k_F). A clearer picture for the rising and decay of the fluorescence is shown on Fig 2.3 with $k_{rlx}=0.1ps^{-1}$ and $k_F=0.05ps^{-1}$. This corresponding to the rising time of τ_{rlx}=10ps and decay time of τ_F=20ps.

By taking the dF(t)/dt=0, one can find the peak of the temporal profile locate at:

$$t_p=(\ln k_{rlx} - \ln k_F)/(k_{rlx}-k_F)=\ln(k_{rlx}/k_F)/(k_{rlx}-k_F).$$

Integrating the equation (2.13a), one can have the total number of the photon emitted in the fluorescence, which is

$$N_F = \int_0^\infty F(t)\ dt$$

$$= k_r [\beta k_{rlx}E/h\nu(k_{rlx} - k_F)] \{ \int_0^\infty [e^{-k_rt} - e^{-k_{rlx}t}]\ dt$$

$$= (k_r/k_F) * (\beta E/h\nu) \quad . \qquad (2.14a)$$

It is the radiative portion of the total absorbed excitation photon number $N_{ex}=(\beta E/h\nu)$. Therefore, using 2.14a, the quantum yield is:

$$\phi_F=k_r/k_F. \tag{2.14b}$$

The Eq. 2.13a can be reduced to

$$F(t)=N_{ex}[k_r k_{rlx}/(k_{rlx} - k_F)] \{e^{-k_r t} - e^{-k_{rlx} t}\} \tag{2.13b}$$

further since $k_{rlx}>>k_F$ to

$$F(t)=Nex\ k_r\{e^{-k_r t} - e^{-k_{rlx} t}\} \tag{2.13c}$$

and $F(0)=0$.

To further simplify the case, let us assume that $t>0$, k_{rlx} is so much larger than k_F equation (2.13) can become

$$F(t) = k_r\ [\beta E/h\nu]\ e^{-k_r t} = A\ e^{-k_r t} \tag{2.15}$$

for a very short time after the molecules were pumped ($t > 0$). Let

$$\tau_F = k_F^{-1}, \tag{2.16}$$

equation (2.15) can also be expressed as

$$F(t) = A\ e^{-t/\tau_F} \tag{2.17}$$

where τ_F is the observed fluorescence decay time.

As is very noticeable in the equations (2.15) and (2.17), the observed fluorescence decay time is related to the summary of radiative decay rate and the non-radiative decay rate. That is

$$\tau_F = k_F^{-1} = [\ k_r + k_{nr}\ ]^{-1}\ . \tag{2.18}$$

This equation shows that if the environment in which the molecule stays gives the excited molecule more chance of non-radiative decay, that is the system with larger k_{nr}, than the

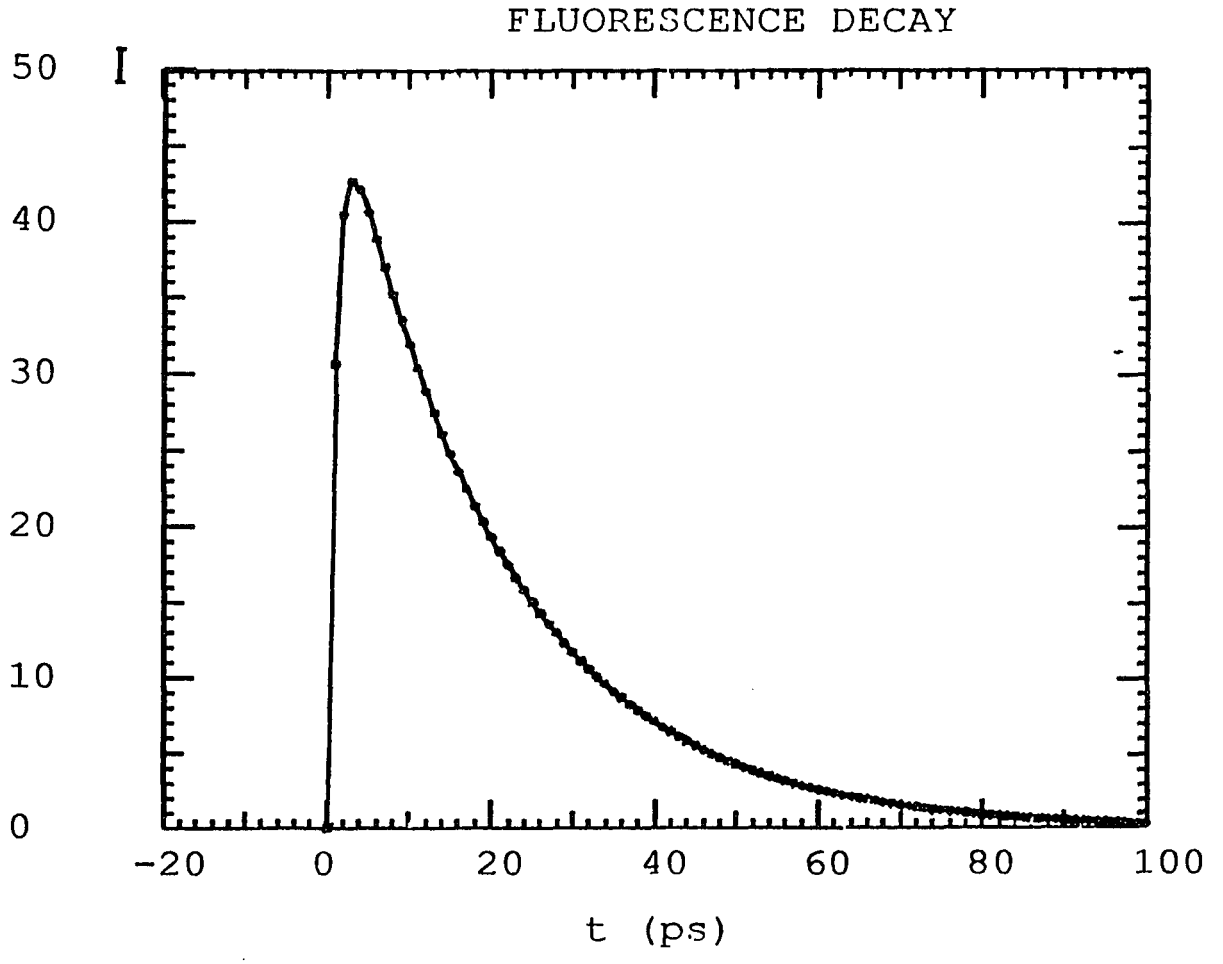

Figure 2.2 Fluorescence decay curve calculated from theoretical model (Equation 2.13) with k_{rlx}=1 ps^{-1} and k_F=0.05 ps^{-1}.

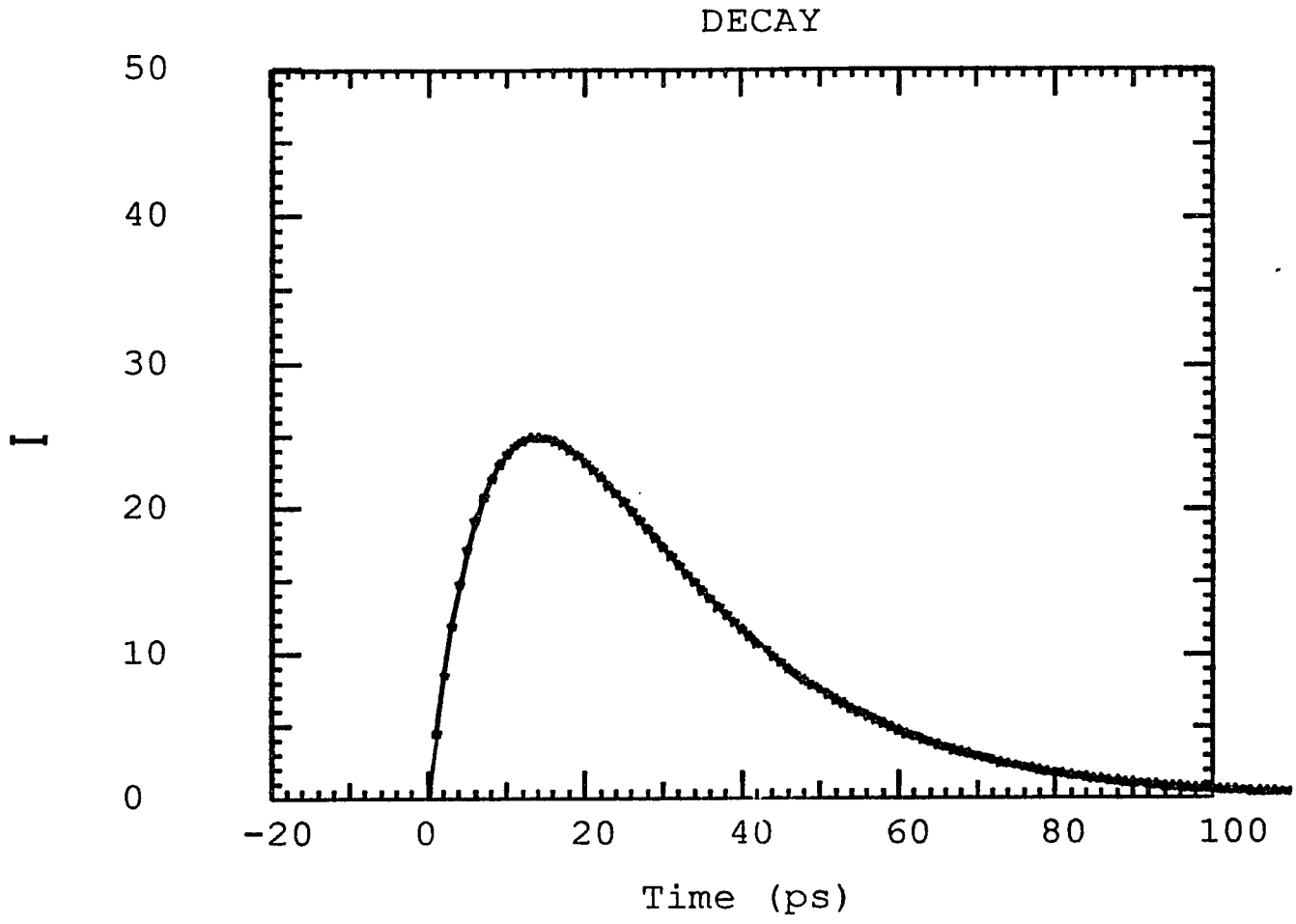

Figure 2.3 Fluorescence decay curve calculated from theoretical model (Equation 2.13) with k_{rlx}=0.1 ps^{-1} and k_F=0.05 ps^{-1}.

observed fluorescence decay time τ_F will be smaller.

In the case of mixture of several kinds of fluorophors, the observed fluorescence decay will be a mixture of several exponential decay

$$F(t) = \Sigma \; A_i \; e^{-t/\tau_{Fi}} \tag{2.19}$$

As in the steady state fluorescence study, one uses a CW laser or continuous light source to excite the molecules. Those CW light sources, which can be mathematically considered as pumping pulses come one after another on continuous basis, can be expressed as:

$$\begin{aligned} I_0(t) &= \int_{-\infty}^{t} [\, P(t-\theta)/A_1] \; d\theta \\ &= \int_{-\infty}^{t} \{(P_0/A_1) \exp[\, -(t-\theta)^2 / \tau^2 \,]\} \; d\theta \\ &= (P_0/A_1) \int_{-\infty}^{0} \exp(\, \theta^2/ \tau^2) \; d\theta \\ &= \sqrt{\pi} P_0 \tau / 2A_1 = \text{Const.} = I_0 \;, \end{aligned} \tag{2.20}$$

Here, A_1 is the laser beam cross section area.

Fluorescence intensity can also be considered as each single fluorescence decay coming out on a continuous basis. Then fluorescence intensity shall be:

$$\begin{aligned} I_F(t) &= \int_{-\infty}^{t} [h\nu F(t-\tau)/A_2] \; d\tau \\ &= k_r \; (\beta E/A_2) \; (\int_{-\infty}^{t} e^{-(t-\tau)/\tau_r} \; d\tau) \\ &= k_r \; \tau_F \; \beta E/A_2 = I_F \;, \end{aligned} \tag{2.21}$$

here, A_2 is the area of the fluorescence detector. Therefore, as one kind of fluorophor in different environments if k_r is the same, the relationship between the CW fluorescence intensities I and the time resolved fluorescence decay time τ_F

will be:

$$I_{F1} / I_{F2} = \tau_{F1} / \tau_{F2} \quad (2.22)$$

In the experimental case, the fluorescence intensity is dependent of the intensity of the excitation light and the optical properties of samples as following. The intensity of the excitation light in the substance obeys the Beer-Lambert law,

$$I = I_0 \, e^{-2.303\varepsilon(\lambda_e)cl} \quad (2.23)$$

where I_0 is the excitation beam intensity, $\varepsilon(\lambda_e)$ is the absorption coefficient at the exciting wavelength, c is the concentration of the absorption molecules, and l is the path length.Take the first order expansion

$$I = I_0 \, [\, 1 - 2.303 \, \varepsilon(\lambda_e) cl] \quad (2.24)$$

The concentration of the excited molecules will be proportional to the light which was absorbed:

$$I_0 - I = 2.303 \, \varepsilon(\lambda_e) cl I_0 \quad (2.25)$$

And fluorescence intensity is proportional to the light that has been absorbed and several other factors. That is

$$I_F(\lambda) = 2.303\varepsilon(\lambda_e) cl I_0 \phi_F f(\lambda) d = g\varepsilon(\lambda_e) \phi_F f(\lambda) c I_0 \quad (2.26)$$

where $f(\lambda)$ is the fraction of total emission that occurs at wavelength λ, and d is the fraction of radiation actually collected by the detection. g=2.303*l*d. ϕ_F is the probability of the excited molecular emitting photon as fluorescence at all. It is (as 2.14b)

$$\phi_F = k_r / k_F = k_r / (k_r + k_{nr}) \quad (2.27)$$

Quantum efficiency of the fluorescence is defined as the

fluorescence intensity at peak where $f(\lambda)=1$ over the incident light intensity

$$Q = I_{Fmax} / I_0 = g*\varepsilon(\lambda_e)*c*\phi_F \qquad (2.28)$$

For mixture of several components, we obviously have

$$I_F(\lambda) = [\ \sum \varepsilon_i(\lambda_e)\ \phi_{iF}\ f_i(\lambda)\ c_i\ ]\ I_0\ k \qquad (2.29)$$

If one put all the other factors together but the function $f_i(\lambda)$ in order to only consider the spectral profile, we have

$$I_F(\lambda) = \sum B_i\ f_i(\lambda) \qquad (2.30)$$

where

$$B_i = \varepsilon_i(\lambda_e) * \phi_{iF} * c_i * I_0 * k \qquad (2.31)$$
$$= \varepsilon_i(\lambda_e) *[k_{ir}/(k_r+k_{nr})]* c_i * I_0 * k$$

Chapter 3. Experimental Methods

In this thesis, I have used three experimental methods based on fluorescence. They are fluorescence emission spectroscopy, excitation spectroscopy, and time resolved fluorescence spectroscopy. Absorption spectra were used during the work. The research included measuring the fluorescence spectra excited by light from CW laser beam, measuring emission and excitation fluorescence spectra excited by quasi monochrometer light from a lamp based light source, and measuring the fluorescence kinetics excited with picosecond laser pulses.

These methods are described in this chapter.

3.1 Steady state laser induced fluorescence methods

The experimental setup is shown in the Figure 3.1. The laser source is the model 95 CW argon-ion laser (from Lexel Co.). The output of the laser wavelength and the laser power can be changed. For choosing a certain output laser wavelength, one can use the vertical & wavelength knob which

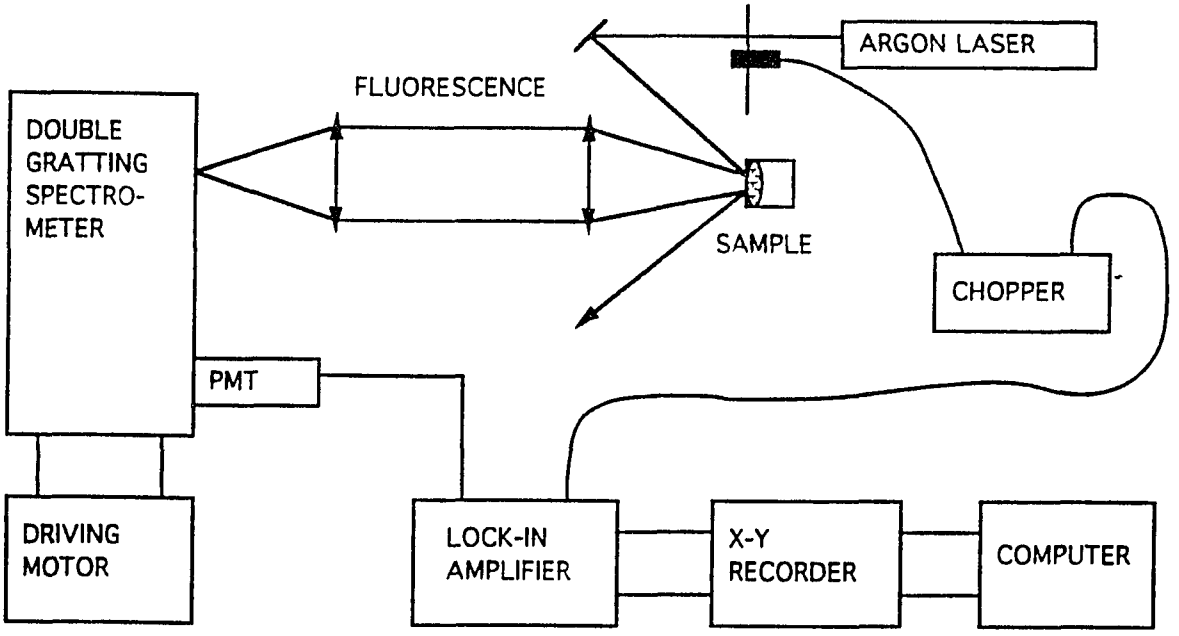

Figure 3.1. Schematic diagram of the experimental setup of the steady state laser excited fluorescence spectra.

controls the length of the oscillating cavity, then use a narrow band laser line filter to cut off the surrounding weak spectral lines from the discharge of the laser which surrounded the major output laser line. For controlling the output laser power, one can adjust the control light knob on the control panel. Natural density filters can also be used. The laser line 488nm and 457nm have been chosen because they are able to excite the flavin molecular groups in the tissue and cell samples. (see the flavin's absorption spectra in Figure 1.27). Only the results excited by wavelength 488nm are reported in this thesis because of the general similarities in the study results between 488nm excitation and 457nm excitation.

The selected laser beam passes through a mechanical beam chopper with frequency (100Hz or 200Hz). Then the beam is focused on to the front surface of the samples with a spot size of about 200μm diameter. The incident angle is adjusted so the reflected beam from the cuvette surface will not fall into the fluorescence collection beam path. The fluorescence was collected through a pair of lenses with diameter of 4 inches to a spectrometer. The first lens was been placed at where the sample is at its focus point so it collected the fluorescence from the sample and paralleled it to the second lens. The second lens focused the paralleled fluorescence beam on the slit of a double 1/2m grating spectrometer (Spex Industries) blazed at 500nm. A photomultiplier tube (Model

RCA 7265, S-20) was placed at the output of the spectrometer. The photomultiplier tube was connected to a lock-in-amplifier (EG&G princeton Applied Research) with 1 mΩ. The lock-in-amplifier worked with the laser beam chopper on the same frequency so the modulated signal can be amplified but not the non-modulated noises. This make the signal to noise ratio higher. The output signal from lock-in amplifier is at a few mV range. It is recorded by a X-Y recorder and/or a personal IBM computer.

This experimental setup enabled me to measure the laser induced fluorescence spectra for study of the human malignant and non-malignant cells (see Chapter 4) and tissues (see Chapter 5). In the experiment, the intensity of the excitation beam was adjusted to be as low as possible (if there is enough output signal) to avoid the possible light induced changes in the tissues and cells (See Chapter 4 and 5 for details). The power of the excitation beam is usually around a few milliwatt.

I only used this setup for measuring the fluorescence, mostly from flavins, around the range 500nm to 700nm because of the limitation of the laser lines.

3.2 The Method of Steady State Fluorescence Induced by Lamp Based Light Source

Most of the steady state fluorescence spectra were measured by using Perkin-Elmer luminescence spectrometer LS-50. Software was developed by Mediscience Technology to diagnose samples called CD scan. Its optical design is shown in the Figure 3.2. The light source is Xenon flash tube. There are two monochrometers. One each on both excitation beam path (called excitation monochrometers) and emission beam path (called emission monochrometers). The Xenon flash lamp produces intense, short duration pulses of radiation on almost a continued basis. The radiation from the lamp is focused by an ellipsoidal mirror and reflected by a toroidal mirror onto the entrance slit of the excitation monochrometer with a grating (G1440mm^{-1}). The excitation wavelength were selected by adjusting the angle of the grating which was controlled by a step motor and a fixed slit. The selected excitation wavelength beam were reflected and focused by toroidal mirror to the sample. A small portion of the excitation beam were reflected by a beam splitter to the reference photomultiplier tube for the purpose of correction of the excitation intensity difference vs wavelength. The emission light from the sample is focused by a toroidal mirror through emission entry slit to the emission monochrometer with another grating (G1200mm^{-1}). The emission wavelength is also selected by adjusting the

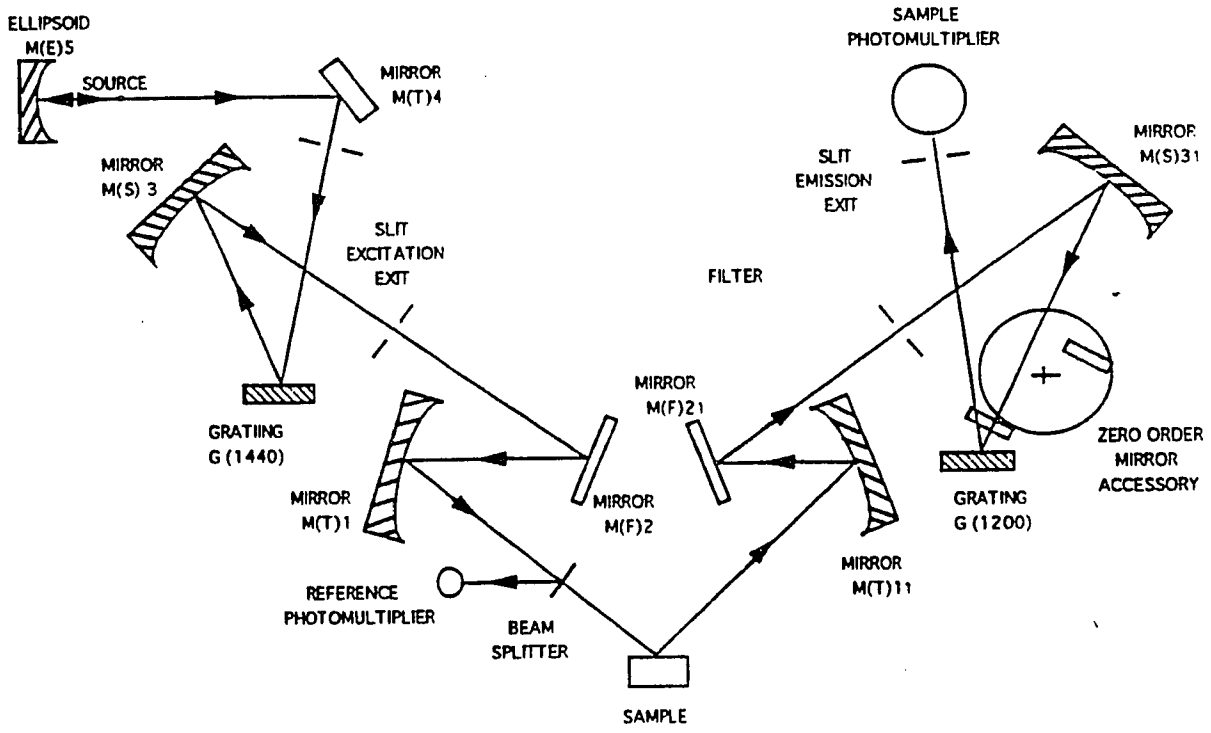

Figure 3.2. Schematic diagram of the optical setup in LS-50.

angle of the grating which was also controlled by a stepper motor. The emission light at the selected wavelength went into the signal photomultiplier tube. The computer output signal is proportional to the division of the output from the signal photomultiplier tube by the output from the reference photomultiplier tube. Therefore, the variations of intensity of the excitation light from lamp source vs. wavelength were corrected.

Both excitation and emission monochrometers can be scanned independently, or be set on certain wavelengths. The excitation beam width and the spectral resolution can be adjusted by changing both the excitation and emission slits width. They were usually set to have the spectral resolution at about 3 to 4nm half width in my measurement. One can use this system to get both emission spectra and excitation spectra by fixing excitation wavelength or emission wavelength and then scanning the other wavelength respectively. The power of the excitation light source is around a half microwatt.

This spectrometer is reliable in the wavelength range from 250nm to 800nm for both excitation and emission spectroscopy. The sensitivity is lower in the longer wavelength range (over 600nm) because the photomultiplier response is weaker.

Using this system, I measure both excitation and emission fluorescence spectra from the human malignant and non-

malignant cell and tissue samples. Due to the system's light source and photomultiplier tube, I mostly use it for measuring the spectra in the range from 250nm to 600nm.

3.3 Time Resolved Fluorescence Measurement

The time resolved fluorescence spectroscopy contains certain information one can not get from steady state fluorescence spectroscopy. As has been shown in Chapter 2, about the physics model of fluorescence, the time resolved fluorescence profile presents how the molecules relax from first singlet excitation state back to singlet ground state. Therefore it is important to measure the time-resolved fluorescence spectroscopy in some case, especially when the molecular binding or interacting is apparent.

Time-resolved spectroscopy was studied with the following method. The samples were pumped by the laser pulse with a wavelength of 351nm, 8ps duration and energy of 1uJ. The size of the pumping laser spot was less then 0.5mm in diameter. The fluorescence decay times were measured by a streak camera system. The details of the setup are described below.

The picosecond Laser pulse is generated by a picosecond mode locked Nd:glass laser system. The setup is shown in the Figure 2.3. The laser oscillator consists of a Nd^{3+} -doped phosphate laser rod surrounded by a flashlamp and a saturable

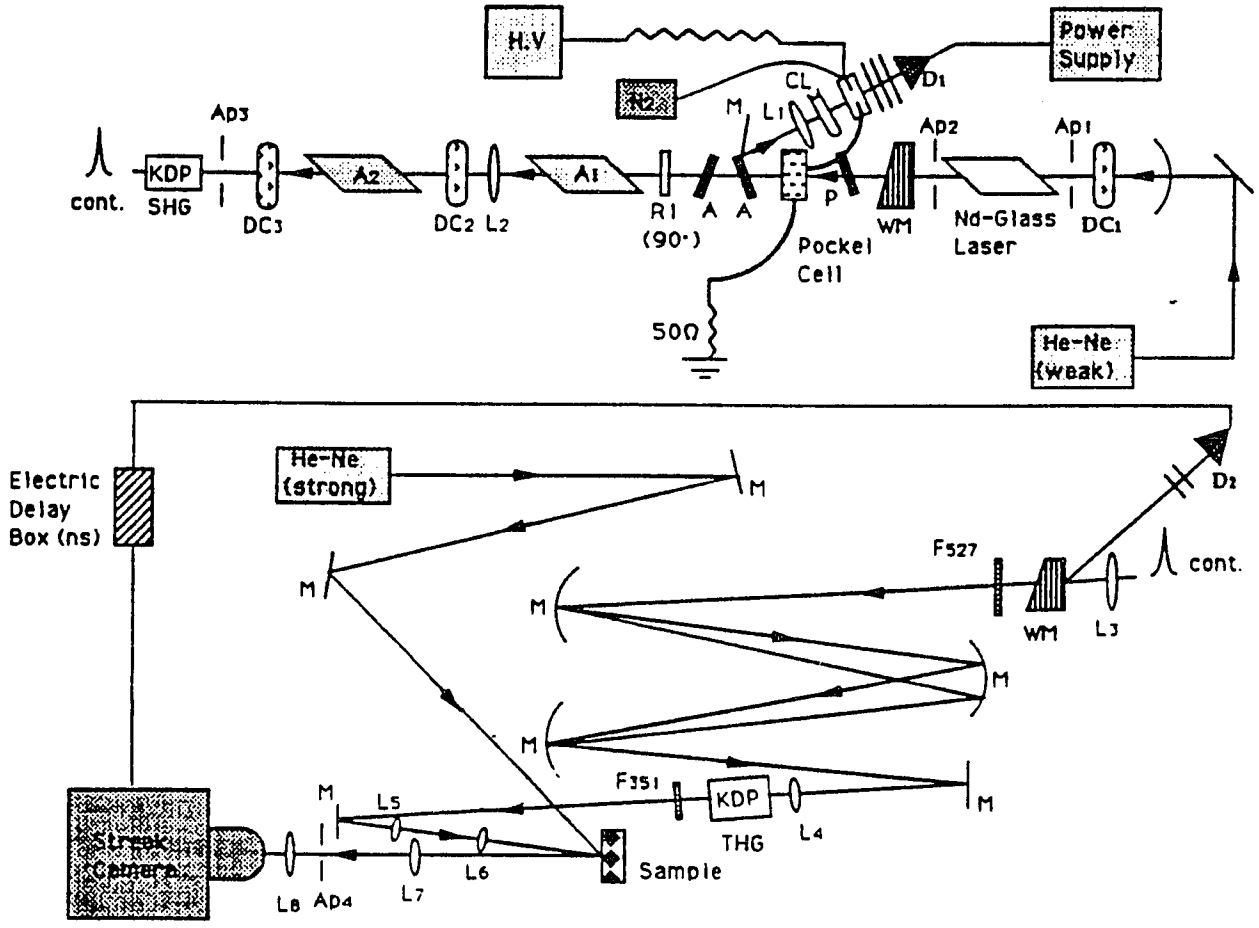

Figure 3.3. Schematic diagram of the experimental setup for time-resolved fluorescence studies using a picosecond mode-locked Nd:glass laser.

absorber dye between one high reflectivity mirror and another 70% reflectivity mirror at the end. The spectral width of the gain profile is due to inhomogeneous broadening and its FWHM is 30 cm^{-1}. The two end of the laser rod are cut at Brewster's angle. The rod is pumped optically by discharging a bank of capacitor (5kV) through a helical water cooled halogen flashlamp. The saturable absorber medium is made by dissolving a certain amount of dye "Kodak 9860" in 1,1' dichloroethane (from Kodak). The transmission of this medium is 64% through a 1cm dye cuvette. The longitudinal modes of the laser are determined by the round trip time (about 2.1m/c ≈ 7 nsec) within the laser cavity and limited by the gain profile G(w) which can be phase locked by saturable absorbing medium. This passive mode locking of the longitudinal modes generates a train of about 100 pulses separated from each other by the round trip time (≈7ns) in the cavity. The pulses come out of the cavity from the 70% transparent mirror.

A single pulse is selected from the pulse train with a transverse laser-triggered spark gap connected to a KD*P Lasermetric Pockels cell with double-shielded coaxial cable. The pulse selection is accomplished by applying a high voltage pulse to the Pockels cell which is placed in between a pair of perpendicular polarizes. When the voltage is applied on the Pockels cell, one half wave retardation is induced by the electra-optic effect. This rotates the plane of the polarization by 90° so that the pulse is transmitted through

the second polarizer. The high voltage (15.8KV, which corresponds to twice the one half wave retardation at wavelength 1054nm) is applied through a high impedance current limiting resistor (10 megohms). This resistor is connected in a series with spark gap (filled with N_2 with pressure around 100psi) and the pockels cell. Most voltage is loaded on the spark gap in the normal situation. However, when the laser pulse train path through the gap, it will ionize the N_2 gas which trigger an electric spark between the two electrodes of the gap. This spark delivers the voltage on the pockels cell through the gap. This voltage pulse over the pockels cell makes the KD*P rotate the polarization of one of the laser pulses by 90°. The length of the electric line between the gap and the pockels cell and its impedance are adjusted so this voltage pulse can path through with less time than the time duration between the two consecutive laser pulses. On the other end, the pockels cell is connected to a long transmission line (20nsec) which is terminated into a matched resistive load (50ohms) to prevent reflections. Therefore, only this selected pulse can path the second polarizer. Figure 3.4 shows the pulse train with a selected single pulse.

The single pulse is then amplified by two stages of amplifiers. The two amplifiers are two Nd^{+3} glass rods with diameter of a half inch. The flashlamps that excite the rods are triggered simultaneously with the laser oscillator flashlamp via common electrical pulses so the maximum gain in

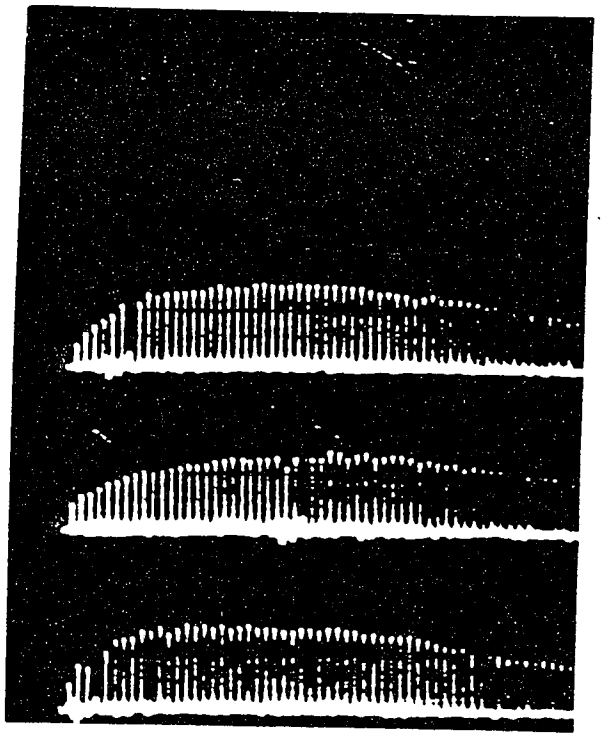

Figure 3.4 The photograph of the laser pulse train with a single pulse selection.

the amplifier is available when the pulse arrives at the amplifier. This timing is relatively easy since the amplifier gain follows the flashlamp intensity which has a broad peak of one millisecond width. The first amplification is about 7 times. The second amplification is about 3 times. Total amplification is around a factor of 20. The amplified 1054nm pulse was frequency doubled through a KDP crystal of length 25mm (efficiency 10%) to obtain 527nm pulse. This pulse was split into three parts by a wedge shape beam splitter: one strong transition and two weak reflections. One of the weak reflection beams went into a silicon photodiode (S-20) to produce a trigger signal for triggering the streak camera. An electric delay unit is connected in between for the perfect matching with the optical arriving time. Another weak reflection went into an energy meter detector (Prinston Procession Inc.) to monitor the energy level of each pulse. The rest of the pulse path went through to the main optical path. It went through the white cell for an optical delay, so the optical signal arrive at the streak camera after the trigger signal. Then this pulse (mixed 1054nm and 527nm) path through another KDP crystal with length of 25mm to produce a frequency tripled (over 1054nm) pulse with wavelength 351nm. The Corning color glass filters 7-51 and 7-60 is placed after the crystal for only selecting 351nm pulse. The 351nm pulse is then focused on the sample. The total energy of the 351nm pulse with twice amplifications is about 1 to 2 uJ.

The induced fluorescence is collected and passed through a window and then focused on the streak cream slit. There is a Corning color glass filter O-51 placed at the window to block the scattering laser light. Neutral density filters have sometimes been placed at the window to reduce the intensity of the fluorescence for the streak camera to collect.

A 10ps streak camera (Model # C979, Hamamatsu) is used to detect the temporal change information and display them as an time vis. intensity two dimension profiles. The Streak camera is a device which convert the temporal information into the spacial information. The basic structure of the streak camera tube (See Figure 3.5) consist of (1) photocathode; (2) Mesh electrode; (3) Sweeping electrode; (4) Microchannel plate; (5) phosphor screen. The photons strike on the photocathode (multialkali) which produce emission of the electrons which are proportional to the incident light intensity. The high voltage (1.5 kV) mesh electrode accelerates the electrons into the tube. The sweeping voltage on the electrodes gives a time dependent vertical electric field to sweep the electrons with a known time vis distance rate (15, 7.5, 3 and 1.5mm/ns). This sweeping voltage is started to apply on the sweeping electrode by the input trigger signal (2V into 50ohm). These accelerated and swept electrons strike on the microchannel plate which are capable of producing electron multiplication through secondary emission. The electrons which come out of

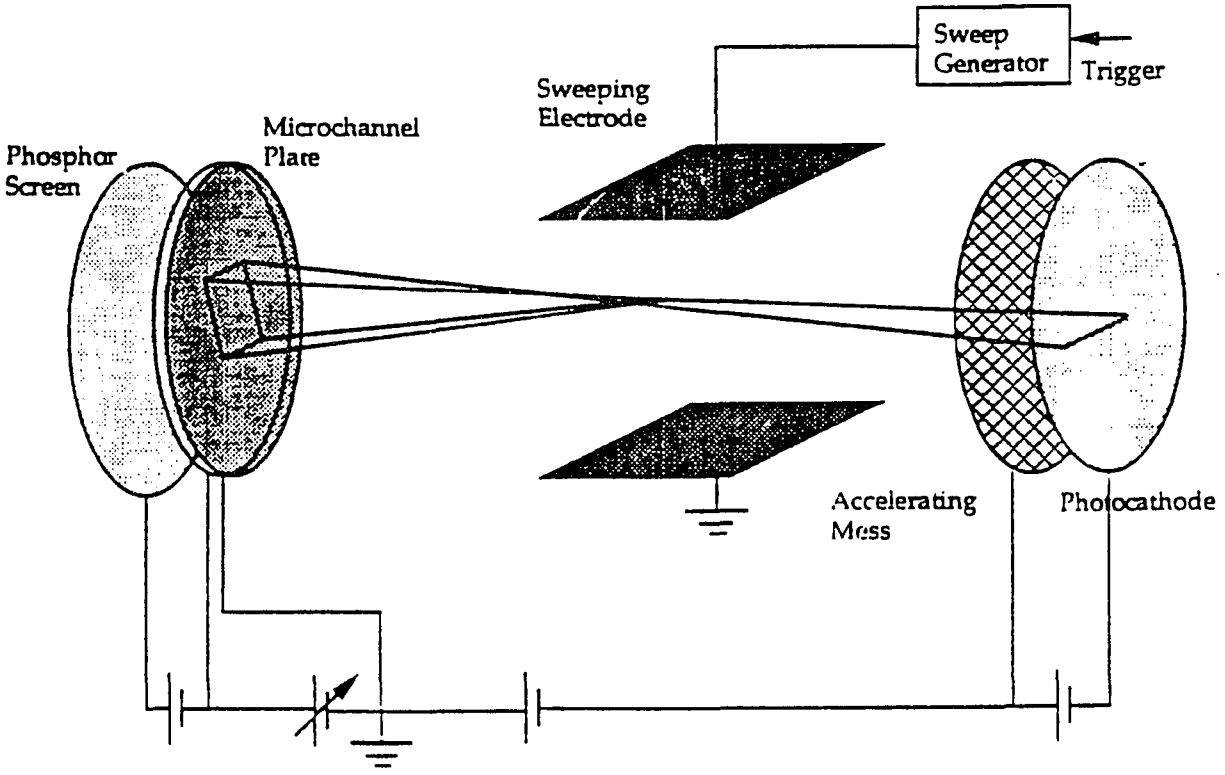

Figure 3.5. Schematic diagram of a streak camera.

the multichannel plate (about 3 KeV) will strike on the phosphor screen (P-11, 50 photons/electron) to show temporal information.

The streak camera is used with a direct video readout consisting of a silicon intensifier target vidicon camera, an analyzer, a monitor, and a computer for data recording. The SIT vidicon camera (S-20 photocathode) monitors the streak image on the phosphor screen. The video signal is analyzed by temporal analysis microcomputer (Model C1000, Hamamatsu, Inc.) which converts the image information from analog to digital. The output is corrected for dark current and sensitivity variations in the SIT vidicon. It integrates and outputs the video intensity along each horizontal scanning line over the window settings. The output of the time vis. intensity profile is displayed on the monitor. The data is transferred and saved in the PC computer for data analysis and model fitting. The models are usually multi-exponential decay according to the formula 2.19 in the Chapter 2. (It is double exponential function in my study. See Chapter 5.3.4 for detail.) The VAX unix system is used to operate the computer fitting. The used computer program are listed in Appendix I.

The time axis of the streak camera is calibrated by using etalon. The streak camera response is over checked by measuring the certain dye whose decay time is known. The detail process are presented in the Appendix II.

Chapter 4. STEADY STATE AND TIME RESOLVED FLUORESCENCE SPECTROSCOPY FROM THE CULTURED HUMAN MALIGNANT AND NORMAL BREAST CELL LINES

It is well known that cancer is a disease which results in the uncontrolled reproduction of cells. It is believed to be caused by genetic mis-coded in reproduction controlling genes. Since the DNA interacts with enzymes and other parts in the cellular system, many biochemical changes will occur in the neoplasm cells. However, the whole cancer picture of the changes has not yet been well understood.

The study of the fluorescence from malignant and non-malignant cells is done for the following purposes. One is to probe some of the biochemistry changes in the transformed cells and help us to understand what has happened during those changes. Another is for helping us to analyze the fluorescence spectroscopies from malignant and non-malignant tissues (see chapter 6) because of the "purity" of the cell sample due to the absence of blood and connective proteins etc. Therefore, I can evaluate the effects on the structure

of features where different molecule are located on the fluorescence spectra.

The cell samples preparation and the various inspected fluorescence spectra from human cultured normal and malignant cells are presented below.

4.1) Cell Preparation

The cell samples used in this experiment were cultured human breast cell lines which originally were purchased from American Type of Culture Collection (ATCC), Rockville, MD. These cell lines were further subcultured to increase the cell population. The cell lines used in the study were: normal human breast cell line ATCC HTB125, malignant human breast cell lines ATCC HTB22 (Adenocarcinoma Pleural Effusion), ATCC HTB126 (Ductal Carcinoma) and also ATCC HTB19 (Carcinoma). The HTB125 (normal) and HTB126 (carcinoma) lines were obtained from the same patient according to ATCC Catalogue of Cell Lines & Hybridomas, 6th Edition, 1988.

For the first experiment which related to flavins (see Chapter 4.2), the cancerous cell samples of HTB19, HTB22, HTB126 were initially supplied by Dr. Kamiyama at the St. Lukes Hospital with my help and then further supplied by Dr. Oka at New York Medical College. The normal cell sample and both the cancerous and normal cell samples for all the other

experiments were cultured in Prof. Steinberg's biochemistry Laboratory by myself with his help. All the cells were cultured and prepared with using the following procedure. It is also shown in a flow chart (Figure 4.1).

The purchased cells were in the deep freeze and protected by of the dry ice when it was shipped. They were usually packed with 1M of cells within a completely sealed 1ml glass tube. They were quickly unfrozen by a 37°C water bath. Then the cells were moved into the prepared culture flasks (size 50ml) with 7ml culture medium. The cell culture medium was made with 90% modified Dulbeco's minimal essential medium (Eagle) (GIBCO Co.) with 10% of fetal bovine serum (GIBCO Co.). After slightly shaking the flask to make the cells to be uniformly distributed in the flask, the cell culture flasks were then placed in an incubator with humidified atmosphere of 4% CO_2 at 37° C to start culturing. After a while, the cells were sunk and attached to the bottom of the flask. These breast cells stay attached to the bottom of the flask when they are in the stable growing condition but flow up if the cell has died. It is important to often check the cells under the microscopy to see if they are in good condition. If the cells were flowing up or the medium is opaque or there is unusual substance in the flask, that means the cell has died or has been contaminated as the result of a mistake in the process. The whole flask cells should then be discard. If the cells are still attached to the bottom and

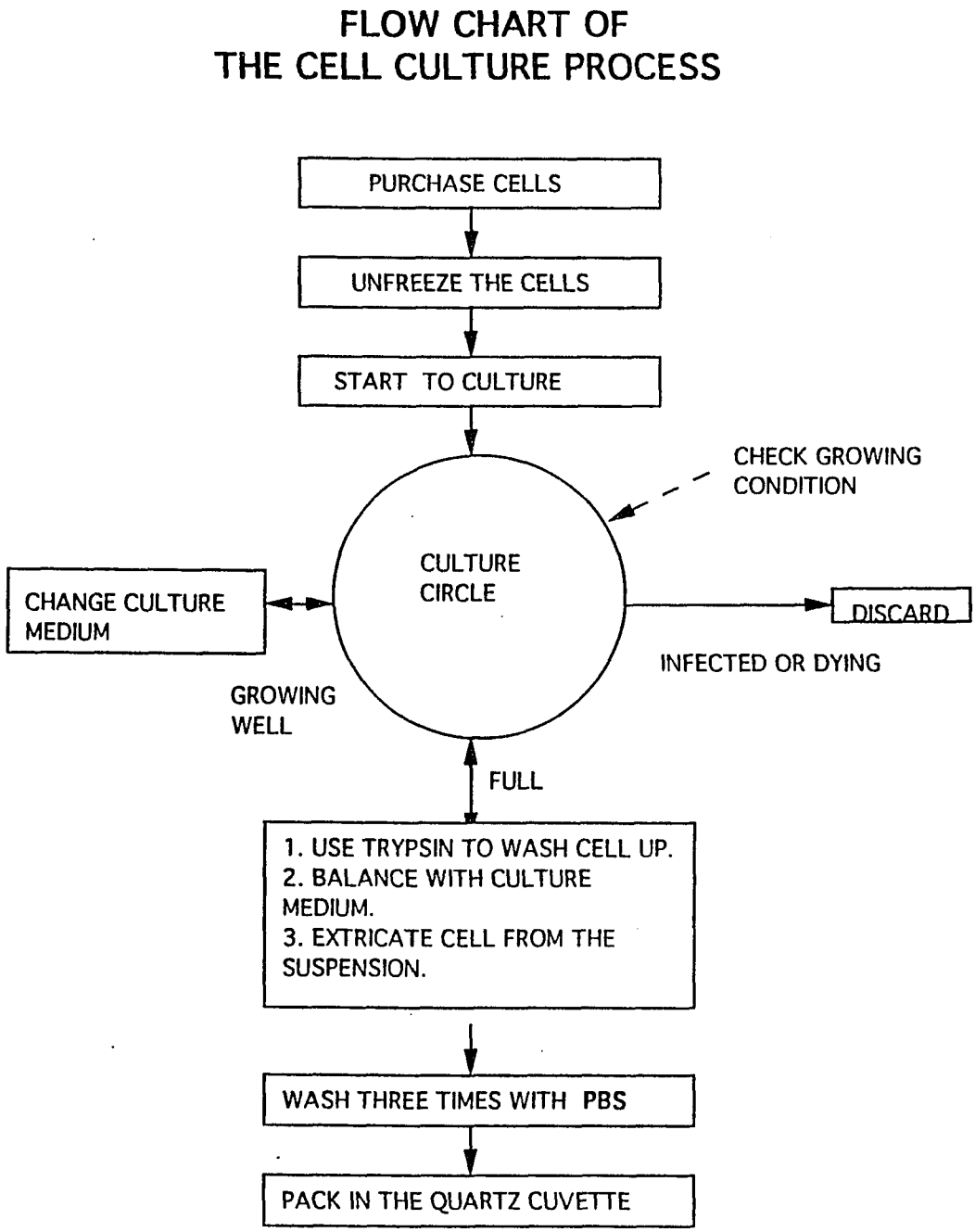

Figure 4.1 Flow chart of the cell culture process.

nothing looks unusual except for a few flowing dead cells, the cells are still in the good condition for continuing the culture. The cell culture medium should be changed every two to three days. This is done by simply pulling the old culture medium out and adding in the new culture medium; but the process should be carried out as fast as possible to avoid the cells being damaged when there is no culture medium. When the cells fill up the flask (when the cells looks like crowded), one have to split one flask cells to two or three flasks in order to continue culturing, or move the cells into a bigger culture flask (100ml size with 14ml culture medium in it). This is done by first treating the cells with trypsin EDTA (5% trypsin and 5.3mM EDTA; from GIBCO) for 5 - 10 minutes, gently shaking the flask to help the cells flow up, then diluting them into an equal or more amount of the culture medium to balance out the trypsin's function. The cells are isolated by centrifugation, then moved into new culture flasks with new culture medium for further culturing. When the cell amount is enough for preparing a sample (usually two full flasks of 100ml size), those isolated cells will be repeatedly washed by 40ml PBS (SIGMA CO.), then isolated again three times. The final isolated cells will be packed into a 3x3x24 mm^3 quartz cuvette (Type 507 from ESCO). The cell concentration was about 10^8 to 10^9 cells/ml. [$100X10^6$ /$(3x3x4)x10^{-3}cm^{-3}$=$(10/36)x10^{9ml}$-1)= $0.3x10^9$ ml^{-1}= 3 x 10^8 ml^{-1}].

The experiments were carried out immediately at room temperature (about 20°C), the cell suspensions were stored at 4°C incubation between measurements. For the cell sample used in the experiment related to flavins (experiments in Chapter 4.2), two to three hours of delivery time were be added.

4.2 Steady State Fluorescence From Cells Primary By Flavins in 500-700nm Range

Flavins' biochemical function and optical properties were previously described in section C of the Chapter 1. It is known that the native cellular fluorescence in the range 500-600nm is most likely due to Flavins[71]. It has been found that there are fluorescence spectral differences in the wavelength range 500 to 600nm between human malignant and non-malignant breast tissues in vitro [10,11,12,13] when the excitation wavelength is 488nm. These research results show that the spectra from the non-malignant breast tissues in vitro contained one major band associated with two subbands profile while spectra from malignant breast tissues in vitro contained only one major band profile[10,11,12,13]. The question is if this observed fluorescence difference comes directly from cells. Therefore, it is of interest to study the fluorescence emission spectra in this range from the malignant and non-malignant human breast cells.

The experimental method (Figure 3.1) used for these experiments is described in the Chapter 3.1. It was also the method which has been used for study the fluorescence of the tissues around the range 500nm to 600nm.[10,11,12,13] The power level of the pump laser was around a few milliwatts at 488nm.

The average experimental results for each of the cell line samples are shown in Figure 4.2 to Figure 4.5. The spectral profiles emitted from both cultured human breast normal cell line (HTB125, Figure 4.2) and cancerous cell lines (HTB126, Figure 4.3, HTB22, Figure 4.4, HTB19, Figure 4.5) have only one broad band spectral profile. The peak position of each cell line was slightly, but not significantly, different from each other. The peak position of the normal cell line HTB 125 were at 535$\pm$10nm, cancerous cell line HTB126 at 530$\pm$10nm, and HTB22 and HTB19 at 525$\pm$10nm. The shifts may be caused by the pH changes in the cell medium around flavins. These peak positions differences have also reported by other researcher in their study results of the malignant and non-malignant rat tissues.[82]

All the spectral profiles of these cell lines are close in the sharp to the flavin spectral profile. However, it is obvious that the spectral profile from human normal breast cell line <u>in vitro</u> is different than the fluorescence spectral profile of normal human breast tissues <u>in vitro</u>. The spectral profile of the most normal human breast tissues in vitro contains one major peak and two subpeaks[10,11,12,13] and so

were the normal gynecological tissues (see Chapter 5.2). This show us that the complex spectral profile from the normal tissues were not responsible by the cells inside the tissues. It may caused by the surrounding media other than the cells.

This study result supports the view point that the complication of the spectra from the normal tissues is caused by the reabsorption by the blood residue in the tissues[12,72]. More study results on this point will be present in the Chapter 5.2.

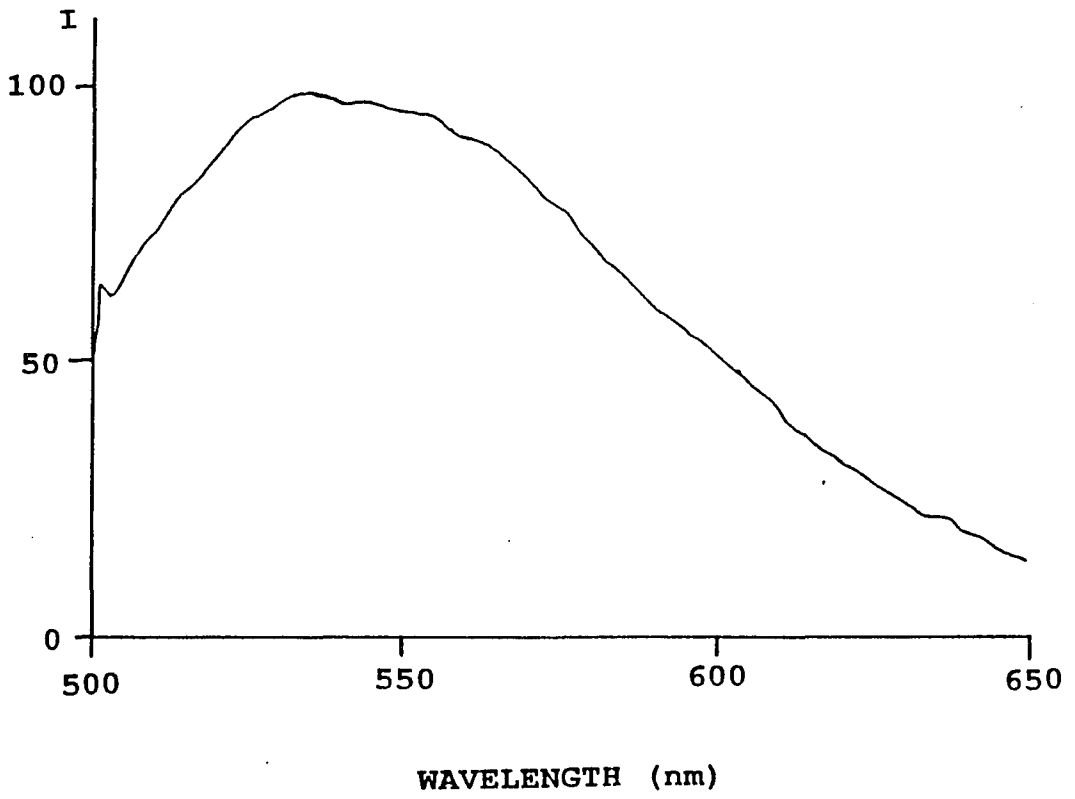

Figure 4.2. Steady state fluorescence spectrum from human normal breast cell line ATCC HTB125 excited by laser line 488nm. (Intensity axis is in the arbitrary unit).

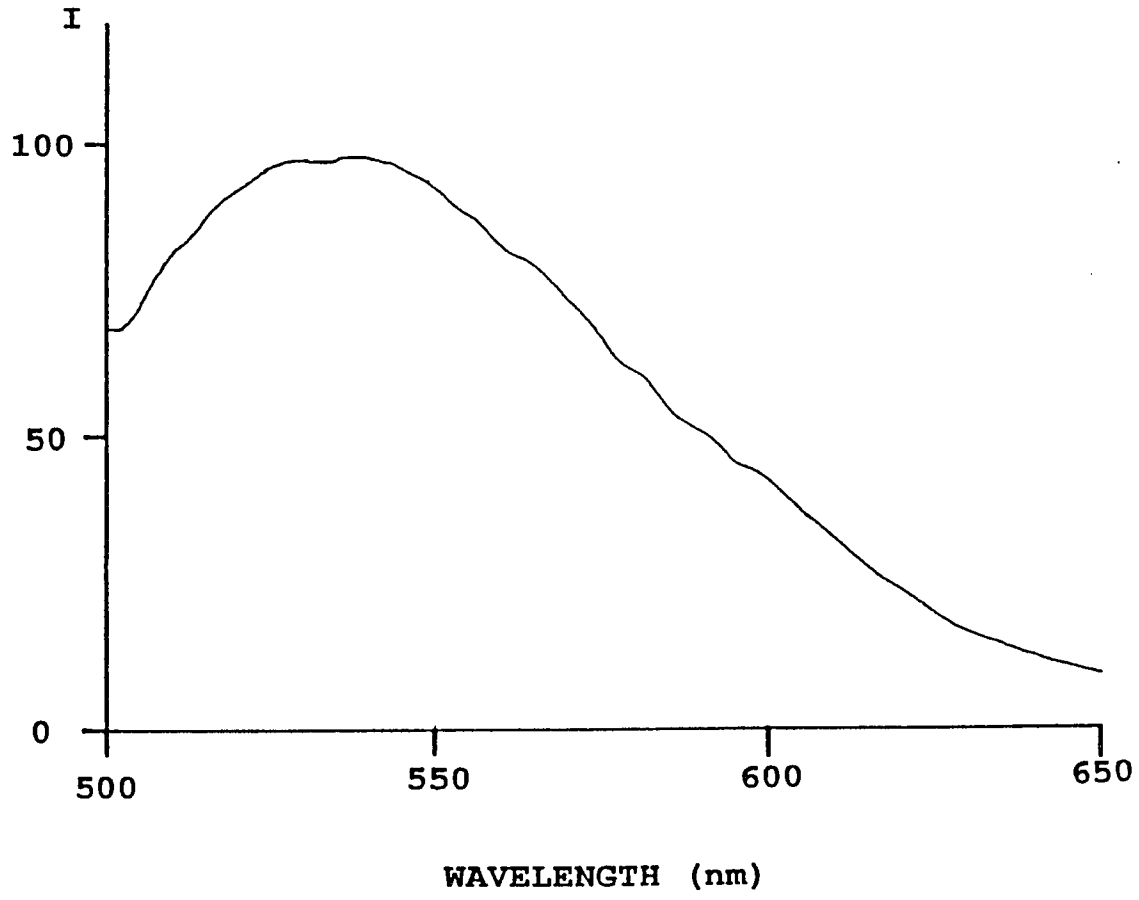

Figure 4.3. Steady state fluorescence spectrum from human cancerous breast cell line ATCC HTB126 (ductal carcinoma) excited by laser line 488nm. (Intensity axis is in the arbitrary unit).

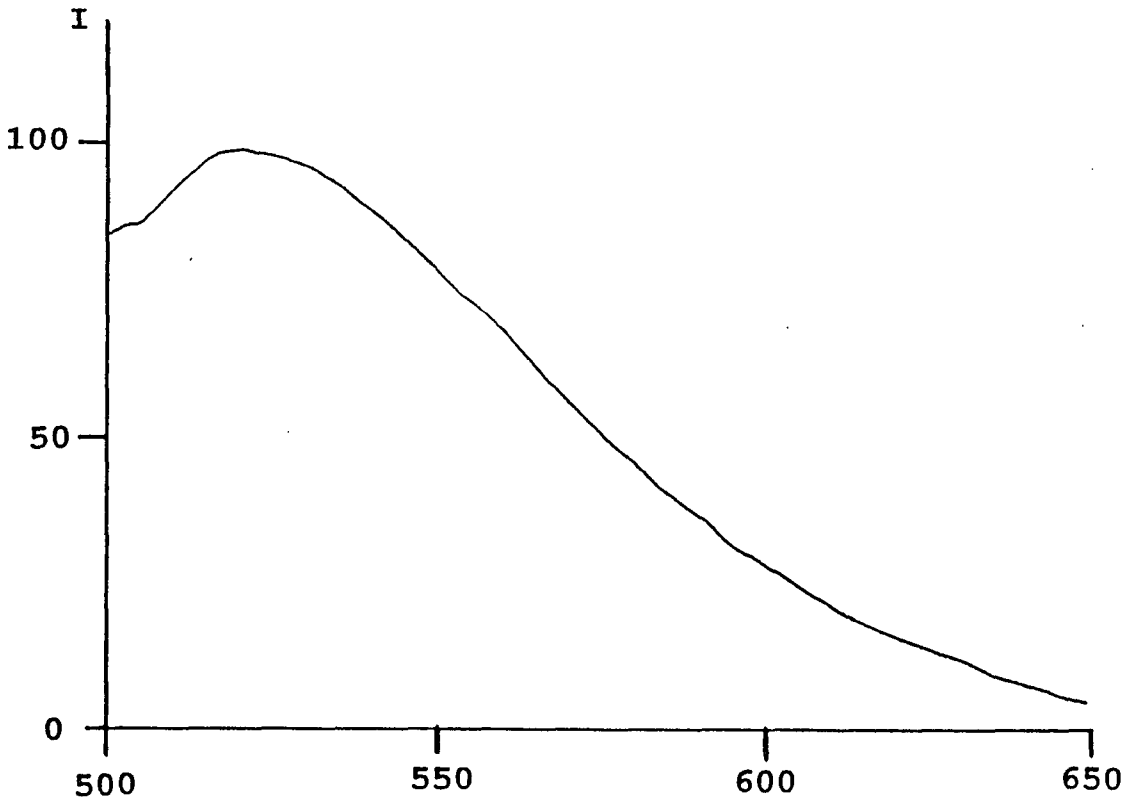

Figure 4.4. Steady state fluorescence spectrum from human cancerous breast cell line ATCC HTB22 (adenocarcinoma pleural effusion) excited by laser line 488nm. (Intensity axis is in the arbitrary unit).

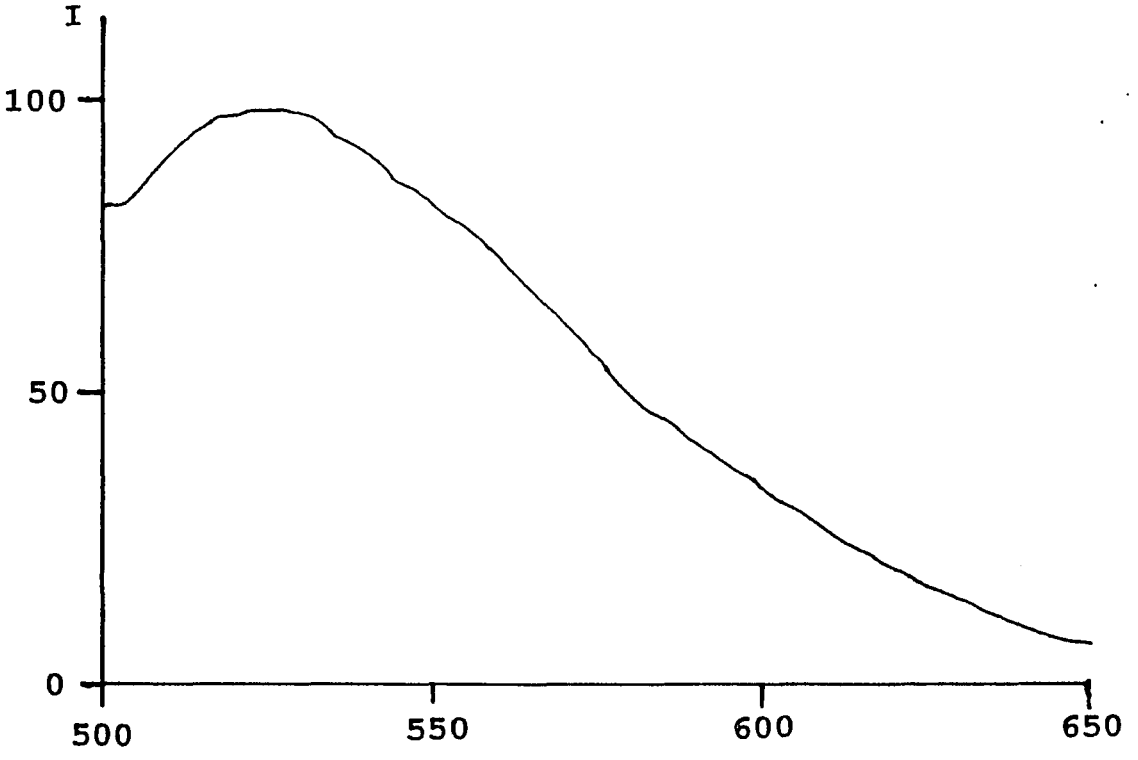

Figure 4.5. Steady state fluorescence spectrum from human cancerous breast cell line ATCC HTB19 (carcinoma) excited by laser line 488nm. (Intensity axis is in the arbitrary unit).

4.3 Fluorescence from cells primary by NADH in the wavelength range of 400nm-500nm.

As I described in section C of Chapter 1 (pages 40 to 48), nicotinamide adenine dinucleotide (NAD) and Nicotinamide adenine dinucleotide phosphate (NADP) are important components for energy transforming, and redox phosphorylation in mitochondria of cells. The ratio of the oxidative state $NAD(P)^+$ over reduced state NAD(P)H is an indicator of the metabolic capabilities of the cells. Free NAD(P)H gives a fluorescence spectrum with a peak at 460nm and decay time around 0.4ns and has absorption band maximum at 340nm.[57] Oxidized NAD (NAD^+) does not fluorescence efficiently[65] because of its lack of absorption around 340nm (see Figure 1.22 [64]). The fluorescence from NADH predominates over NADPH[65, 73] about four fold. Studies have also shown that the bound NAD(P)H in the mitochondria is primarily responsible for the blue fluorescence from cells and tissues[54, 2, 74]. The bound NADH fluorescence shows a blue shift on the emission peak (from 460nm to about 450nm)[75] and also may show a blue shift on the absorption peak over the free NADH[76].

The fluorescence from NADH has been widely used in biochemistry and medical research. Some examples are: kinetics of enzymes[76], the tissues' metabolic state[77]; regions of cerebral ischemia[2], and imaging of isolated cardiac myocyte[65].

In related cancer research, measurements performed on the NADH fluorescence intensities from ascites tissue culture cells and ascites tumor cells showed that the tumor cells emit more than the tissue cells[78], but no direct spectral comparison was made. It has been mentioned in section A of the Chapter 1 that some recent studies results have also shown that invasive cancerous tissue areas show two to six folds stronger NADH fluorescence than the normal tissue area.[43,44,45,46] On the other hand, biochemical studies have been done on the relationship between growth factor and the NAD^+ and NADH concentrations and NAD^+:NADH ratio in normal and transformed fibroblast cells from rat kidney.[79] The result showed that fast growth is associated with a low NAD^+:NADH ratio[79]. It also seems that the amount of NADH contained by the normal cells was changed from more to less when those normal cells changed from growing in the logarithmic phase to being in the stationary phase[79]. Although the biochemical reasons for those NAD (NAD^+ and NADH) level changes are not yet clear. These changes show that NADH can reveal the metabolism changes in the cells which are caused by transformation of cells from normal to malignant.

Thus, it is of interest to study the NADH fluorescence spectroscopies and their kinetics from normal and cancerous cells for two purposes. The first is to see if there is an NADH fluorescence spectral differences between human normal breast cells and cancerous breast cells. The second is to

probe what may have happened around the NADH when the cells are transformed from normal to cancerous.

4.3.1 Steady state fluorescence emission spectroscopy from cultured human malignant and non-malignant breast cells

The steady state fluorescence measurement gives information on the spectral profiles and the relative intensities of the fluorescence spectroscopies from human malignant and non-malignant cells.

These experiments were performed on Mediscience Technology CD Scan which was based on Perkin Elmer's Luminescence Spectrometer LS-50. The details of the experimental setup are described in Chapter 3.2. The fluorescence emission spectra were measured by using 353nm (about 4nm half-width) excitation for correspondence with the laser pulse pump (center wavelength 351nm) for time resolved fluorescence decay time study which will be presented later (see 4.3.4 for details). This wavelength (353nm) was also chosen because there are almost no measurable fluorescence from the culture medium, trypsin EDTA and PBS buffer which were used in the cell sample preparations (see Figure 4.6). The measurements of the absorption spectra of the culture medium, trypsin EDTA, and PBS buffer are shown in Figures 4.7, 4.8 and 4.9, respectively. These absorption spectra show that the 353nm is located at the dips of the absorption spectra of

the culture medium and of the trypsin EDTA and at near zero in the absorption spectrum of the PBS.

Typical steady-state fluorescence spectra from each cell line HTB125, HTB126, and HTB22 which were excited with 353nm are shown in Figures 4.10, 4.11 and 4.12, respectively. These fluorescence spectral profiles from various cell lines all consist of a band centered at 450nm and a shoulder around 525nm. The 450nm band is assigned to NADH[80] and the 525nm shoulder is due to the weak emission of flavins[80]. Meanwhile, according to the emission spectra of the elastin (Figure 1.17), the elastin in the cells should also contribute the fluorescence which would form a background under the NADH and flavins' peak structure. This background should be stronger around 420nm range and weaker in the longer wavelength range (see Figure 1.17). Comparing the spectral profiles from the normal cell line and the cancerous cell lines, the relative intensity of the 450nm band to the 525nm shoulder is larger for the cancerous cell lines than for the normal cell line. There were several sharp peaks which appeared in the original spectra which have been recognized as ghost lines caused by the spectrometer and have been corrected in the displayed spectra.

Calculating the ratio of the intensity at 450nm to the intensity at 525nm, the cancerous cell lines have values greater than 2 while the normal cell line has values less than

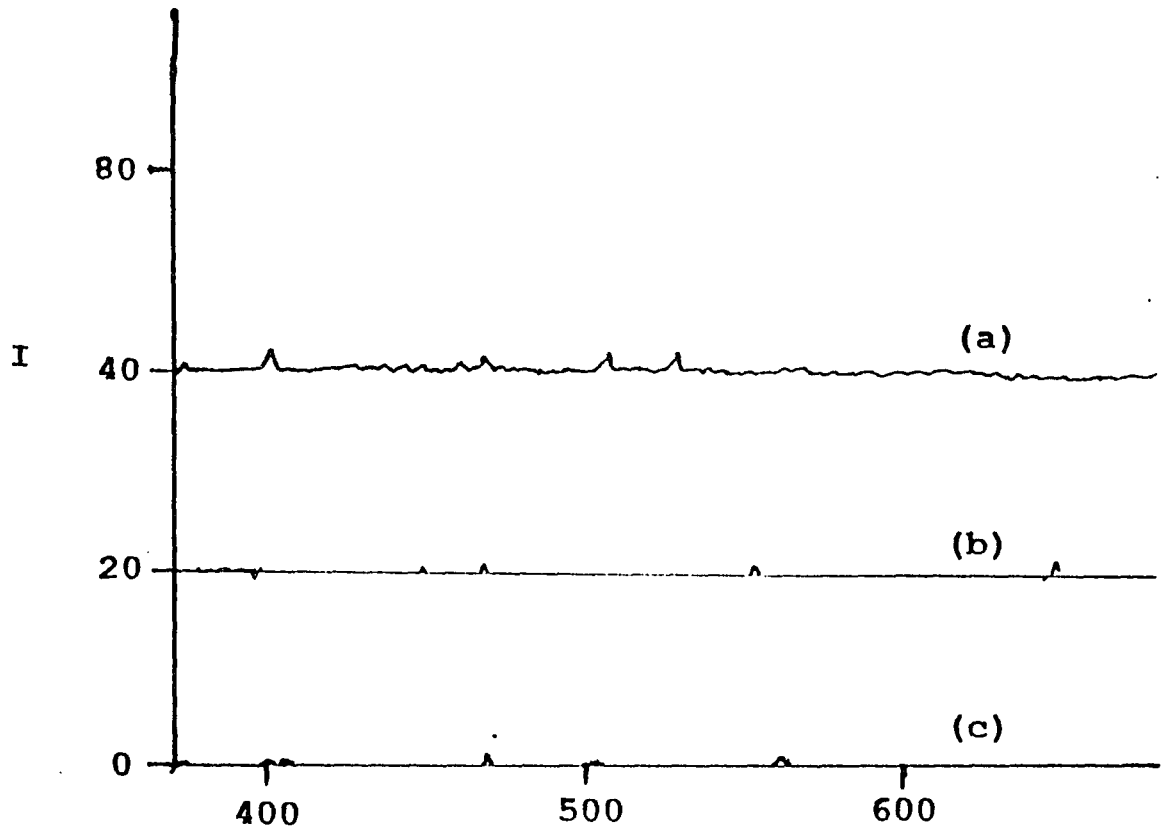

Figure 4.6. Steady state fluorescence spectra of (a) culture medium; (Intensity is equal to the reading minus 40), (b) trypsin EDTA; (intensity is equal to the reading minus 20), (c) PBS buffer; when they were excited at 353nm.

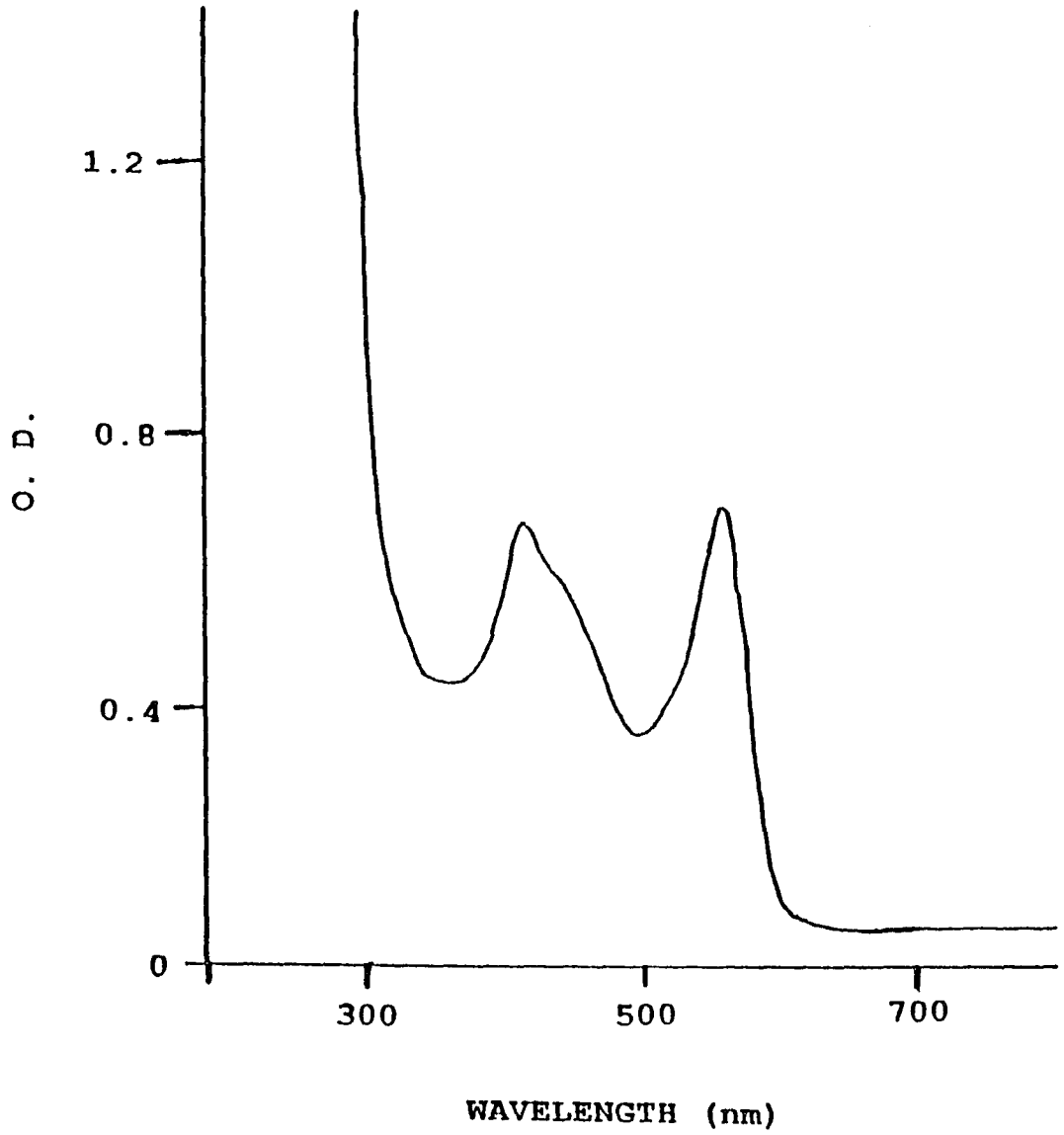

Figure 4.7. Absorption spectrum of modified culture medium. The penetration length is 1cm.

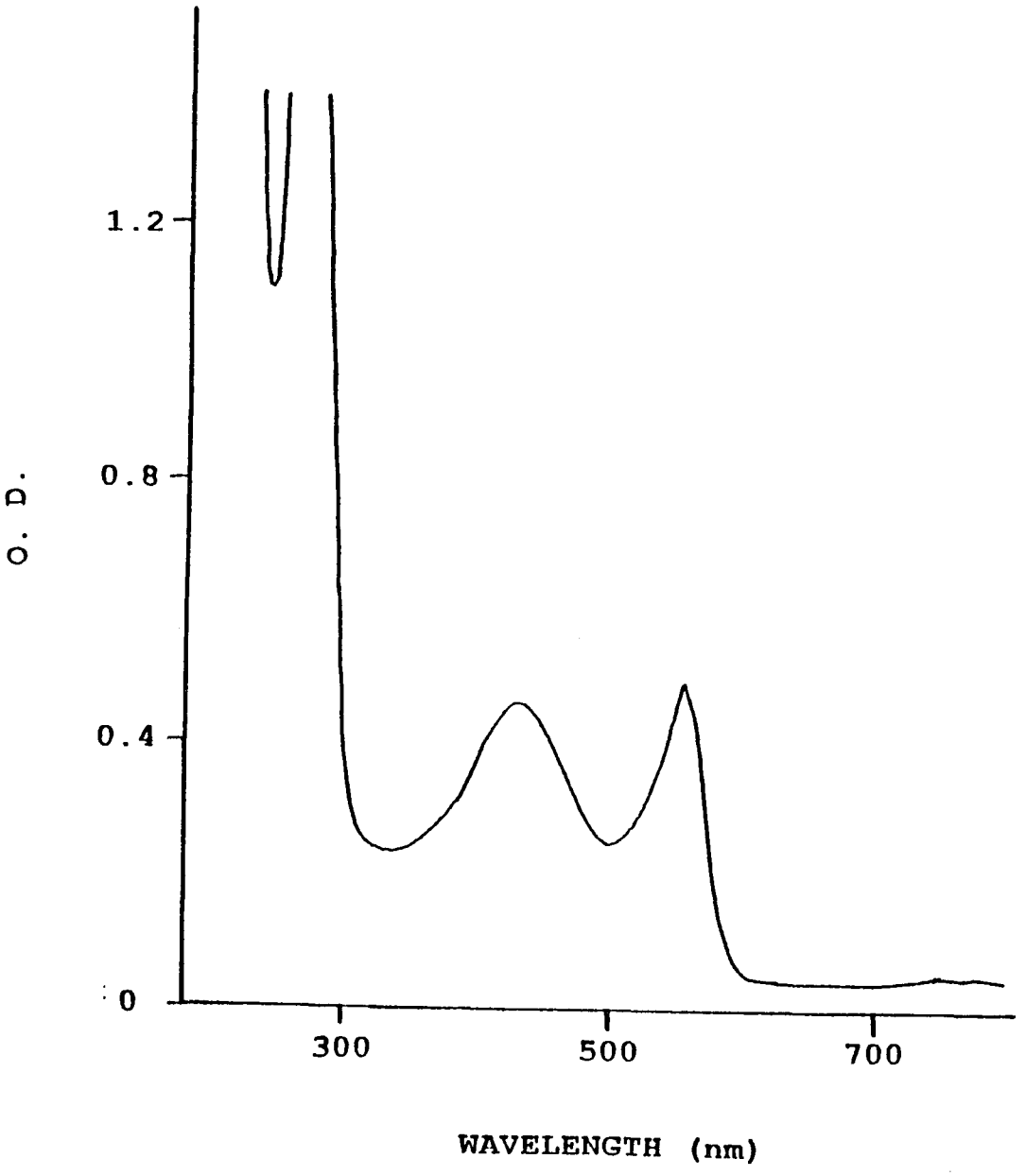

Figure 4.8. Absorption spectrum of trypsin EDTA. The penetration length is 1cm.

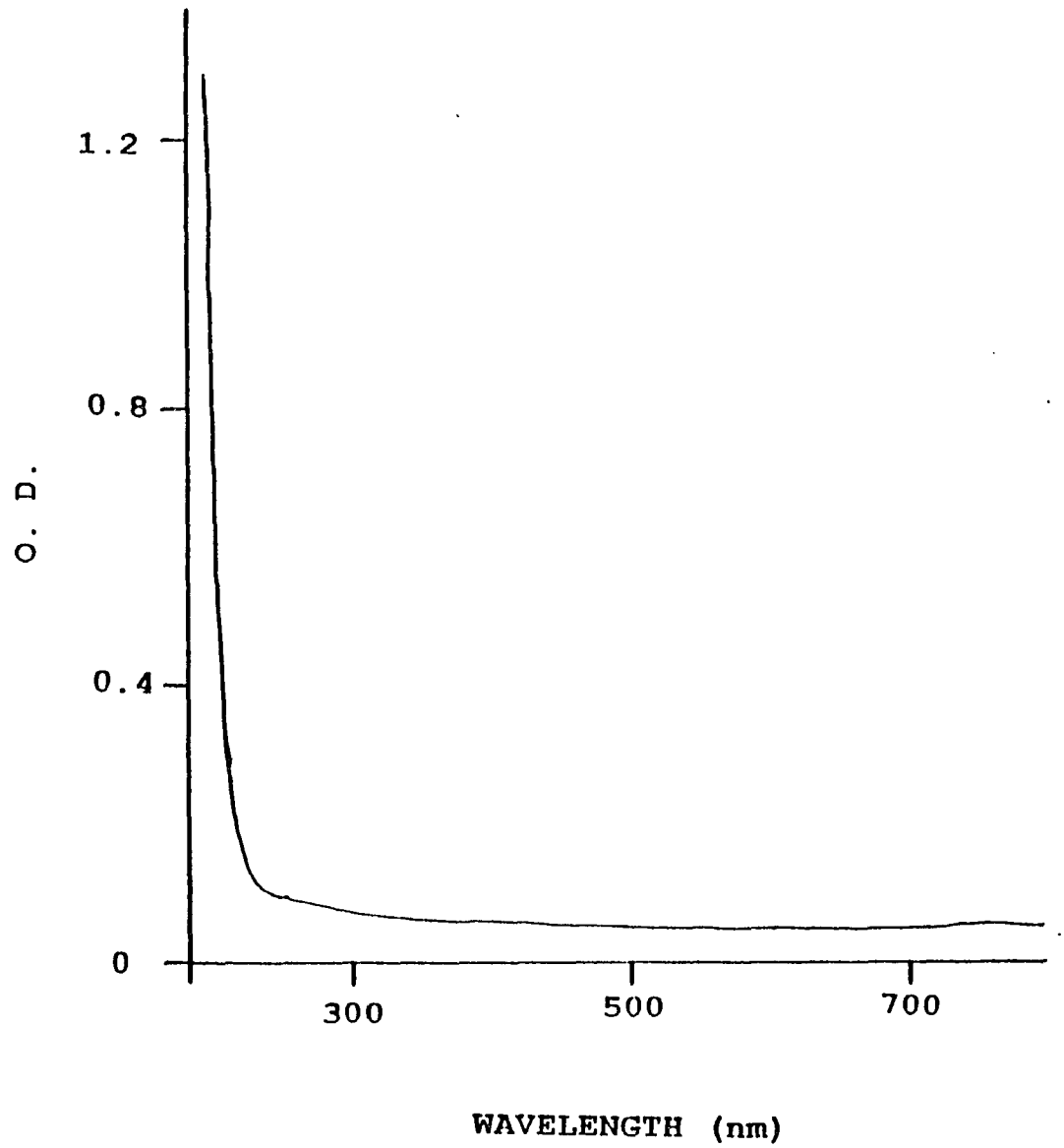

Figure 4.9. Absorption spectrum of PBS buffer. The penetratio length is 1cm.

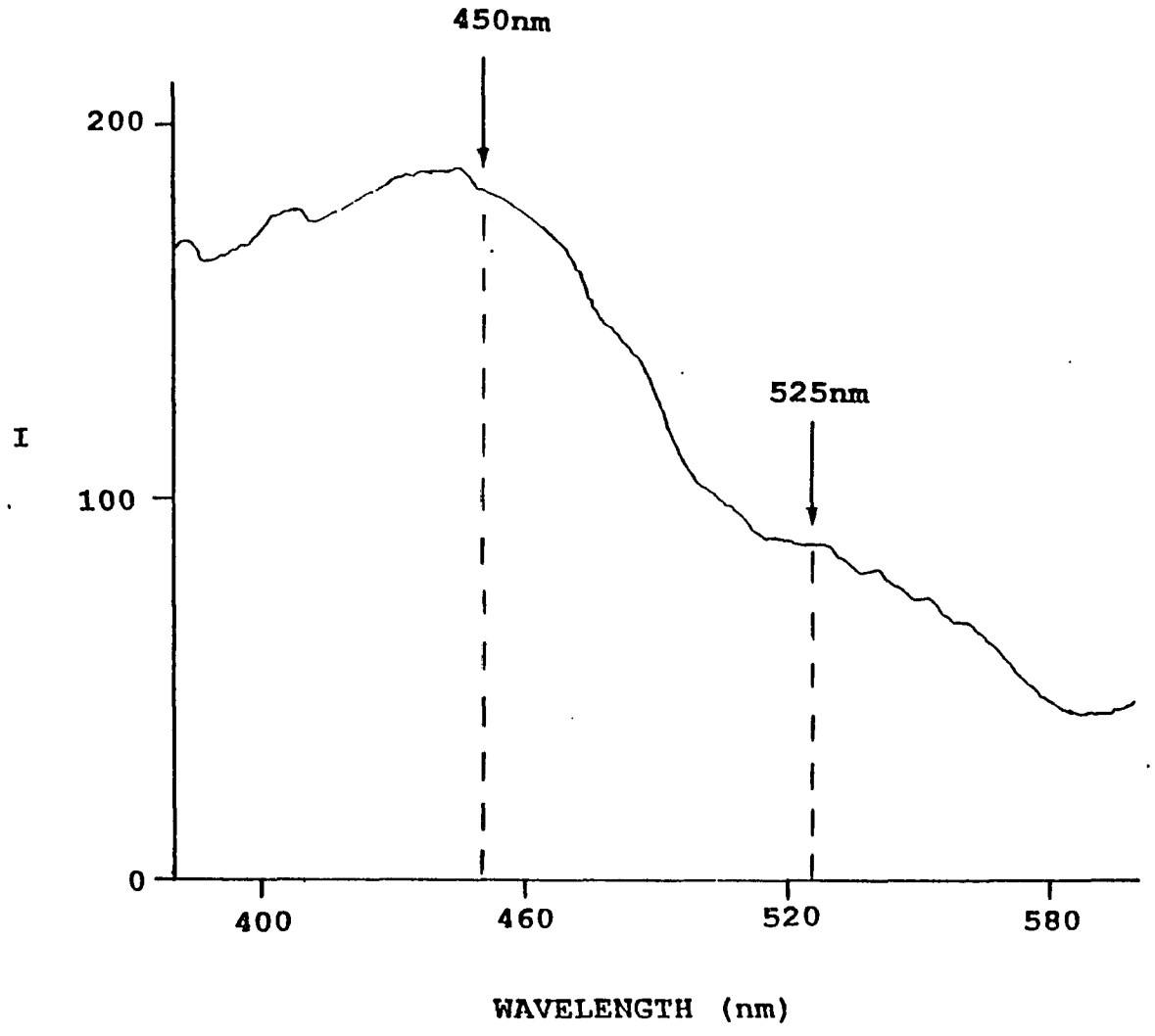

Figure 4.10. Steady state fluorescence emission spectrum of the human normal cell line ATCC HTB125 excited at 353nm. (Intensity axis is in the arbitrary unit).

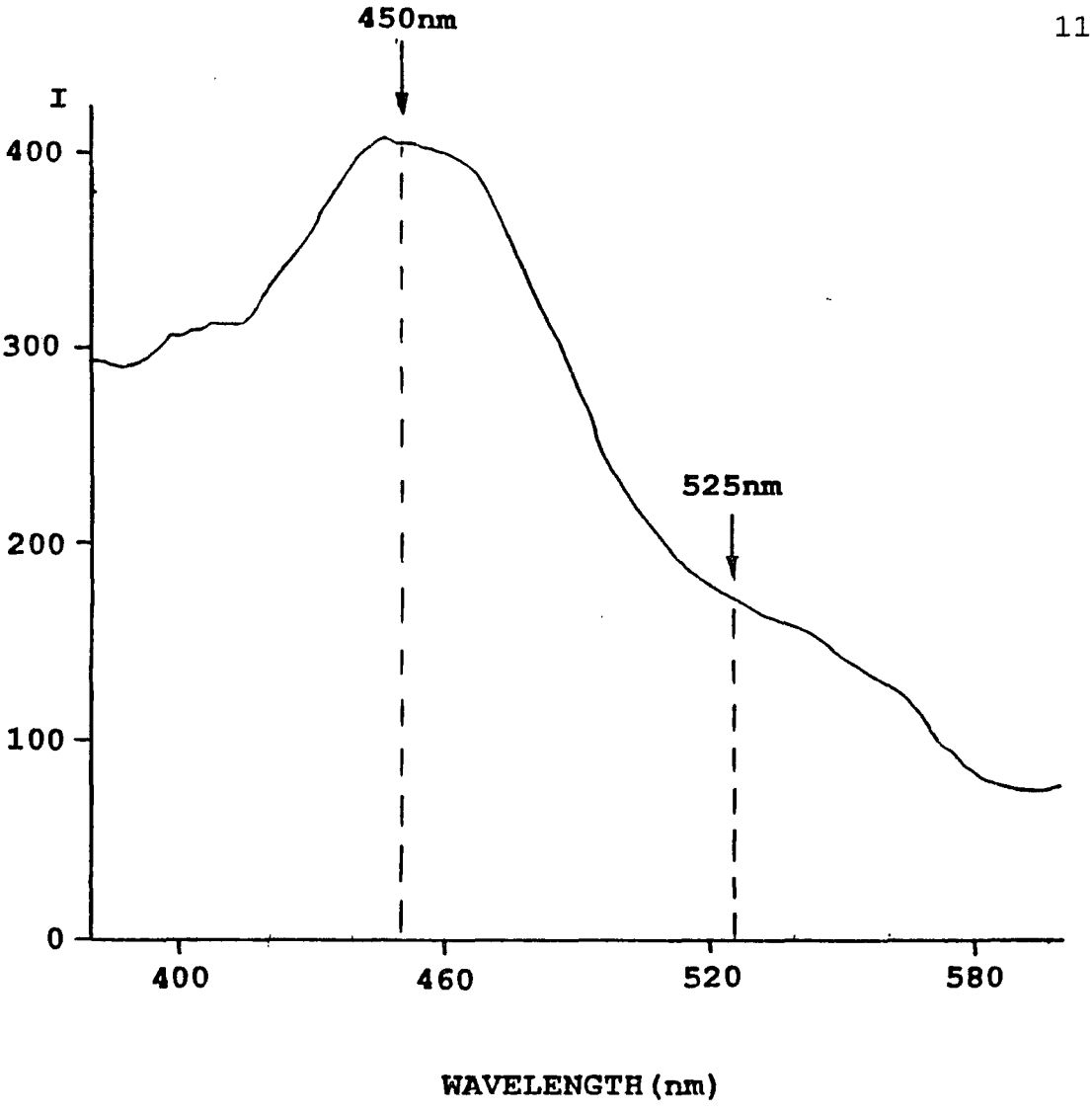

Figure 4.11. Steady state fluorescence emission spectrum of the human cancerous cell line ATCC HTB126 (ductal carcinoma) excited at 353nm. (Intensity axis is in the arbitrary unit).

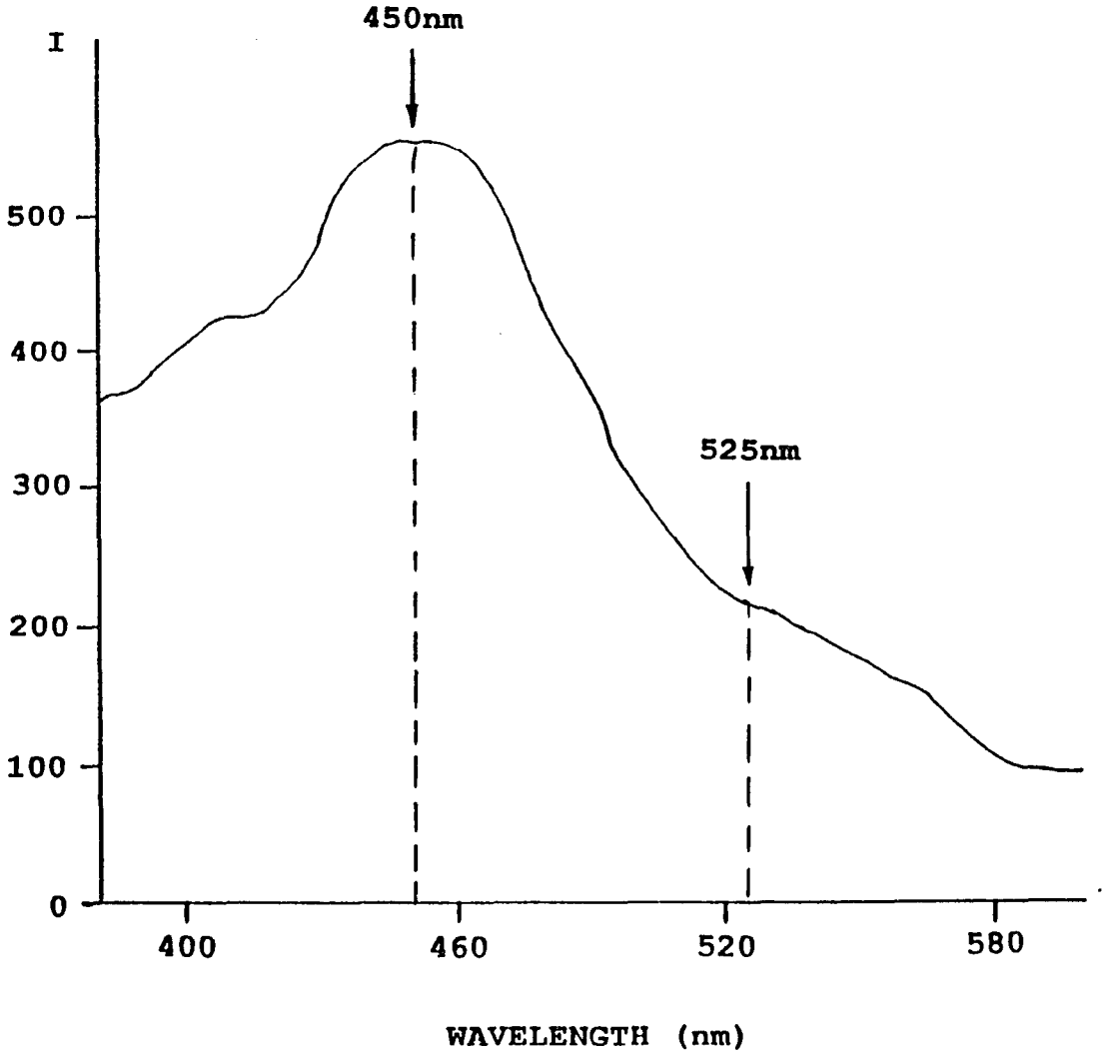

Figure 4.12. Steady state fluorescence emission spectrum of the human cancerous cell line ATCC HTB22 (adenocarcinoma pleural effusion) excited at 353nm. (Intensity axis is in the arbitrary unit).

2. These ratio values are listed in Table 4.1 for the measured samples. Selecting one pair of the normal (HTB125) and cancerous (HTB22) cell samples with about the same amount of cells, the absolute intensity of the 450nm band for the cancer cell line was about twice the intensity of the 450nm band of the normal cell line, while the intensity at 525nm only differed by about 30% (See Fig. 4.13).

To check the reproducibility of our results, experiments were carried out 4 times for the normal cell line HTB125, 5 times on the cancerous cell line HTB22, and 3 times on the cancerous cell line HTB126. The experiments were performed at different cell passage numbers, or different shipments of cells, on the same day and on different days (in which the experimental setup conditions may have been different), and on different numbers of cells. The results from all these runs were fairly consistent. Steady-state spectral measurements carried out on a given sample twice in the same experiment after a 30 minutes interval at room temperature revealed no significant differences between measurements (see Figure 4.14). These lack of significant differences precludes the possibility of changes in spectra which might result from the incubation of the samples over the duration of an experiment.

Table 4.1 Ratio of the fluorescence intensity I_{450nm}/I_{525nm} from cultured human breast cell lines. The excitation wavelength was λ_{ex}=353nm.

HTB126	HTB22	HTB125
2.8	2.7	1.4
2.4	2.2	1.7
2.3	2.3	1.9
	2.7	1.3
	2.2	
Average 2.5	**Average** 2.4	**Average** 1.6

HTB126, Ductal Carcinoma (ATCC); HTB22, Adenocarcinoma Pleura Effusion (ATCC); HTB125, Normal (ATCC).

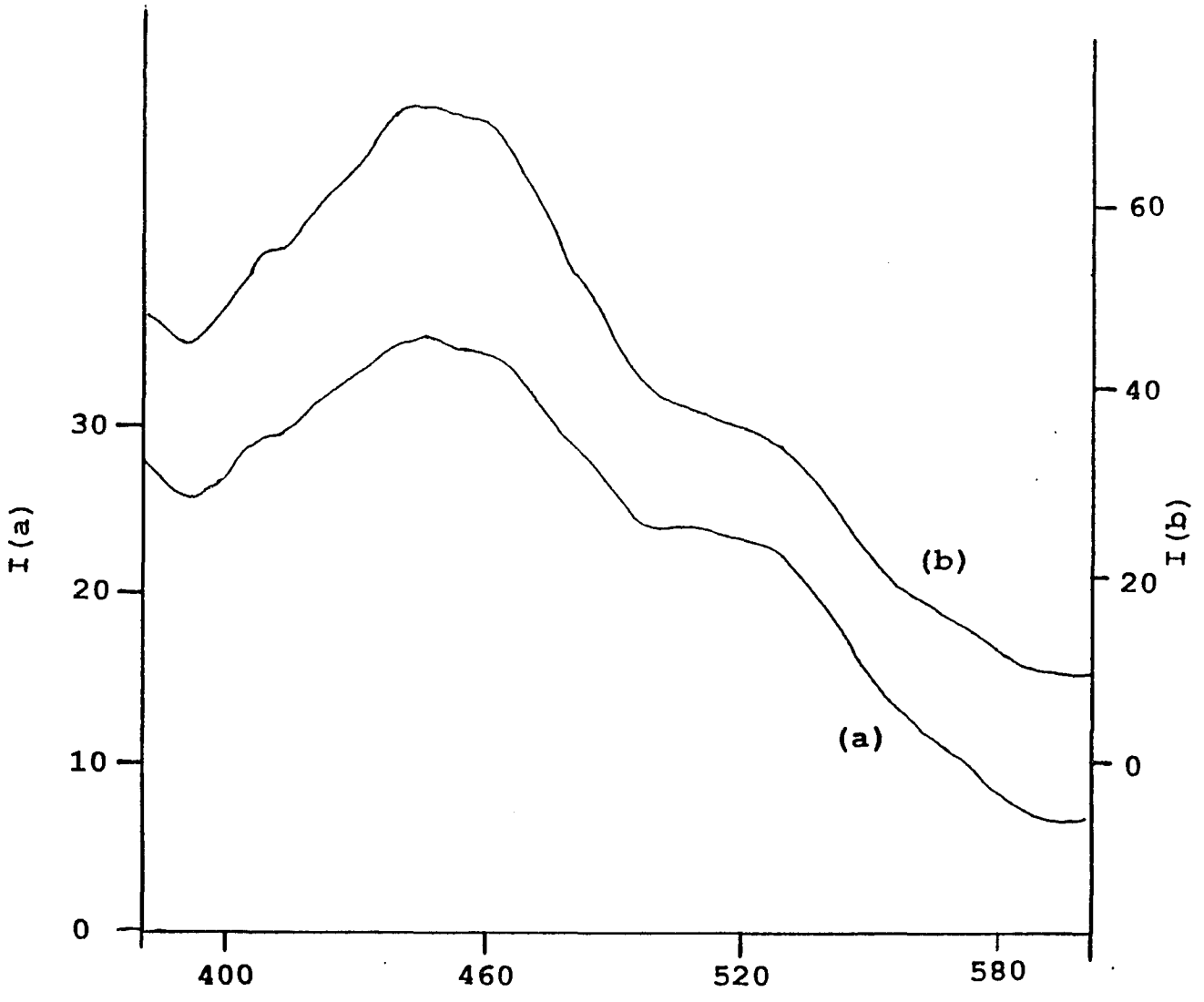

Figure 4.13. Steady state fluorescence emission spectrum of the human (a) normal cell line ATCC HTB125 and (b) cancerous cell line ATCC HTB126 excited by 353nm. The two samples contain approximately the same amount of cells. (Intensity axis is in the arbitrary unit).

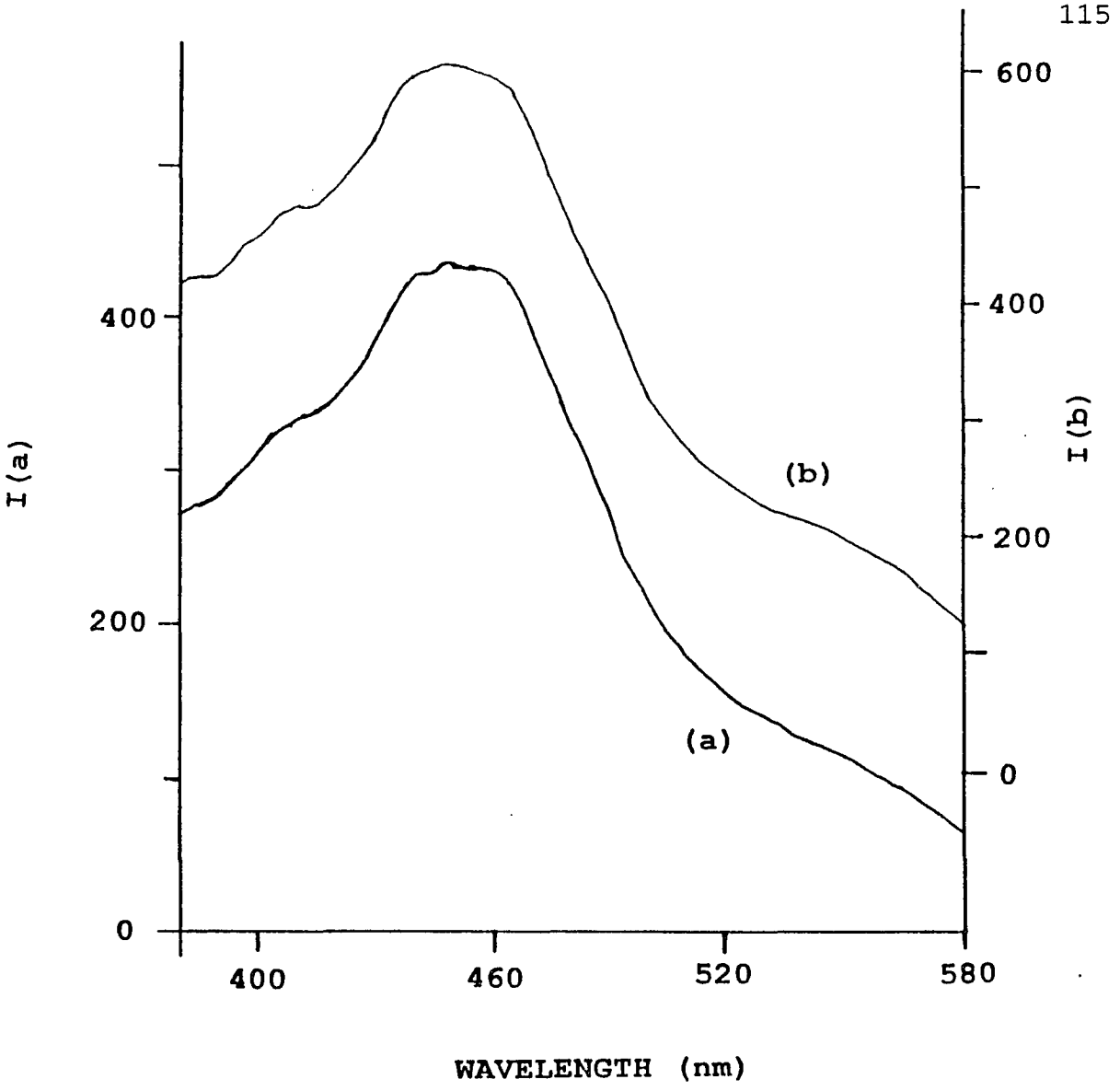

Figure 4.14. Steady state fluorescence excitation spectrum of the human cancerous cell line ATCC HTB22 (adenocarcinoma pleural effusion) with the emission wavelength at 460nm (a) at time t="0", emission collection through a I-75 filter, (b) at t="30" min. (Note: Intensity is in the arbitrary unit).

4.3.2 Theoretical model for numerical fitting of the fluorescence emission spectra from the cells.

In order to build a simple theoretical model of the physics process, I assume that the monochromatic incident light with intensity I_0 and wavelength λ_e is illuminated on the surface of the cell sample whose attenuation coefficient is $\mu_t(\lambda)$. μ_t includes both the absorption (which includes all the fluorophors absorption) and scattering coefficient.

$$\mu_t = \mu_{ta} + \mu_{ts} \tag{4.1}$$

According to the Beer-Lambert Law, the intensity of the excitation light should be reduced along the penetration depth along x-axis as

$$I = I_0 \exp[-\mu_t(\lambda_e)x] \tag{4.2}$$

The fluorescence from the i kind of fluorophors in the tissue at local x is proportional to the excitation light intensity at local x, that is

$$dI_{Fi}(\lambda,x) = Q_i\, f_i(\lambda)\, I(x)\, dx \tag{4.3}$$

where $f_i(\lambda)$ is the fraction of emission that occurs at wavelength λ of the fluorophor i. Q_i is a constant which is proportional to the absorption coefficient $\varepsilon_i(\lambda_e)$ of the fluorophor, the concentration of the fluorophor c_i, and ϕ_F which is the probability of the excited molecular emitting photon as fluorescence.

$$Q_i = 2.303\varepsilon_i(\lambda_e) * c_i * \phi_{Fi} \tag{4.4}$$

The fluorescence contributed from the i fluorophor at the distance range dx should be

$$dI_{Fi}(\lambda,x) = Q_i\ f_i(\lambda)\ I(x)\ dx$$

$$= Q_i\ f_i(\lambda)\ I_0\ \exp[-\mu_t(\lambda_e)x]\ dx \qquad (4.5)$$

This part of the fluorescence has to penetrate out of the cell surface for the detector to receive. Therefore, using the Beer-Lamber's Law again, the fluorescence which can be received by the detector from this contribution of $dI_{Fi}(\lambda,x)$ should be

$$\delta dI_{Fi}(\lambda,x) = \nu\ dI_{Fi}(\lambda,x)\ \exp[-\mu_t(\lambda)x] \qquad (4.6)$$

$$= \nu Q_i f_i(\lambda) I_0\ \exp[-(\mu_t(\lambda_e)+(\mu_t(\lambda))x]\ dx$$

where the ν is a constant. ν is the fraction of radiation actually collected by the detector.

The excitation light intensity is weak, and the sample is turbid, so the excitation light decays to near zero before it travels far. Collecting all the fluorescence at the front surface from the various depth x, the detected fluorescence spectrum should be

$$\delta I_{Fi}(\lambda) = \int_0^\infty \nu Q_i f_i(\lambda) I_0\ \exp[-(\mu_t(\lambda_e)+(\mu_t(\lambda))x]\ dx$$

$$= \nu Q_i f_i(\lambda) I_0\ /[\mu_t(\lambda_e)+(\mu_t(\lambda)] \qquad (4.7)$$

In the case there are several kind of fluorophors in the tissues, the fluorescence spectrum should be

$$I_F(\lambda) = \sum \nu Q_i f_i(\lambda) I_0\ /[\mu_t(\lambda_e)+\mu_t(\lambda)] \qquad (4.8)$$

For further simplifying the case, I assume that the attenuation coefficient of the cell sample can be considerate as an constant in the wavelength range in which we are interested. Thus, let

$$\eta = \mu_t(\lambda_e)+\mu_t(\lambda) \qquad (4.9)$$

then,

$$I_F(\lambda) = \sum \nu Q_i f_i(\lambda) I_0 / \eta \qquad (4.10)$$

or simply be expressed as

$$I_F(\lambda) = \sum B_i f_i(\lambda) \qquad (4.11)$$

According to the fluorescence properties of various intrinsic fluorophors (discussed in section C of the Chapter 1, and shown in Figure 1.32), I assume that there are collagen, elastin, NADH, and flavins. These four fluorophors are most involved in this emission spectra with excitation wavelength 353nm. Therefore,

$$I_F(\lambda) = B_1 f_1(\lambda) + B_2 f_2(\lambda) + B_3 f_3(\lambda + 10nm) + B_4 f_4(\lambda) + Const. \qquad (4.12)$$

Here, 1 presents collagen, 2 presents elastin, 3 presents NADH, 4 presents flavins, and Const. covers the background which might be caused by other weak fluorophors, $f_i(\lambda)$ are the normalized fluorescence spectra from each of the fluorophors.

It is important to note that the NADH fluorescence used in the model has been blue shifted 10nm because of the known fact of the blue peak shift caused by NADH binding (see first paragraph of Chapter 4.3 for detail). The fluorescence peak of the flavins is considered at 325nm. Using the least square error method to numerically fit the measured spectra (Figure 4.10, 4.11, and 4.12), I can obtain the relative B_1, B_2, B_3, B_4. and Const. values and the ratios between them. χ^2 gives the averaged least square fittinng error for each fit. It is equal to

$$\chi^2 = \Sigma [y_i - I_i]^2 / (N-k),$$

where the y_i is the fit data according to the model at the point i, I_i is the experimental data at point i, N is the number of the points in the data set, k is the number of the parameters in the fitting model. For the individual set of data, the smaller is χ^2, the batter is the fit model. The best χ^2 value is 0.

Suppose that

$$R = B_3 \; / \; (B_1 + B_2 + B_4 + \text{Const.}) \qquad (4.13)$$

present the ratio of the relative fluorescence intensity of the NADH over combined fluorescence intensity of all the others, I obtained that R_{HTB126} is 1.86, R_{HTB22} is 1.65, but R_{HTB125} is 0.65. These values are listed in the Table 4.2. The results show that the cancerous cells HTB126 and HTB22 contain relatively stronger NADH fluorescence intensity over the fluorescence intensities from elastin than the normal cells HTB125 does.

The goodness of fit curve over the measured spectra curve of the HTB125, HTB126, and HTB22 are shown in the Figures 4.15 to 4.17, respectively. The fitting in the range of 500nm to 560nm were slightly mis-matched in all three spectra. This may have been caused by the flavins peak shifting toward the longer wavelength or some other weak fluorophor emission which we do not know of. The flavins peak shifting will cause the obtained B_4 values to be smaller than they should be. And this mismatching also causes B_1 and B_2 and Const. slightly larger than they should be.

Table 4.2 List of the fitting parameters of the model equation 4.12 for the emission spectra of the cultured human breast cell lines. The excitation wavelength is 353nm.

	HTB125	HTB126	HTB22
B1 (Collagen)	105.67	62.43	154.85
B2 (elastin)	1.08	0.0447	0.0006
B3 (NADH)	117.41	319.46	480.05
B4 (flavins)	15.02	25.73	32.27
Const.(background)	42.84	80.77	100.3
$\chi^2=\sum[y_i-I_i]^2/(N-5)$	0.87	2.42	3.62
R=B3/(B1+B2+B4+Const.)	**0.71**	**1.89**	**1.67**

HTB126, Ductal Carcinoma (ATCC); HTB22, Adenocarcinoma Pleura Effusion (ATCC); HTB125, Normal (ATCC).

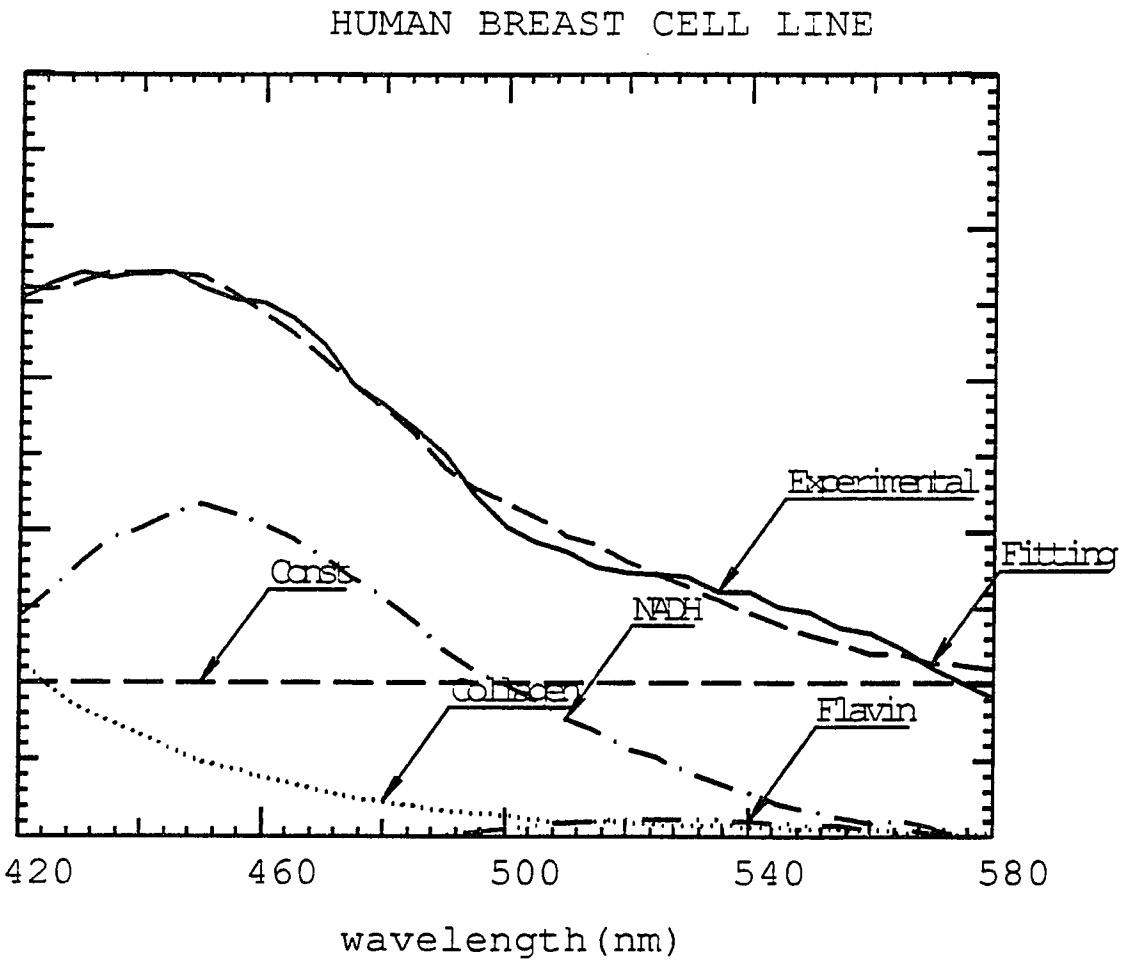

Figure 4.15 Goodness of fit with model (equation 4.12 to the emission spectrum of normal cell line HTB125 with excitation wavelength 353nm. The fitting parameters are listed in Table 4.2.

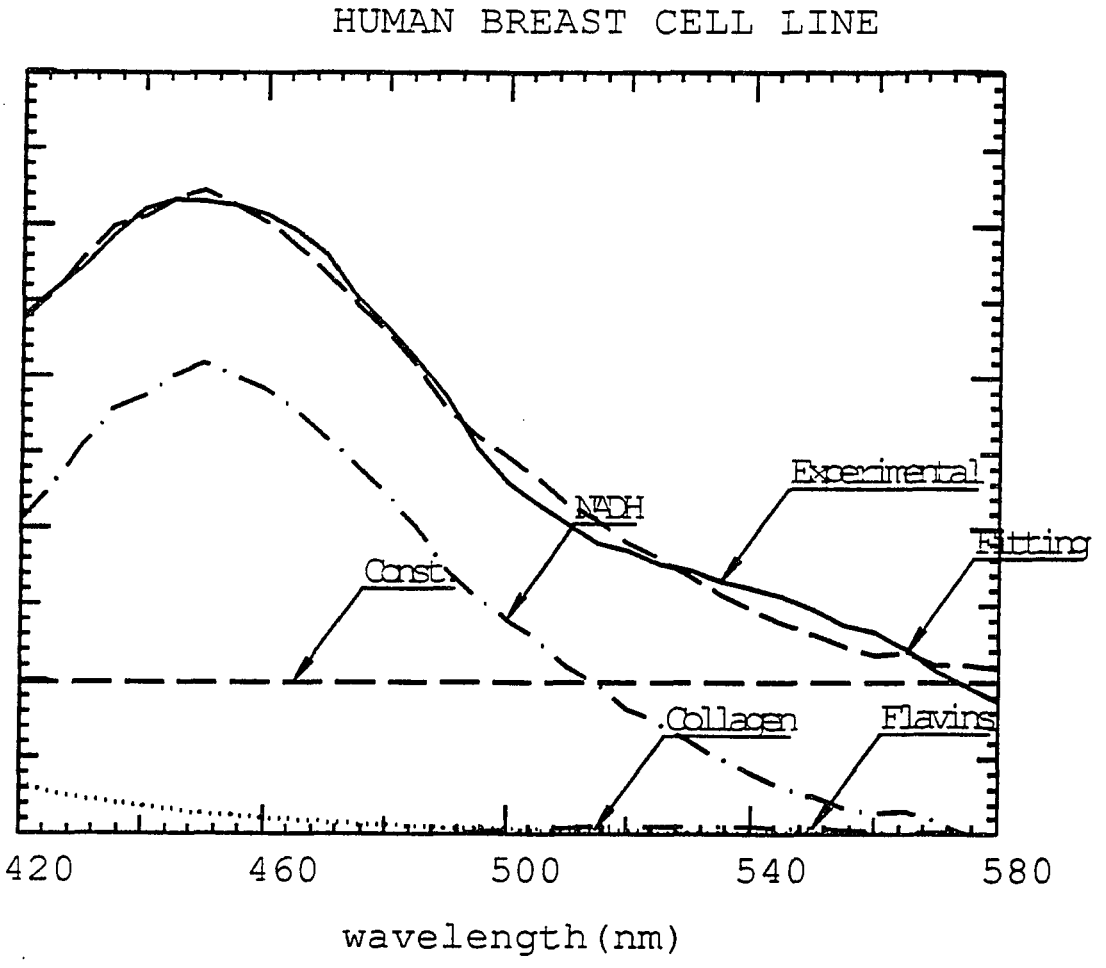

Figure 4.16 Goodness of fit with model (equation 4.12 to the emission spectrum of cancerous cell line HTB126 with excitation wavelength 353nm. The fitting parameters are listed in Table 4.2.

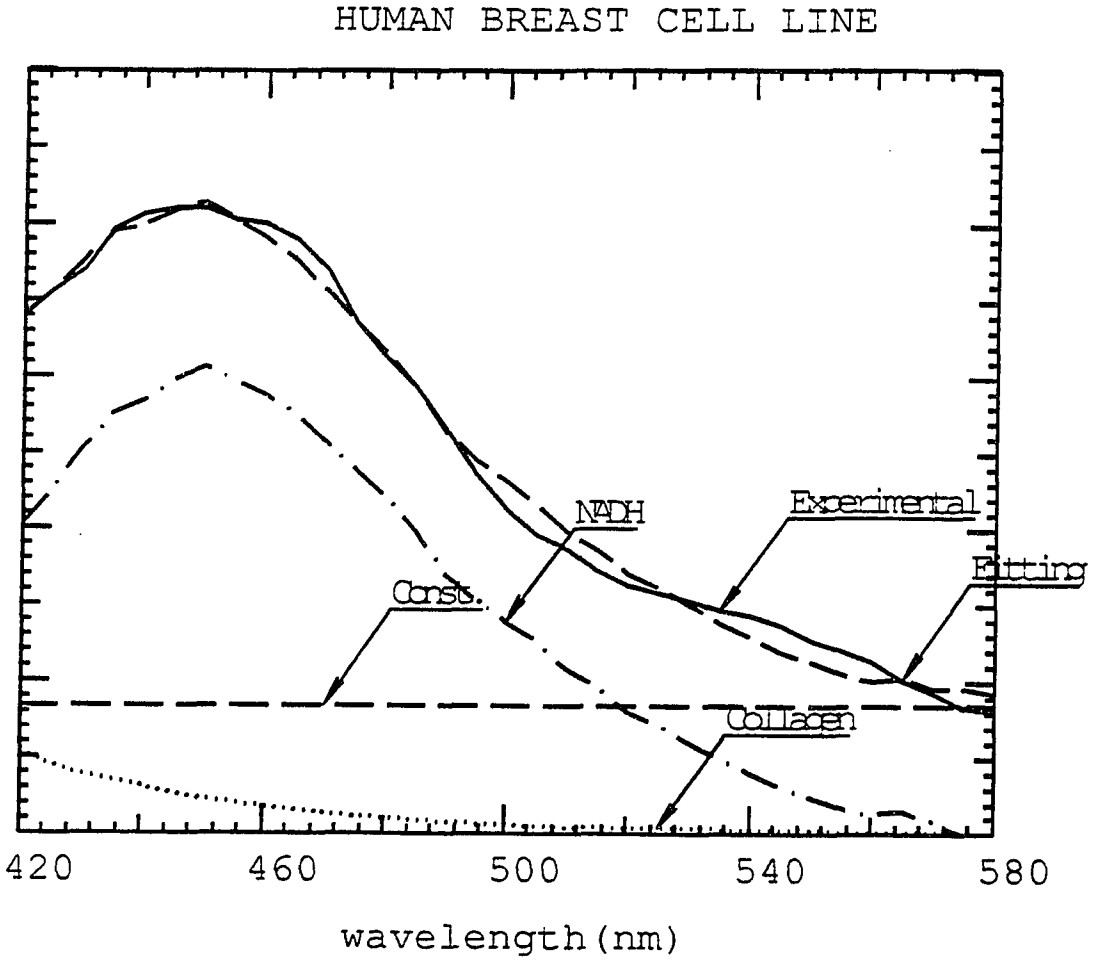

Figure 4.17 Goodness of fit with model (equation 4.12) to the emission spectrum of cancerous cell line HTB22 with excitation wavelength 353nm. The fitting parameters are listed in Table 4.2.

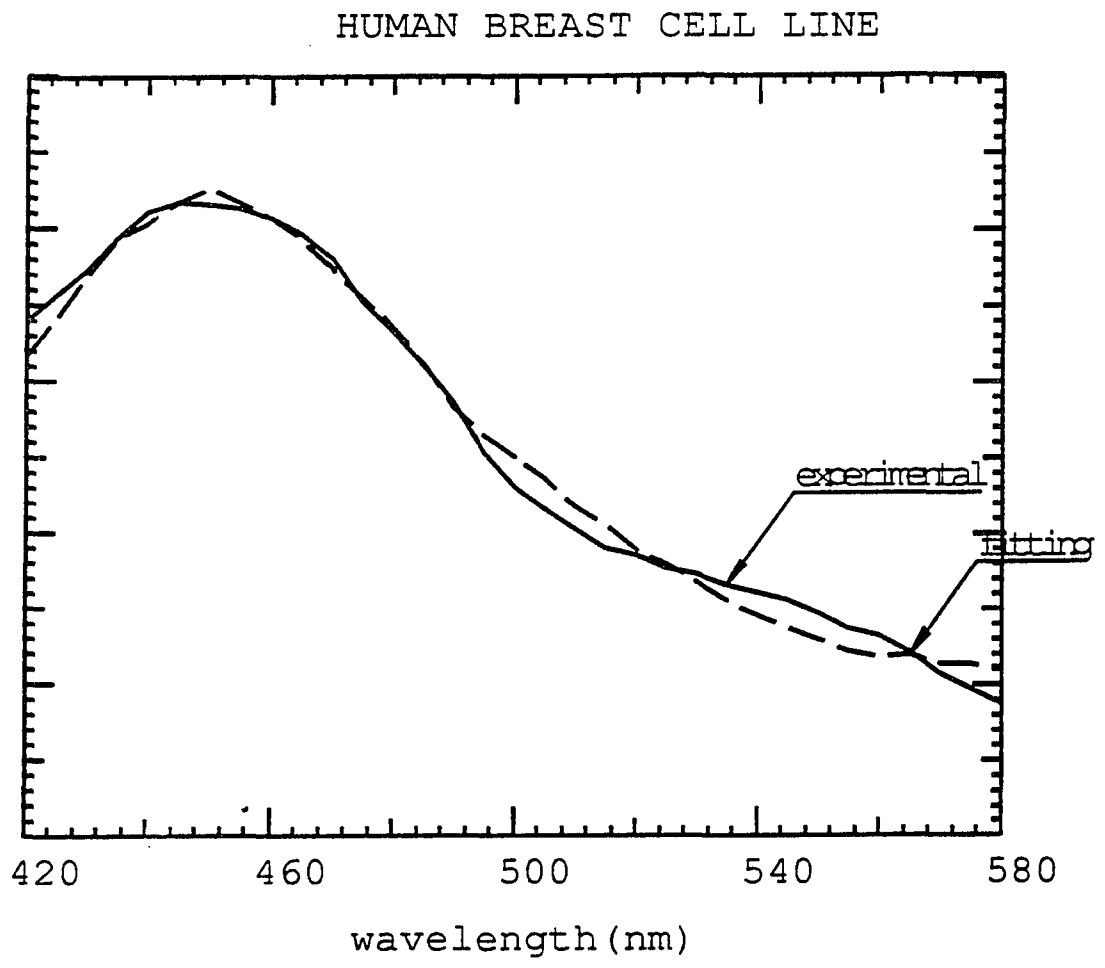

Figure 4.18 Goodness of fit with model (equation 4.12 but without collagen and elastin) to the emission spectrum of cancerous cell line HTB126 with excitation wavelength 353nm.

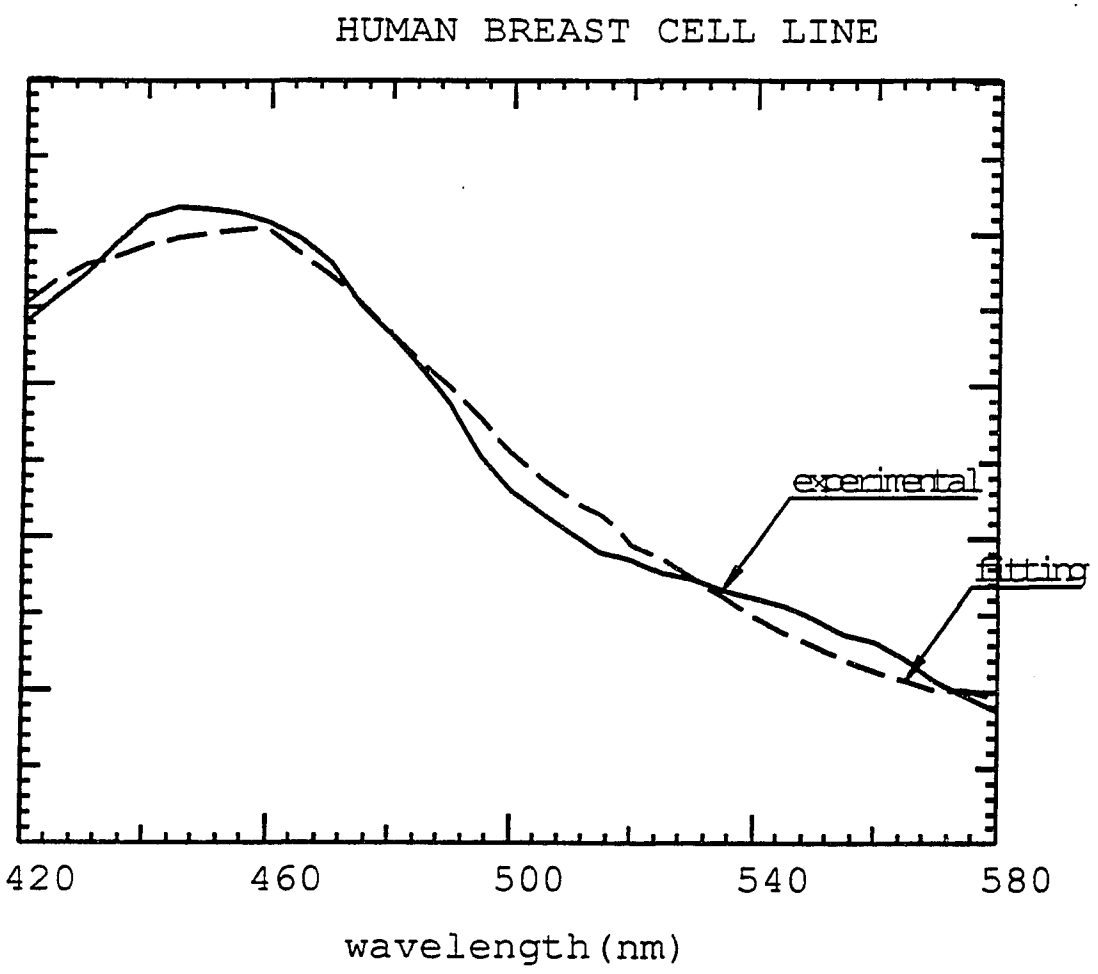

Figure 4.19 Goodness of fit with model (equation 4.12 but without NADH blue peak shift) to the emission spectrum of cancerous cell line HTB126 with excitation wavelength 353nm.

The same fitting as Eq. 4.12 but without considering collagen's and elastin's contributions has been tried on the spectra from HTB126. The result shows the mismatching (see Fig. 4.18) between the experimental curve and fitting curve around the shorter wavelength range.

The same fitting as Eq. 4.12 but without considering NADH peak blue shifting has also been tried on the spectra from HTB126. The result shows the obvious peak mis-matching at around 450nm range (see Fig. 4.19). Therefore, it is true that the fluorescence from the NADH in the cells has a blue shift of about 10nm relative to the fluorescence from the free NADH dissolved in water.

By assuming that the fluorescence from flavins in the cells excited with 353nm has the peak shifted from 525nm to 535nm, one can use the model (similar to Eq. 4.12)

$$I_F(\lambda)=B_1f_1(\lambda)+B_2f_2(\lambda)+B_3f_3(\lambda+10nm)+B_4f_4(\lambda-10nm)+Const. \quad (4.14)$$

to fit the experimental data. The fitting results are better matched to experimental data (as shown in Figures 4.20 to 4.22) with the averaged square fitting errors χ^2 decreases around 30%. The results are listed in Table 4.3.

With the further consideration of the flavins' fluorescence peak at 545nm:

$$I_F(\lambda)=B_1f_1(\lambda)+B_2f_2(\lambda)+B_3f_3(\lambda+10nm)+B_4f_4(\lambda-20nm)+Const. \quad (4.14a)$$

The averaged square fitting errors χ^2 decreases about 70%. The fitting results are listed on Table 4.4. The goodness of fit are shown on the Figs. 4.23 to 4.25.

The improvement on the goodness of fitting may suggest that there is a red peak shifting of the fluorescence spectrum of the flavins in the cells. The peak may shift from 525nm to 10 or 20nm longer in wavelength. The shift may be caused by the environment around the flavins in the cells. This red peak shift has been observed in the fluorescence spectra from the cells (see Chapter 4.2) and tissues[82] with excitation wavelength 488nm.

However, the largest red peak shifting has only been observed at 540nm but not 545nm. This suggests that there is a possibility of the existance of the another weak fluorophor. This fluorophor should fluorescence around the 545nm range. This possibility is also supported by the following arguments. The relative elastin amount given in the fitting results with flavins' peak at 525nm or 535nm are quite small in all three cell line cases (see Table. 4.2 and 4.3, and Figs. 4.15 to 4.17 and Figs. 4.20 to 4.22). However, the relative elastin amount given in the fitting results with flavins' peak at 454nm is quite a bit larger in the normal cell line HTB125 than in the cancerous cell lines (Table 4.4, and Figs. 4.23 to 4.25). This large amount of elastin in the normal cell line should contribute to the time resolved fluorescence spectra which I will discuss in the next section 4.3.4. Pure elastin has a large portion of the slower fluorescence decay component (2 portion with 2.1ns) and smaller portion of the fast component (1 portion of 47ps). NADH in water has only a fast

component about 400ps (see Table 1.2 for detail). I should observe a much larger portion of the slower component in the normal cell line than in the cancerous cell line. This does not agree with my experimental results on the cells' time resolved fluorescence measurement (see section 4.3.4). There, the ratios of the fast to slow components are 3 ± 1 for normal cell line HTB125 and 4 ± 1 for cancerous cell lines HTB126. The slower component takes larger portion in the normal cell line than in the cancerous cells, but not larger enough to agree with the fitting results with flavins at 545nm. Therefore, it is possible that there might another weak fluorophor which gives the fluorescence around 545nm. The theoretical model fit gives the relative values of each of the fluorophors contributing to the whole spectra. The relatively more intense NADH fluorescence from cancerous cell lines as opposed to those from normal cell lines can not be caused by the possible difference of the cell concentrations between the different cell samples. This is because the contribution of all the fluorophors will change by the same factor, but not the relative contribution of one kind of fluorophors, if this is the case. However, the interior cell structure changes are excluded from the contribution to this spectral observation.

It should be mentioned again that I assume that the attenuation coefficients (which includes absorption and scattering) of these cell samples are constant versus

wavelength range 420nm to 580nm in our theoretical model. This may not be true, which would cause our fitting results to change a bit. However the goodness of the fit are quit high so I do not except the attenuation coefficients to change much with the wavelength in this range. The constant attenuation coefficients will effect all the fluorophor's contribution by dividing a constant (see equation 5.10) only, but not the relative value between each fluorophor.

Table 4.3 List of the fitting parameters of the model equation 4.14 for the emission spectra of the cultured human breast cell lines. The excitation wavelength is 353nm. The flavins emission peak is assumed at 535nm.

	HTB125	HTB126	HTB22
B1 (Collagen)	107.10	59.62	149.09
B2 (elastin)	0.0025	0.116	0.032
B3 (NADH)	108.96	301.13	452.57
B4 (flavins)	6.035	5.64	0.247
Const.(background)	50.24	96.75	125.24
$\chi^2=\sum[y_i-I_i]^2/(N-5)$	1.37	3.30	4.62
R=B2/(B1+B3+Const.)	**0.65**	**1.86**	**1.65**

HTB126, Ductal Carcinoma (ATCC); HTB22, Adenocarcinoma Pleura Effusion (ATCC); HTB125, Normal (ATCC).

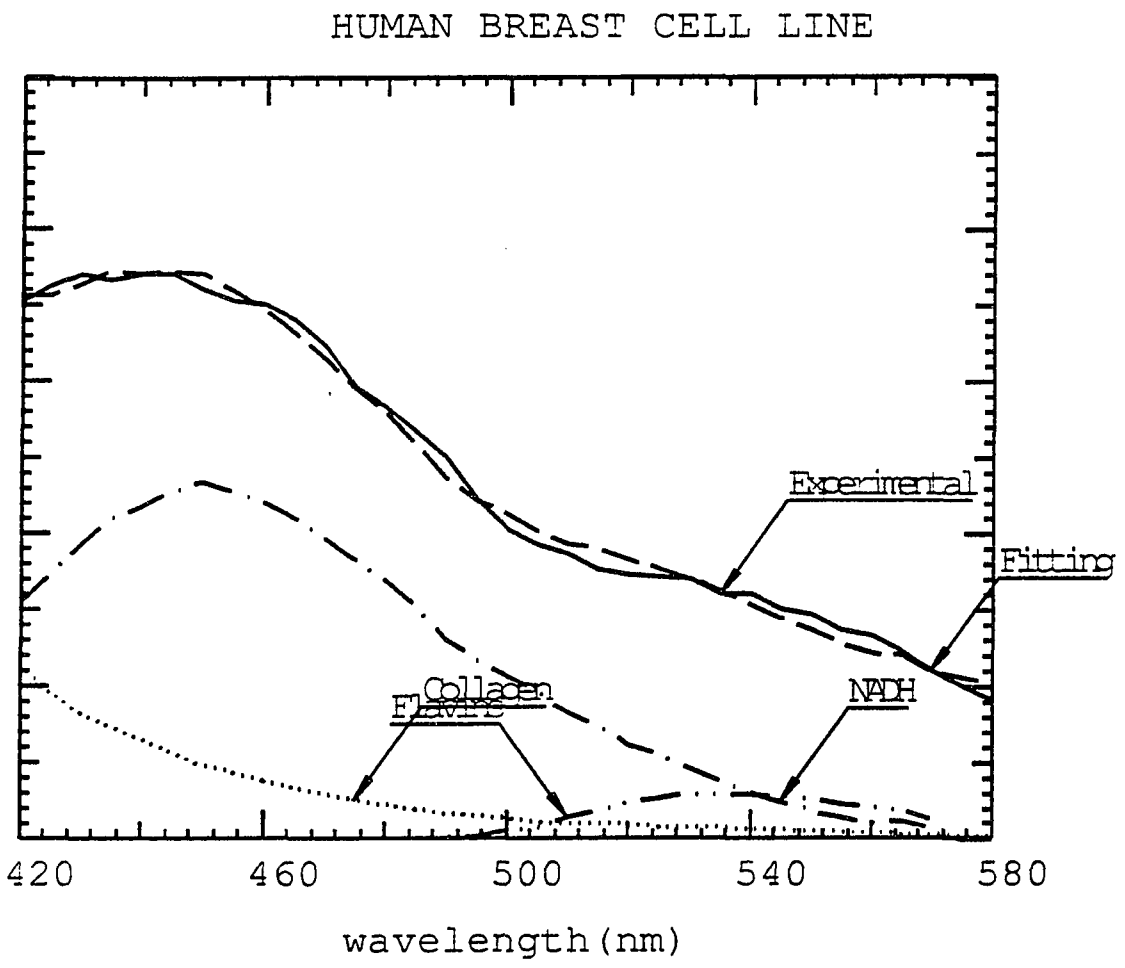

Figure 4.20 Goodness of fit with model (equation 4.14) to the emission spectrum of normal cell line HTB125 with excitation wavelength 353nm. The fitting parameters are listed in Table 4.3.

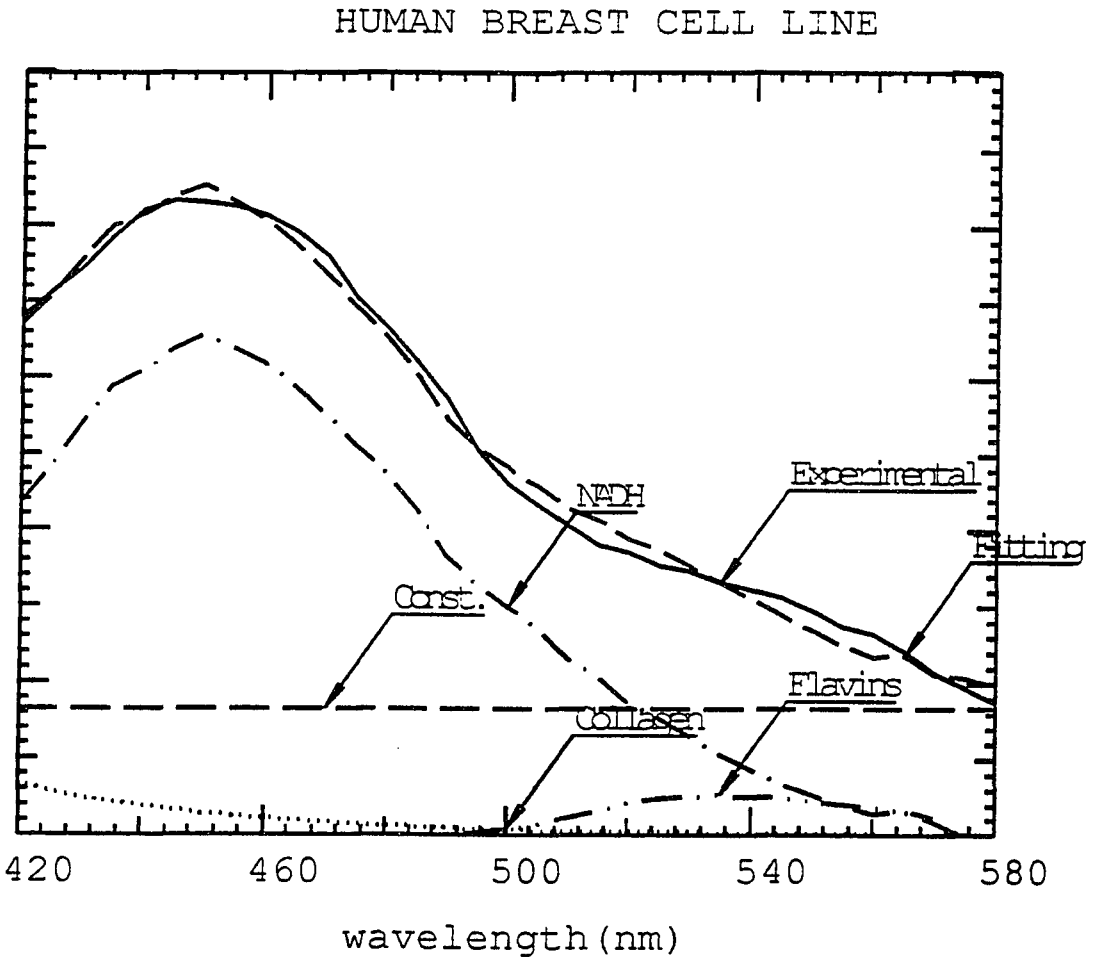

Figure 4.21 Goodness of fit with model (equation 4.14) to the emission spectrum of cancerous cell line HTB126 with excitation wavelength 353nm. The fitting parameters are listed in Table 4.3.

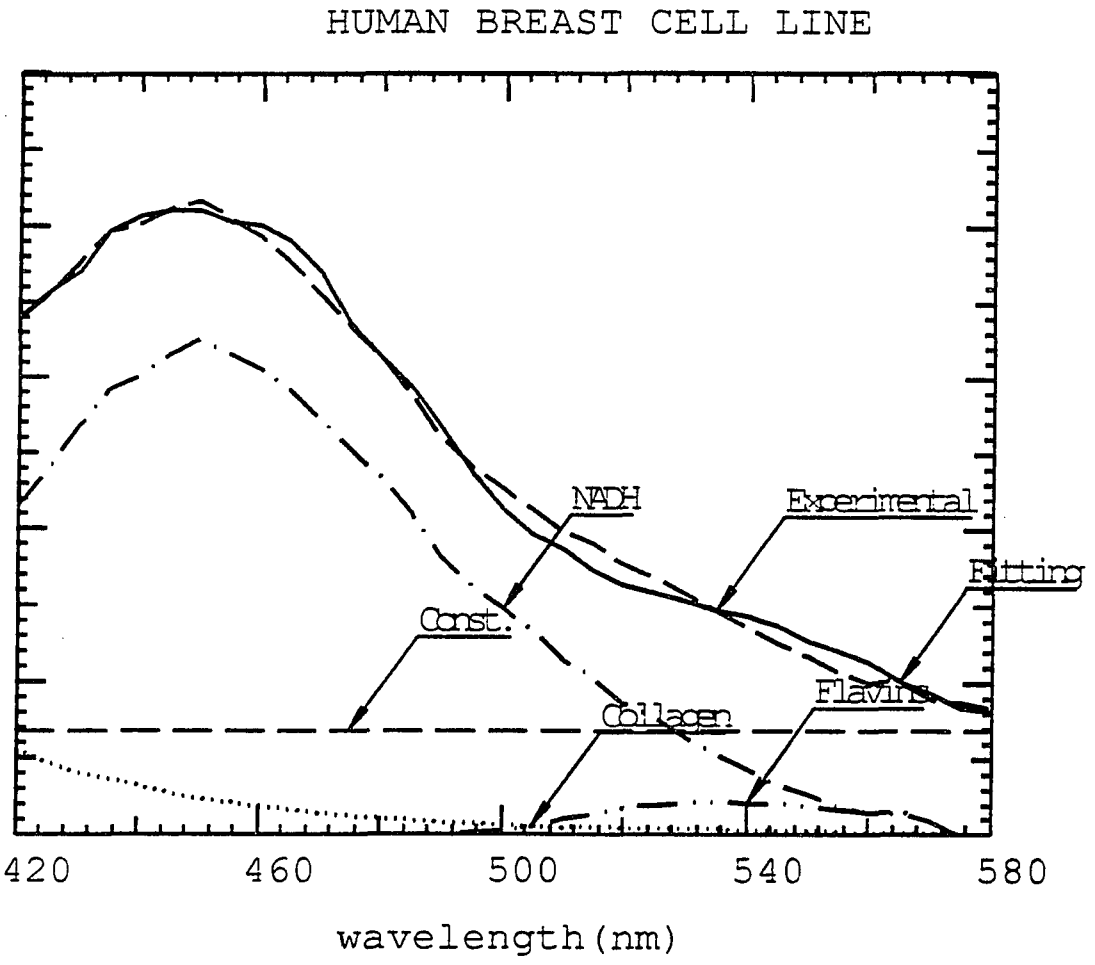

Figure 4.22 Goodness of fit with model (equation 4.14) to the emission spectrum of cancerous cell line HTB22 with excitation wavelength 353nm. The fitting parameters are listed in Table 4.3.

Table 4.4 List of the fitting parameters of the model equation 4.12a for the emission spectra of the cultured human breast cell lines. The excitation wavelength is 353nm. The flavins emission peak is assumed at 545nm.

	HTB125	HTB126	HTB22
B1 (Collagen)	30.79	0.603	143.63
B2 (elastin)	76.98	62.99	0.23
B3 (NADH)	85.75	303.39	512.70
B4 (flavins)	22.04	36.55	60.65
Const.(background)	31.26	63.24	77.47
$\chi^2=\Sigma[y_i-I_i]^2/(N-5)$	0.41	1.36	1.68
R=B3/(B1+B2+B4+Const.)	**0.53**	**1.86**	**1.83**

HTB126, Ductal Carcinoma (ATCC); HTB22, Adenocarcinoma Pleura Effusion (ATCC); HTB125, Normal (ATCC).

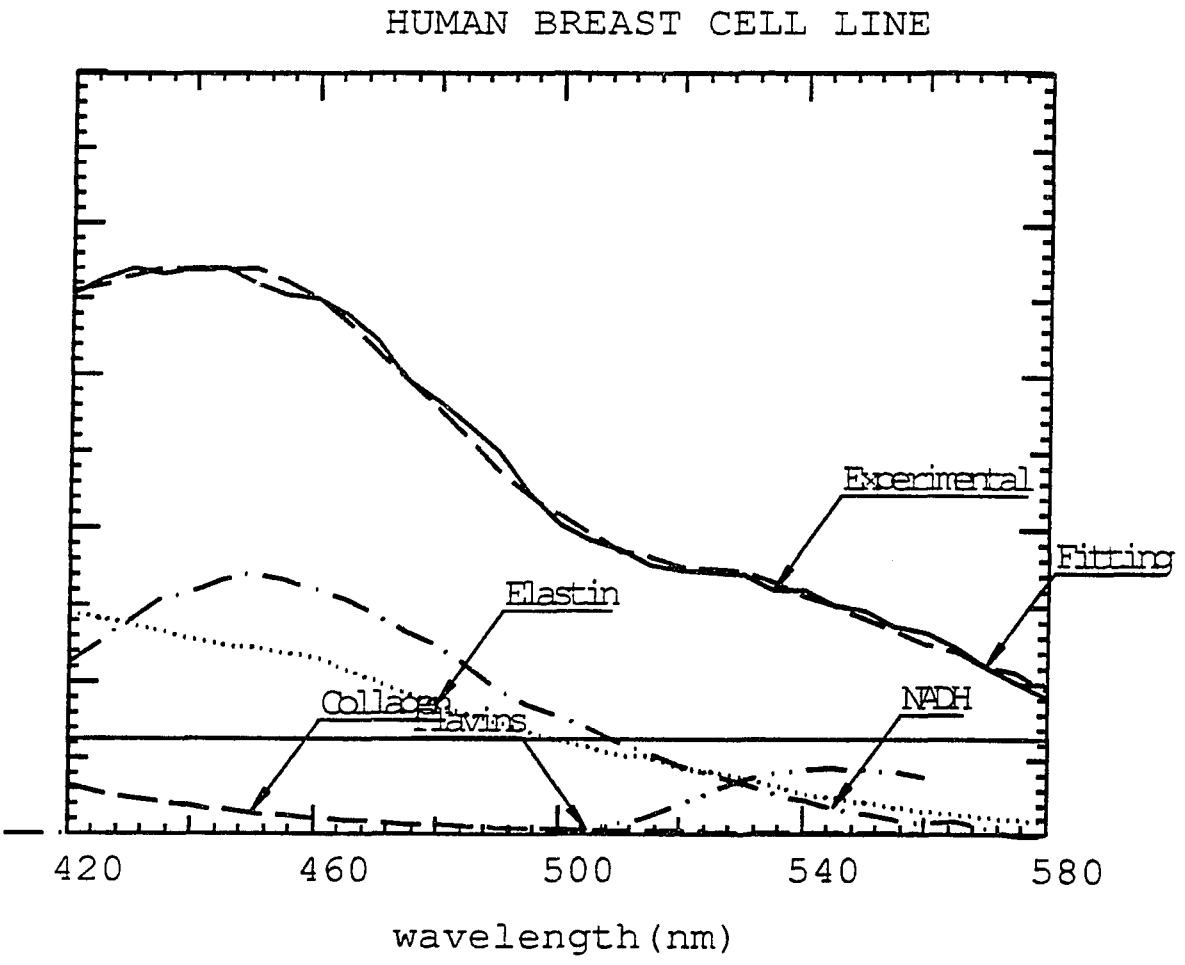

Figure 4.23 Goodness of fit with model (equation 4.14a) to the emission spectrum of normal cell line HTB125 with excitation wavelength 353nm. The fitting parameters are listed in Table 4.4.

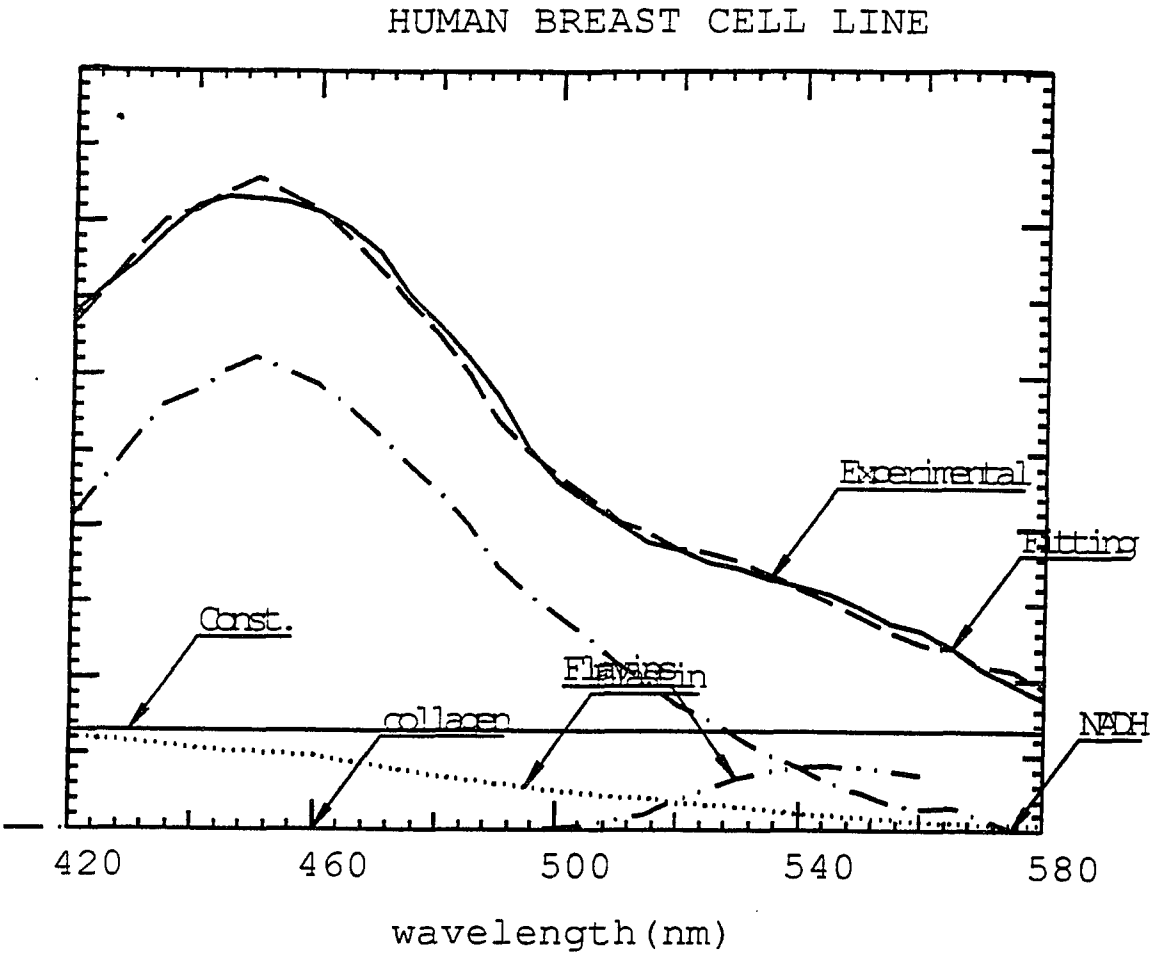

Figure 4.24 Goodness of fit with model (equation 4.14a) to the emission spectrum of cancerous cell line HTB126 with excitation wavelength 353nm. The fitting parameters are listed in Table 4.4.

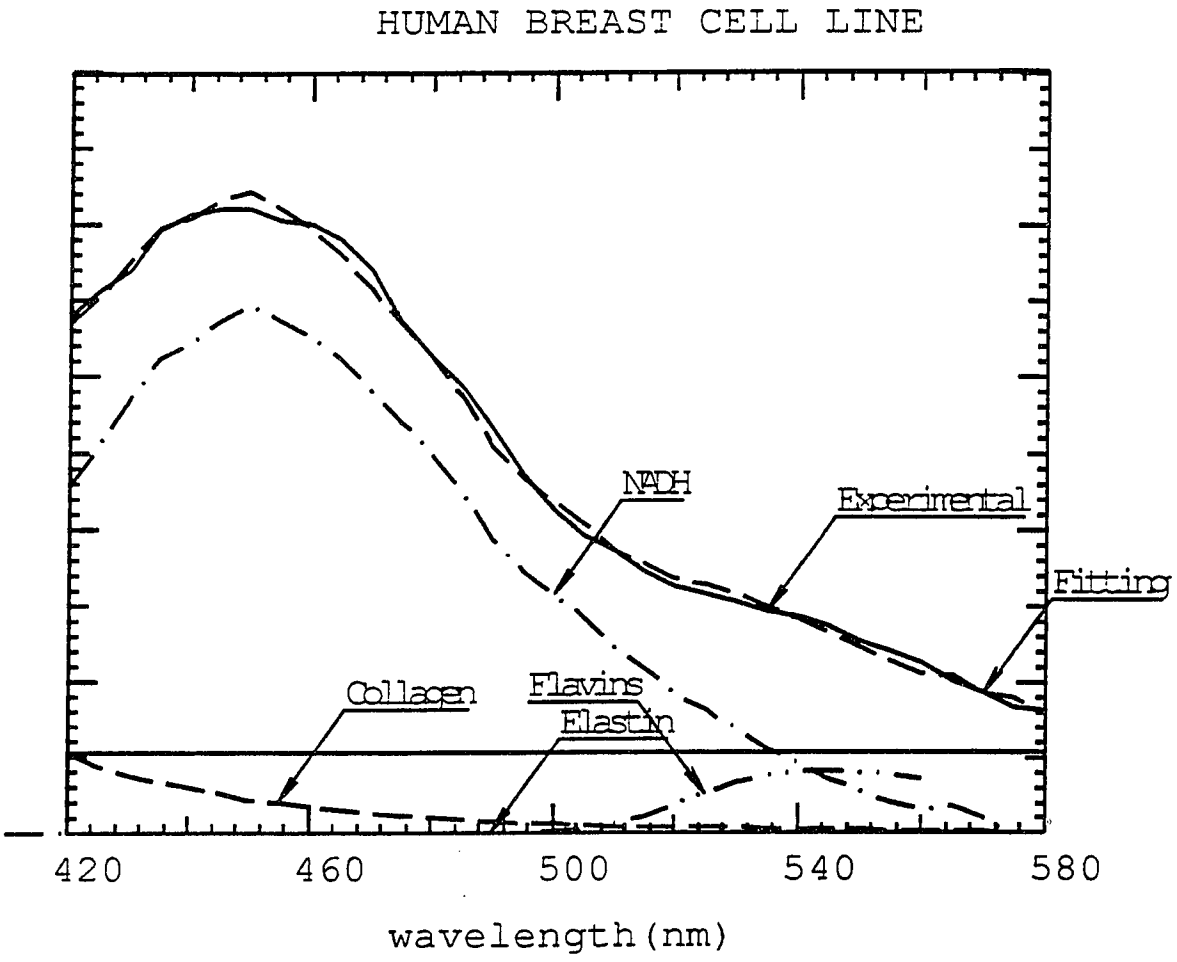

Figure 4.25 Goodness of fit with model (equation 4.14a) to the emission spectrum of cancerous cell line HTB22 with excitation wavelength 353nm. The fitting parameters are listed in Table 4.4.

4.3.3 Steady state fluorescence excitation spectroscopy from cultured human malignant and non-malignant breast cells

The corresponding typical excitation spectra for these cell lines HTB125, HTB126 and HTB22 with the emission wavelength at 460nm are displayed in Figures 4.26, 4.27, and 4.28. The excitation spectra from the various types of cell lines were measured with the emission wavelength at 460nm which corresponds to the emission peak of the free NADH. The peak positions are around 335nm for the normal cell line HTB125 (Figure 4.26), and around 340nm for the cancerous lines HTB126 (Fig. 4.27) and HTB22 (Fig. 4.28). This peak is due to NADH which has an absorption peak at 340nm (as shown is section C of the Chapter 1). Consequently, there is a slight blue shift in the excitation peak of the spectral profile for the normal cell line HTB125, as compared to the excitation peaks of the cancerous cell lines HTB126 and HTB22.

The emission peak located at 450nm, instead of the 460nm as the free NADH, indicated that the fluorescence mostly came from the bound NADH. In addition, the slight blue shift of the excitation peak from normal cell lines compared to that of the cancerous cell lines suggested that the NADH in the normal and cancerous cells may be bound differently. The differences between the fluorescence intensities between the normal and cancerous cell lines in both emission and excitation spectra may have been caused by the different amount of NADH in

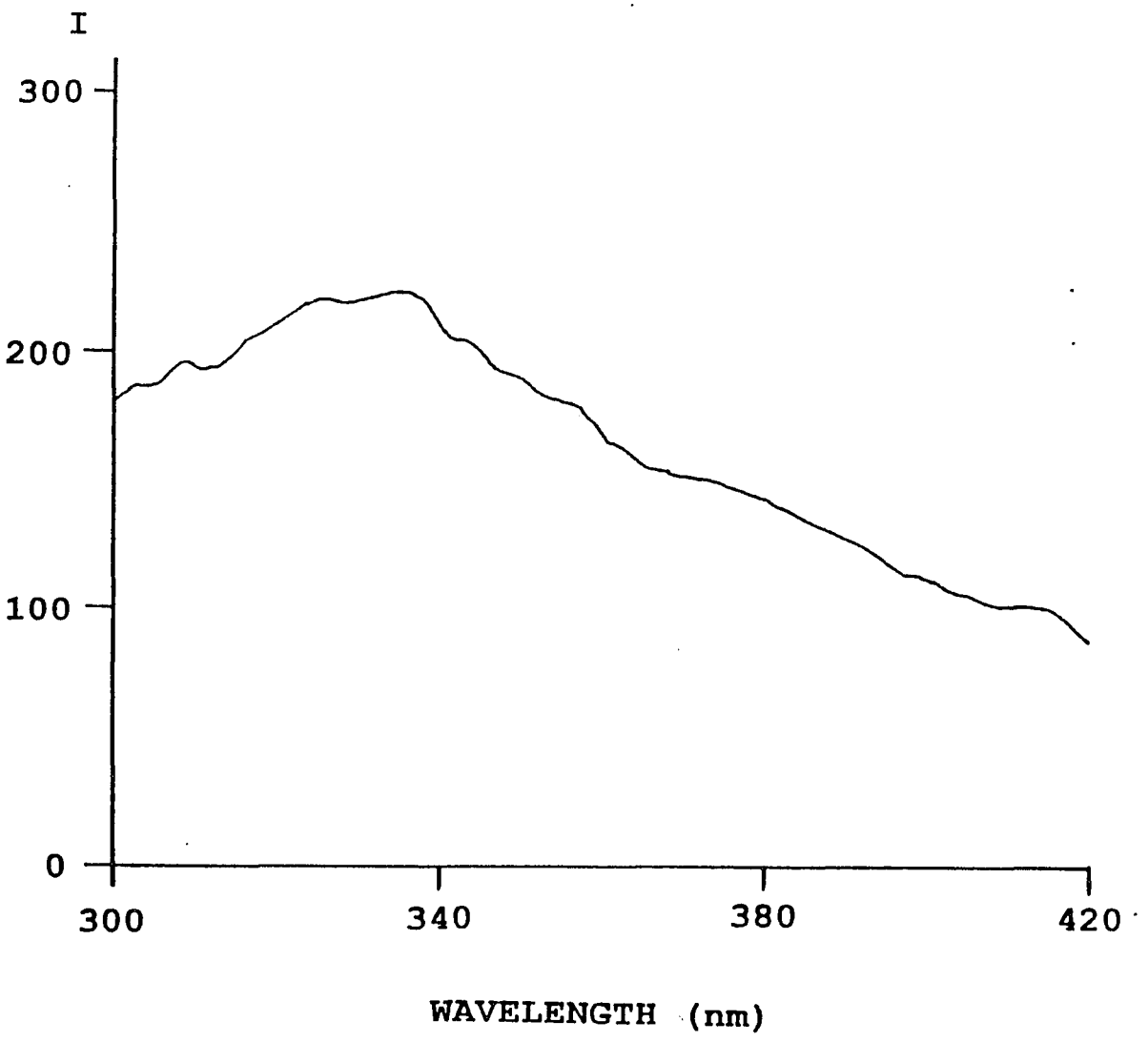

Figure 4.26. Steady state fluorescence excitation spectrum of the human normal cell line ATCC HTB125 with emission wavelength at 460nm. (Intensity axis is in the arbitrary unit).

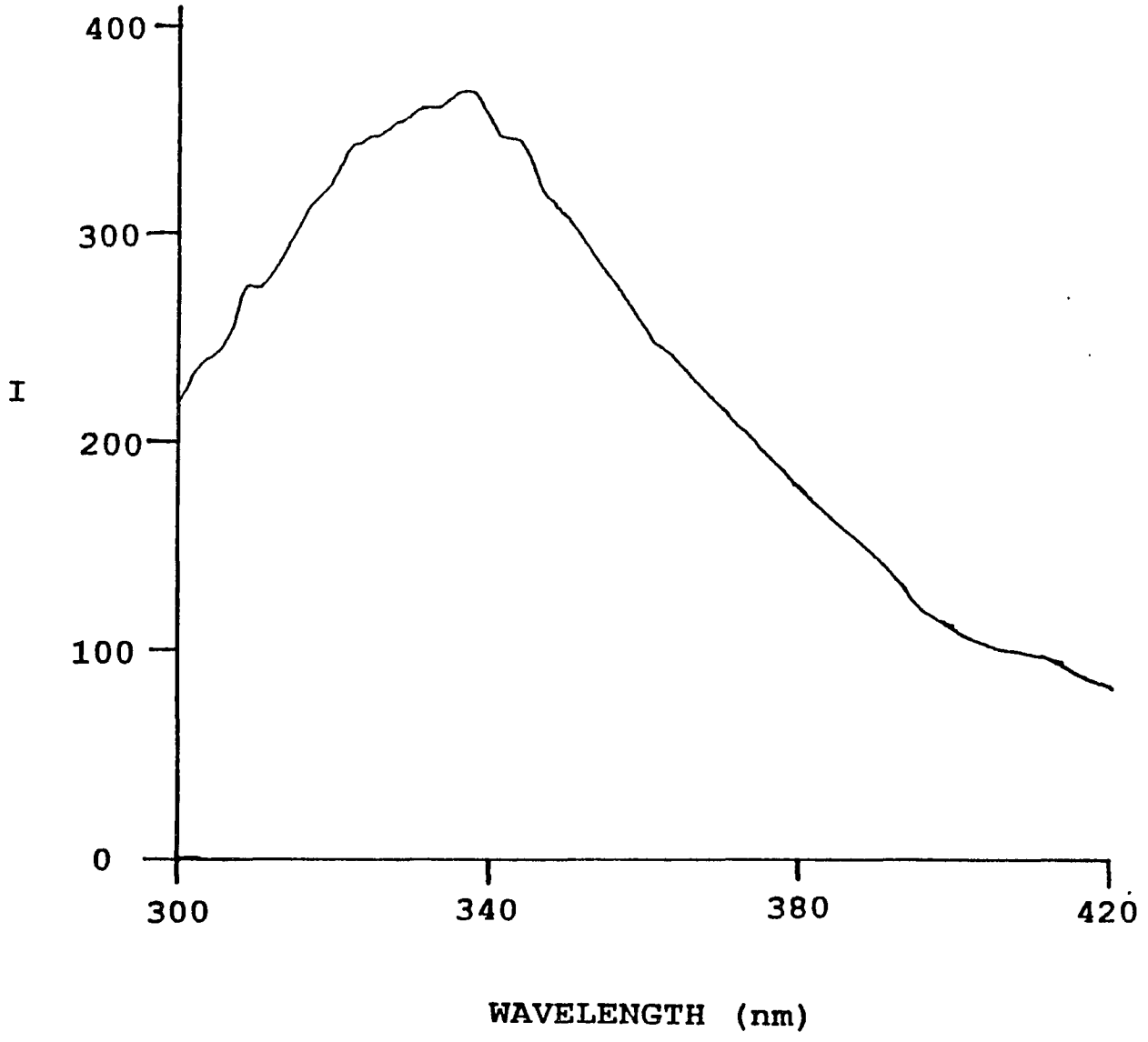

Figure 4.27. Steady state fluorescence excitation spectrum of the human cancerous cell line ATCC HTB126 (ductal carcinoma) with emission wavelength at 460nm. (Intensity axis is in the arbitrary unit)

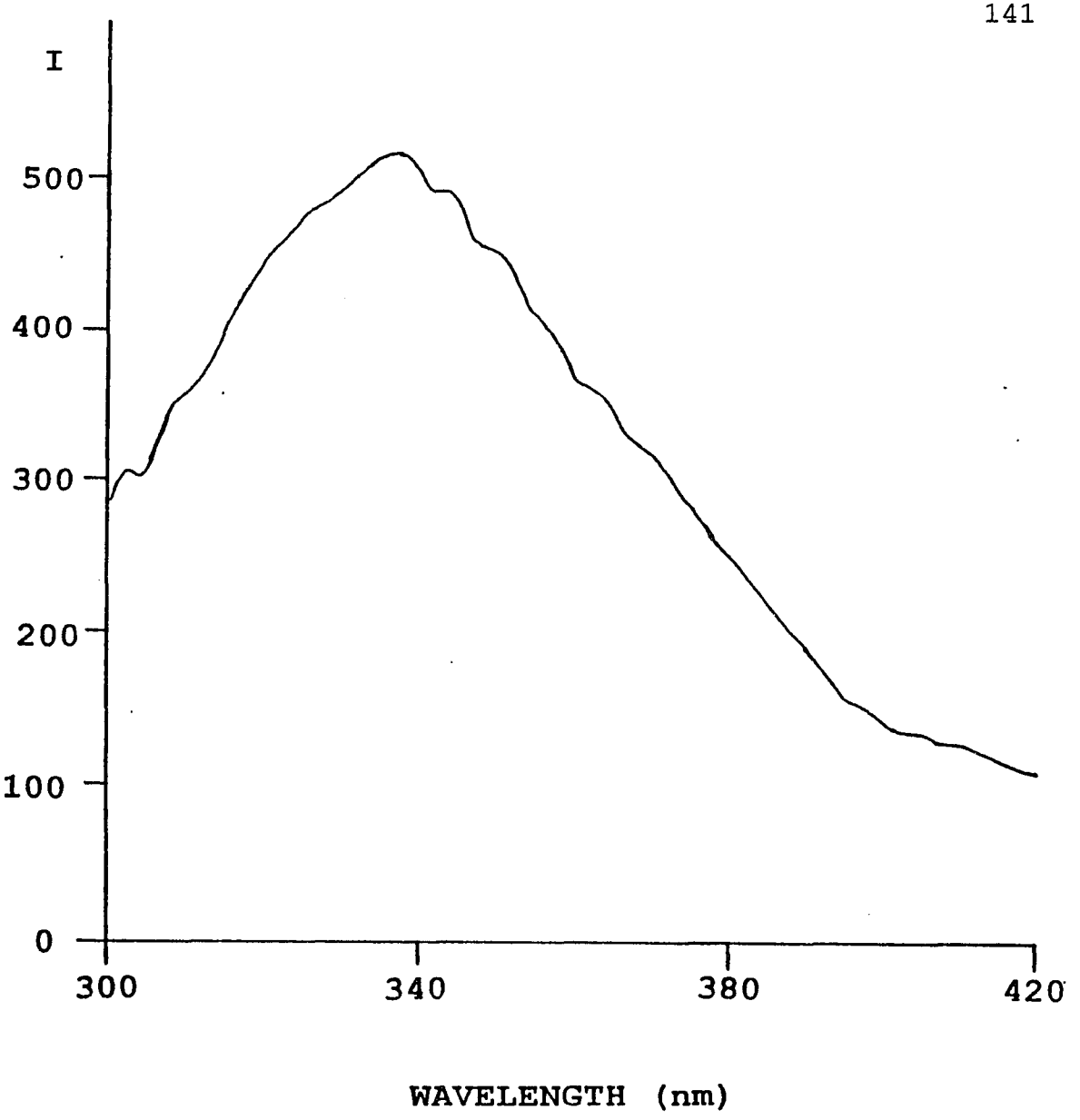

Figure 4.28. Steady state fluorescence excitation spectrum of the human cancerous cell line ATCC HTB22 (adenocarcinoma pleural effusion) with emission wavelength at 460nm. (Intensity axis is in the arbitrary unit)

these cell lines or the different fluorescence efficiency of the NADH in the normal and cancerous cell lines due to the environment around the NADH. These will be further discussed in the next section 4.3.4 after the study results of the fluorescence kinetics have been presented.

4.3.4 Time resolved fluorescence kinetics of cultured human malignant and non-malignant breast cell lines.

The fluorescence intensity not only depends on the numbers of fluorophors, but also on the radiative rate k_r and the fluorescence decay time τ_F as it has shown in equation 3.21. Fluorescence decay time τ_F is closely related to the environment and the non-radiative processes the fluorophors stay in. This can be studied by measuring the time resolved fluorescence spectroscopies.

Since the fluorescence from bound NADH in the cells is predominant over the free NADH fluorescence [65], there should be a high chance of resonance energy transfer from NADH to the bound molecules (NADH related enzyme proteins) -- This is quenching. This expectation is also supported by the fact that the NADH fluorescence intensity from mitochondria is greatly enhanced when the mitochondrion is at low temperature[80].

As it has been discussed in Chapter 2, the fluorescence decays with an exponential function as (from Equation 2.17):

$$F(t) = A\, e^{-t/\tau_F} \tag{4.15}$$

Assume there are two samples with the same radiative rate k_r but different kind of non-radiative rates k_{nr}, their steady state fluorescence intensities ratio will be related to the fluorescence decay times as (from Eq. 3.22):

$$I_{F1} / I_{F2} = k_{F2} / k_{F1} = \tau_{F1} / \tau_{F2} \tag{4.16}$$

when τ_{Fi} is the measured lifetime which is:

$$\tau_{Fi} = 1 / [k_r + k_{nri}] \tag{4.17}$$

With this relationship, I can examine if the difference in the steady state NADH fluorescence intensities between normal and cancerous cell lines might be caused by quenching. That is, to see whether there is an environmental difference around NADH between normal and cancerous cells, rather than only the NADH concentration difference between normal and cancerous cells.

The experimental setup for time resolved fluorescence kinetics study with excitation 351nm is described in Chapter 3.3. The excitation laser pulse energy was about a microjoule. The laser was focused on the sample with a spot size of about 0.5mm. Since the fluorescence was weak, narrow wavelength range selection was not possible. The fluorescence for λ >400nm was collected through the color filters O-51

(Corning Color Glass Filter, from ESCO Products Inc.) which can also be used to block scattering laser light.

The kinetic data were analyzed using a double exponential model for the intensity as:

$$I(t) = A_f \exp [-t/t_f] + A_s \exp [-t/t_s] \qquad (4.7)$$

where A_f is the amplitude and t_f is the decay lifetime of the fast components, and A_s is the amplitude and t_s is the lifetime of the slow components. The double exponential model was chosen because I assume that collected fluorescence were contributed mostly by NADH along with others like flavins, elastin and background. NADH has a fast decay time (around 400ps)[57] and flavins and elastin have mostly slow decay components[67, 81]. The fluorescence decay time of the FMN is 4.5ns, FAD is 200ps and 3ns (with ratio fast/slow=1/3 at room temperature)[67], and elastin is 46ps and 2.6ns (with ratio fast/slow=0.48 at room temperature)[81].

Typical time resolved fluorescence kinetic profiles of the total emission beyond 400nm are displayed in Figures 4.29, 4.30, and 4.31 for these three cell lines.

The temporal profile from normal cell line HTB125 (Fig. 4.39) displayed a faster decay time than the profile from cancerous cell lines HTB126 (Fig. 4.30) and HTB22 (Fig. 4.31). The normal cell line HTB125 had a fast decay time of 240 ± 25ps and a slow decay time of 1.6 ± 0.2ns. The cancerous cell line HTB126 had a fast decay time of 390 ± 40ps and a slow decay time of 4.1 ± 0.5ns, and the cancerous cell line HTB22 had a fast

decay time of 410±50ps and a slow decay time of 2.7±0.3ns. The fast component is assigned to the fluorescence decay of NADH in the cells and the slow component is assigned to the flavins, elastin and other background molecular as I had discussed in the previous paragraph.

The Table 4.5 lists the fitting parameters A_f/A_s, t_f, t_s for the kinetics results from these cell lines and Table 4.6 lists the average results. The relaxation rates of the fast components are about two times faster in the normal cells than in the cancerous cells.

To check the reproducibility of our results, the time resolved measurements were carried out 3 times for the normal cell line HTB125, 4 times on the cancerous cell line HTB22, and 3 times on the cancerous cell line HTB126. The experiments were performed at different cell passage numbers, on different shipments of cells, on the same day and on different days (in which the experimental setup conditions may have been different), and on different numbers of cells. The results from all these runs were fairly consistent. Time resolved fluorescence decay measurements on two identical samples with different pre-incubation times at 4°C revealed similar decay times within the measurement error variation (Figure 4.32). These results preclude the possibility of changes in kinetics which might result from the incubation of the samples over the time course of an experiment.

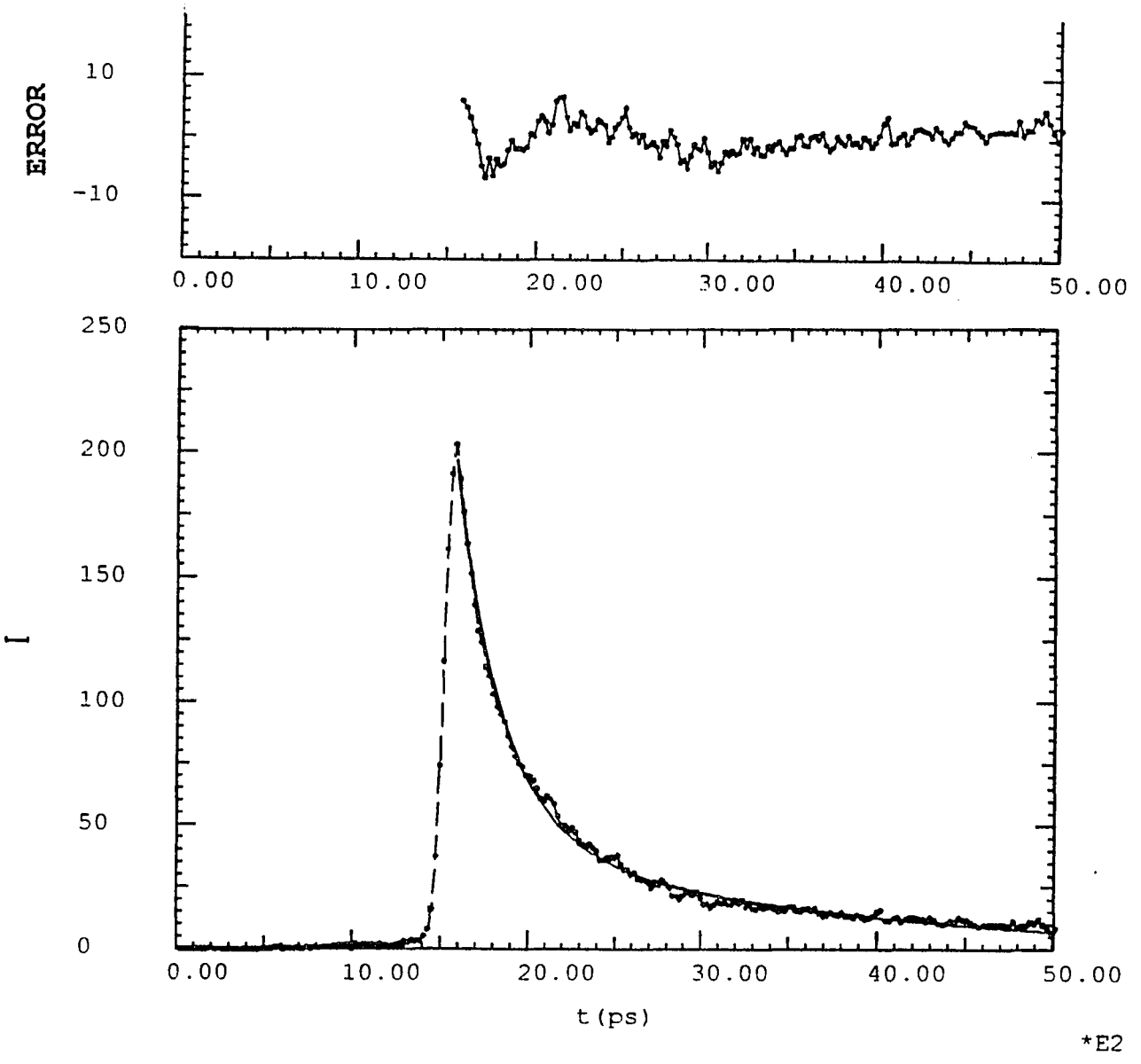

Figure 4.29. Time resolved fluorescence decay from the human normal cell line ATCC HTB125. The excitation laser pulse has wavelength 351nm and time duration around 8ps. τ_f=258ps, τ_s=1.77ns, and A_f/A_s=3.0.

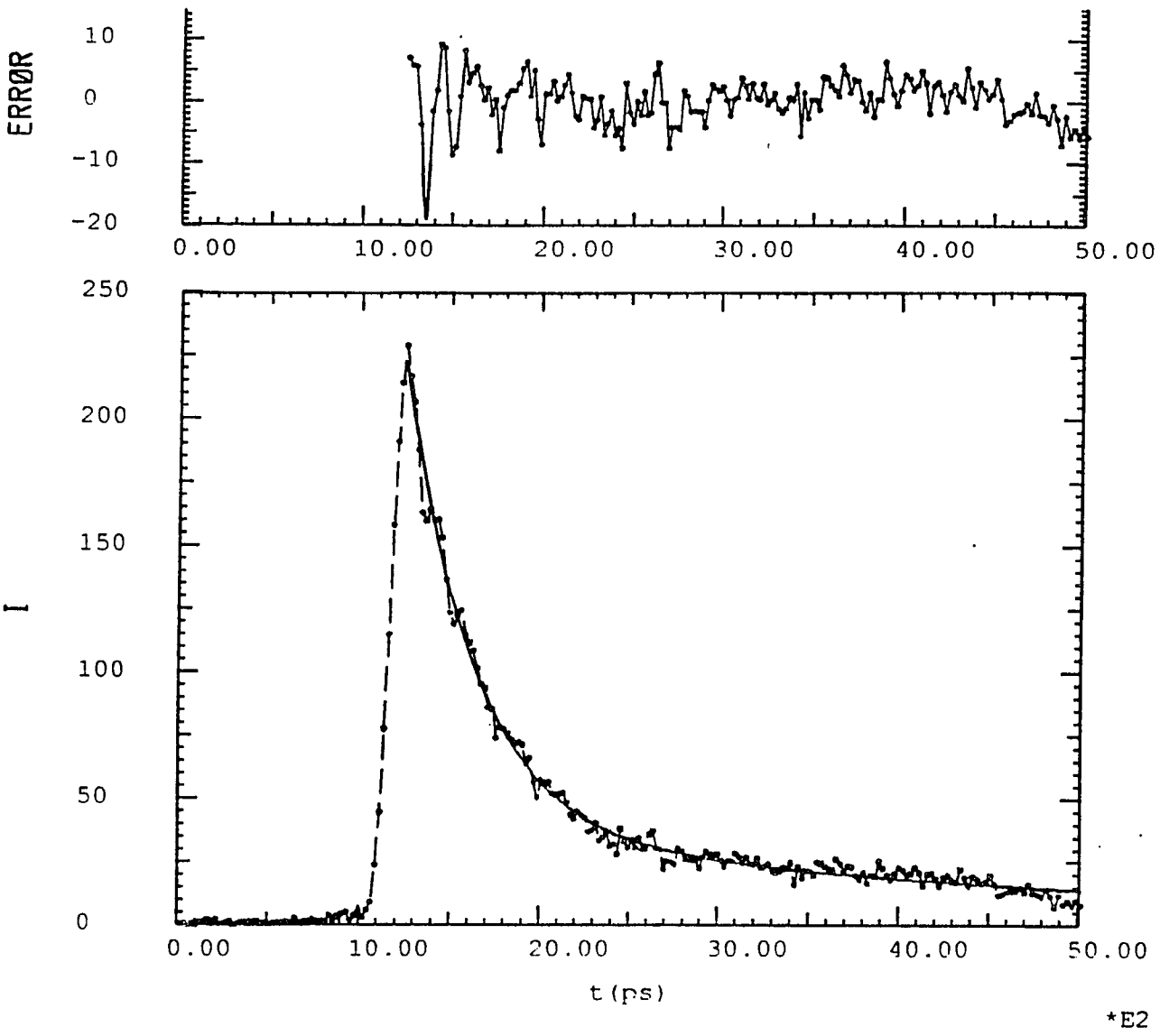

Figure 4.30. Time resolved fluorescence decay from the human cancerous cell line ATCC HTB126 (ductal carcinoma). The excitation laser pulse has wavelength 351nm and time duration around 8ps. τ_f=382ps, τ_s=3.77ns, and A_f/A_s=5.0.

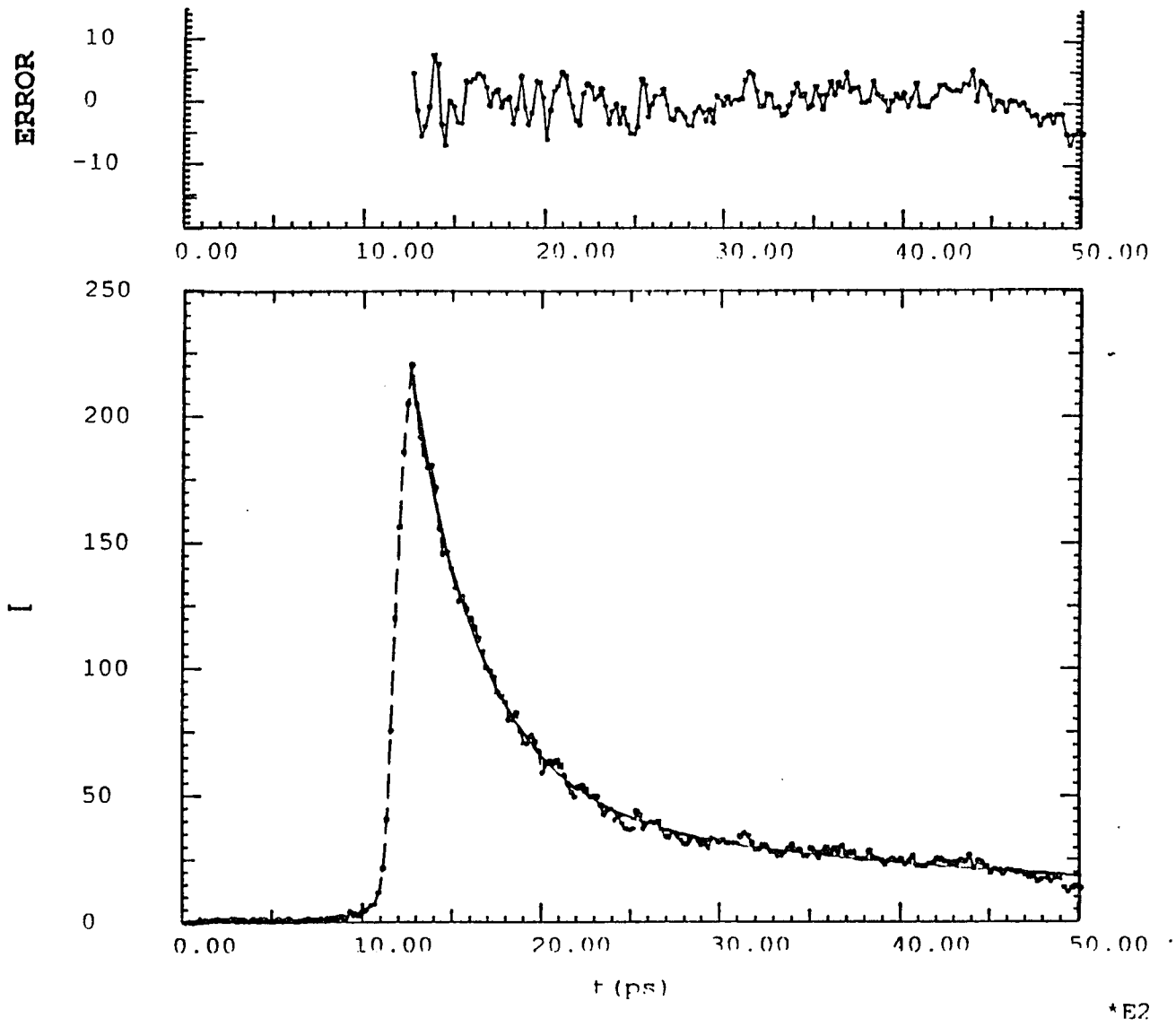

Figure 4.31. Time resolved fluorescence decay from the human cancerous cell line ATCC HTB22 (adenocarcinoma pleural effusion). The excitation laser pulse has wavelength 351nm and time duration around 8ps. τ_f=404ps, τ_s=4.33ns, and A_f/A_s=3.9.

Table 4.5 List of the time resolved double exponential fitting parameters, τ_f, τ_s, A_f/A_s for various samples.

Cell line	τ_f(ps)	τ_s(ns)	A_f/A_s	Fig. No
	218	1.77	2.7	
HTB125	251	1.47	1.6	
	258	1.77	3.0	Fig.5.24
	406	4.30	5.6	
HTB126	382	3.77	5.0	Fig.5.25
	649	4.50	4.9	
	366	2.51	2.4	
HTB22	404	4.33	3.9	Fig.5.26
	637	2.78	2.8	
	450	2.95	3.7	

HTB126, Ductal Carcinoma (ATCC); HTB22, Adenocarcinoma Pleura Effusion (ATCC); HTB125, Normal (ATCC). A_f/A_s is the ratio of the amplitudes of the fast and slow components; t_f is the life time of the fast decay component; t_s is the life time of the slow decay component.

Table 4.6 Fitting parameters of the fluorescence kinetics of human normal and cancerous cell lines.

	HTB126	HTB22	HTB125
A_f/A_s	5±1	4±1	3±1
t_f	390±40ps	410±50ps	240±25ps
t_s	4.1±0.5ns	2.7±0.3ns	1.6±0.2ns

HTB126, Ductal Carcinoma (ATCC); HTB22, Adenocarcinoma Pleura Effusion (ATCC); HTB125, Normal (ATCC). A_f/A_s is the ratio of the amplitudes of the fast and slow components; t_f is the life time of the fast decay component; t_s is the life time of the slow decay component.

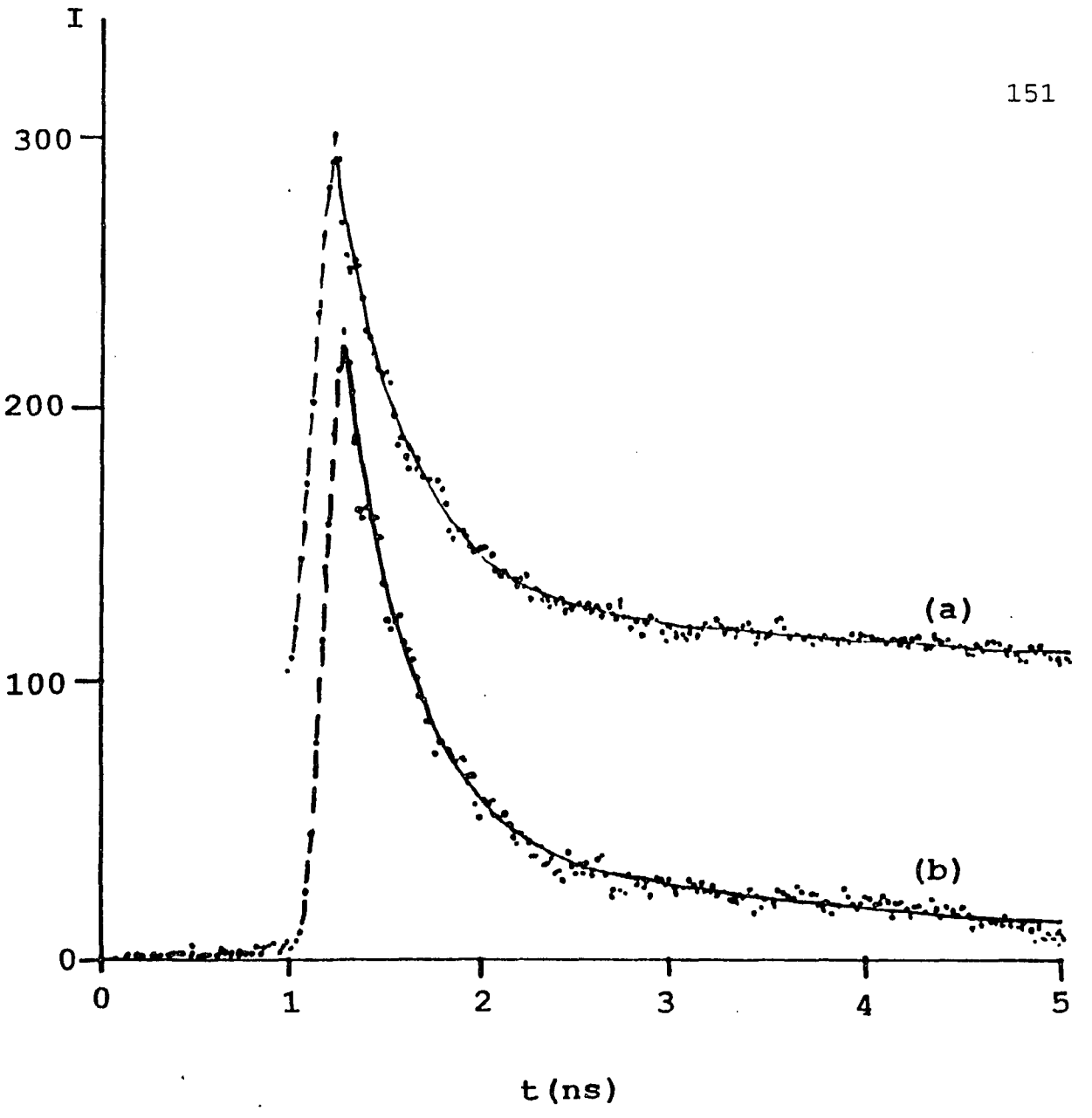

Figure 4.32. Time resolved fluorescence decay from the human cancerous cell line ATCC HTB126 (ductal carcinoma). The results come from two identical cell samples that have different incubation times under 4°C. (a) t="0" min, (b) t="1-2" hr. The excitation laser pulse has wavelength 351nm and time duration around 8ps.

4.3.5 Analysis and Conclusion

For explaining our experimental results, we must return to equation 4.6. We can clearly see that the steady state fluorescence intensities are closely related to the fluorescence kinetics. So, the experimental results from steady state and time resolved studies should be considered together.

The fluorescence peak at 450nm arise from NADH[80]. The stronger NADH fluorescence band with slower relaxation from the cancer cell lines as compared to normal cell line indicates that there is a difference in the underlying photophysics. Combining the information taken from the steady state fluorescence with the time-resolved fluorescence decays for these cell lines supports a model in which the differences arise from the environment around the NADH molecules in normal and cancerous cell lines. This difference affects the fluorescence efficiency and kinetics of NADH in the two states.

It is well known that NADH in cells are mostly bound, which would be shown in a blue shift of the peak position of the emission spectrum[75]. This is also indicated in our results by a blue shift in the NADH peak position for emission spectrum when compared to the peak position (460nm) of NADH in H_2O[67]. It was also observed that there is a blue shift of the peak position in the absorption spectra from the NADH in the intact cell, which was presumably due to binding of the

NADH[76]. In our results, the blue shift of the peak position in the excitation spectra and the faster fluorescence decay time of the normal cell line HTB125 as compared to those of the cancerous cell lines HTB126 and HTB22 may indicate that NADH is **more strongly bound** in the normal cell lines than in the cancerous cell lines. The stronger binding causes an enhancement of the non-radiative processes because it facilitates quenching of RPN energy by the bound molecular groups according to the Forster theory. The enhanced non-radiative process will result in an observed faster fluorescence decay and a weaker fluorescence intensity for normal cells. In addition, it is known that oxidized PN (NAD^+, $NADP^+$) forms do not significantly fluoresce in this wavelength range because of its lack of absorption in the 351nm range.[64] Biochemistry research has shown that stronger-growth conditions are associated with a lower NAD^+:NADH ratio.[79] It has also been shown that cells growing in the logarithmic phase contain more NADH in cells than the cells in the stationary phase.[79] Thus, it might be possible that the concentration of NADH in the cancerous cell line are higher than those in the normal cell line because cancerous cells grow faster. This difference would have resulted in stronger fluorescence from the cancerous cell lines; however, it would not account for the slower fluorescence decay times.

In conclusion, differences in the spectral and time resolved profiles of the fluorescence between cultured human

normal and cancerous cell lines have been found. The increase in non-radiative relaxation and spectral blue shift of the excitation spectra in the normal cells in comparison to cancerous cells may indicate that NADH is bound more strongly in normal cells than in the cancerous cells.

Fluorescence spectra in time and wavelength studies provides information about the microscopic metabolic states of normal and cancerous cells which are not available from direct chemical analysis.

4.4 The Relative Steady-State Fluorescence Intensities from Tryptophan, Collagen, and Elastin in the Malignant and Non-malignant Cells (300m Excitation).

The wavelength 300nm is at the red side tail of the absorption spectra (Figure 1.5) of the tryptophan and at the blue side front of the excitation spectra of the collagen (Figure 1.11), elastin (Figure 1.18) and NADH (Figure 1.22). Using 300nm as excitation wavelength, one is able to excite tryptophan, collagen, elastin and NADH molecular groups at the same time. This enables one to compare the relative fluorescence intensities of different molecular groups. This overcomes certain difficulties in the study of the absolute fluorescence intensities caused by the experimental setup variations and the sample variations, especially in the tissue's case.

It is important to point out that the culture medium and the trypsin-EDTA contains tryptophan. This will directly influence the tryptophan level in the cultured cells. Therefore, the results of this study will only be used as a reference for similar kind of study on tissue fluorescence, but not used as a primary result or conclusion for the states of the cells in malignance or non-malignance. However, in the case of studying tissues, these artificial culturing effects do not exist. Tissue is controlled by the instinct chemical

adjustments of the human body. In this case the study results take on a different tenor. (see Chapter 5.3 for results).

These experiments were also done on the Luminescence Spectrometer LS-50 (Perkin Elmer, see Chapter 3.2 for details). The excitation wavelength were chosen to be 300nm.

The fluorescence spectra of the culture media and trypsin-EDTA excited by 300nm has been examined. The spectral profile are displayed in Figure 4.33 (culture media) and Figure 4.34 (trypsin-EDTA). They obviously contain the tryptophan fluorescence band with peaks around 340nm.

The fluorescence emission spectra from both cancerous and normal cell lines excited by 300nm contain a very strong band at 340nm but a very weak and flattened tail afterwards in the longer wavelength range (Figures 4.35 & 4.36).

The strong 340nm band might be because the tryptophan is a highly efficient fluorophor, so it still gives a relatively very strong fluorescence; even 300nm is at the red edge of its absorption spectra. On the other hand, there is a smaller amount of collagen and elastin in the cultured cells than in the tissues. In that case collagen and elastin will contribute less to the fluorescence spectra of the cells.

The very low fluorescence intensity and the longer wavelength of the spectra of cells suggests that the NADH in the cells did not contribute much to these fluorescence spectra.

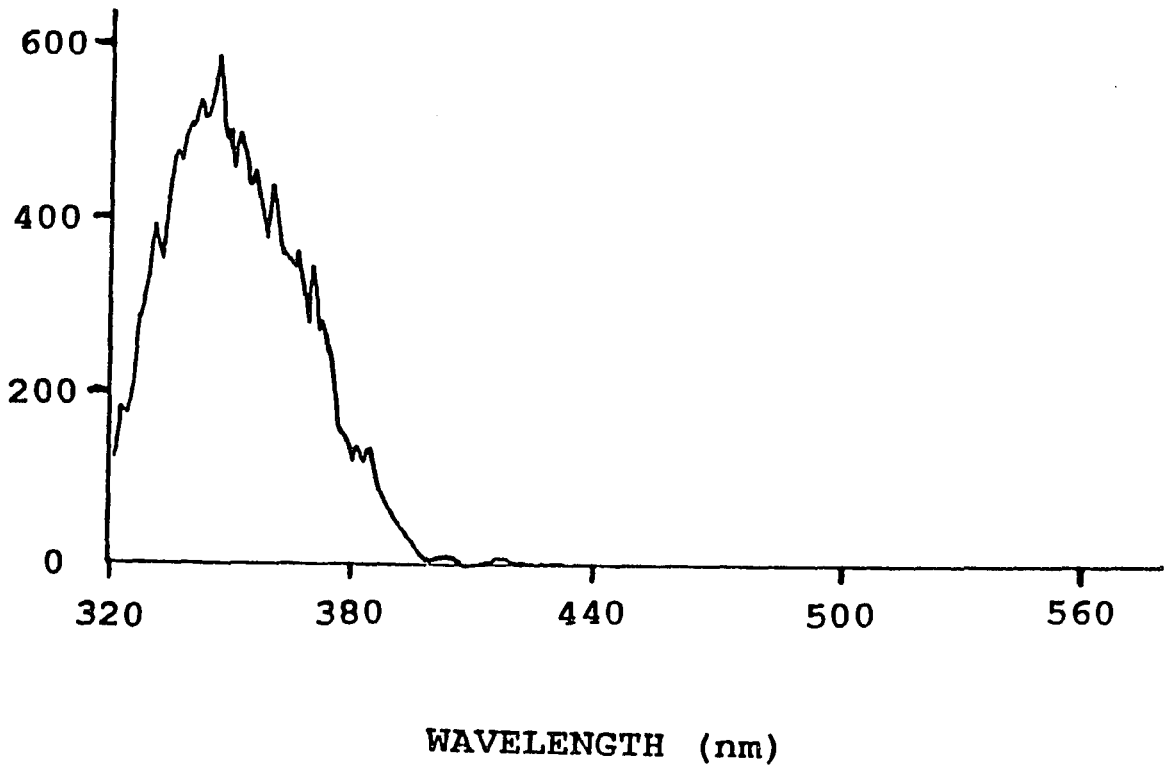

Figure 4.33. Steady state fluorescence spectrum from Modified culture medium excited at 300nm.

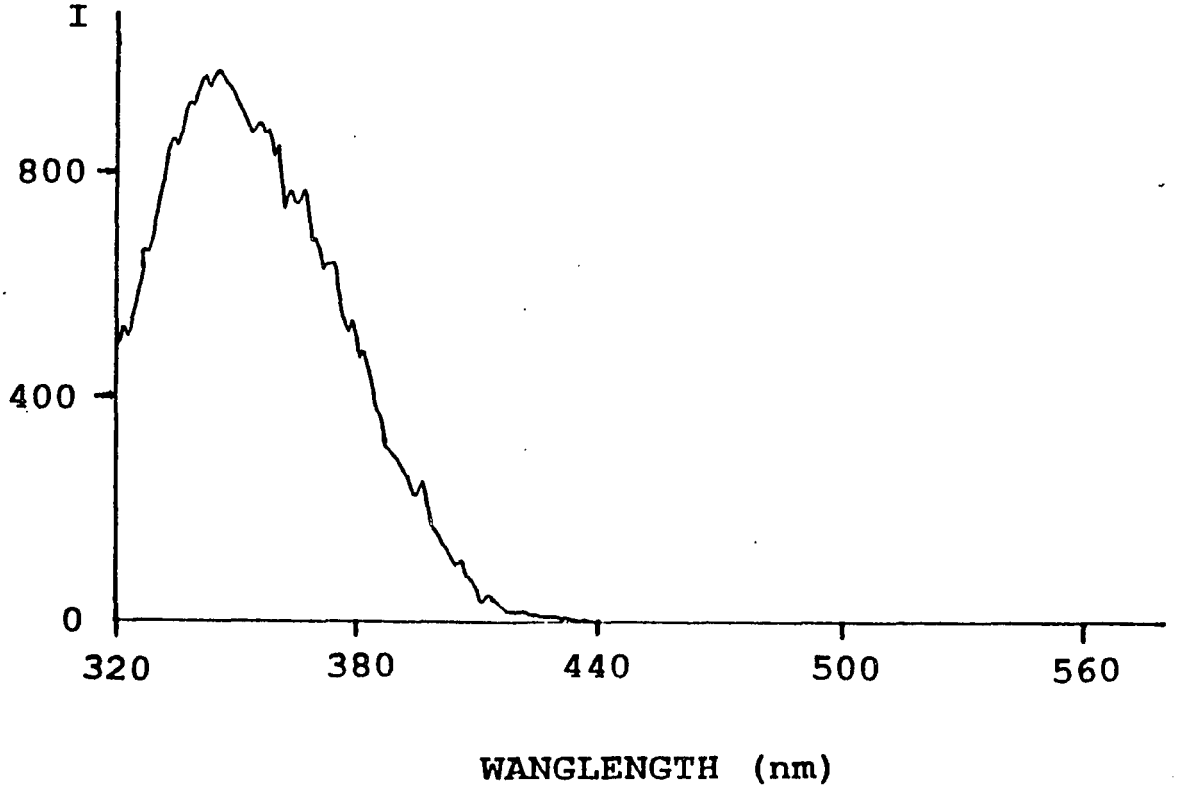

Figure 4.34. Steady state emission fluorescence spectrum from trypsin EDTA excited at 300nm.

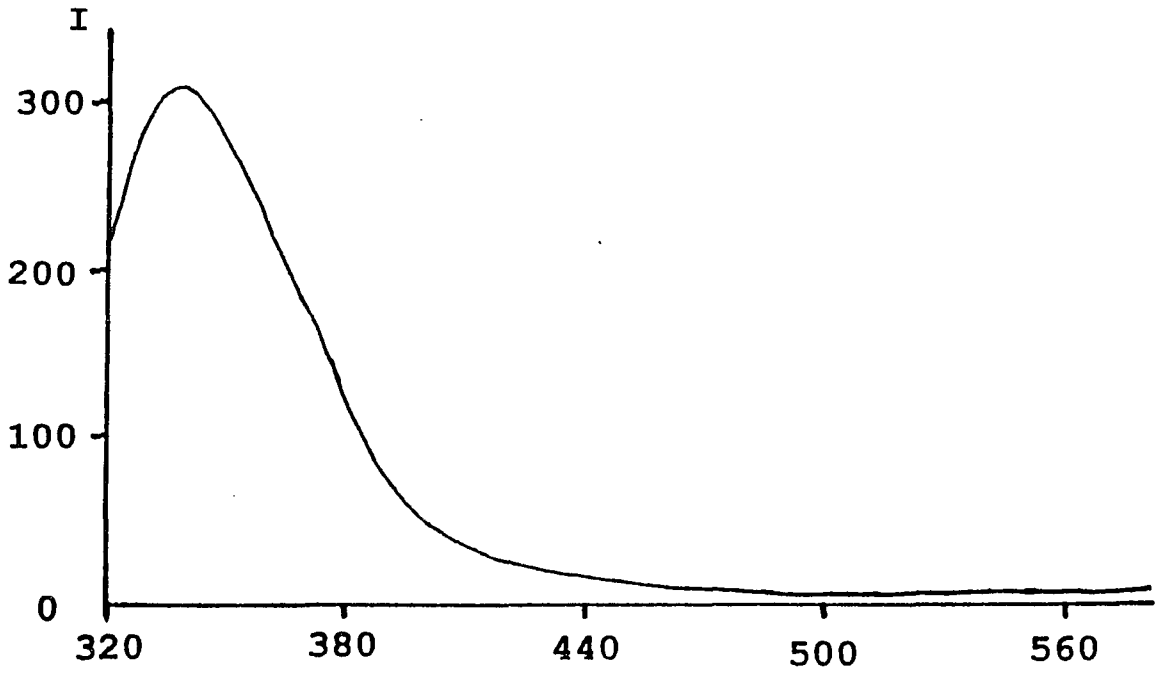

Figure 4.35. Steady state emission fluorescence spectrum from human normal breast cell line ATCC HTB125 excited at 300nm.

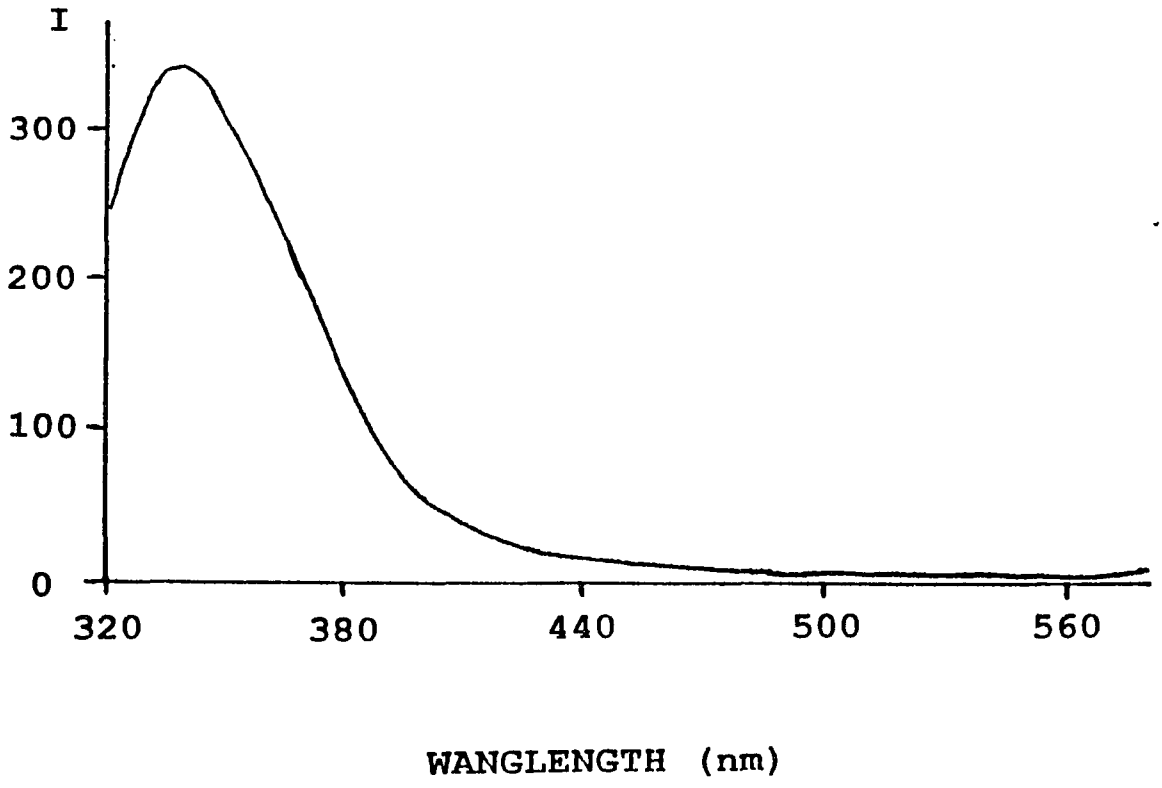

Figure 4.36. Steady state emission fluorescence spectrum from human cancerous breast cell line ATCC HTB126 (ductal carcinoma) excited at 300nm.

A shoulder appears in the spectra of the tissues in the longer wavelength around 450nm (see Chap. 5.3) which dose not appear in the spectra of cells. That suggested the shoulder in the spectra of tissues might very well come from the emission of the collagen and elastin, or less possibly from NADH.

4.5. The Relative Steady-state Fluorescence Intensities from Collagen, Elastin, NADH and Flavins in the Malignant and Non-malignant Cells (Excited with 320nm).

As has been discussed in the Section C of the Chapter 1, the wavelength 320nm will be able to excite the fluorescence from collagen, elastin, NADH and flavins. Therefore, it is possible to compare the relative fluorescence intensities from those fluorophors in a single spectrum. Meanwhile, we also know that the cell samples contain less of the collagen and elastin than the tissue samples do. So the spectral information from the cells will also provide us with a base for analysis of the spectra from the tissues.

Experiments were also done on the Luminescence Spectrometer LS-50 (Perkin Elmer). The excitation wavelength was set at 320nm.

The fluorescence spectral profiles from the human normal cell line HTB125 and human cancerous cell line HTB126 and

HTB22 were almost all flatter at the shorter wavelength range from 360nm to 420 nm with the band peaking at around 450nm (Figures 4.37, 4.38 and 4.39). The intensities of the 450nm peaks from malignant cell line HTB126 (shown in the Figure 4.38) and HTB22 (shown in the Figure 4.39) were relatively higher than the 450nm peak from the non-malignant cell line HTB125 (shown in the Fig. 4.37). The flattened spectral structure at the shorter wavelength from 360nm to 420nm may be partially attributed to the small amount of collagen and elastin in the cell membrane and other weak fluorophors. The 450nm fluorescence peak may come from NADH in the cells. The fluorescence from flavins are not noticeable because the flavins absorbs quite a bit less at the wavelength 320nm. (see Figure 1.33) The results of the stronger 450nm peak from the cancerous cell lines HTB126 and HTB22 than from the normal cell line HTB125 suggest those the NADH fluorescence intensities from the malignant cell lines were relatively stronger then that from the non-malignant cell line. This result is consistent with the results from the fluorescence spectra excited with wavelength 353nm (see Chapter 4.3 for details).

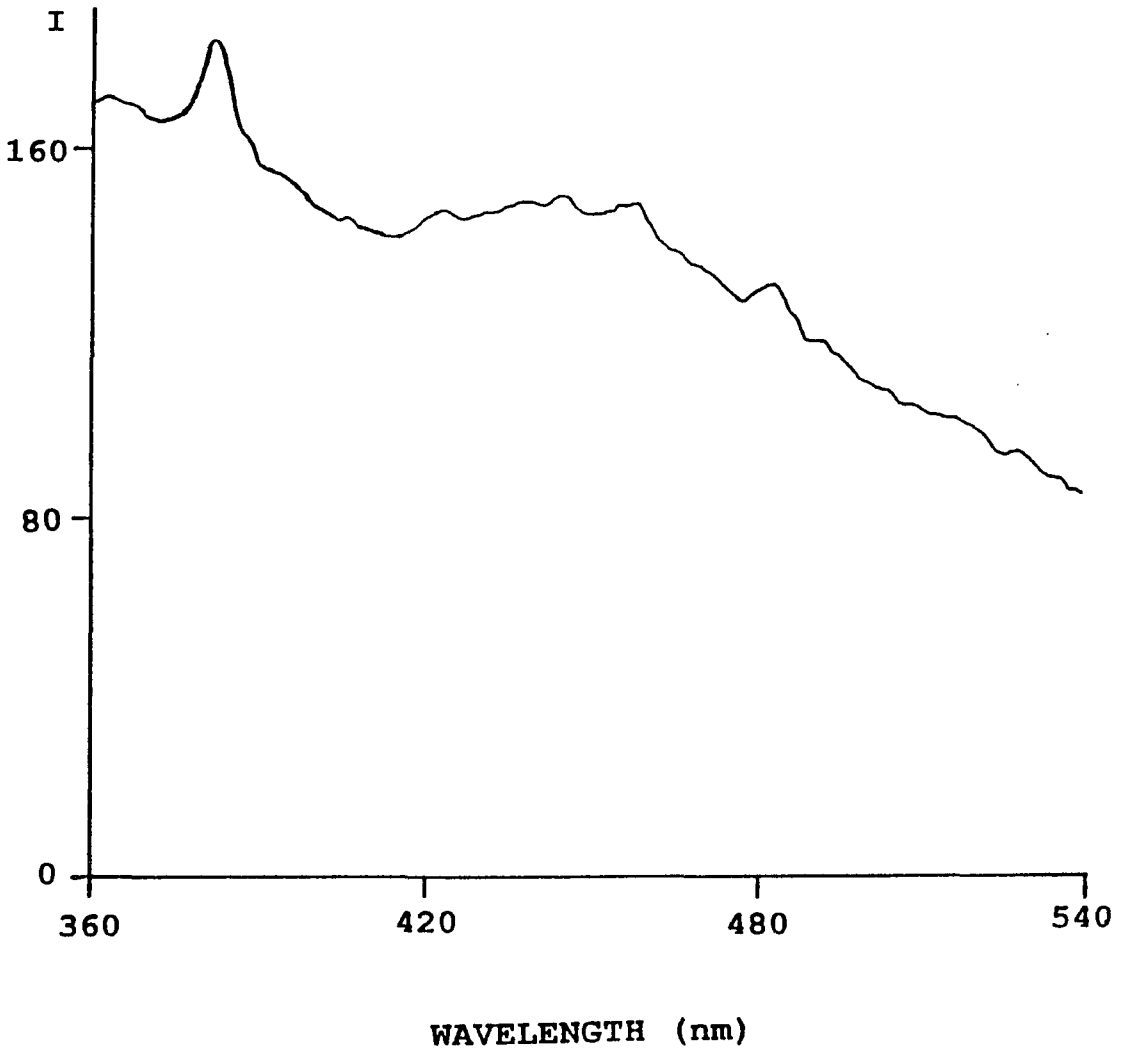

Figure 4.37. Steady state emission fluorescence spectrum from human normal breast cell line ATCC HTB125 excited at 320nm.

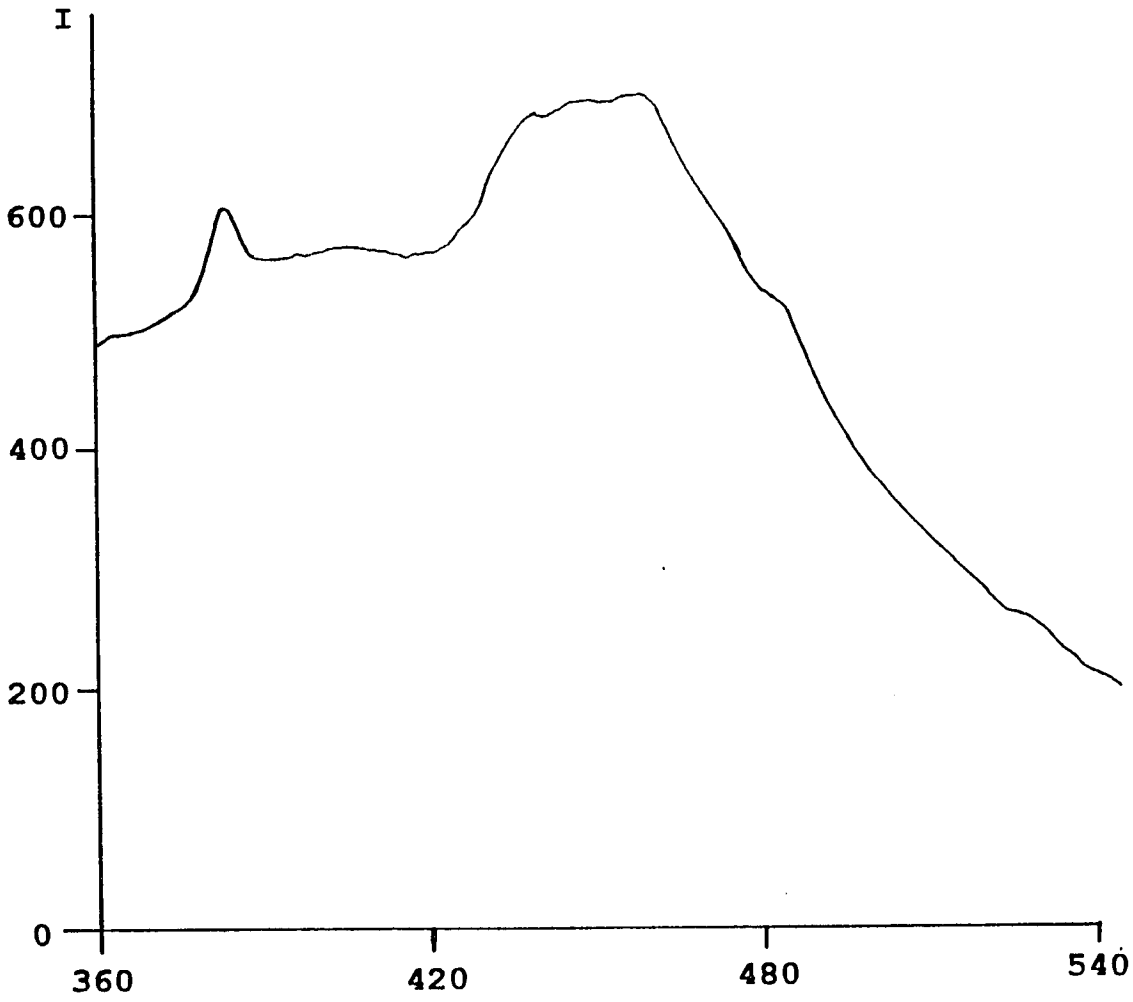

Figure 4.38. Steady state emission fluorescence spectrum from human cancerous breast cell line ATCC HTB126 (ductal carcinoma) excited at 320nm.

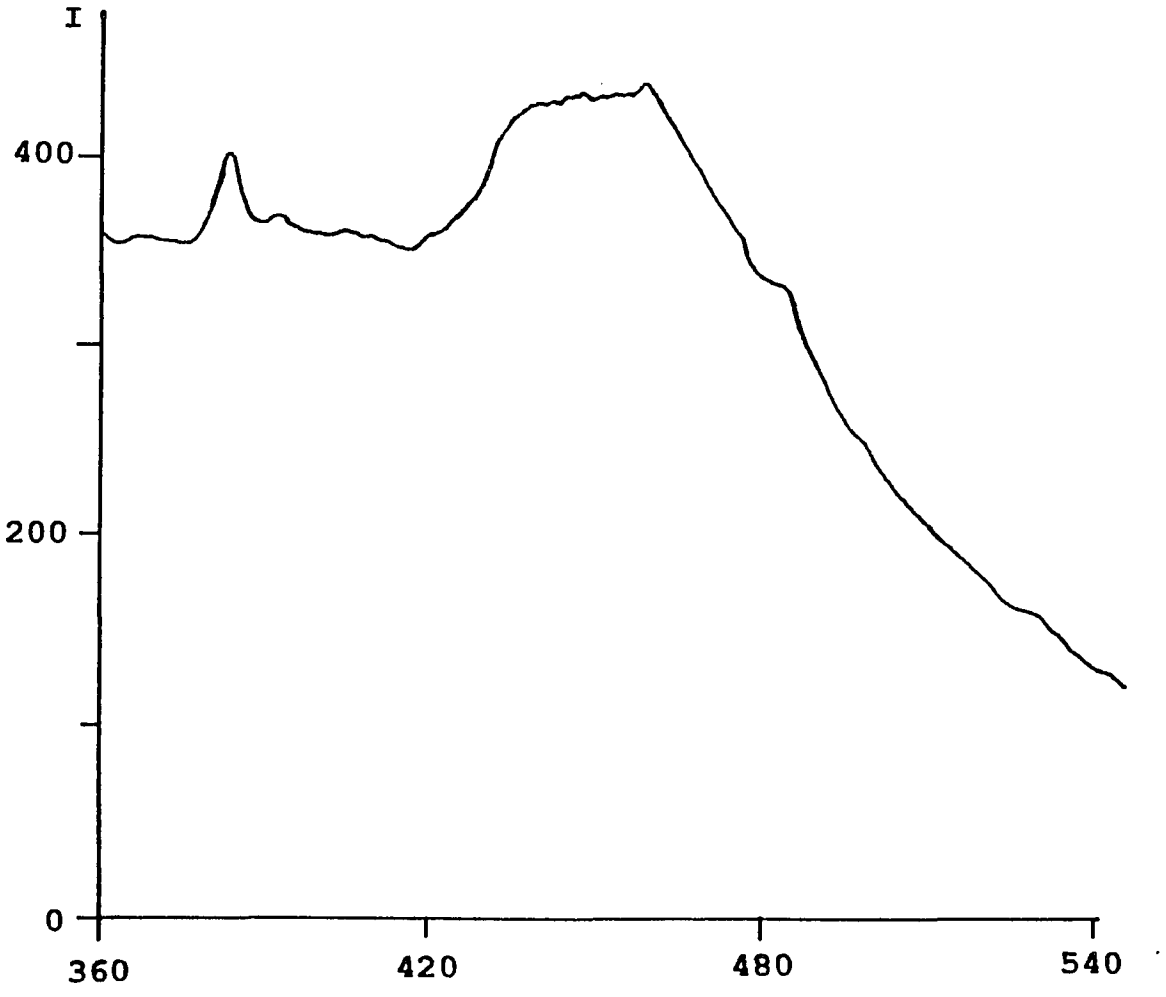

Figure 4.39. Steady state emission fluorescence spectrum from human cancerous breast cell line ATCC HTB22 (adenocarcinoma pleural effusion) excited at 320nm.

Chapter 5. Fluorescence from Human Malignant and Non-malignant GYN Tissues

It is important to study the fluorescence spectra from normal and diseased tissues because of its potential as an optical histochemical method for in vivo clinical applications. It is important to understand what spectral features are related to certain physiology changes during the malignancy. A numbers of study results, cited in Section A of the Chapter 1, have shown the great success of this LIF optical pathology method.

Although studying the fluorescence spectroscopies from malignant and non-malignant cells can give us a lot of basic information about the alteration of the cells from normal to cancerous (as it has shown in chapter 5), this spectral information may change because of the different optical properties of tissues and cells (see Section B of the Chapter 1 for details). Therefore, it is still important to study the LIF spectroscopies of the tissues, and analyze the spectra of the tissues along with the spectral information of the cells. My studies on fluorescence spectroscopy from malignant and non-malignant cells (presented in the chapter 4) provides a good base for analyzing the fluorescence spectroscopies of the

tissues. Since my colleagues at IUSL have been working on the human malignant and non-malignant breast tissues, my research concentrated on human malignant and non-malignant gynecological (GYN) tissues - in particular ovary, cervix, and uterus tissues. Some of my measurements on the GYN tissues were extended after their success on breast tissues, such as using the excitation wavelength 488nm and 300nm to distinguish the malignant and non-malignant human breast tissues.[10,11,14]

The early detection of cervix, uterus and ovarian cancers in women has long been a medical priority. Over the years, mortality rate for these types of cancers have been high[83]. This is partly attribute to the inefficiency of the medical techniques currently available and used to detect these forms of cancers. The technique most often used for cervix cancer is the PAP test. It is helpful, but it is a complicated process with a high degree of failure (about 70% effective). Ovarian and uterus cancer are more difficult for doctors to discern due to the position of the cancer, and they often remain undiagnosed until the tumor becomes an obvious growth. The subsequent surgical procedure used to treat this type of cancer is often inadequate. The surgeon is frequently unable to remove all cancerous tissue. This leads to a high level of recidivism among the cancer patients, and a very low long term survival rate. A new and more effective method is needed to detect and treat the cancers. The light induced fluorescence

spectroscopy may just provide the help to detect gynecological neoplasms.

As I have cited in the section C of the chapter 2, there are several intrinsic fluorophors in the human tissues. Their fluorescence cover from UV to visible wavelength range (see Figure 1.32). Various excitation wavelength can excite these fluorophors in various ways (see Figure 1.33). Since these fluorophors are playing important roles in the biological system, especially tryptophan, NAD and flavins, their fluorescence spectroscopy from tissues may reveal the states of the tissues. It is also important to remember that there are various amounts of blood residue in the tissues. Their existence can complicate the fluorescence spectral profiles.[72]

5.1 Tissue Samples

The tissue samples used in my studies are <u>in vitro</u> tissues. Malignant and non-malignant tissue samples for fluorescence study were supplied by Dr. S.Lubicz (Gynecologist and Oncologist). They were obtained at the time of diagnostic or therapeutic procedures from patients with benign or malignant neoplasms. A small portion of each sample was separated. Most parts of the sample were submitted to the department of pathology to be evaluated through standard pathology test methods. A small portion was sent to us for

fluorescence spectral analysis study. We were later informed of the pathology result.

The tissue samples which were used in the experiment were non-chemical treated and fresh tissues. The time between the tissue being removed and the fluorescence experiment was between six and forty eight hours because of transportation and equipment availability. The tissues were stored at 4°C. A series of experiments were carried out to check the repeatability of the spectra of the tissues versus the tissues' in vitro time. The results show very few spectral changes occurred during this period of time (see Figure 5.1, 5.2, and 5.3)

The pathology test was done as standard procedure. The steps, according to the pathologist, are listed below.

1) all tissues are fixed in Formalin 10% and then treated in alcohol (2 steps).
2) all tissues are dehydrated in absolute alcohol and then treated in Xylene (8 steps).
3) all tissues are placed in cassettes and embedded in Paraffin blocks (3 steps). Depending on the size of the samples, small or large, the short (4 hours) or long (14 hours) processing method is used.
4) in order to obtain the histologic slice, the blocks are placed on ice trays and with a microtome slice of 3-5 microns are obtained and placed on

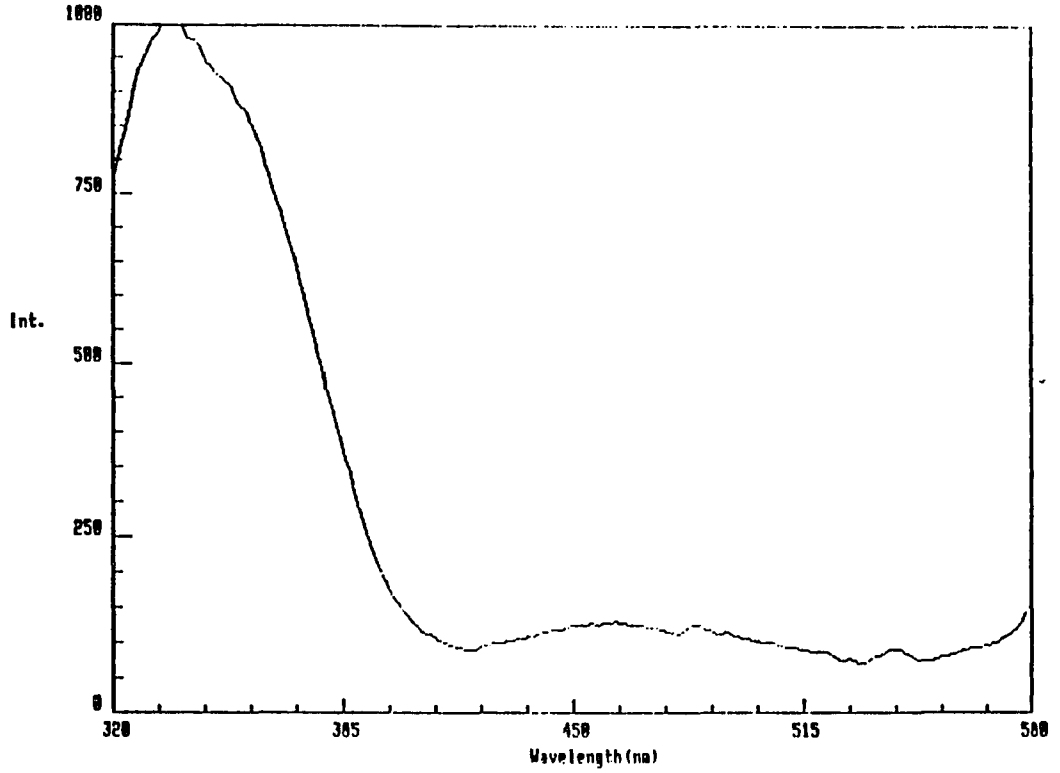

Figure 5.1 Fluorescence spectrum from a tissue A at approximately 20hr after removed from the patient.

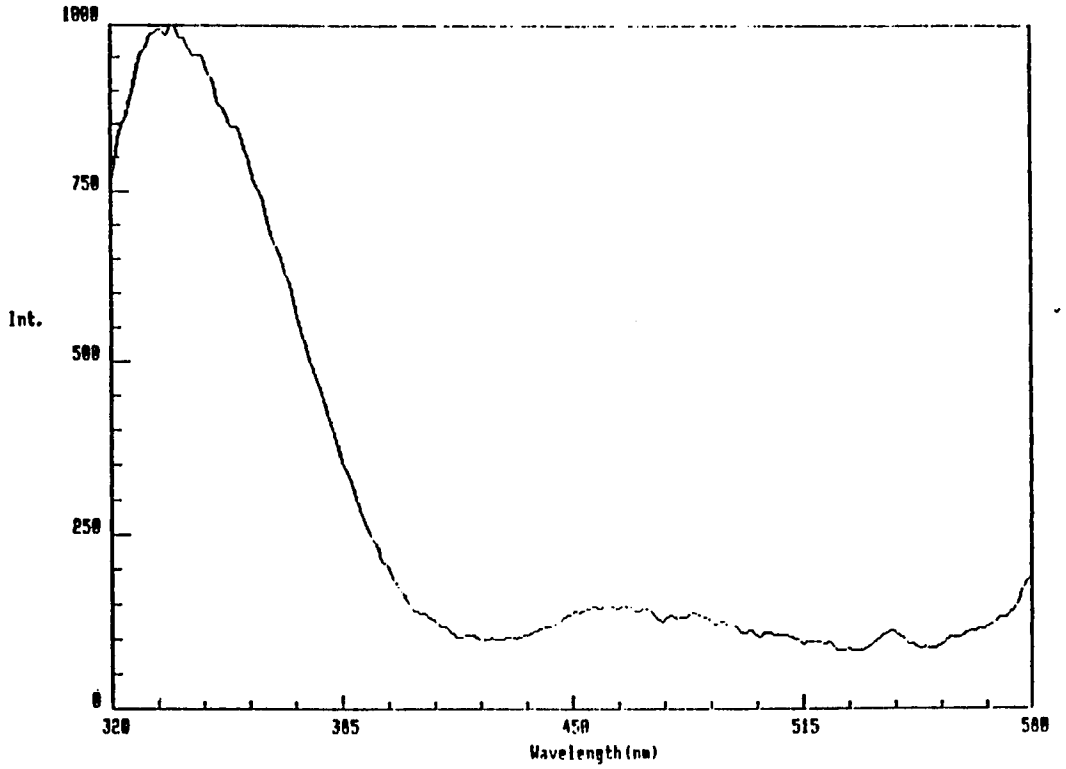

Figure 5.2 Fluorescence spectrum from the tissue A at time approximately 26hr after removed from the patient.

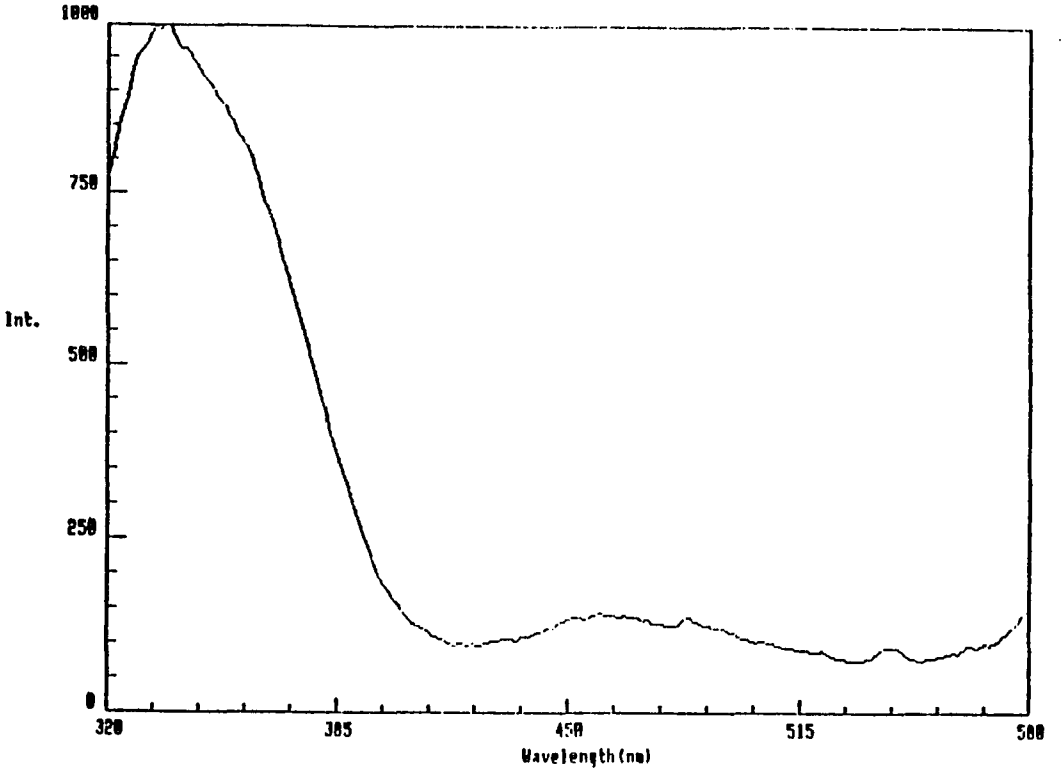

Figure 5.3 Fluorescence spectrum from the tissue A at time approximately 44hr after removed from the patient.

microslides.

5) the slides are then stained with Hematoxylin/Eosin (21 sequences are involved in this procedure).

6) as a final step the stained slides are mounted (cover slip and mounting solution)

Most of these steps are performed by automatic systems. The most common staining method used is the HE (Hematoxylin-Eosin). At this point the pathologist will study the slides with a microscope to determine the HS state.

5.2 Steady State Fluorescence From Tissue Primary by Flavins In 500-700nm Range

My research started by using 488nm laser excitation and measuring fluorescence in the range 500nm to 700nm. It is known that the intrinsic fluorophor flavins (oxidized form: FAD, FMN, riboflavin) give rise to fluorescence in the range of 520nm and absorption around 450nm and 375nm (Fig. 1.27)[64]. It is know that the fluorescence from cells in the wavelength range from 500nm to 600nm are mostly from flavins[71]. According to the absorption spectrum of the flavins (Figure 1.27) and others (Figure 1.33), one can excite the flavins but not others in the tissues with the excitation wavelength 488nm from the argon laser, which is in our laboratory.

This study is concentrated around the fluorescence emission spectra from the malignant and non-malignant GYN tissues at the 500 to 700nm range, which is excited by the argon laser line at 488nm. The fluorescence spectra from the flavins in the malignant and non-malignant tissues may be modified by the different environments around the flavins in these two types of tissue. My colleagues have done extensive work and found that there are fluorescence spectra differences between the normal and cancerous human breast and lung tissues with the excitation wavelength at 488nm[10, 11]. I wanted to see if the spectral differences also exist in the GYN tissues. I also thought it is important to study what is responsible for these differences.

The experiment setup is described in the chapter 4.1. The laser power was around a few milliwatts. The tissues were placed in a glass tube with 1cm diameter for the measurement.

There are 11 malignant and 11 non-malignant uterus (endometrium) tissues and 5 non-malignant and 6 malignant ovary tissues investigated with the excitation wavelength 488nm. The typical spectrum from non-malignant and malignant endometrium tissues are shown in Figures 5.4 and 5.5. The non-malignant endometrium tissues were mostly shown as one major band with peaking at 516$\pm$5nm and two subbands with peaks at 558$\pm$5nm and 599+5nm. The two dips occur between the adjoined peaks at 545+10nm and 580+10nm. The malignant

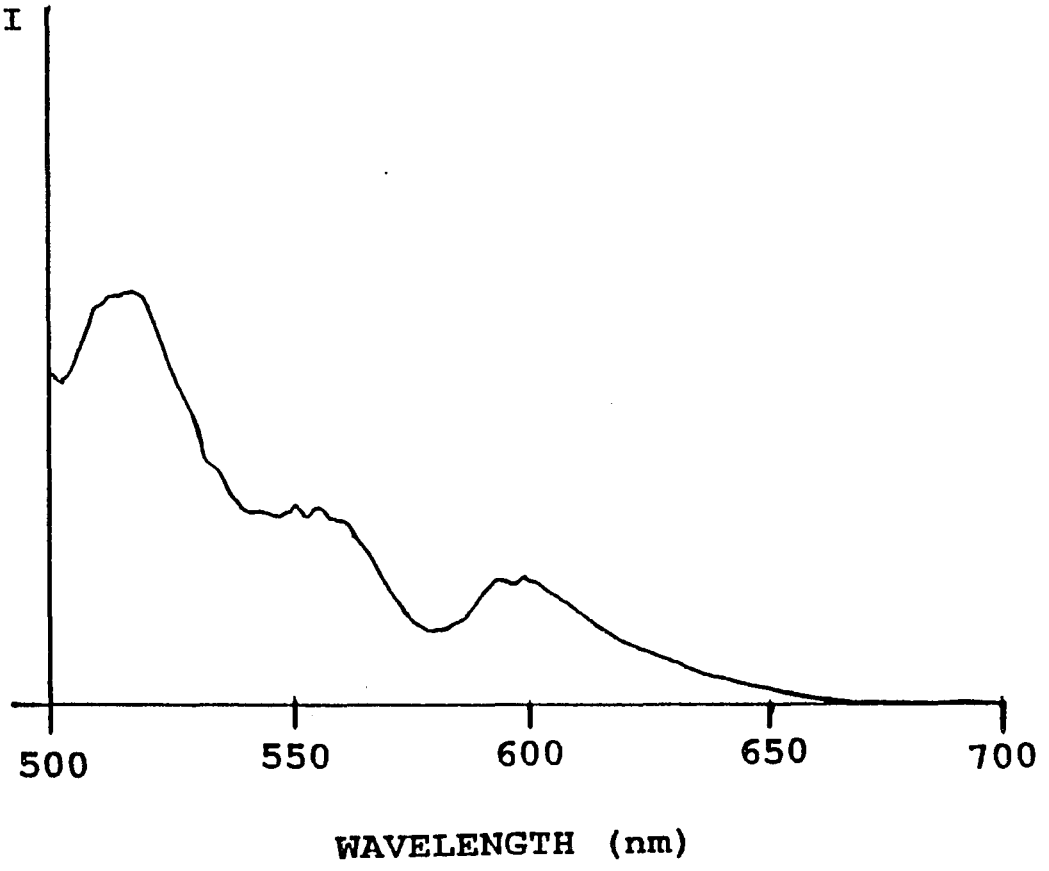

Figure 5.4. Steady state emission spectrum form human normal uterus (endometrium) tissue in vitro excited at 488nm.

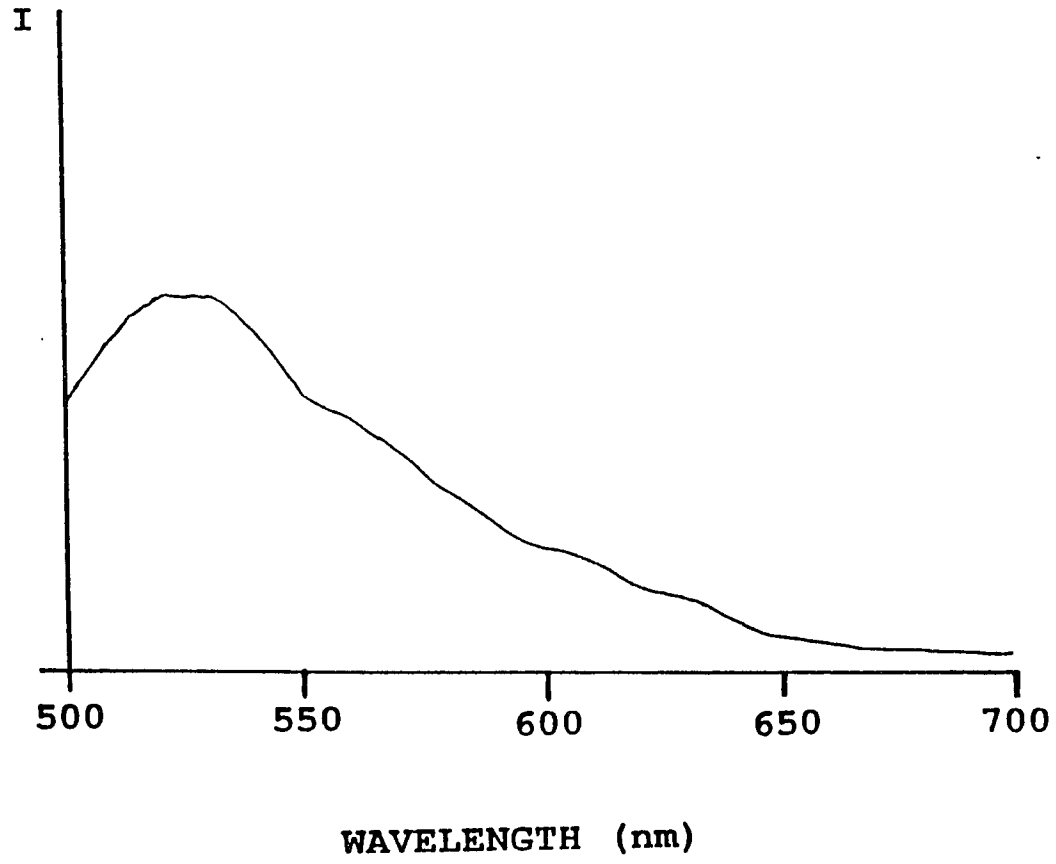

Figure 5.5. Steady state emission spectrum from human cancerous uterus (endometrium) tissue in vitro excited at 488nm.

Table 5.1. Statistic results on malignant and non-malignant uterus (endometrium) tissues when excited by 488nm.

Sample Name	Number	Smooth Curve	Complex Curve
Normal Tissue	11	3	8
Tumor Tissue	11	9	2

Negative	False Negative	Positive	False Positive
8	3		
		9	2

Specificity (True Negative)	Sensitivity (True Positive)	False Negative	False Positive
0.73	0.82	0.27	0.18

endometrium tissues mostly showed one band simple profile with peak at 525±10nm. The statistical results are shown in Table 5.1. The typical spectra for cervix tissues are shown in Figure 5.6 and 5.7. The non-malignant cervix tissues mostly showed as one major band with peaking at 514±5nm and two subbands with peaks at 558±5nm and 596+5nm. The two dips occurring between the adjoining peaks were at 545+10nm and 580+10nm. The malignant cervix tissues mostly showed one band simple profile with peak at 531±10nm. The statistical results are shown in the Table 5.2.

In Tables 5.1 and 5.2, the **sensitivity** (also called **true positive**) is defined as the percentage of the malignancy detection in agreement with the pathologic report. The **false negative** is defined as the percentage of the malignancy detection which does not agree with pathologic report. The **specificity** (also called **true negative**) is defined as the percentage of the non-malignant detection in agreement with pathologic report. The **false positive** is defined as the percentage of the non-malignant which does not agree with the pathologic reports.

The statistical results show about 75% success of the distinguishability of the spectral differences between the spectra of the non-malignant tissues and malignant tissues of both kinds.

The typical spectra (Figure 5.8) from malignant ovary tissues shows a simple profile with one peak at 525±5nm. The

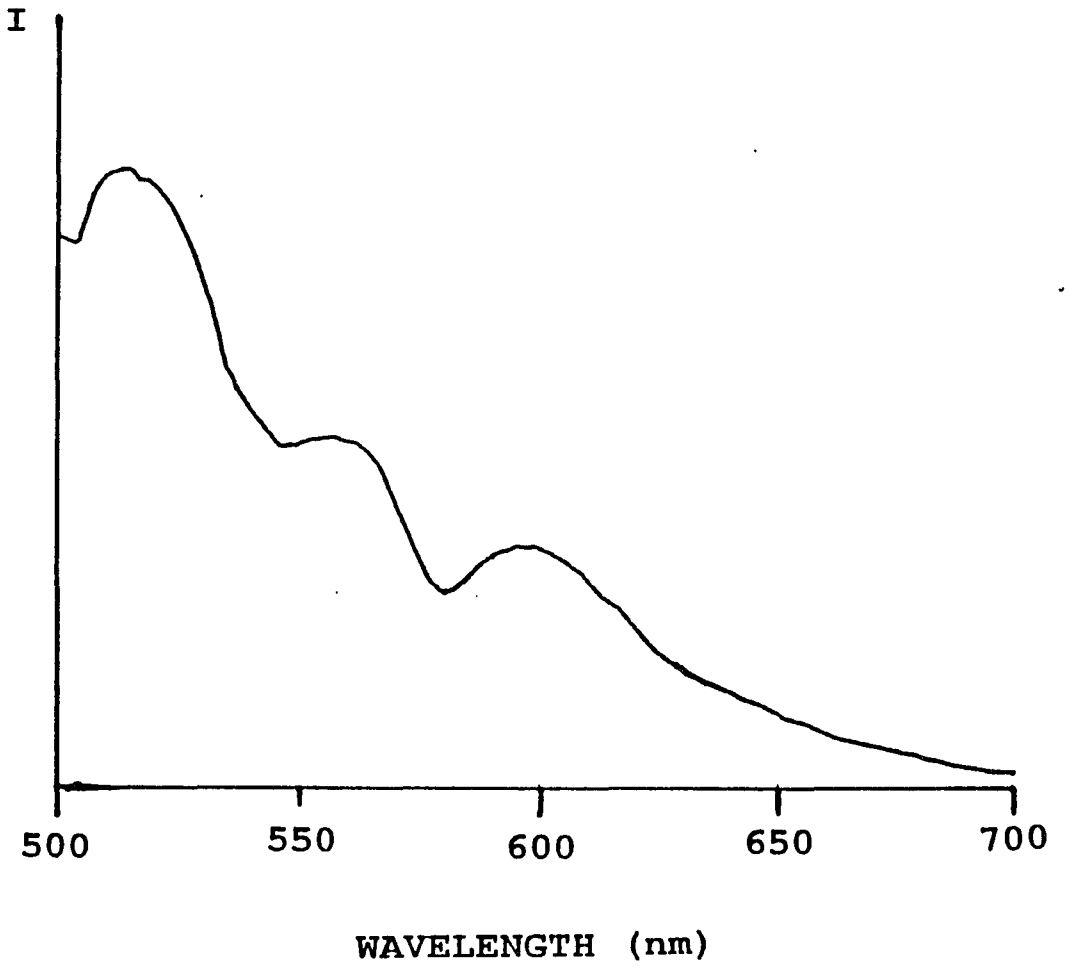

Figure 5.6. Steady state emission spectrum from human normal cervix tissue in vitro excited at 488nm.

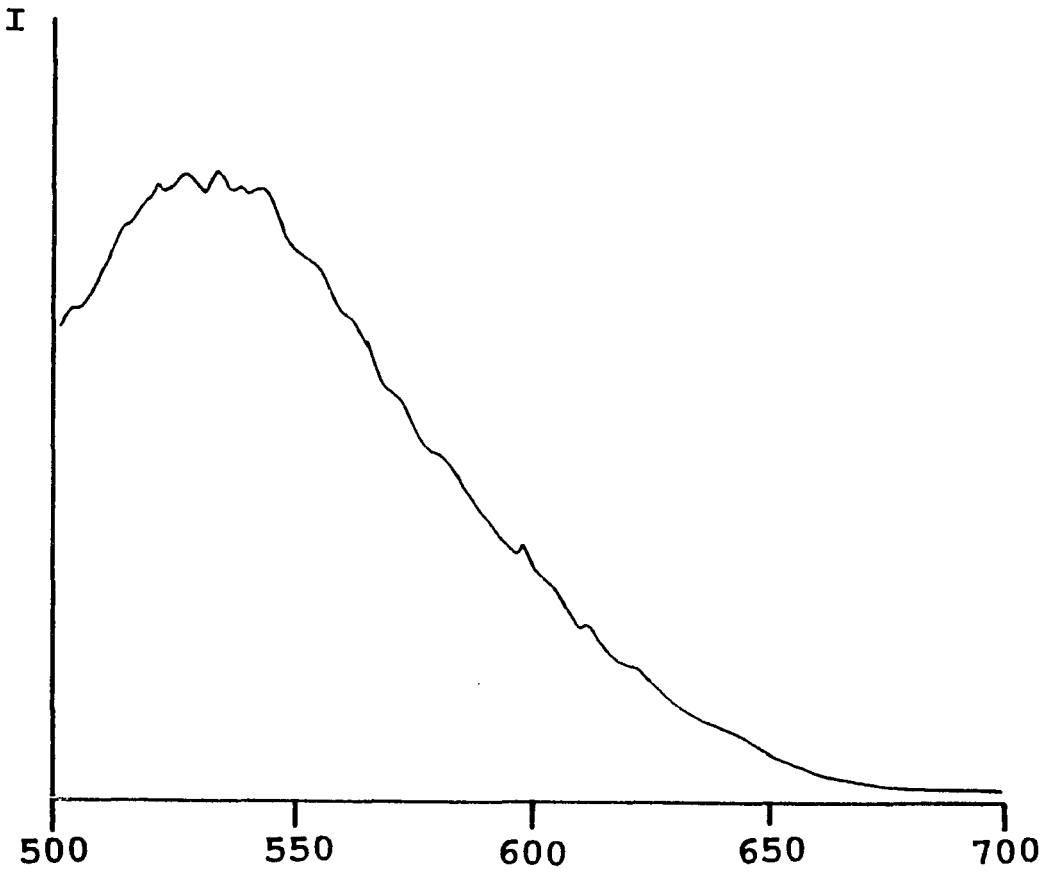

Figure 5.7. Steady state emission spectrum form human cancerous cervix tissue in vitro excited at 488nm.

Table 5.2. Statistic results on malignant and non-malignant cervix tissues when excited by 488nm.

Sample Name	Number	Smooth Curve	Complex Curve
Normal Tissue	5	1	4
Tumor Tissue	6	4	2

Negative	False Negative	Positive	False Positive
4	1		
		4	2

Specificity (True Negative)	Sensitivity (True Positive)	False Negative	False Positive
0.8	0.67	0.2	0.33

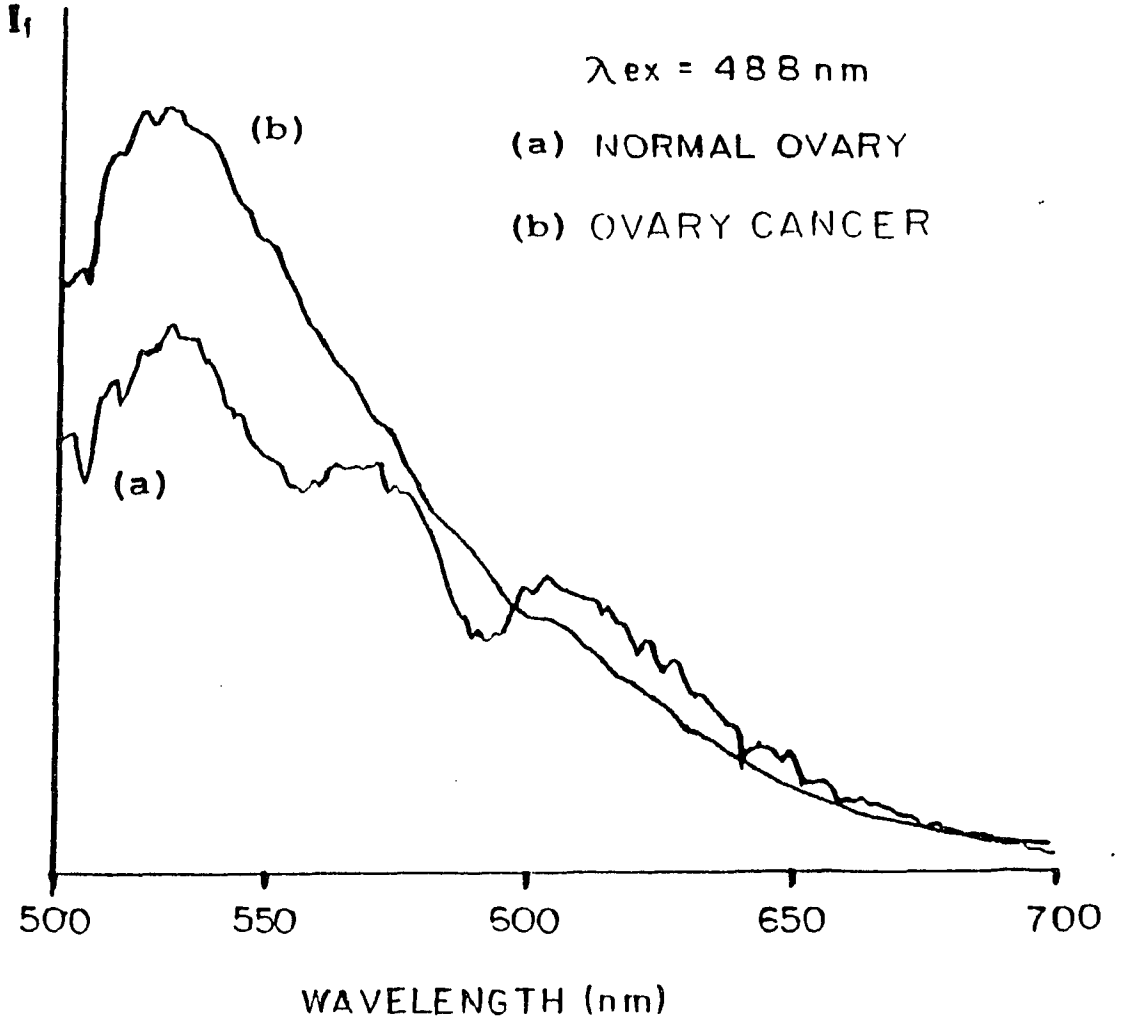

Figure 5.8. Steady state emission spectrum from human normal and cancerous ovarian tissues in vitro. The normal tissue spectrum is from the one of the selected fresh human normal ovary tissue in vitro measured before the extraction of interstitial medium. Excitation wavelength is 488nm.

typical spectra (Figure 5.8) from non-malignant ovaries show complex profiles with a major band peak at 528±5nm and two sub-peaks at 570+5nm and 610+5nm. The dips between the peaks are located at 560±5nm and 590±5nm. Four out of five investigated malignant tissues have a one peak smooth spectral profile. And both investigated non-malignant tissues had a one peak with two sub-peaks complicated spectral profile.

The above results were similar to those results, obtained from rat and human malignant and non-malignant breast tissues and lung tissues, found by my colleagues[9,10,11]. The big question is what physiologic changes in in vitro malignant tissues are related to the fluorescence spectral changes. The coincident between the spectral dips position and the blood absorption peaks position[53] tells us it is possible that this difference was caused by the secondary absorption of the blood residue in the tissues.

Experiments and calculation which carried out by me and my colleagues supports this blood residue reabsorption model. The experiment used the NH_4Cl solution to extract the blood residue in the fresh normal tissues, continuing to measure the fluorescence spectra during certain time periods.[12] A self absorption model has been used to calculate the blood residue absorption effect on the one band simple spectral profile which comes from the malignant tissues.[72] The results agree with the blood reabsorption assumption.

Tissue is composed of cells, connective proteins, and interstitial medium (which include water and blood, vitamins, etc.). The fluorescence spectra from human normal and cancerous cells shows that they bear the same kind of spectral profile as flavins' spectrum with one band in spite of the slight differences in the shape and peak position (see Chap. 4.2 of this thesis). Is it something different around the cells which causes the spectral differences?

The flavin molecules exist inside and outside of the cells[84]. By extracting the interstitial medium out of the fresh tissues and then measuring the fluorescence spectra from the dried tissue and the interstitial medium, it may reveal which part of the tissue is responsible for the complex spectral profile from the non-malignant tissues.

The experiment is performed in the following procedure.

1) Fluorescence spectra (used same experimental setup as described in Chap. 3.1) was measured from a fresh normal ovary tissue (shown in Figure 5.8).
2) Interstitial medium and dried tissue were obtained by the following process: put a fresh normal tissue (after measure its fluorescence spectra) on the top of a screen inside the sterilized falcon tube (Figure 5.9), then centrifuge it about 8 min. The centrifuge force will force the interstitial medium to flow down and the screen will keep the dried tissue up.

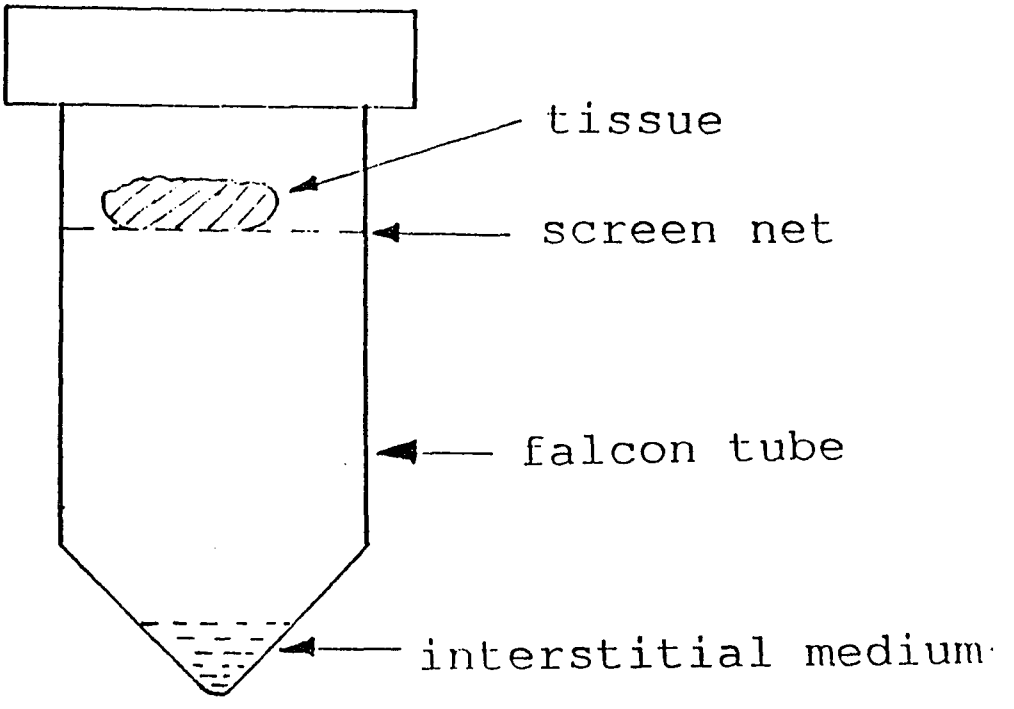

Figure 5.9. The diagram of the experimental set up for extracting the interstitial medium from the tissue <u>in vitro</u>.

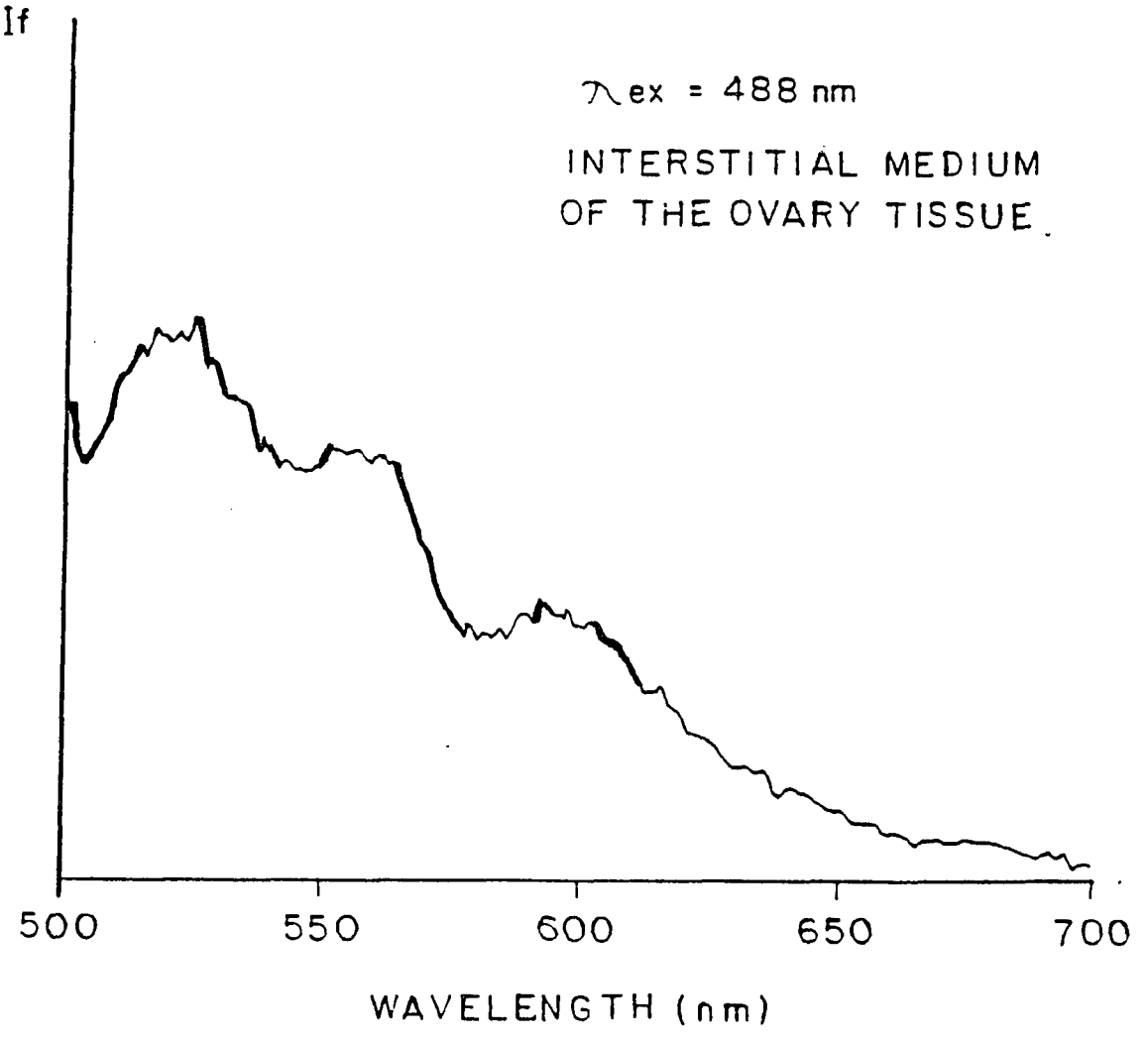

Figure 5.10. Steady state emission spectrum form the interstitial medium extracted from the selected fresh human normal ovary tissue in vitro. Excitation wavelength is 488nm.

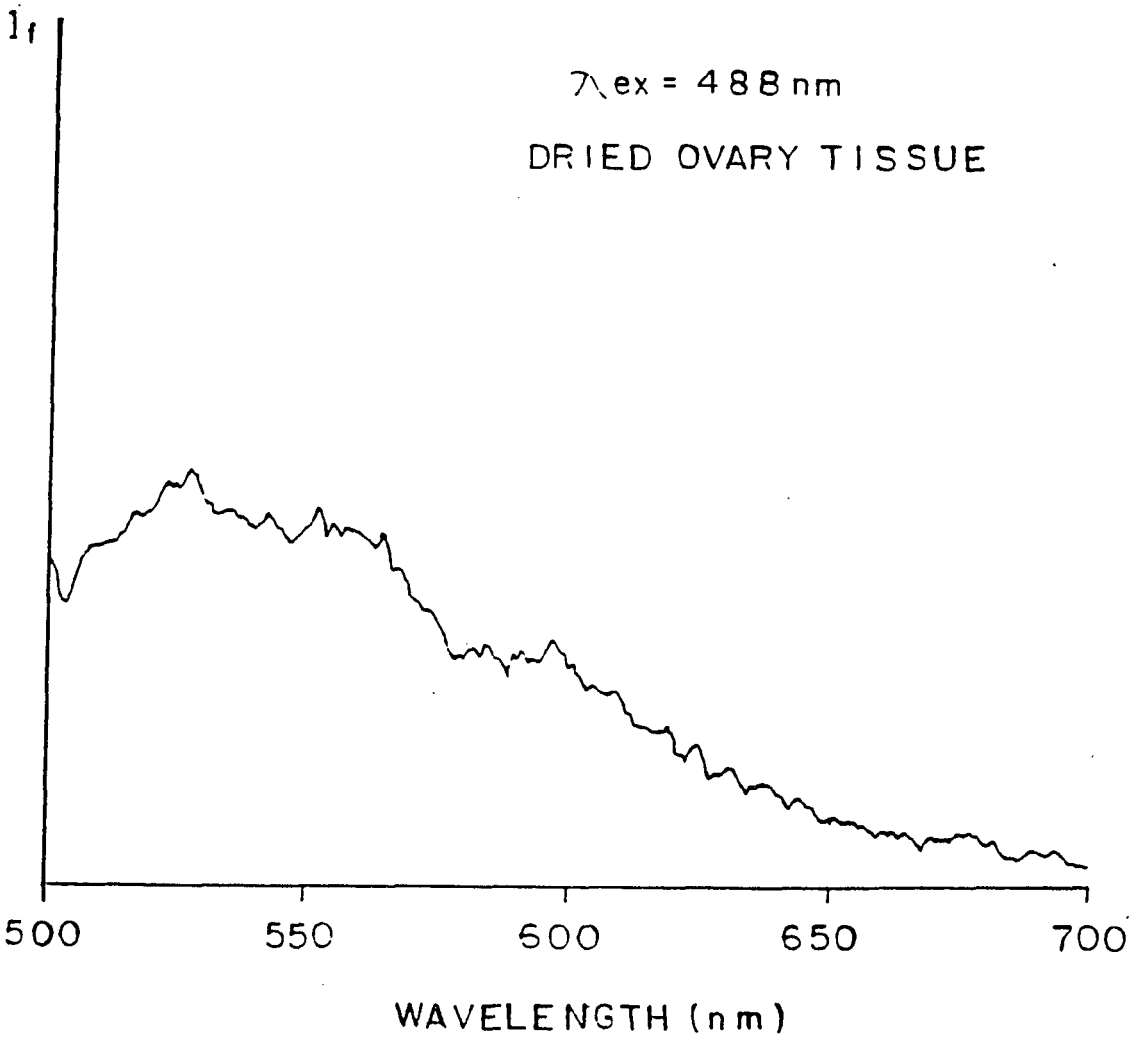

Figure 5.11. Steady state emission spectrum form the dried tissue after the interstitial medium has been extracted from the selected fresh human normal ovary tissue in vitro. Excitation wavelength is 488nm.

3) Fluorescence spectra from the dried tissue and the interstitial medium were measured.

The experimental results showed that the interstitial medium gave almost the same profile as the fresh tissue did (Figure 5.10 and Figure 5.8), but the dry tissue gave a profile which showed intent to change from complex to smooth (Figure 5.11). This is because the blood residue in the dried tissue will be less than that in the fresh tissue after a lot of blood residue flows out with the interstitial medium. In that case, the dip in the dried tissue should be less deep, and the interstitial medium may about the same as the fresh tissue. These results point out that it is the interstitial medium which is responsible for the complex profile of the normal tissues. Blood residue might be modifying the flavin's spectrum to make the spectra profile complex.

It seems the complex fluorescence spectra profile arise mostly from non-malignant tissues and are caused by modification by other molecular groups on the flavins fluorescence spectra profile-- possibly by hemoglobin in the blood. The fact that most malignant tissues showed one peak profiles and most non-malignant tissues showed complex profiles suggests that there was more blood residue in the normal tissues <u>in vitro</u> than in the cancerous tissues <u>in vitro</u>.

5.3. The Relative Steady-state Fluorescence Intensities mostly from Tryptophan, Collagen, Elastin and NADH in the malignant and non-malignant tissues.

As discussed in section C of chapter 2 (page 22), it is known that tryptophan gives a very strong fluorescence emission spectrum centered around 350nm and has an absorption peak around 275nm[56]. It is also known that the fluorescence peak is blue shifted to 340nm when the tryptophan is bound.[57, 59] The collagen fluorescence emission is centered at 390nm with excitation spectral peak at 350nm and the elastin fluorescence emission is centered at 420nm with excitation spectral peak at 335nm. These two fibre proteins give weaker fluorescence relative to tryptophan. Tryptophan is a very basic molecular in forming proteins. It has been known for years that abnormal tryptophan metabolism occurs in patients with cancer.[85]

It is difficult to compare the absolute fluorescence intensities of the tryptophan between malignant and non-malignant tissues because the tissues in vitro come with different sizes and contain different amounts of blood. Wavelength 300nm is at the longer wavelength edge of the absorption spectrum of the tryptophan (See Fig. 1.5) and at the shorter wavelength edge of the excitation spectrum of collagen and elastin (See Figures 1.15 and 1.18) as well as NADH (see Figure 1.22). These facts make 300nm a good choice

as excitation wavelength for comparing the relative fluorescence intensities between the tryptophan, collagen, elastin and NADH.

My colleagues first successfully used this method to distinguish human malignant and non-malignant tissues.[14] Intensity at 340nm is picked to represent the intensity of tryptophan. Intensity at 440nm should be picked[14] to represent the emission of collagen and elastin instead of using 390nm to 420nm. This is because of the same absorption coefficient of the blood at 340nm and 440nm.[53] The ratio I(340nm)/I(440nm) should reveal if there is any difference in the intensity of tryptophan fluorescence relative to the intensity of the other molecules between malignant and non-malignant tissues, with the least blood residue affection.

The experiment was carried out on the Luminescence Spectrometer as described in the Chapter 3.2 of this thesis. The tissue samples were placed in the 10 x 10 x 30mm^3 quartz curvatter (ESCO Co., Type Q-1) for the measurement.

The typical spectral profiles from malignant and non-malignant GYN tissues are shown in the Figures 5.12 and 5.13. They generally have a very strong band centered around 340nm and a weak band at around 460nm. The dip between the two bands are located at 420nm.

The band at 340nm is obviously from the emission of the tryptophan. The tail beyond 450nm should come from the

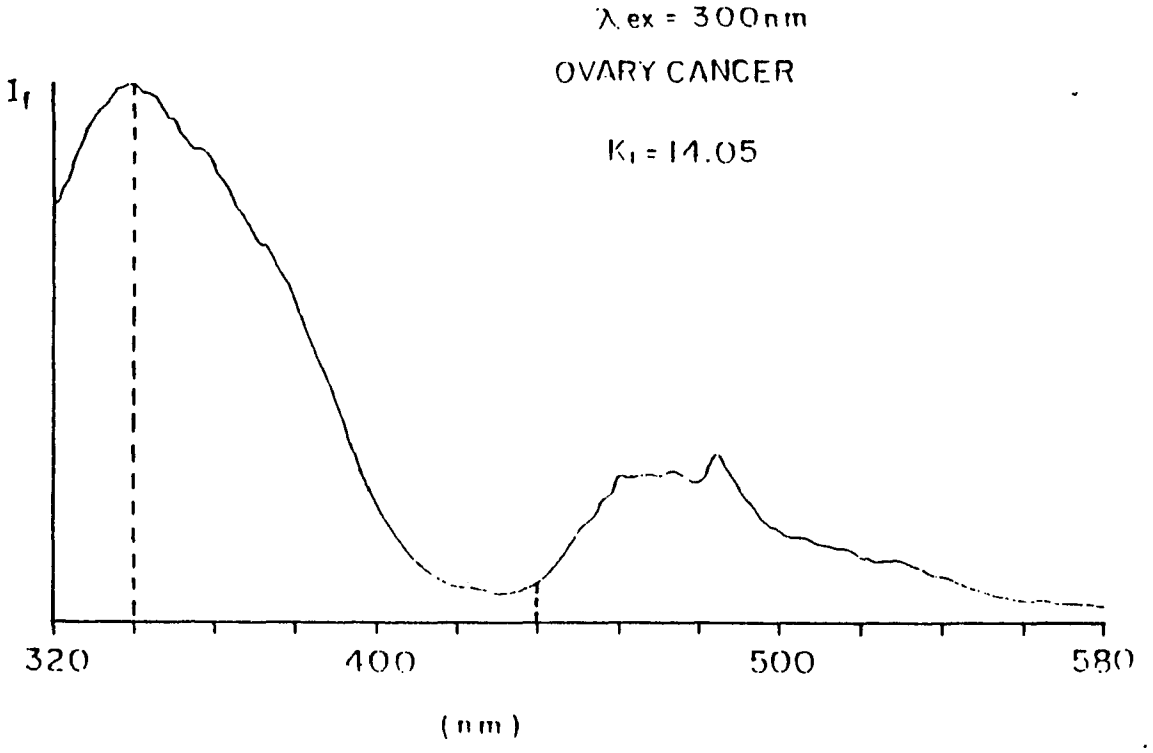

Fig. 5.12. Steady state fluorescence emission spectrum from human malignant ovary tissue <u>in vitro</u> excited at 300nm.

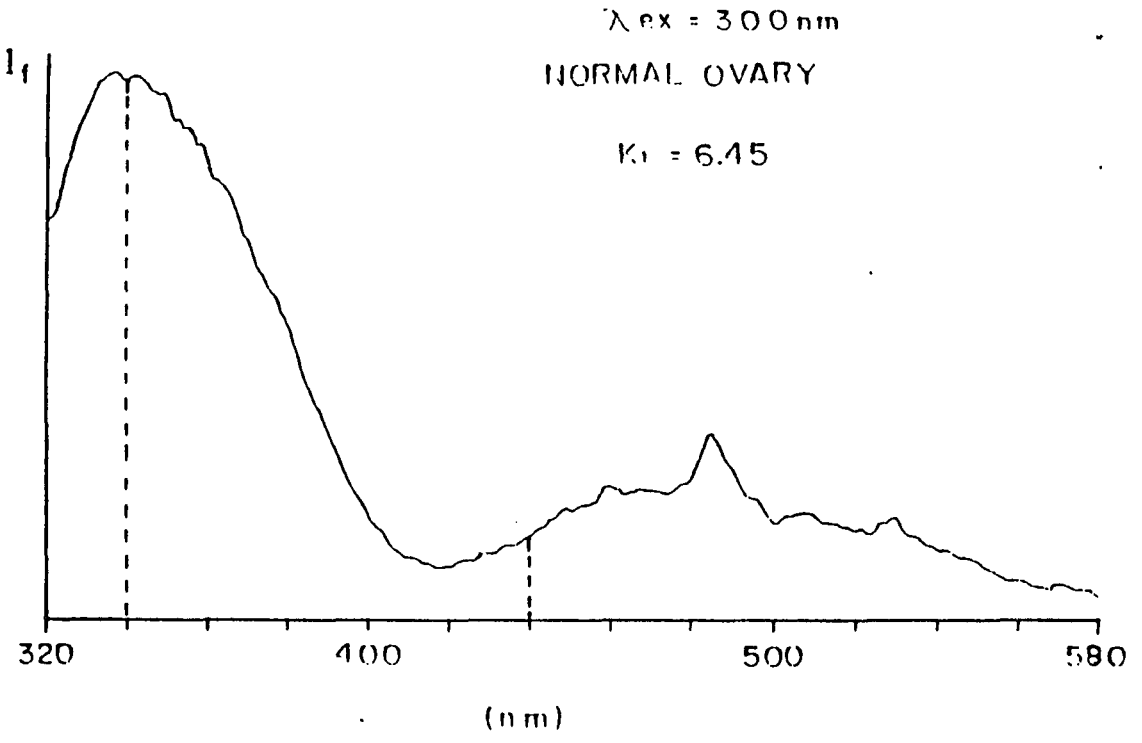

Fig. 5.13. Steady state fluorescence emission spectrum from human non-malignant ovary tissue <u>in vitro</u> excited at 300nm.

mixture emission of collagen, elastin and NADH. The dip at 420nm should be caused by the reabsorption of the blood residue because of the strong absorption peak at 420nm from the blood (see Figure 1.2). This absorption peak modulated the whole emission spectra. The appeared 460nm peak is partially due to this effect. The spectral part form 380nm an to 580nm from the tissues might be contributed by the collagen, elastin over the NADH. It is because the extra weak of this part of the structure in the fluorescence spectra from cells which are also excited by 300nm (see chapter 4.4 in this thesis). The ratio I (340nm) / I (440nm) minimizes the effects of the blood absorption (see two previous paragraphs for details).

Thirty four samples of the malignant tissue and eleven samples of the non-malignant tissue have been measured. Their ratio of the intensities K1 = I(340nm) / I(440nm) have been calculated. The results and the sample statistic results have been listed in Table 5.3. The relative histogram is shown in Figure 5.14. The result shows a fairly good cut at the ratio value K1 = I(340nm) / I(440nm) = 11.5. Thirty-one out of thirty-four of the malignant tissues have a ratio above this value. This gives a Sensitivity of 95%, False Negativity of 5%, Specificity of 93% and False Positiveness of 7%. (see chapter 5.2 for the definition of the Sensitivity, False Negativity, Specificity and False Positiveness)

Table 5.3 List of the measured ratio K1 values from malignant and non-malignant GYN tissues with excitation wavelength at 300nm (K1 = I(340nm)/I(440nm)).

Non-malignant Tissues	K1	Malignant Tissues	K1
Ovary	7.0	Endometrium	23.0
Cervix	11.0	Cervix	21.0
Ovary	6.5	Ovary	14.0
Cervix	7.6	Cervix	12.0
Cervix	10.4	Endometrium	12.0
Myometrium	7.6	Ovary	19.0
Uterus	5.4	Ovary	16.0
Myometrium	8.1	Endometrium	14.0
Cervix Benign	5.7	Cervix	12.0
Cervix Benign	5.8	Endometrium	35.0
Uterus	2.8	Ovary	35.0
Ovary	5.7	Endometrium	35.0
Uterus	9.5	Myometrium	35.0
Uterus	18.1	Ovary	35.0
		Endometrium	16.0
		Endometrium	29.0
		Ovary	33.0
		Uterus	20.0
		Endometrium	10.0
		Cervix	12.0
		Uterus	18.0
		Uterus	18.0
		Ovary	27.4
		Uterus	21.3
		Endometrium	12.4
continue to next page			

continue from front pege			
		Cervix	16.0
		Endometrium	8.4
		Ovary	20.1
		Myometrium	23.5
		Myometrium	18.45
		Uterus	22.2
		Endometrium	15.45
		Ovary	22.0
		Uterus	16.75
		Cervix	25.9
		Uterus	25.9
		Uterus	17.2
		Vagina	29.1
		Uterus	18.1
		ovary	25.8
		Uterus	24.8
Standard	< 11.5		> 11.5
False Negative			5%
False Positive	7%		
Sensitivity			95%
Specificity	93%		

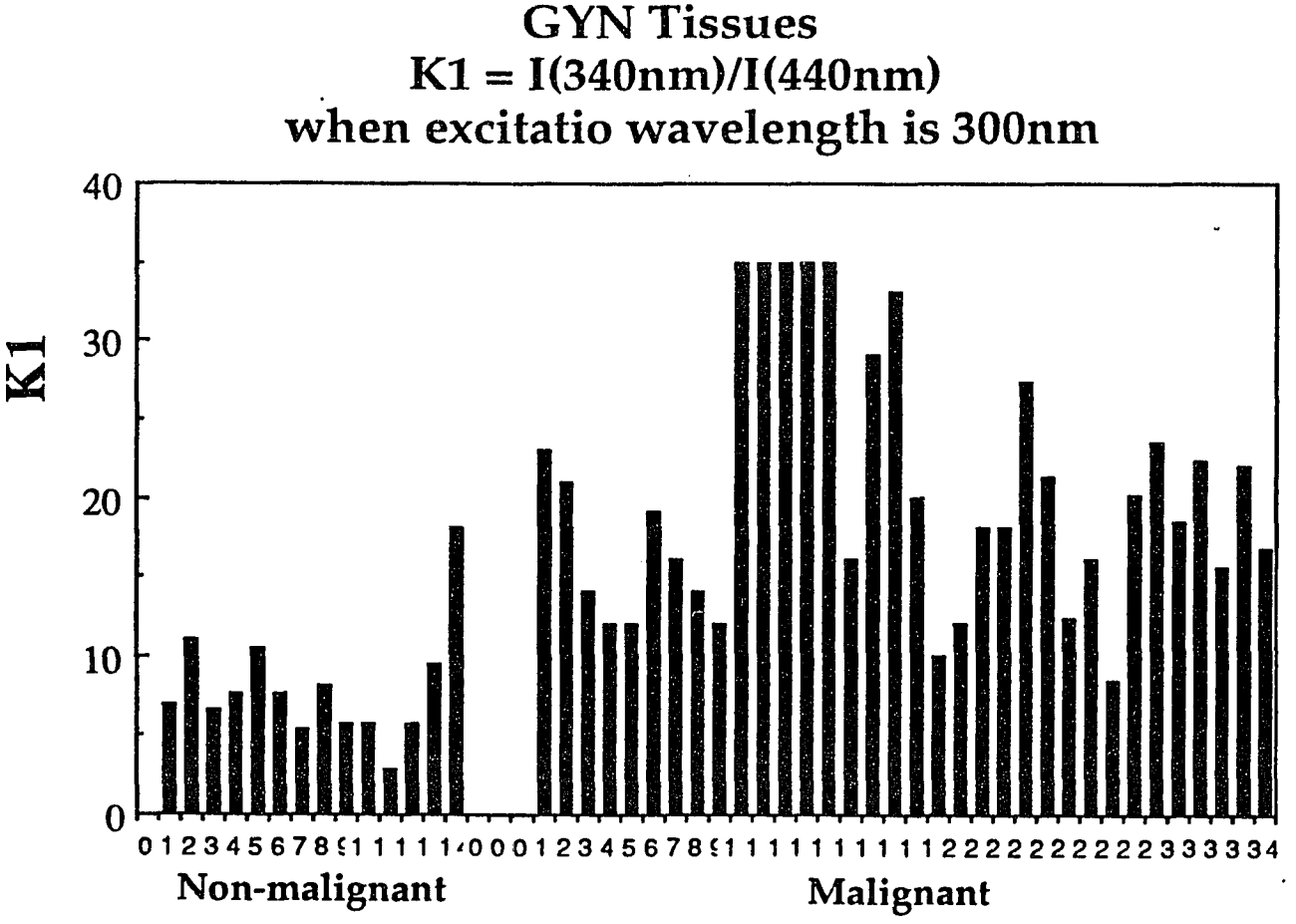

Fig. 5.14. Histogram of the fluorescence intensities ratio K1 [I (λ=340nm) / I (λ=440nm)] over the examined tissues in vitro with excitation wavelength at 300nm.

This result shows that the relative fluorescence intensities of the tryptophan over the collagen, elastin and NADH are relatively higher from malignant tissues than from non-malignant tissues. It is fairly consistent with the results obtained by my colleagues on the same kind study performed on human malignant and non-malignant breast tissues[14].

Medical studies have found that cancer tumor bearing patients have higher plasma free tryptophan levels[86]. This studies has traced the 12 lung and 16 breast cancer patients' plasma free tryptophan levels before and after the surgical removal of the tumor. The free tryptophan levels significantly decreased after tumor ablation. The plasma free tryptophan level of the lung cancer patients changed from 1.09 ± 0.52 umol/dl to 0.71 ± 0.26 umol/dl. The plasma free tryptophan level of the breast cancer patient changed from 0.66 ± 0.32 umol/dl to 0.46 ± 0.11 umol/dl. It is believed, as a result of this study, that the tumor itself may be responsible for the higher free tryptophan level in the cancer patients.

Our study results may support a similar model of the tumor containing higher levels of free tryptophan. In the usual cases, the free molecular gives stronger fluorescence than the bound molecular because the free molecular has less chance to transfer its energy to the other molecular group. That is free molecular has smaller k_q, therefore larger k_r/k_F which corresponds with the stronger fluorescence. (see chapter

3 for detail). This model may also be supported by a fluorescence kinetics study performed by my colleagues[16]. They used a 310nm femotsecond laser pulse to excite the human malignant and non-malignant tissues and then measure the decay time of the 340nm band. The obtained results showed that the malignant tissues had a lower ratio value of the fast decay component over the slow decay component than non-malignant tissues.[16] If one considers that the free tryptophan has a slower decay time (smaller k_F because the k_q is zero or small) and bound tryptophan has a faster decay time (larger k_F because the k_q is larger), than the lower ratio value of the fast decay component over the slow decay component from the malignant tumor, it means that the malignant tumor contains a higher level of free tryptophan.

5.4. The Relative Steady-state Fluorescence Intensities from Collagen, Elastin, and NADH in the Malignant and Non-malignant Tissues

The essential idea of this experiment is the same as the one described above, to compare the relative intensities from a single spectrum. The wavelength 320nm excites collagen, elastin, and NADH. As I discussed in section C of chapter 2 (page 21), collagen and elastin emit fluorescence mostly around 390nm to 420nm, and bound NADH emit fluorescence mostly

around 450nm. The spectrum will give us the relative fluorescence intensities of the NADH over collagen and elastin if we compare intensities around these two ranges.

The experiment was carried on the Luminescence Spectrometer as described in Chapter 3.2 of this thesis. The tissue samples were also placed in the 10 x 10 x 30mm^3 quartz curvatte (ESCO, Type Q-1) for the measurement.

The fluorescence spectra from malignant and non-malignant GYN tissues are shown in Figure 5.15 and 5.16. They generally show two bands: one centered at 383nm and another one centered at 460nm. A deep dip existed at 420nm. Comparing these spectra to the spectra from cells (see chapter 4.6), I believe that the peak at 383nm is mostly from collagen and elastin and the peak at 460nm is mostly from NADH. The deep dip at 420nm is caused by blood re-absorption because of the very strong absorption peak at 420nm (see Figure 1.2). This absorption also made the collagen associated with elastin peak blue shift to 383nm and the NADH peak red shift from around 450nm to around 460nm. And it also made both peaks appear narrower than the collagen, elastin, and NADH fluorescence profiles. The ratio K2= I(383nm)/I(460nm) is used in our study.

There were totally eighteen malignant and ten non-malignant GYN tissues measured. For comparing the relative intensity from NADH with the intensity from collagen and elastin, I chose to take the ratio of the intensities at two

peaks, 383nm and 460nm. The calculated ratio values and the statistic results are shown in Table 5.4. The histogram is shown in the Figure 5.17. The result shows a fairly good cut at the ratio K2 value (= I(383nm) / I(460nm)) of 1.2. Thirteen out of the eighteen malignant tissues have a ratio below this value. Seven out of ten non-malignant tissues have a ratio above this value. This gives sensitivity of 72%, False Negativity of 28%, Specificity of 70% and False Positiveness of 30%. (see chapter 5.2 for the definition of the sensitivity, false negativity, specificity and false positiveness).

This result shows that fluorescence intensities of the NADH are generally stronger relative to the fluorescence intensity of the collagen and elastin in the malignant tissues (as opposed to the non-malignant tissues). This result agrees with my study results from cancerous and normal cells. That study also showed that the NADH fluorescence intensity from the cancer cells were relatively stronger than those from the normal cells. (see chapter 4.3 and 4.5 in this thesis). The study results of human normal and neoplastic colon tissues <u>in vitro</u>, which was done at the Yale University School of Medicine, has also shown a relatively higher intensity at 460nm range when comparing the 380nm range from the neoplastic tissues to that from the normal tissues[33]. The study results of the pulse induced fluorescence spectra from human

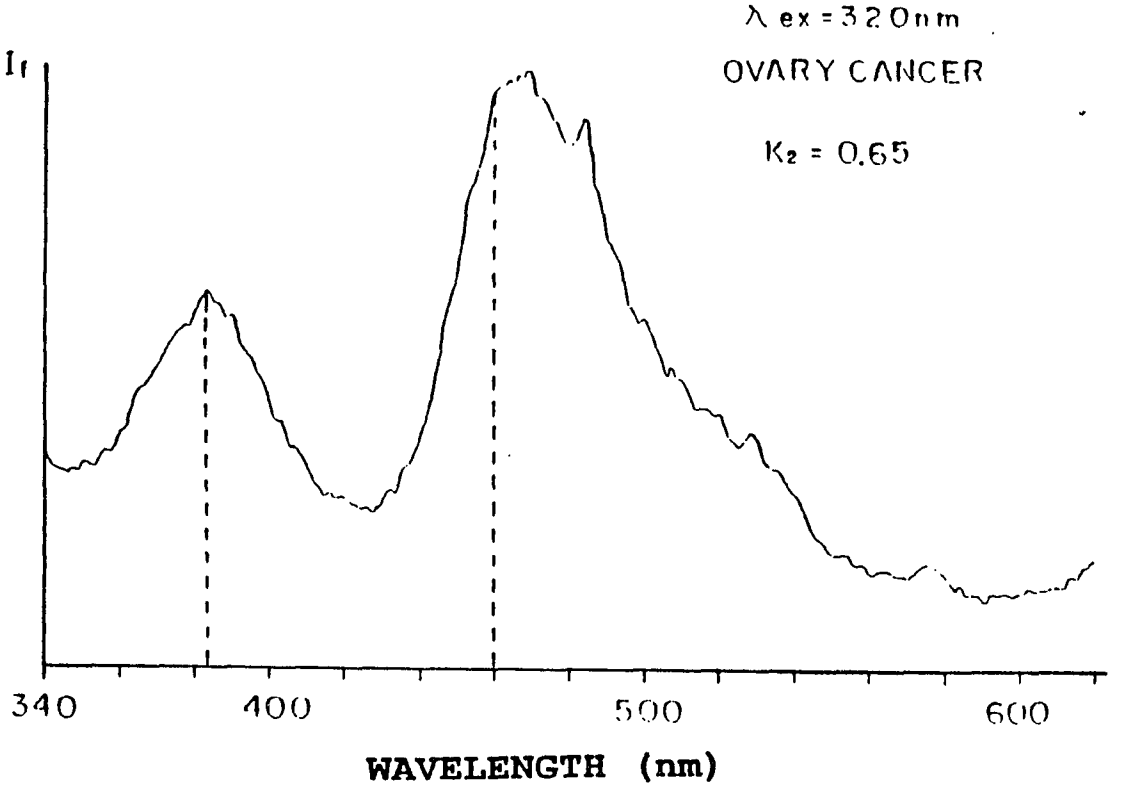

Fig. 5.15. Steady state fluorescence emission spectrum from human malignant ovary tissue <u>in vitro</u> excited at 320nm.

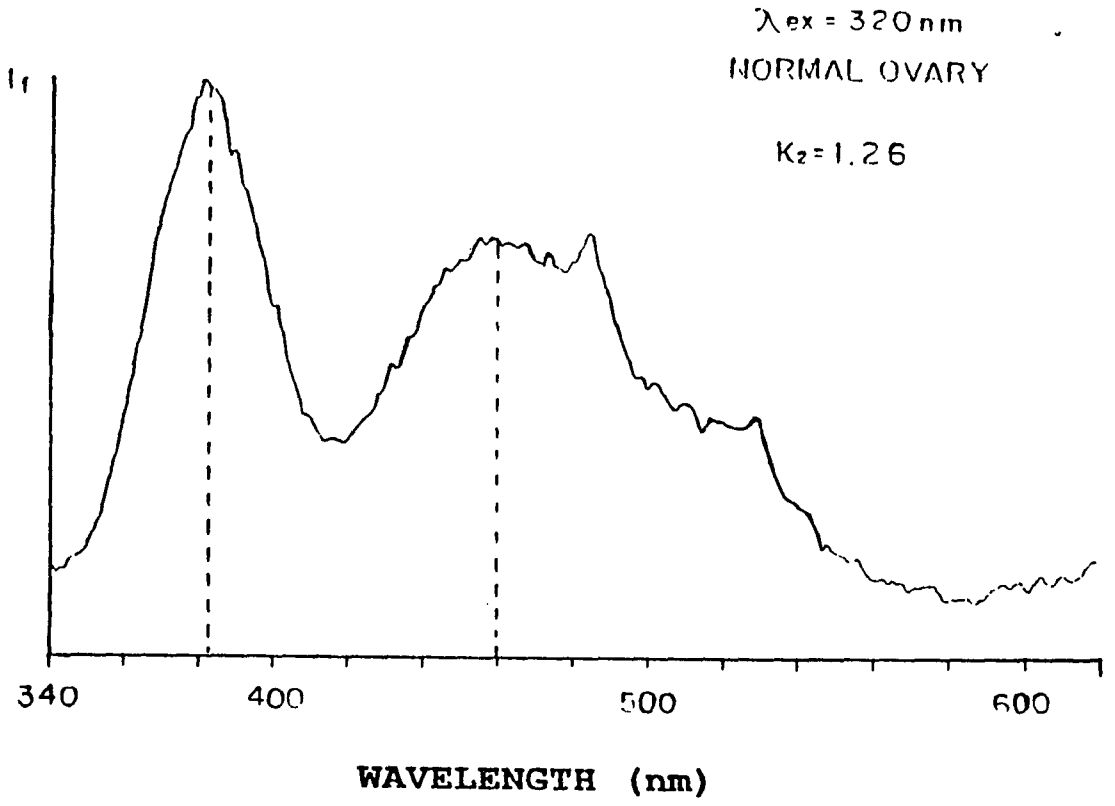

Fig. 5.16. Steady state fluorescence emission spectrum from human non-malignant ovary tissue <u>in vitro</u> excited at 320nm.

Table 5.4 List of the measured ratio K2 values from malignant and non-malignant GYN tissues with excitation wavelength at 320nm (K2 = I(383nm)/I(460nm)).

Non-malignant Tissues	K2	Malignant Tissues	K2
Ovary	0.78	Endometrium	0.84
Cervix	1.1	Cervix	0.67
Ovary	1.4	Ovary	0.14
Cervix	1.4	Cervix	0.49
Cervix	0.55	Endometrium	0.98
Myometrium	2.5	Ovary	0.65
Uterus	1.3	Ovary	0.86
Myometrium	2.6	Endometrium	0.74
Cervix Benign	1.6	Cervix	0.46
Cervix Benign	2.0	Endometrium	1.19
		Ovary	0.19
		Endometrium	0.05
		Endometrium	0.65
		Uterus	1.8
		Endometrium	1.5
		Cervix	2.0
		Uterus	1.4
		Uterus	1.4
Standard	> 1.2		< 1.2
False Negative			28%
False Positive	30%		
Sensitivity			72%
Specificity	70%		

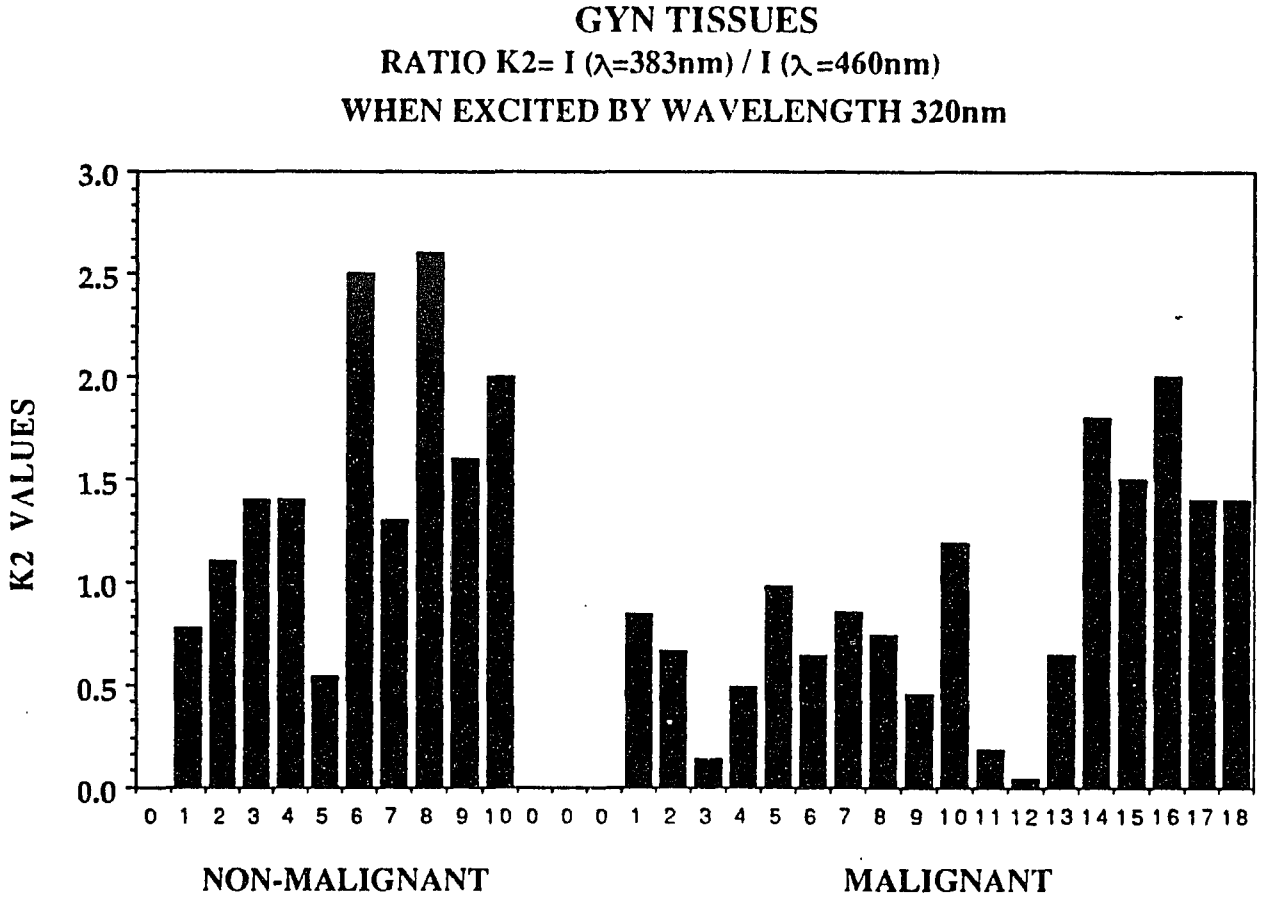

Fig. 5.17. Histogram of the fluorescence intensities ratio K2 = I(λ=383nm)/ I(λ=460nm) over the examined tissues in vitro with excitation wavelength at 320nm.

normal and cancerous breast tissues which was done by my colleagues also showed a relatively higher intensity at 460m range compared to the 520nm range from the cancerous tissues when opposed to normal tissues.[12] Lohman also found that the fluorescence intensity around 460nm is several fold higher at the rim of the malignant tumor than at the normal site.[44,45] All these study results may suggest that the NADH fluorescence in the higher growth fraction site is relatively stronger.

It is noticeable that the sensitive and the specificity were only 70% of the result. This large error may be due to the different amounts of collagen and elastin in those different tissues in the top surface layer within 500u of the depth. Another reason for this difference might be because of the modulation by the reabsorption of the blood residue. The reabsorption of the blood residue gives a negative effect on the statistical results of the ratio K_2 = I(383nm)/I(460nm) because of the higher absorption rate at 383nm than at 460nm (see Figure 1.2, the absorbance of the blood). It is very possible that non-malignant tissues <u>in vitro</u> contain more blood residue than malignant tissues <u>in vitro</u>. Thus, the effective results will be that the ratio of the non-malignant tissues which appear lower, will move towards the ratio range of the malignant tissues. The statistical results may also affected by the lack of knowledge of the exact site of the measured tissue. Lohman's results seem to point out that the intensity of the NADH fluorescence changes along the measured

site of the tumor, in which the growth factor is different along at different positions.

5.5. Models for the Numerical Fitting of the Fluorescence Spectra from the Tissues.

As I mentioned in the previous sections, the blood residue in the tissues affects the fluorescence spectroscopies by the self-absorption. To build a simple model based on physics, I assume that the monochromatic incident light with intensity I_0 and wavelength λ_e is illuminated on the surface of the tissues whose attenuation coefficient is $\mu_t(\lambda)$ when there is no blood residue. μ_t is including both the absorption and scattering.

$$\mu_t = \mu_{ta} + \mu_{ts} \tag{5.1}$$

The blood's specific absorption coefficient is $\alpha(\lambda)$. I also assume that the distance between the detector and the sample site are much larger than the dimension of the fluorescence volume of the sample. The angle between the incident light and the detection is small. In addition, I assume the physical properties are uniform in the tissue. This is not true since the tissue is localized.

According to the Beer-Lambert Law, the intensity of the excitation light should be reduced along the penetration depth along x-axis as

$$I = I_0 \exp[-(\mu_t(\lambda_e)+\alpha(\lambda_e)c)x] \quad . \tag{5.2}$$

in the Eq. 5.2, c presents the relative blood residue concentration in the tissue. The fluorescence contributed from the i fluorophor at the distance range (x.dx) should be (according to Eq. 2.28)

$$dI_{Fi}(\lambda,x) = Q_i\ f_i(\lambda)\ I$$
$$= Q_i\ f_i(\lambda)\ I_0 \exp[-(\mu_t(\lambda_e)+\alpha(\lambda_e)c)x]\ dx \tag{5.3}$$

where Q_i is the quantum efficiency of the fluorescence of each fluorophor in the tissue. $f_i(\lambda)$ is the normalized fraction function of the spectral distribution function of each fluorophor. This part of the fluorescence has to penetrate out to the tissue surface for detector to receive it. Therefore, using the Beer-Lamber's Law again, the fluorescence which can be received by the detector from this contribution $dI_{Fi}(\lambda,x)$ will be

$$\delta dI_{Fi}(\lambda,x) = \nu\ dI_{Fi}(\lambda,x) * \exp[-(\mu_t(\lambda)+\alpha(\lambda)c)x] \tag{5.4}$$
$$= \nu Q_i f_i(\lambda) * I_0 \exp[-(\mu_t(\lambda_e)+\alpha(\lambda_e)c+(\mu_t(\lambda)+\alpha(\lambda)c)x]\ dx.$$

The ν is a constant which covers the geometric factor and detector factor, and the tissue surface effects which determine part of the fluorescence which can be received by the detector. Collecting all the fluorescence from the various depths x at the front surface, the detected fluorescence spectrum should be,

$$\delta I_{Fi}(\lambda) = \int_0^\infty \nu Q_i f_i(\lambda) I_0 \exp[-(\mu_t(\lambda_e)+\alpha(\lambda_e)c+(\mu_t(\lambda)+\alpha(\lambda)c)x]\, dx$$

$$= \nu Q_i f_i(\lambda) I_0 / (\mu_t(\lambda_e)+\alpha(\lambda_e)c+\mu_t(\lambda)+\alpha(\lambda)c) \quad . \qquad (5.5)$$

In the case there are several fluorophors in the tissues, the fluorescence shall be

$$I_F(\lambda) = \sum \nu Q_i f_i(\lambda) * I_0 / (\mu_t(\lambda_e)+\alpha(\lambda_e)c+\mu_t(\lambda)+\alpha(\lambda)c) . \qquad (5.6)$$

For further simplifying the case, I assume that the blood absorption modifies the spectrum, therefore the attenuation coefficient of the tissue without blood can be considered as a constant in the wavelength range in which I am interested. Thus, let

$$\eta = \mu_t(\lambda_e)+\alpha(\lambda_e)c+\mu_t(\lambda) \quad . \qquad (5.7)$$

The Eq. 5.6 becomes,

$$I_F(\lambda) = \sum \nu Q_i f_i(\lambda) * I_0 / (\eta+\alpha(\lambda)c) \quad . \qquad (5.8)$$

Consider the Eq. 2.30, this equation can be expressed as

$$I_F(\lambda) = \sum B_i f_i(\lambda) / (\eta+\alpha(\lambda)c) \quad . \qquad (5.9)$$

Under the assumption that 320nm excites collagen, elastin, NADH and flavins according to the Figure 1.33, the fluorescence emission spectrum from a tissue excited with 320nm can be expressed as:

$$I_F(\lambda) = [B_1 f_1(\lambda)+B_2 f_2(\lambda)+B_3 f_3(\lambda)+B_4 f_4(\lambda)] / (\eta+\alpha(\lambda)c)+C \qquad (5.10)$$

where 1 is corresponding to collagen; 2 to elastin; 3 to NADH; and 4 to flavins. C presents the possible background which may be caused by other weak fluorophors. I can use this model to fit the experimental data with the least square error method to obtain the B_i (i=1,2,3,4) and relative blood

concentration c and relative tissues attenuation coefficient μ and C. It is important to emphasize here that the obtained c and η are not the real values of the blood concentration and tissue attenuation coefficient of the tissue but only a relative value. This is because I am fitting this model to the spectra in which the fluorescence intensity is in arbitrary unit. The obtained values should tell us the relative contributions of each fluorophor and the relative blood re-absorption contribution.

The obtained values of B_i (i=1,2,3,4), η, c and C for the fitting of the spectra from malignant and non-malignant tissues are listed in Table 5.5. χ^2 gives the average least square fitting error for each fitting as defined in chapter 4.3.2 (pages 218,219). The goodness of the fitting are sown in Figures 5.18, 5.19 and 5.20. The computer fitting program is listed in Appendix I.

The best fitting for the spectrum from the non-malignant tissue is when the NADH peak is assumed to be at 450nm. However, the best fitting for the spectra from malignant tissues is when the NADH peak is assumed to be at 460nm. The fitting difference is quite small (χ^2 changes less than 0.005) when I chose the flavins peak at 525nm or at 535nm. This may be caused by the quite weak contribution from the flavin to the fluorescence spectra. The error in this fitting may caused by other weak fluorophors and other quenching molecules. For example, the over sharp of the 460nm peak in

the spectra of the malignant tissue may be caused by the quenching of myoglobin at the blue side of the NADH peak[65]. This also causes the peak appearing red shifted. The obtained ratio of the portions between collagen and elastin is 7/1 for non-malignant tissue (Tab. 5.5 and Figs. 5.19 & 5.19a) and 0/7 for malignant tissue (Tab. 5.5 and Figs. 5.18 & 5.18a). The ratio 7/1 for non-malignant (normal) tissue is close to the ratio of the portions between collagen and elastin in the normal human uterus, which is 6/1. The reasons the obtained fitting components of collagen and elastin changed a lot between the malignant and non-malignant tissues are unknown. It may agree with the fact that the amount of collagen has dropped a lot in the tissue when the tissue changes from non-malignant to malignant.[87] It may also be because the peaks of collagen and elastin are close (390nm and 420nm) and the elastin spectrum has a long tail. Therefore, the elastin fitting may be affected by the non-constant background and have to make up the unfitted parts. This then further affects the fitting of the collagen and NADH. The higher the portion of elastin is mistaken, the more portions of collagen and NADH that will be given in the fitting values of less than what they should be.

I also tried to fit the spectra of the malignant tissues, with assumption that the ratio of the portions between collagen and elastin is 7/1 as it is obtained from the fitting result of the non-malignant tissue. In another word, assume

the ratio of the portions between collagen and elastin does not change when the tissue changes from non-malignant to malignant. The obtained fitting result is also listed in Table 5.5. The goodness of fit is shown in Figure 5.20, and the contribution from each fluorophor is shown in Figure 5.20a. The average square fitting error χ^2 is increased from 0.19 to 0.24 with this model (see Tab. 5.5). The result actually shows that the 383nm peak is better fit on the peak location, except for the larger mismatch at the 350nm range. The reason for that is unknown. It might be attributed to the weak emission of the free tryptophan in the tissues because the malignant tissues contained more free tryptophan.

I will expect the real case is in between these two fitting results I have obtained for the malignant tissue.

Calculating the ratio value of the NADH component over the summary of the components of collagen, elastin, flavins and the background as

$$R = B_3 / (B_1 + B_2 + B_3 + C) \qquad (5.11)$$

I will have that R value for non-malignant tissue as 0.29, and the R value for malignant tissue as 0.34 or 0.78 in case I choose the ratio of the portions of collagen over elastin as 7 (see Table 5.5 for the calculation). The actual R value for the malignant tissue here may be higher than 0.34 because the intensity of the experimental data at 460nm is higher than the fitting result. The higher R value of the malignant tissues agree with the previous conclusion that the NADH fluorescence

is relatively stronger from the malignant tissue than from the non-malignant tissue. (see Chapter 5.4)

In addition, I have tried the various fitting cases in which I omitted each individual component: blood, collagen, elastin, and NADH. The purpose of this trying is to show the necessity of the each component in the Eq.5.10. The cases, corresponding figure number, and their results are listed on the Tables 5.6 and 5.7. The results has generally shown that every component is necessary for the fairly fit to the both malignant and non-malignant tissues. Blood re-absorption can not be ignored in both malignant and non-malignant tissues. In the non-malignant tissue case, the fit without collagen is not right, but the fit without elastin or NADH show a fair match. In the malignant tissue case, the fit without elastin or NADH is not right, but fit without collagen show a very good match.

Table 5.5 List of the fitting parameters* of the model equation 5.5 for the emission spectra of malignant and non-malignant GYN tissues. The excitation wavelength is 320nm.

Fitting Parameters	Malignant	Malignant (limited B1/B2=7)	Non-malignant
B_1 (Collagen)	<0.001	4.35	7.88
B_2 (Elastin)	7.22	0.62	1.12
B_3 (NADH)	2.48	4.42	2.96
B_4 (Flavins)	<0.001	<0.01	0.47
η (relative tissue penetration coefficient)	0.43	0.35	0.45
c (relative blood concentration)	3.7	3.0	3.1
C (background constant)	0.10	0.69	0.61
$\chi^2 = \sum [Y(i)-f(i)]^2 / (N-7)$	0.19	0.24	0.029
$R = B_3/(B_1+B_2+B_4+C)$	**0.34**	**0.78**	**0.29**

*Note: The absolute values of these parameters (B_1, B_2, B_3, B_4, d and C) is not meaningful because the fluorescence intensities are in the arbitrary unite. They are only considerable when they are compared with each other.

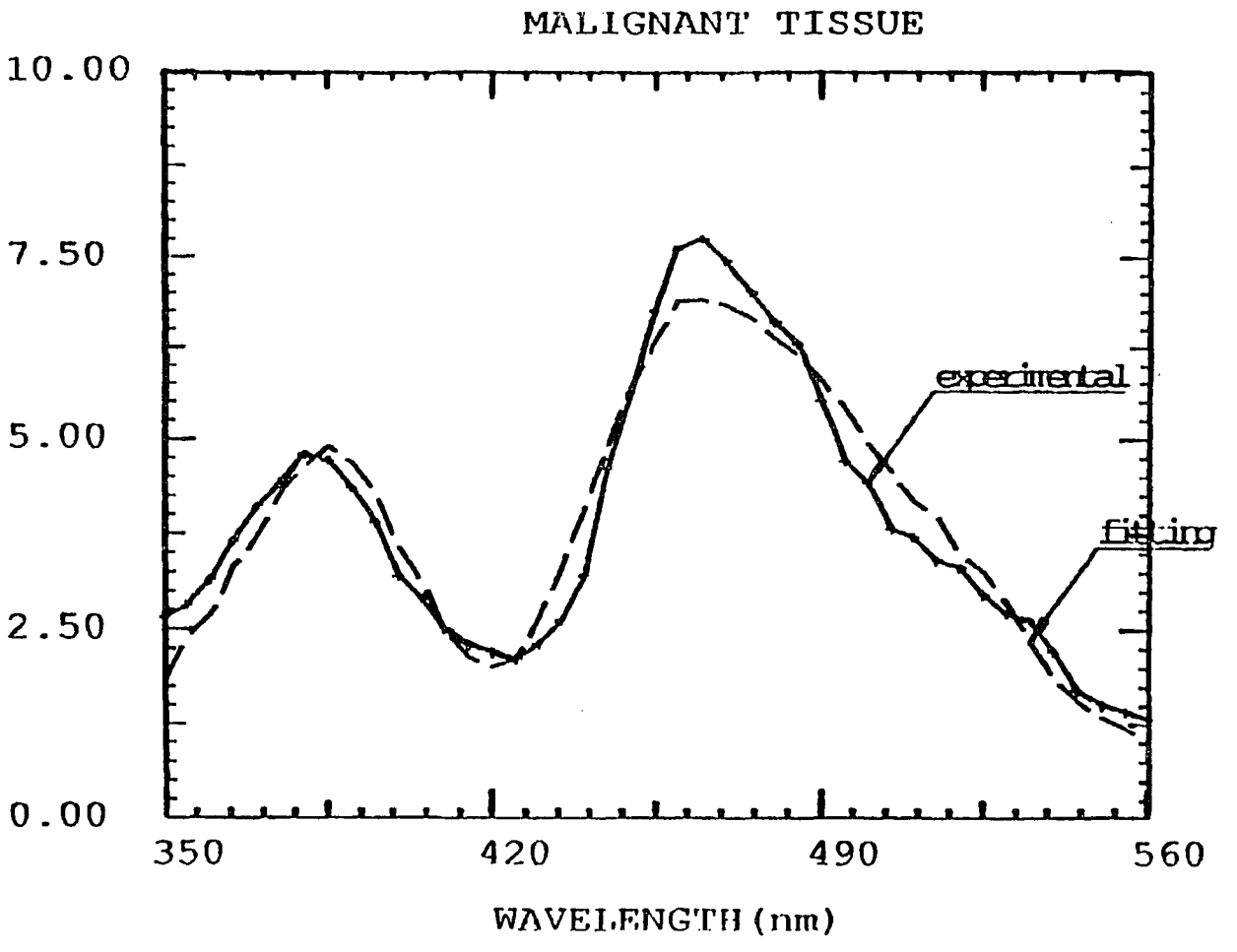

Fig. 5.18. Goodness of fit with model Eg. 5.5 to the emission spectra from malignant tissue excited with 320nm.

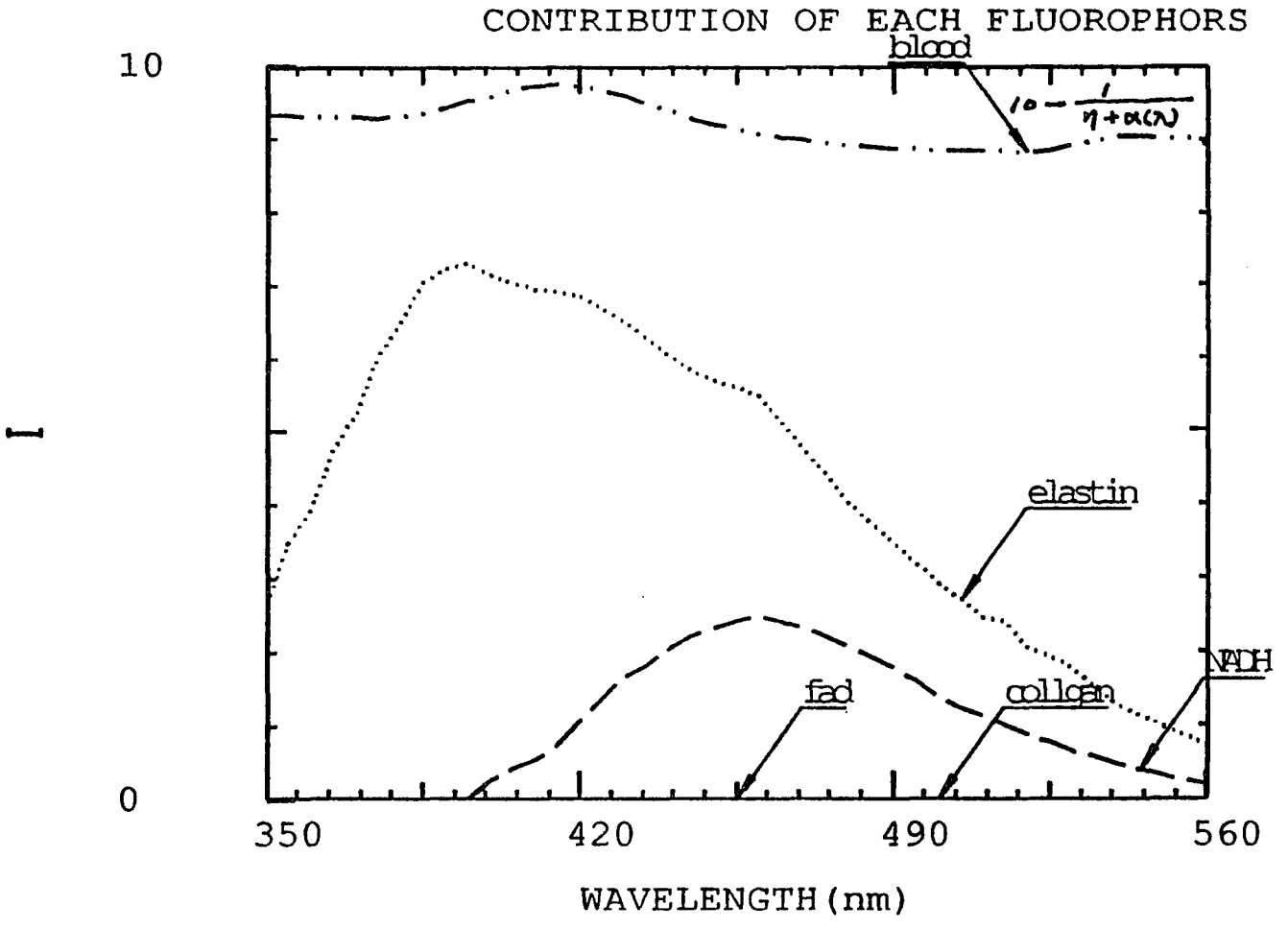

Figure 5.18a The fitting results of the contribution from each fluorophor to the fluorescence from malignant tissue excited with 320nm.

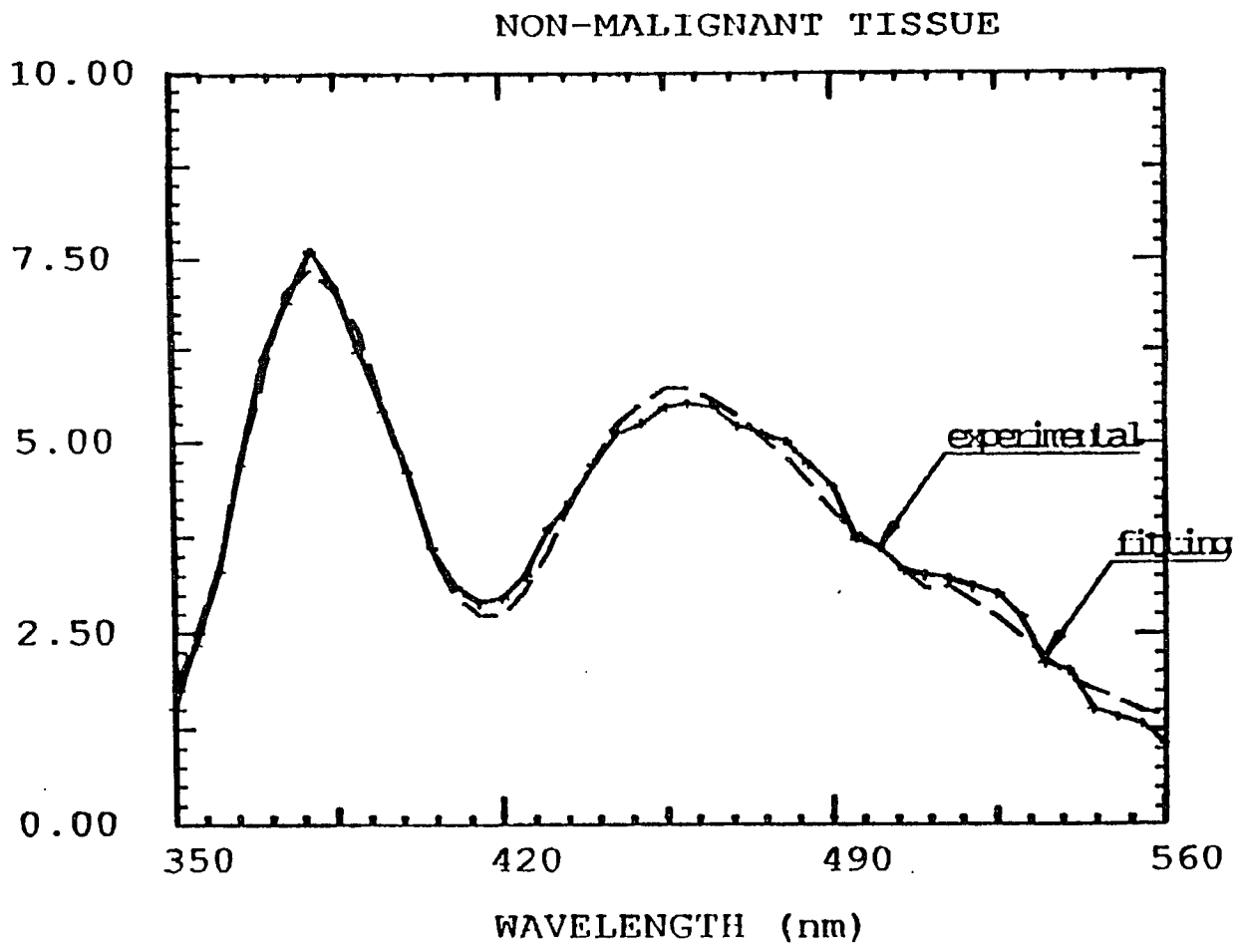

Figure 5.19 Goodness of fit with model Eg. 5.5 to the emission spectra from non- malignant tissue excited with 320nm.

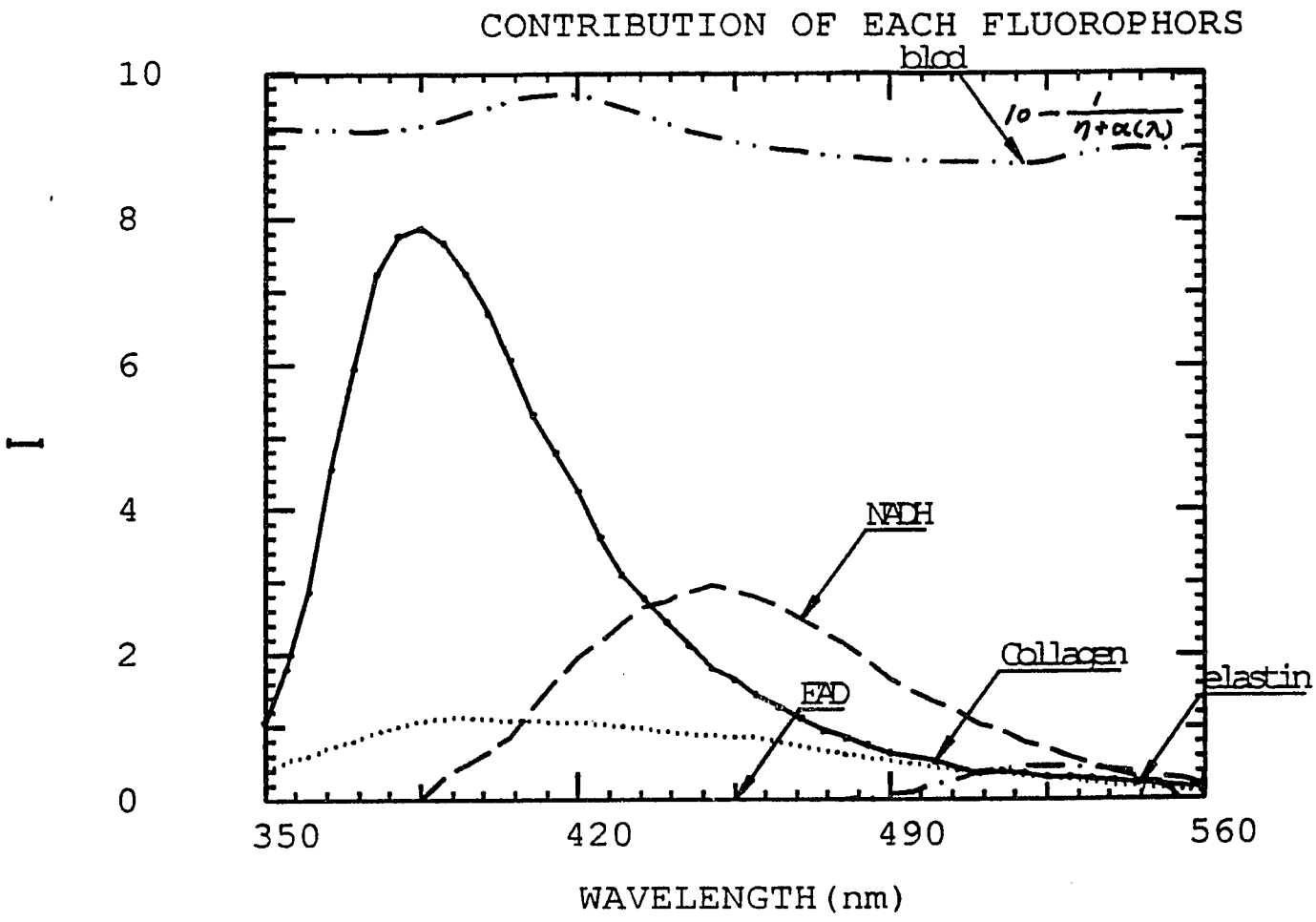

Figure 5.19a The fitting results of the contribution from each fluorophor to the fluorescence from non-malignant tissue excited with 320nm.

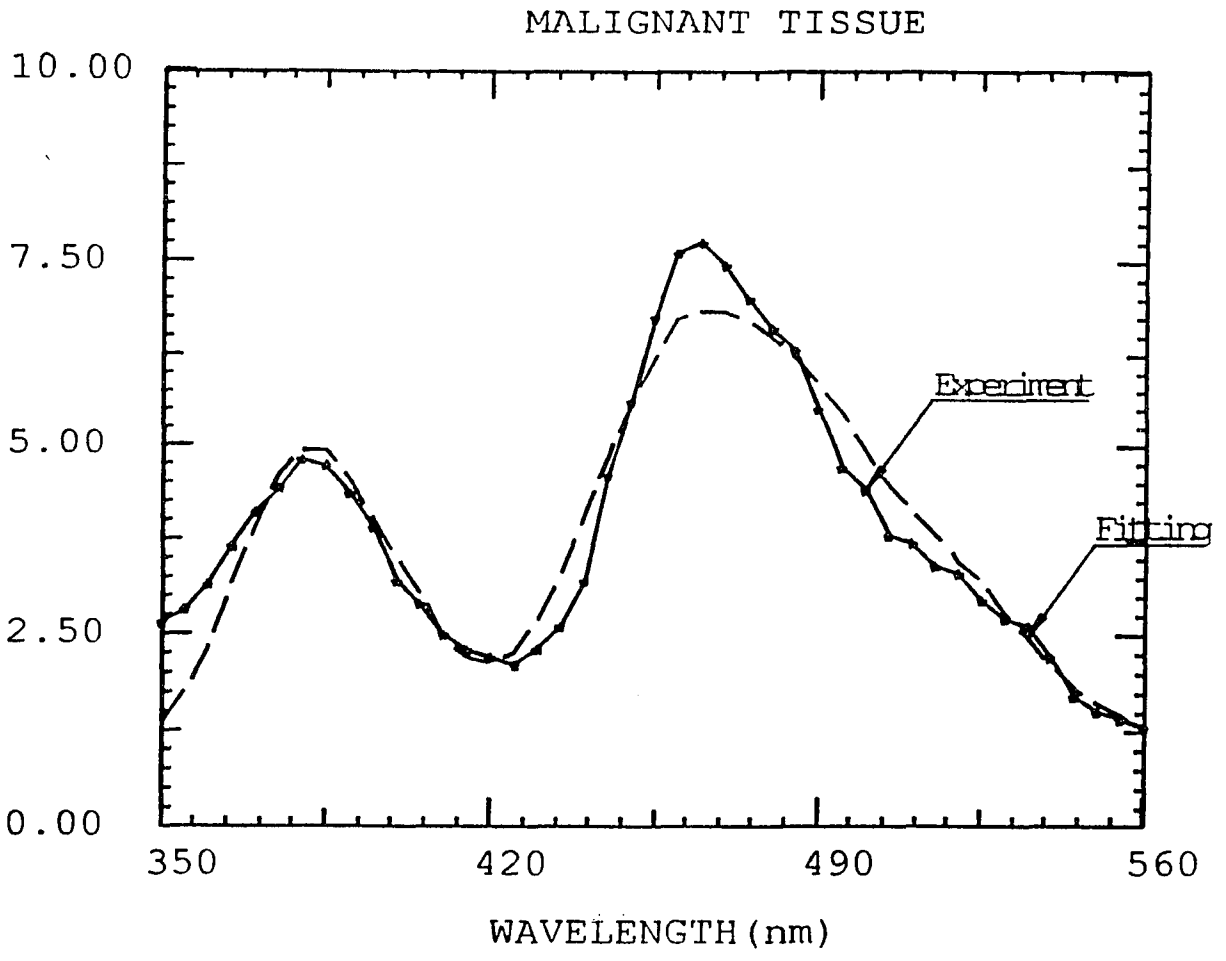

Figure 5.20 Goodness of fit with model eg. 5.5 to the emission spectra from non- malignant tissue excited with 320nm. It is limited that the contribution from collagen over elastin is 7.

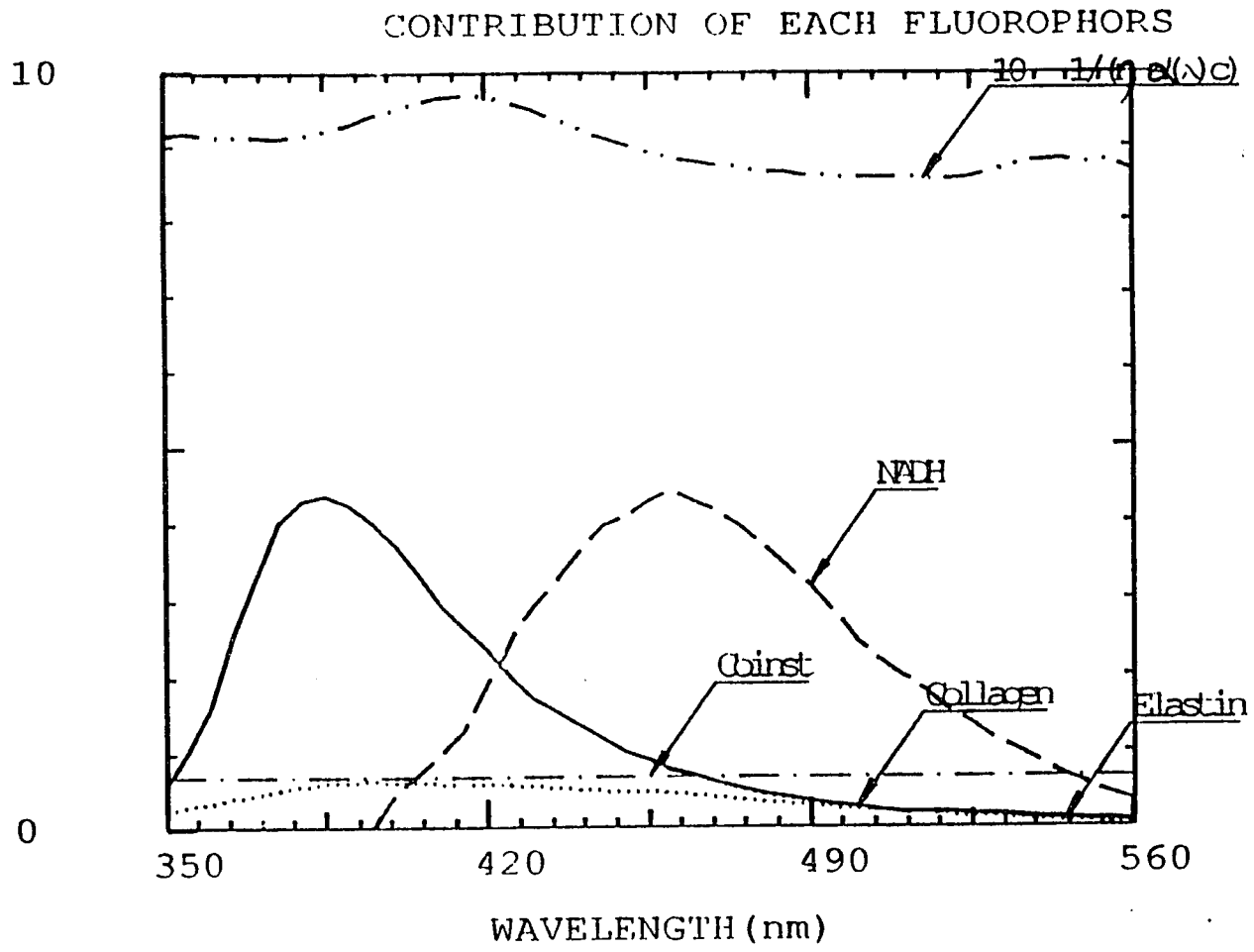

Malignant tissue, excited with 320nm.
ct11.ds

Figure 5.20a The fitting results of the contribution from each fluorophor to the fluorescence from malignant tissue excited with 320nm. It is limited that the contribution from collagen over elastin is 7.

Table 5.6 List of the fitting results on various trying of the non-malignant GYN tissues. The excitation wavelength is 320nm.

Fitting Parameters	No blood	No collagen	No elastin	No NADH
B_1 (Collagen)	3.85	**0**	8.89	5.49
B_2 (Elastin)	10^{-10}	5.4	**0**	12.8
B_3 (NADH)	2.53	10^{-9}	4.05	**0**
B_4 (Flavins)	$3x10^{-3}$	0.27	0.86	0.91
η (relative tissue penetration coefficient)	0.86	0.44	0.65	0.97
c (relative blood concentration)	**0**	1.28	1.87	5.03
C (background constant)	1.29	10^{-8}	0	10^{-9}
$\chi^2 = \Sigma[Y(i)-f(i)]^2/(N-7)$	0.87	0.24	0.06	0.067
Figure No.	Fig.5.21	Fig.5.22	Fig.5.23	Fig.5.24
fit well? ($\chi^2<0.2$?)	no	no	OK	OK

*Note: The absolute values of these parameters (B_1, B_2, B_3, B_4, d and C) is not meaningful because the fluorescence intensities are in the arbitrary unite. They are only considerable when they are compared with each other.

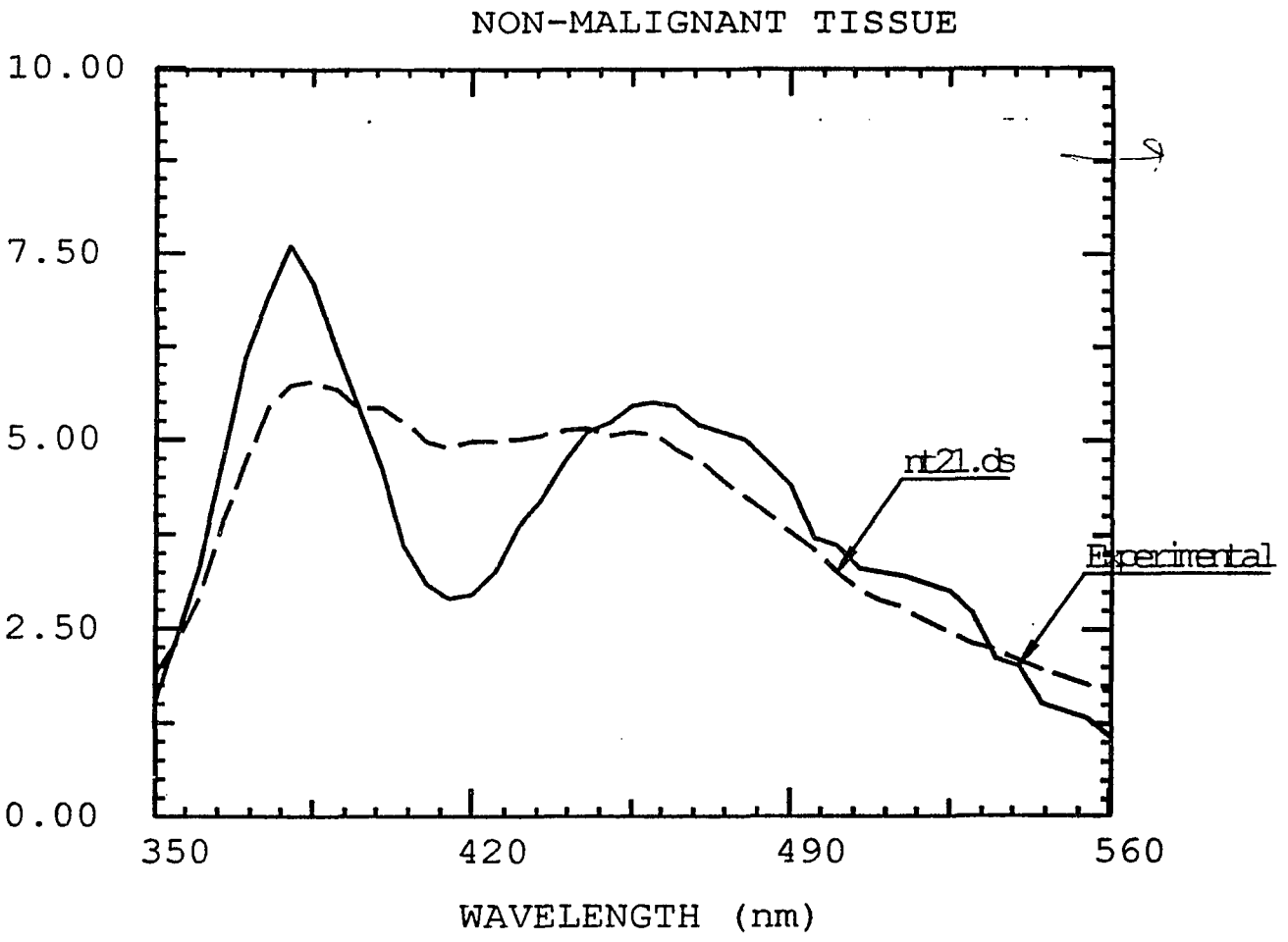

Figure 5.21 Best fit of the non-malignant tissue spectrum with the model Eq.5.5, but assuming there is no blood reabsorption.

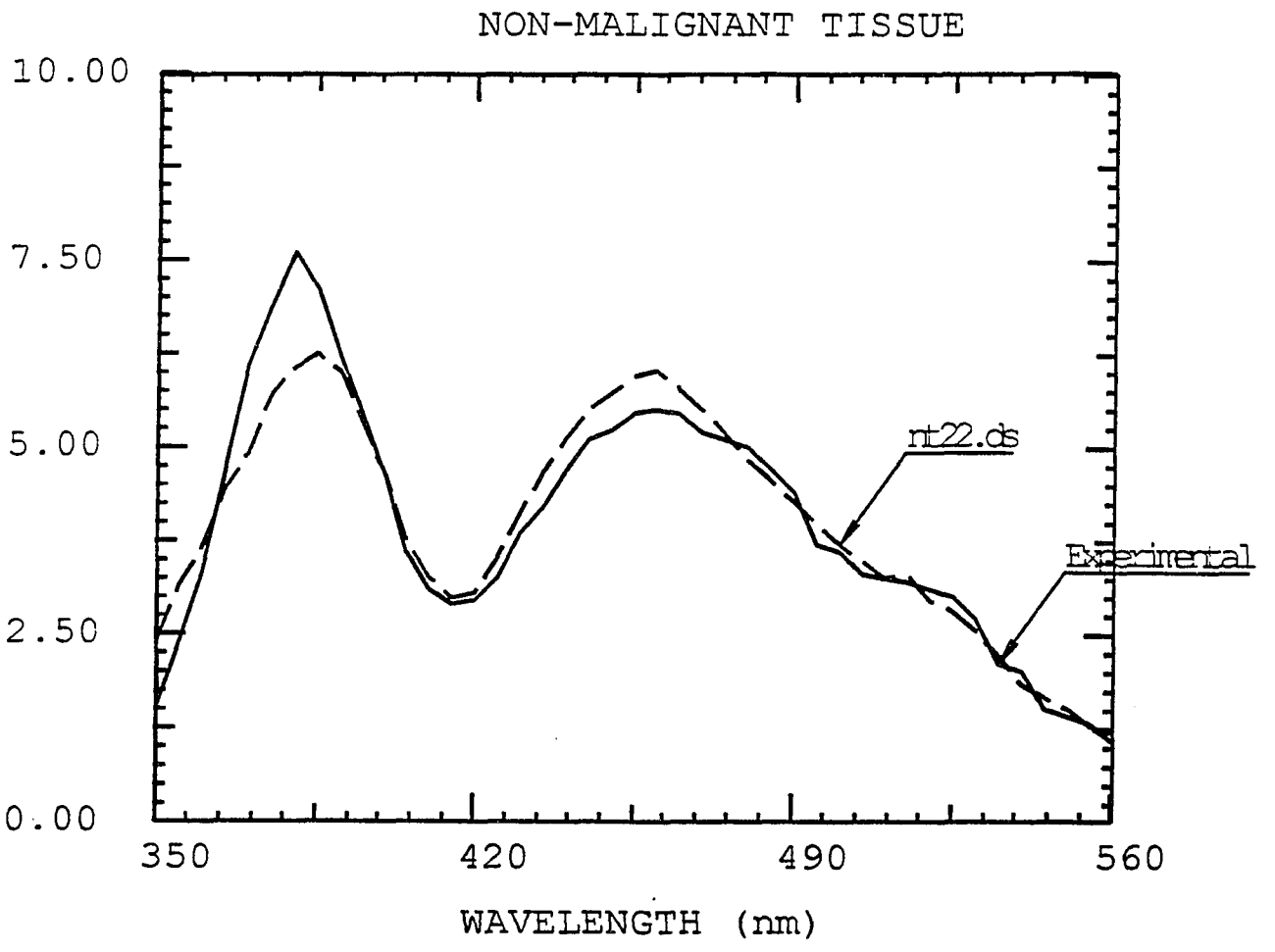

Figure 5.22 Best fit of the non-malignant tissue spectrum with the model Eq.5.5, but assuming there is no collagen.

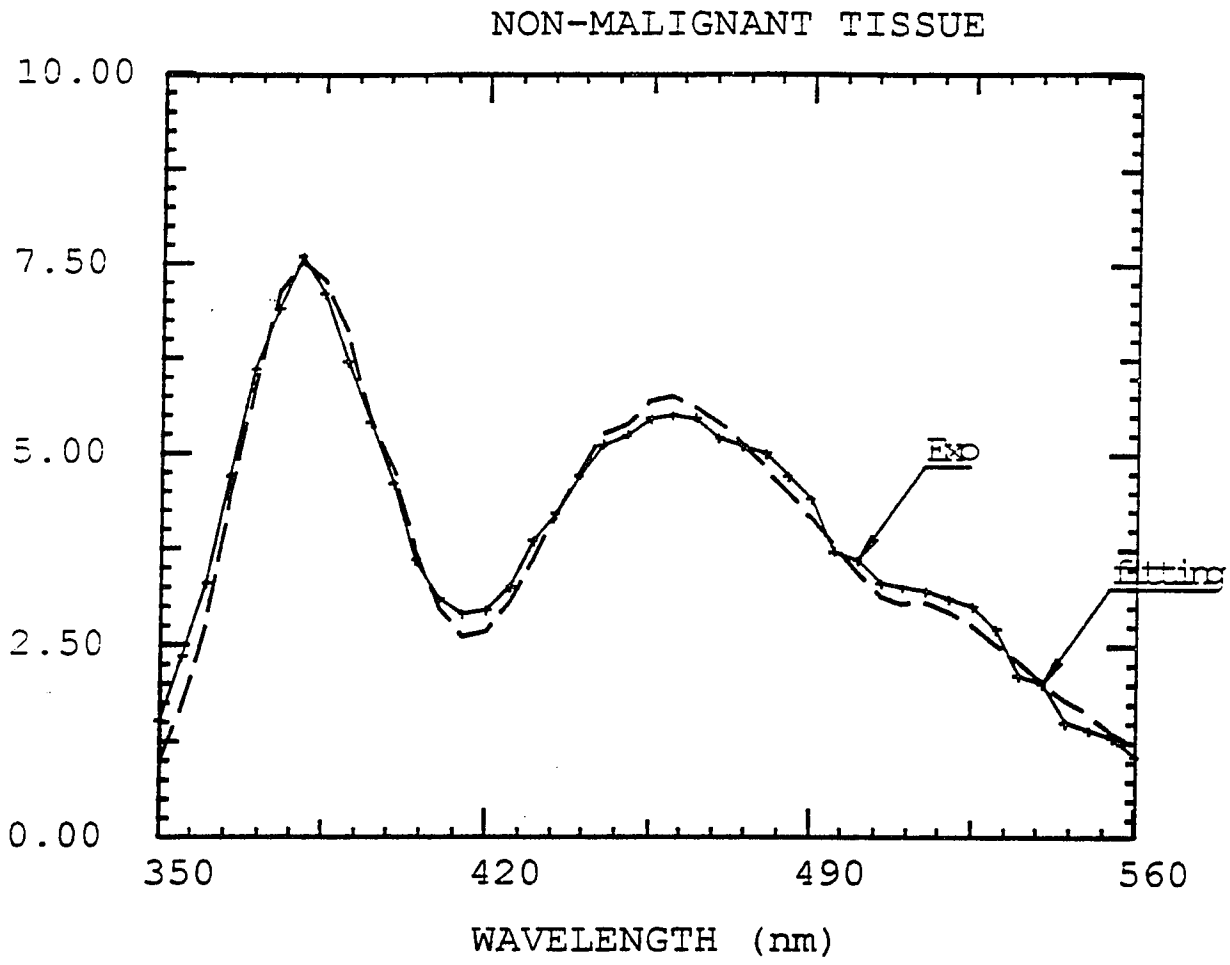

Figure 5.23 Best fit of the non-malignant tissue spectrum with the model Eq.5.5, but assuming there is no elastin.

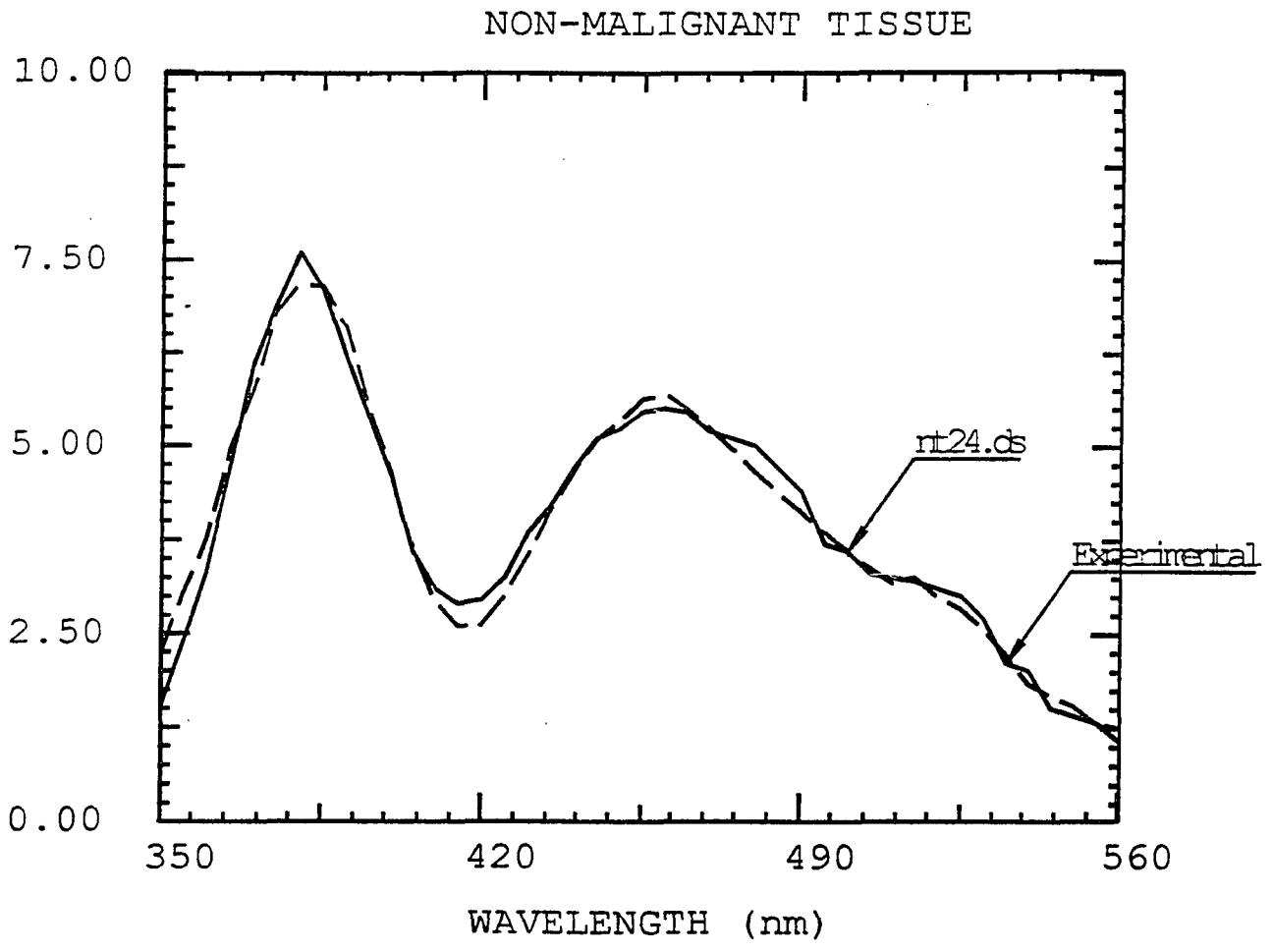

excited with 320nm

Figure 5.24 Best fit of the non-malignant tissue spectrum with the model Eq.5.5, but assuming there is no NADH.

Table 5.7 List of the fitting results on various trying of the malignant GYN tissues. The excitation wavelength is 320nm.

Fitting Parameters	No blood	No collagen	No elastin	No NADH
B_1 (Collagen)	1.42	**0**	6.0	10^{-9}
B_2 (Elastin)	10^{-13}	5.77	**0**	2.63
B_3 (NADH)	3.1	1.99	4.5	**0**
B_4 (Flavins)	10^{-11}	10^{-9}	0.39	10^{-9}
η (relative tissue penetration coefficient)	0.78	0.34	0.28	0.032
c (relative blood concentration)	**0**	3.0	2.9	1.48
C (background constant)	1.68	0.10	0	0.071
$\chi^2 = \Sigma[Y(i) - f(i)]^2/(N-7)$	1.62	0.19	0.41	0.46
Figure No.	Fig.5.25	Fig.5.26	Fig.5.27	Fig.5.28
fit well? (χ^2 <0.2 ?)	no	OK	no	no

*Note: The absolute values of these parameters (B_1, B_2, B_3, B_4, d and C) is not meaningful because the fluorescence intensities are in the arbitrary unite. They are only considerable when they are compared with each other.

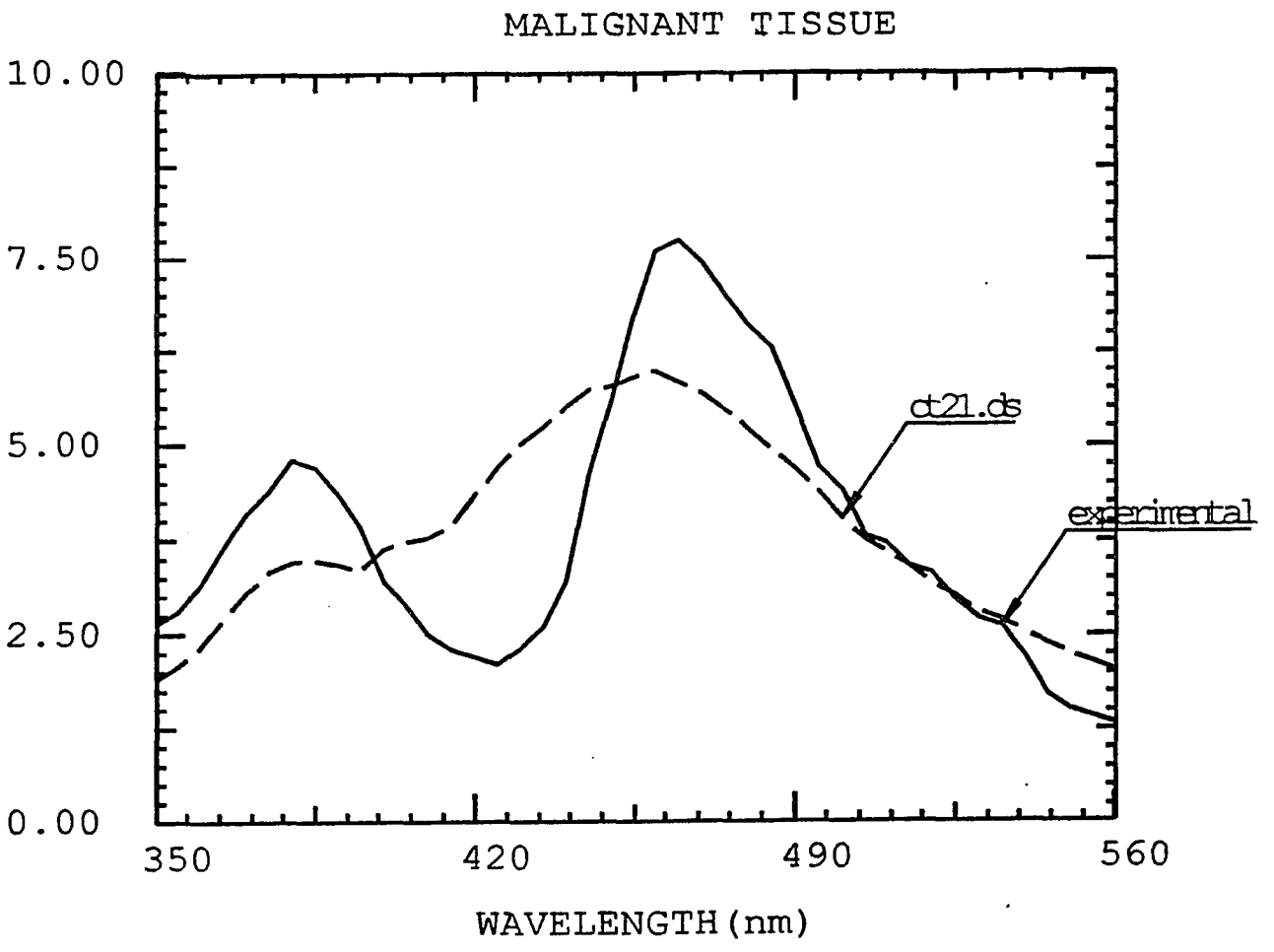

Figure 5.25 Best fit of the malignant tissue spectrum with the model Eq.5.5, but assuming there is no blood reabsorption.

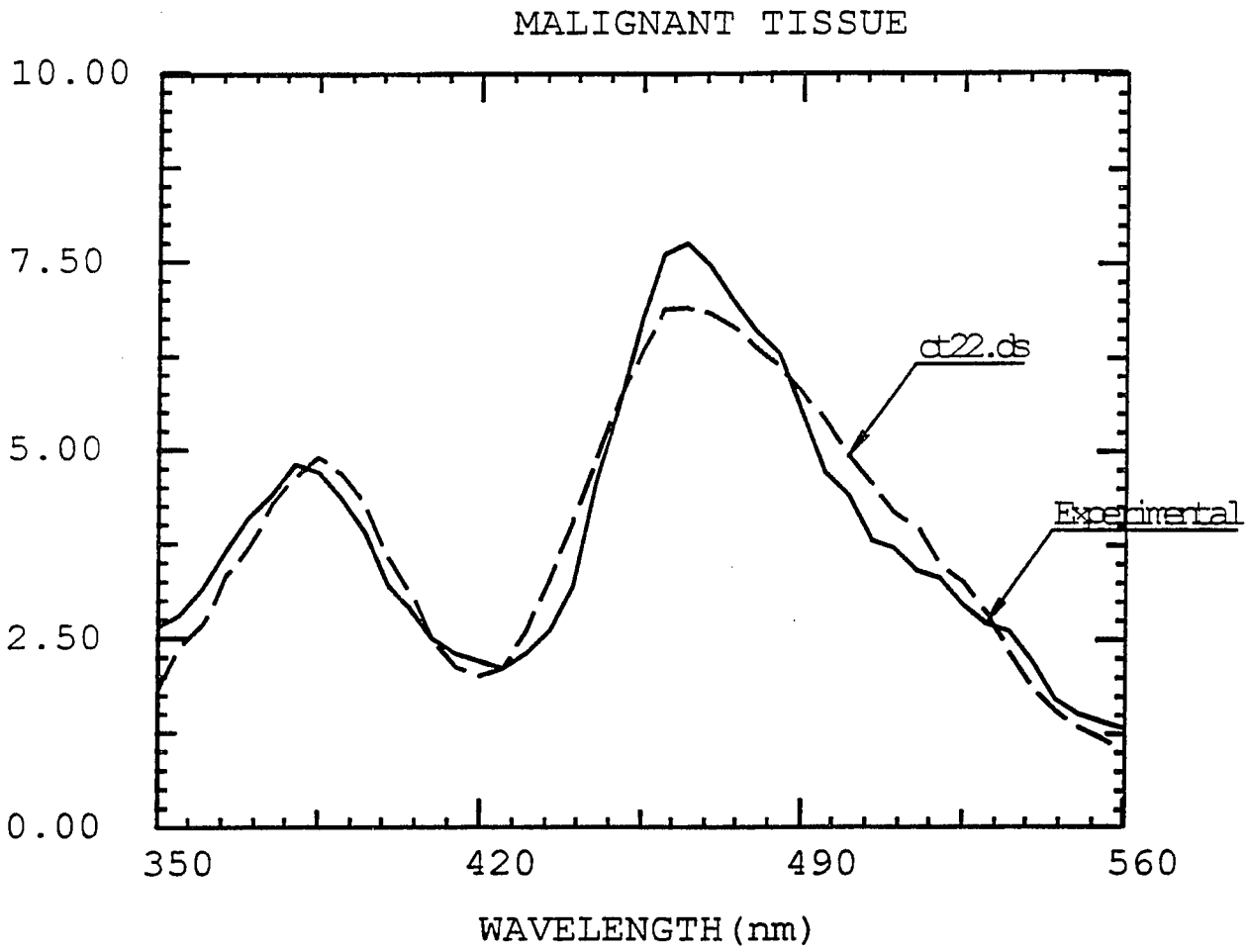

Figure 5.26 Best fit of the malignant tissue spectrum with the model Eq.5.5, but assuming there is no collagen.

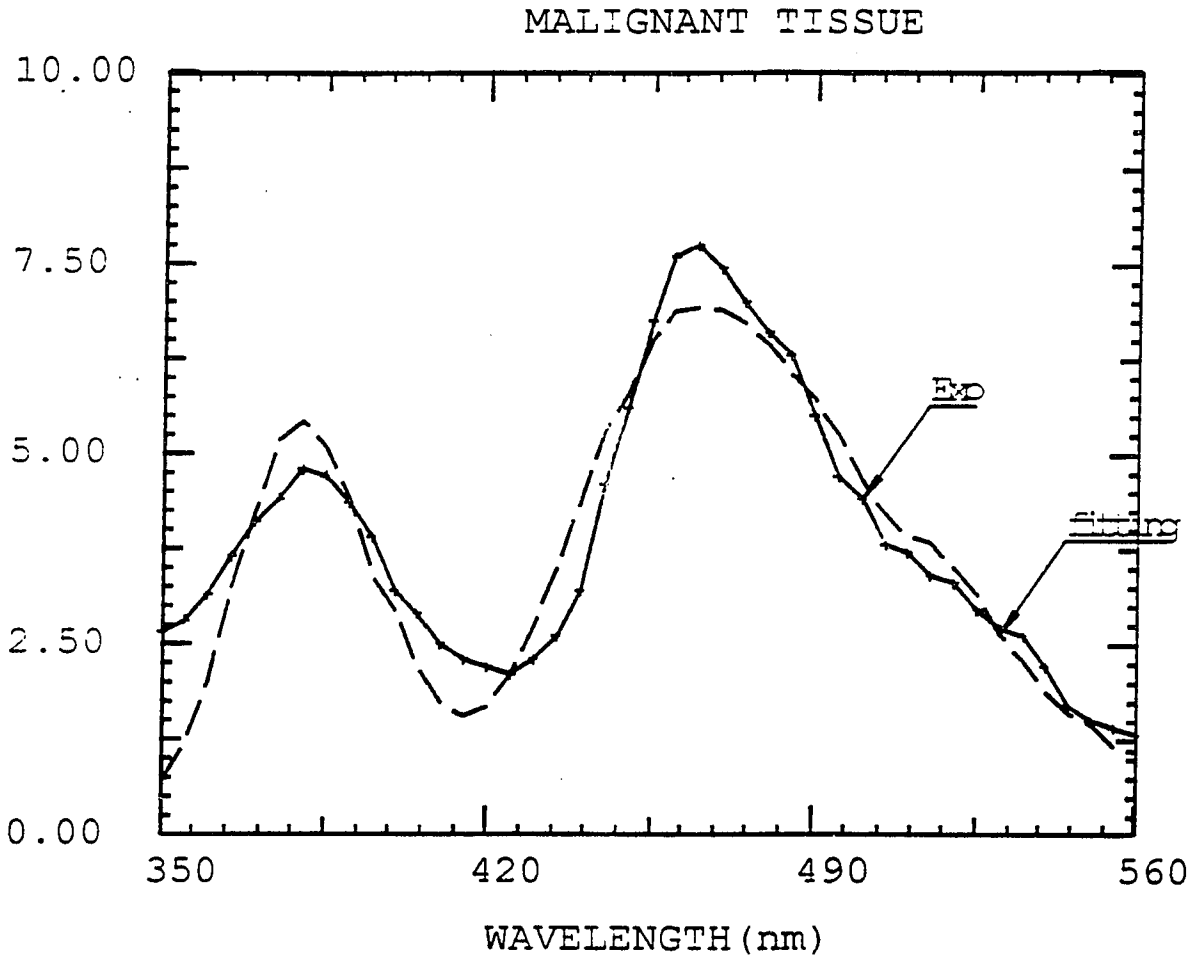

Figure 5.27 Best fit of the malignant tissue spectrum with the model Eq.5.5, but assuming there is no elastin.

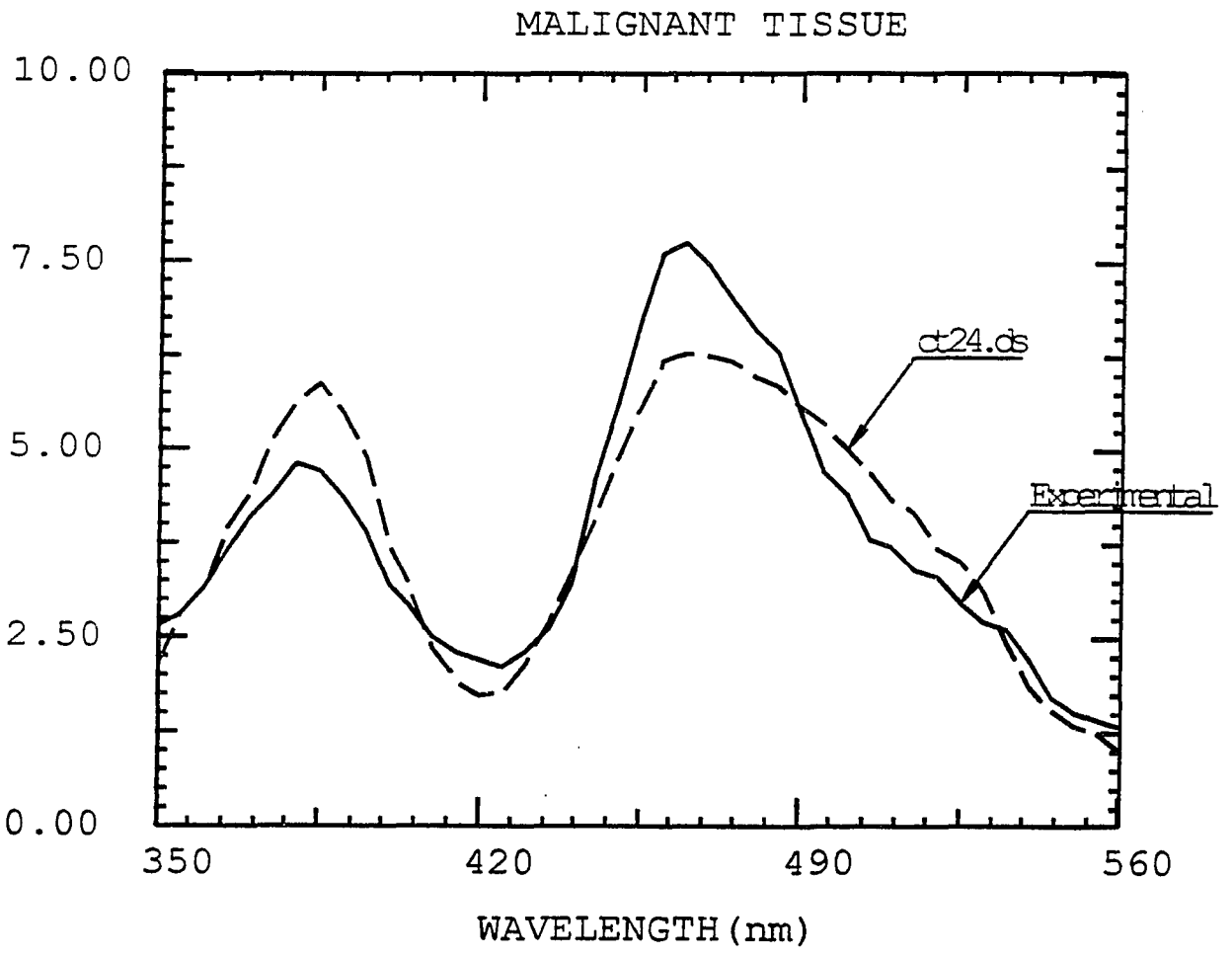

Figure 5.28 Best fit of the malignant tissue spectrum with the model Eq.5.5, but assuming there is no NADH.

5.6 Excitation Spectroscopies with Emission Wavelength at 460nm from Elastin Collagen and NADH in Malignant and Non-malignant tissues.

Excitation spectroscopy is another way to study the fluorescence properties of a substance. With the selected emission wavelength, excitation spectrum presents the emission intensity vs excitation wavelength. In this section, I present the results on the excitation spectra from malignant and non-malignant GYN tissues with the emission wavelength at 460nm. As we can see in Figure 1.32, the fluorescence at 460nm can be from NADH, elastin and collagen. Collagen should contribute at a slightly lower rate since it emits weakly at 460nm. Several cells' and tissues' emission spectral results (in Chaps. 4.3.1, 4.3.3, 4.3.5, and 5.4) have shown that the NADH fluorescence is relatively stronger from the malignant tissues and cells than from the non-malignant tissues and cells, when compared to other molecules. Therefore, by measuring the excitation spectra with emission wavelength at 460nm, one can test if there are differences in the relative contributions between NADH and elastin and collagen.

The experiment was performed on the luminescence spectrometer as described in the Chapter 4.2 of this thesis. The tissue samples were also placed in the 10 x 10 x 30mm^3 quartz curvatte (ESCO, Type Q-1) for the measurement. The emission wavelength was fixed at 460nm while the excitation

wavelength was scanned.

The typical excitation spectra from malignant and non-malignant GYN tissues with emission wavelength at 460nm are presented in the Figures 5.29 and 5.30. The question is what molecules contribute to 460nm fluorescence and how much they contribute. There is a peak around 335nm and a shoulder over the 360nm to 385nm range for both malignant and non-malignant GYN tissues. However, the relative intensities of the 335nm peak and the 380nm shoulder are different between malignant and non-malignant tissues. The malignant tissues have relatively higher 335nm peak intensities over the 380nm shoulders than the non-malignant tissue. Calculate the excitation ratio value for 460nm emission of

$$K_3 = I(335nm)/I(380nm) \qquad (5.6)$$

we have K_3=1.61 for malignant tissue and K_3=1.40 for non-malignant tissue.

Ten malignant and six non-malignant GYN tissues were studied. Table 5.8 list all the K_3 values from these samples. Figure 5.31 gives the histogram of these measured values. selecting the K_3=1.5 as a standard for separated K_3 values of range for malignant and non-malignant tissue, eight out of ten of the malignant tissues give the K_3 value above 1.5, while five out of six non-malignant tissues give the K_3 value below the 1.5. This leads to a statistical result with Sensitivity of 80% and Specificity of 83%. (see chapter 5.2 for the definitions of Sensitivity and Specificity).

According to the absorption and excitation spectra of the NADH, elastin and collagen (see Fig. 1.22, Fig. 1.19 and Fig.1.12), the excitation peak at 335nm may be caused by the NADH and the background and the shoulder around 380nm may be caused by the elastin and collagen. The whole spectral structure is the NADH excitation peak overlap on the excitation peak of the elastin and collagen. The spectral structure over the 360nm to 385nm may be due to elastin and collagen. This is also suggested by the lack of this structure in the excitation spectra from the cells with emission wavelength at 460nm in the previous results. (see Fig.4.26 to Fig. 4.27) The K_3 values of the malignant tissues are higher than the K_3 values of the non-malignant tissues. This may once again lead us to the conclusion that the NADH fluorescence is relatively stronger from the malignant tissues than from non-malignant tissues when compared with the fluorescence from connective proteins.

The excitation spectra of the tissues are also modified by the absorption of the blood. The dip at 420nm in the excitation spectra (Figs. 5.29 and 5.30) is caused by the blood absorption peak at 420nm. In this spectral range, the blood absorbance is slightly higher at 380nm than that at 335nm (see Fig. 1.2). The greater blood residue will cause the K_3 value to go higher. Since the non-malignant tissues <u>in vitro</u> usually contain more blood residue, the blood has a destructive effect on the statistical results.

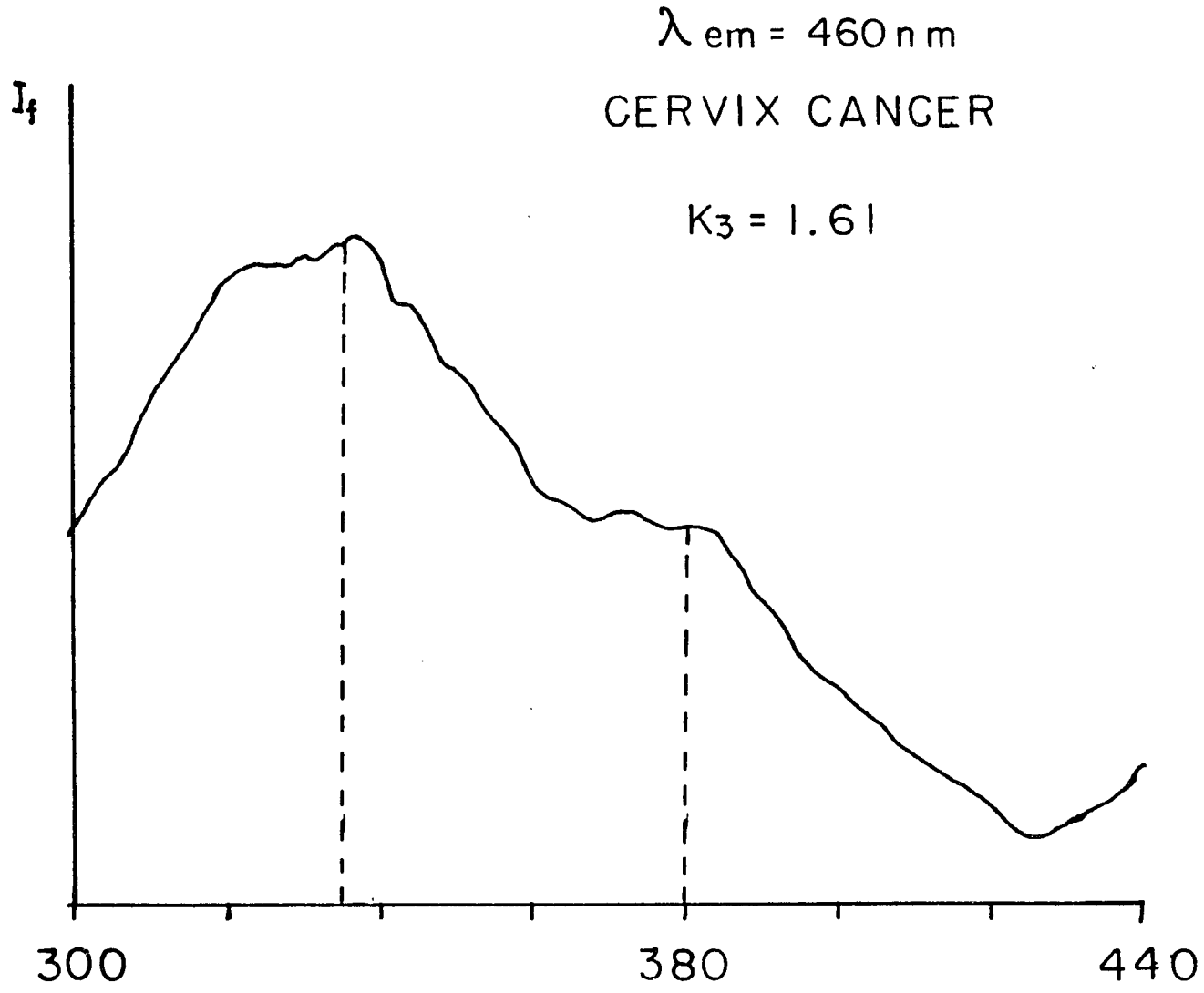

Figure 5.29. Excitation spectrum from malignant GYN tissue with emission wavelength at 460nm.

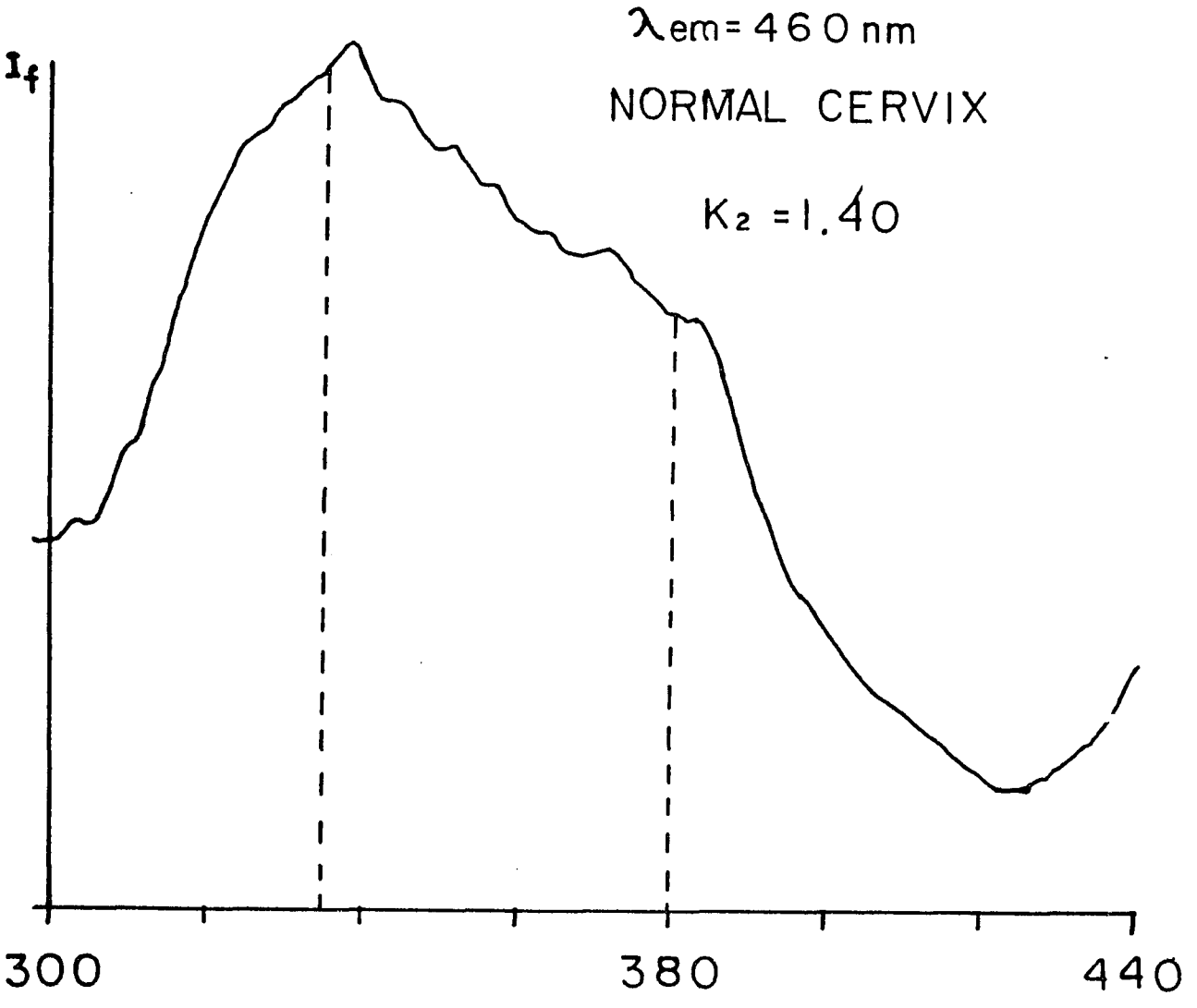

Figure 5.30. Excitation spectrum from non-malignant GYN tissue with emission wavelength at 460nm.

Table 5.8 List of the measured ratio K3 values from malignant and non-malignant GYN tissues with emission wavelength at 460nm (K3 = I(335nm)/I(380nm)).

Non-malignant Tissues	K3	Malignant Tissues	K3
Ovary	1.41	Endometrium	2.44
Cervix	1.27	Ovary	1.92
Ovary	1.45	Endometrium	2.13
Cervix	1.23	Cervix	1.61
Cervix	1.41	Ovary	2.44
Myometrium	1.69	Cervix	1.52
		Endometrium	1.47
		Ovary	2.0
		Ovary	1.96
		Endometrium	1.35
Standard	< 1.5		> 1.5
False Negative			20%
False Positive	17%		
Sensitivity			80%
Specificity	83%		

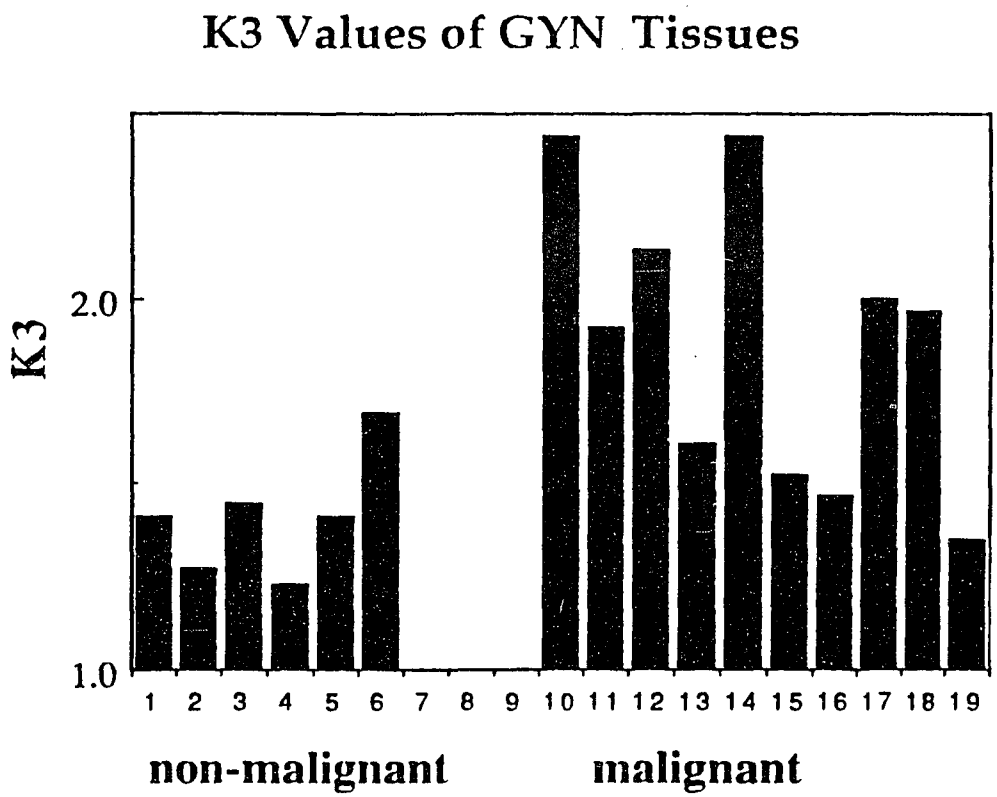

Figure 5.31. Histogram of the fluorescence intensities ratio K_3 = [I(λ=335nm)/I(λ=380nm)] over the examined tissues <u>in vitro</u> with emission wavelength at 460nm.

Chapter 6. Conclusion

This thesis has focused on the fluorescence spectroscopy from the human malignant and non-malignant cells and tissues in the UV and visible range. Based on the fluorescence properties of several important intrinsic fluorophors, an analysis has been done on what possible relative changes have occurred from each of the fluorophors' contribution to the spectra of non-malignant and malignant tissues and cells.

In this thesis, various excitation wavelengths have been used for exciting various groups of fluorophors inside the malignant and non-malignant tissues and cells: 300nm for exciting tryptophan, elastin ,collagen,and NADH; 320nm for collagen, elastin, and NADH; 351nm for elastin, NADH and flavins; 488nm for flavins. The excitation spectra with emission wavelength at 460nm which involved NADH, elastin and collagen, see Fig 1.32 and 1.33, in the tissues and cells has also been measured. The time-resolved fluorescence spectra with excitation wavelength at 351nm and time duration of 8ps has also been measured for studying the kinetics of the NADH in the malignant and non-malignant cells.

The fluorescence spectra profiles from the human cultured malignant and non-malignant cells with excitation wavelength

488nm all present a single band with a peak at the range form 525nm to 535nm. This might possibly arise from flavins in the cells.[100] However, the fluorescence spectra profiles from the human malignant tissues *in vitro* showed (with above 70% probability) a one band profile with peak at the range from 520nm to 530nm, while the fluorescence spectral profile from non-malignant tissues *in vitro* showed (with above 70% probability) a more complex structure of one major band with two subbands and two dips between the bands. The experiments show that these complex structures are caused by some residues in the interstitial medium in the tissues, which very possibly is blood. Therefore, the spectral differences between the malignant and non-malignant tissues *in vitro* may be showing that there is more blood residue in the malignant tissues *in vitro* than in the non-malignant tissues *in vitro*.

The study of the NADH fluorescence from the malignant and non-malignant cells shows that the NADH fluorescence from the malignant cells are relatively stronger than that from the non-malignant cells when compared to other molecules such as elastin. There is also a red peak shift on the excitation spectra from the malignant cells when compared to the peak position of the excitation spectra from the non-malignant cells. The time resolved fluorescence spectra study showed that the fluorescence decay time from the malignant cells are faster than those from the non-malignant cells. All these fluorescence spectral changes may indicate that the NADH is

bound more tightly in the non-malignant cells than in the malignant cells.

With the excitation wavelength 320nm, it was once again observed that the NADH peak at 450nm in the fluorescence spectra from malignant cell lines was relatively stronger than the spectra from the non-malignant cell line. The fluorescence spectra study from the GYN tissues has also shown that the NADH fluorescence peaking at 460nm from the malignant tissues is relatively stronger (over 70% out of the all tested samples) than from non-malignant tissues.

The wavelength 300nm excites tryptophan and most of the other fluorophors weakly. Selecting two wavelength points at 340nm and 440nm where the blood absorption has the same absorbance, the fluorescence intensity ratios at these two points (K1=I(340nm)/I(440nm)) can be calculated. With this ratio, which limited the blood reabsorption effects, the study shows that most of the malignant GYN tissues (over 93%) have ratio values over 11.5, but most of the non-malignant GYN tissues have ratio values below 11.5. This may indicate that the fluorescence from the tryptophan in the malignant tissues is stronger than in the non-malignant tissues. This might be related to the higher concentration of the free tryptophan in the tumor range.[133]

These studies of this thesis indicated that it is malignance related relative to NADH and tryptophan fluorescence intensity. These results might be related to the

metabolism state changes in the cells and tissues from non-malignancy to malignancy. These metabolism changes may have caused the environment around NADH and tryptophan to change.[132, 133, 110] The study results in this thesis can be developed into a new way of diagnosing cancer. It can also help us to understand what information of the biochemical changes and the physical process may be contained in these fluorescence spectra from malignant and non-malignant cells and tissues.

Chapter 7. Future Research Direction

This thesis has presented results on the fluorescence spectra from the human malignant and non-malignant cell lines and tissues. Certain analysis have been done in order to explain the spectral changes from non-malignancy to malignant tissues. This work is far from a full understanding of the whole structure of the spectra, their changes, and chromphores responsible for the spectroscopical changes. Additional studies should be done to make the fluorescence spectroscopy a new medical diagnostic tool.

In this thesis, My work suggests that the NADH in the malignant cells and tissues emits relatively stronger fluorescence than the NADH in the non-malignant cells and tissues. I suggested it may be caused by the different bind site of the NADH in the mitochondria of the malignant and non-malignant cells. However, I can not explain, from this study I did, what enzyme protein changes caused this NADH environment change. Further study should be done on both the biochemistry level and spectroscopy level to understand this change. The study should be related to extract mitochondria from malignant and non-malignant cells and measure their fluorescence spectra.

Fluorescence spectroscopy from malignant and non-malignant cell lines should also be studied to confirm my suggestion. It is known that the cells from different organs contain different amounts of NADH, so the fluorescence intensity will be different. Therefore, the study should be controlled better so that comparison of fluorescence spectra between the malignant and non-malignant cells are to be done on cells from same tissue's type and organ.

It is also suggested that the fluorescence spectra from the various cell components of the malignant and non-malignant cells should be studied. This study may give us a better understanding of the fluorescence spectra from the whole cell and may give us further findings.

The tissue is a complicated system. The malignant tumor grows progressively. The different positions in the tumor range have different physiologic characteristics. There are different types of the cancer. These types of variance have not clearly been taken into consideration in this thesis. The tumors have been considered as a single malignant group. It would be interesting to study the fluorescence spectra subjected to the differences described above. These study results may offer an explanation for the variances in the spectra and the variances of the ratio values in this thesis. This will take an enormous amount of work. The microscopic fluorescence meter is also suggested for the careful match of the pathology site.

The fluorescence model used in this thesis has ignored some fluorophors such as porphyrins, pyridoxic acid etc.. It has also ignored some other secondary absorption substances and only considered blood. Some other spectral modifications on the tissues such as peak shifting and spectral shape change may exist, but are not known at this time. A better model can be built after more information is available.

A study of the free tryptophan level and bound tryptophan should be done on the malignant and non-malignant tissue sites. The relationship between the fluorescence intensity from this free and bound tryptophan should be studied as well as the decay time of the fluorescence.

In this thesis, the GYN tissues have been studied as a group. Further statistical studies based on the individual tissues sub-groups (such as cervix, ovary, etc.) are suggested for a fine understanding of the way individual tissue groups behave.

Basically, more detailed research has to be done for a better understanding of the fluorescence spectroscopic information from the non-malignant and malignant cells and tissues.

Appendix I: Lists of the computer program for data treatment

1. **scmrwt.f** ---- A fortran program for rewriting the streak camera data file with 16 rows and 16 columns of the intensity data into the VAX data file with two columns 256 rows: first column is time axis and second column is intensity data.
2. **avtest.f** ---- A fortran program for averaging several date sets with the same kind of measurement.
3. **fcn01.f** ---- A fortran subroutine program for using double exponential function to fit the temporal fluorescence decay profiles. It works with **taurosv.f** in VAX.
4. **spcfit.f** ---- A fortran subroutine program used in the theoretical model to fit the fluorescence spectral profiles from the normal and cancerous human cell lines excited with 353nm. It works with **taurosv.f** in VAX.
5. **spctsu.f** ---- A fortran subroutine program used in the theoretical model to fit the fluorescence spectral profiles from malignant and non-malignant human GYN tissues excited with 320nm. It works with **taurosv.f** in VAX.

scmrwt.F

```
c       This program is for rewriting the streak camera data file
c       with 16 rows and 16 columns of the intenity data into the
c       VAX data file with two columns 256 rows: first column is
c       time axis and second column is intensity data.

c
c
        dimension x(300)
        character*14 aname, bname, cname
        aname='tsf015.dat'
        n=256
        m=16
        open(1, file=aname)
        do 50 i=1,n
        read(1,*) x(i)
 50     continue
        close(1)
        print*, 'Give data file bname'
        read(5,70) bname
 70     format(a14)
        print*, 'give exit date file cname'
        read(5,80) cname
 80     format(a14)
        open(3, file=bname)
        open(2, file=cname,status='new')
        j=1
        do 100 i=1,m
        read(3,*) a,b,c,d,e,f,g,h,o,p,q,r,s,t,u,v
        write(2,*) x(j), a
        j=j+1
        write(2,*) x(j), b
        j=j+1
        write(2,*) x(j), c
        j=j+1
        write(2,*) x(j), d
        j=j+1
        write(2,*) x(j), e
        j=j+1
        write(2,*) x(j), f
        j=j+1
        write(2,*) x(j), g
        j=j+1
        write(2,*) x(j), h
        j=j+1
        write(2,*) x(j), o
        j=j+1
```

```
      write(2,*) x(j), p
      j=j+1
      write(2,*) x(j), q
      j=j+1
      write(2,*) x(j), r
      j=j+1
      write(2,*) x(j), s
      j=j+1
      write(2,*) x(j), t
      j=j+1
      write(2,*) x(j), u
      j=j+1
      write(2,*) x(j), v
      j=j+1
100   continue
      end file(2)
      stop
      end
```

```
c  This program is for
c  do average to M-experiment data          Jan.24,'90 N.Y.
c  change from input 1-dimension to 2-dimension array      Jan.29.'90

      program avtest

      character filename*20,outdata*20
      dimension a0(300),pmax(10),nmax(10),a(300,10),b(350,10)
      dimension aa(350)
       dimension a1(3000,2)

CCC       m = 10
c       n = 300
       n = 256

c  read the array of exp.-data to array a0
       print *, 'give the number of array m=?'
       read *, m
c       print *, 'give the row number(array size) of the input file n=?'
c       read *, n

       nm = n*m

       print *, 'give the input exp.-data file name: filename?'
       read *, filename
       open(2,file=filename)
       read(2,*) ((a1(i,j),j=1,2),i=1,nm)
CCC       close(5)

        print *,"give output filename= "
        read*, outdata
        open(4,file=outdata)

c         write(6,611) (i,(j,a1(i,j),j=1,2),i=1,n)
 611     format(1x,'i =',i4,3x, 'j =',i3,3x, 'a1(i,j) =',e13.6,3x
     z                          'j =',i3,3x, 'a1(i,j) =',e13.6)

       ii = 1
 11     na = (ii-1)*n
         do 900 i=1,n
 900           a0(i) = a1(na+i,2)
c         write(6,613) (i,a0(i),i=1,n)
 613     format(2x,'i =',i4,4x, 'a0(i) =',e16.8)

c         stop 990

       pmax(ii) = 0.

       do 100 j=1,n
          if(a0(j).gt.pmax(ii)) then
            pmax(ii) = a0(j)
            nmax(ii) = j
```

```
        end if
100   continue

c  making up a 2-dimension array a(j,ii)
      do 110 j=1,n
110     a(j,ii) = a0(j)

      if(ii.ge.m) go to 22
      ii = ii+1
      go to 11

c  selecting one of the peak number maximum and minimum amongs m arrays
22    write(6,621) m
621   format(2x,'m =',i3)

      npmax = nmax(1)
      do 120 i=1,m
120     if(nmax(i).gt.npmax) npmax = nmax(i)
      npmin = nmax(1)
      do 130 i=1,m
130     if(nmax(i).lt.npmin) npmin = nmax(i)

      nd = npmax-npmin
      nn = n+nd
      write(6,631) nd
631   format(2x,'nd =',i3)

c  moving the peak place of array a(i,j) to number npmax
      do 140 i=1,m
        nmi = nmax(i)
        do 150 j=nmi,1,-1
150       b(npmax-(nmi-j),i) = a(j,i)
140   continue

      do 160 i=1,m
        nmi = nmax(i)
        do 160 j=nmi+1,n
        b(npmax+(j-nmi),i) = a(j,i)
160   continue

c       write(6,601) (i,(a(i,j),j=1,m),i=1,n)
c 601   format(/, ('i =',i4,3x, 3('a(i,j) =',e11.3,3x)))
 601    format(/, ('i =',i4,3x, 5(e11.3,3x)))
CCC       write(6,603) (i,(b(i,j),j=1,m),i=1,nn)
c 603   format(/, ('i =',i4,3x, 3('b(i,j) =',e11.3,3x)))
 603    format(/, ('i =',i4,3x, 5(e11.3,3x)))

c  assignning zero into empty place in array b(i,j)
      do 170 i=1,m
        nf = npmax-nmax(i)
        do 170 j=1,nf
          b(j,i) = 0.
170   continue
      do 180 i=1,m
```

```
        nf = npmax-nmax(i)
        ne = nf+n
        do 180 j=ne+1,nn
          b(j,i) = 0.
 180   continue

c  doing average
CCCCC       do 190 j=1,nn
        do 190 j=1,n
        sum = 0.
        do 200 i=1,m
 200        sum = sum+b(j,i)
        aa(j) = sum/m
 190   continue

CCC         print *,"give output filename= "
CCC         read*, outdata
CCC         open(4,file=outdata)

CCC         write(6,605) (j,aa(j),j=1,nn)
 605   format(2x,'j =',i4,4x, 'aa(j) =',e16.8)
CCCCC       write(4,101) (j,aa(j),j=1,nn)
        write(4,101) (j,aa(j),j=1,n)
 101   format(1x,i4,4x, e16.8)

      close(2)
      close (4)
CCC         close (5)
     stop
     end
```

FCN23.F

```
c       This progrram is for the double exponential function
c       to fit the temporal fluorescence decay profiles.


        subroutine fcn(npar, g,f,x,iflag)
c       for use with taurosv.f
c       for Gaussion fit to data
        implicit double precision ( a-h, o-z)
        character * 12 anam
      character * 12 onam
        character * 12 mnam
        dimension  y(300), z(300), x(5),c(300),w(300)
        go to (10,60,60,60,120) iflag


 10     print *, "name of datafile.ext"
        read  *, anam
      print *, "name of output data file"
        read *, onam
        print *,"name of output error file"
        read *,mnam
        print *,"pleasee input n "
        read *,n
 21     format (a10)
        open(1,file=anam)
        do 50 i=1,n
        read (1,*)w(i),c(i)
      y(i) = c(i)
 50     continue
        y(j)=0
        do 20 i=1,n
        if (y(i).lt.y(j)) go to 20
        y(j)=y(i)
        w(j)=w(i)
        m=i
 20     continue
 60     do 65    i=m,n
        z(i)=x(1)*exp(-(w(i)-w(j))/x(2))+x(3)*exp(-(w(i)-w(j))/x(4))
 65     continue
        f=0.0
        do 70 i=m,n
        f=f+(y(i)-z(i))**2
 70     continue
      if (iflag.ne.3) return
        nn=0
        ss=0.0
```

```
      do 75 i=m,n
      c(i)=z(i)-y(i)
      if (z(i).lt.1.0e-5) go to 75
      ss=ss+(y(i)-z(i))**2
      nn=nn+1
75    continue
      chi=ss/nn-2
110   open(2,file="ch")
      write(2,*) 'reduced chi-squared is',chi
      close(2,status="keep")
120   open (6, file="prmeters")
      write (6,*) 'fitting A1,t1,A2,t2=',x(1),x(2),x(3),x(4)
      close (6, status="keep")
      open(2,file=mnam)
      open(4,file=onam)
      do 500 i=1,n
      write(4,*)w(i),z(i)
      write(2,*)w(i),c(i)
      print *,w(i),y(i),z(i)
500   continue
      close(2,status="keep")
      close(4,status="keeP")
      chi=ss/(nn-2)
      print *,"The reduced chi-squared is", chi
      end
```

SPCFIT.F

```
c     This program is used forthe theoretical model to fit the
c       fluorescence spectral profiles from the normal and
c       cancerous human cell lines excited with 353nm.

        subroutine fcn(npar, g,f,x,iflag)
c       for use with taurosv.f
        implicit double precision ( a-h, o-z)
c       character * 12 anam
      character * 12 onam
        character * 12 mnam
c       character * 12 bnam
        character * 12 fnam
        dimension  y(300), z(300), x(5),c(300),w(300)
        dimension  a(300), b(300),d(300), w1(300), w2(300)
        go to (10,60,60,60,120) iflag


 10     print *, "name of datafile.ext"
        read  *, onam
C       print *, "name of nadhdata.ext"
C       read *,  anam
C      print *, "name of  faddata file"
C       read *, bnam
        print *,"name of output error file"
        read *,mnam
        print *, "name of output fitting file"
        read *, fnam
        print *,"pleasee input n "
        read *,n
C
        open(1,file=onam)
        do 50 i=1,n
        read (1,*)  w(i),c(i)
      y(i) = c(i)
 50     continue
        close(1)
C
        open(1,file="nadh.dn")
        do 52 i=1,n+4
        read (1,*) w1(i), a(i)
 52     continue
        close(1)
C
        open(1,file="fad.dn")
        do 54 i=1,n
        read (1,*) w2(i), b(i)
```

```
 54     continue
        close(1)
C
        open(1,file="clst.dn")
        do 56 i=1,n
        read (1,*) w2(i), d(i)
 56     continue
        close(1)
C
 60     do 65 i=1,n
        z(i)=x(1)*a(i+2)+x(2)*b(i)+x(3)*d(i)+x(4)
 65     continue
        f=0.0
        do 70 i=1,n
        f=f+(y(i)-z(i))**2
 70     continue
      if (iflag.ne.3) return
        nn=0
        ss=0.0
        do 75 i=1,n
        c(i)=z(i)-y(i)
        if (z(i).lt.1.0e-5) go to 75
        ss=ss+(y(i)-z(i))**2
        nn=nn+1
75    continue
        chi=ss/(nn-2)
110     open(2,file=fnam)
        do 115 i=1,n
        write(2,*) w(i), z(i)
115     continue
        close(2,status="keep")
120    open (6, file="result")
        write (6,*) 'fitting a,b,c, R =',x(1),x(2),x(3),chi
        close (6, status="keep")
        open(2,file=mnam)
        do 500 i=1,n
        write(2,*)w(i),c(i)
500     continue
      close(2,status="keep")
        stop
        end
```

spctsu.F

```
c       This program is used in the theoretical model fitting to
c       the fluorescence spectral profiles from malignant and
c       non-malignant human GYN tissues excited with 320nm.
        subroutine fcn(npar, g,f,x,iflag)
c       for use with taurosv.f
        implicit double precision (a-h, o-z)
      character * 12 onam
        character * 12 mnam
c       character * 12 bnam
        character * 12 fnam
        dimension  y(300), z(300), p(300), x(7),c(300),w(300)
        dimension  a(300), b(300),d(300), e(300), g(300)
        go to (10,60,60,60,120) iflag
c
c
 10     print *, "name of datafile.ext"
        read  *, onam
        print *,"name of output error file"
        read *,mnam
        print *, "name of output fitting file"
        read *, fnam
        print *,"input n "
        read *,n
C
        open(1,file=onam)
        do 50 i=1,n
        read (1,*)  w(i),c(i)
      y(i) = c(i)
 50     continue
        close(1)
C
        open(1,file="nadh.dn")
        do 52 i=1,n+4
        read (1,*) w(i), a(i)
 52     continue
        close(1)
C
        open(1,file="fad.dn")
        do 54 i=1,n
        read (1,*) w(i), b(i)
 54     continue
        close(1)
C
        open(1,file="elst.dn")
        do 56 i=1,n
        read (1,*) w(i), d(i)
```

```
 56     continue
        close(1)
c
        open(1,file="clgn.dn")
        do 57 i=1,n
        read (1,*) w(i), c(i)
 57     continue
        close(1)
c
        open(1,file="blod.dn")
        do 58 i=1,n
        read (1,*) w(i), g(i)
 58     continue
        close(1)
C
 60     do 65 i=1,n
        p(i)=x(1)*a(i+2)+x(2)*b(i)+x(3)*d(i)+x(4)*c(i)
c       print*, p(i)
        z(i)=p(i)/(x(6)+x(5)*g(i))+x(7)
c       print*,x(1),x(2),x(3),x(4),x(5),x(6),x(7)
 65     continue
        f=0.0
        do 70 i=1,n
        f=f+(y(i)-z(i))**2
 70     continue
      if (iflag.ne.3) return
        ss=0.0
        do 75 i=1,n
        c(i)=z(i)-y(i)
        ss=ss+(y(i)-z(i))**2
75     continue
        chi=ss/(n-2)
110     open(2,file=fnam)
        do 115 i=1,n
        write(2,*) w(i), z(i)
115     continue
        close(2,status="keep")
120    open (6, file="result")
        write (6,*) 'NADH,FAD,elastin,colagen,blood,abs,C,R ='
        write (6,*) x(1),x(2),x(3),x(4), x(5),x(6),x(7),chi
        close (6, status="keep")
        open(2,file=mnam)
        do 500 i=1,n
        write(2,*)w(i),c(i)
500     continue
      close(2,status="keep")
        stop
        end
```

Appendix II The calibration of the time axis of the streak camera

In the streak camera, the temporal intensity profile is recorded by 256 micro channels. The following procedure was done to obtain the time which corresponded to each channel.

1) Set the optical path as shown in Figure II.1. Let the single laser pulse path **Etalon** perpendicularly then into the streak camera. The Etalon is made by two parallel set of the 70% and 50% reflect mirrors and in between with a separation block of length d. The part of the single pulse path the etalon, but part of the pulse, will be reflected in the etalon again and again, so the single pulse become to a pulse train. The streak camera received pulses should be time separated by $\delta t=2d/c$, where c is the light speed in the air.

2) Select a streak camera time sweeping speed and a corresponding separation block with proper δt. Record the tumoral profile. The recorded temporal profile and δt vises each time sweeping speed is listed as follows[1]:

---

[1]. The measurement has been done with the window selected as the full screen. The intensities of the pulses in the pulse train are not appeared as decreasing expenatially because the demaged area in the streak carema screen. This should not affact the time position of the pulses much. The fluorescence decay measurement were done under the selection of the window in the non-demaged area. See the Appendix III.

speed	δt	Profile Fig. No.
1.5mm/ns	330.6ps	Figure II.2
3.0mm/ns	230ps	Figure II.3
7.5mm/ns	59.7ps	Figure II.4
15mm/ns	59.7ps	Figure II.5

3) Read the channel numbers where the pulse peak is located. List the channel numbers vise time with the assumption that the first peak is at time 0. This gives a data file as at several point of the channel vise time for each streak camera sweeping speed.

4) Use the non-linear function

$$y(x) = A + Bx + Cx^2 \qquad \text{(II.1)}$$

to fit the data files which obtained in step 3). The goodness of fitting are shown in Figures II.6 to II.9 for each streak camera sweeping speed, respectively. The fitting results give the function relationship between the channel numbers (as x in Eq. II.1) and time (as y in Eq. II.1). The obtained A, B, and C values for each streak camera sweeping speed are listed below:

Speed	A(ps)	B(ps/ch)	C(ps/ch^2)
1.5mm/ns	-732.5	20.03	5.6×10^{-3}
3.0mm/ns	-496.09	12.44	-2.95×10^{-3}
7.5mm/ns	-94.48	4.223	2.7×10^{-3}
15mm/ns	-44.99	2.426	-8.24×10^{-4}

5) Use function

$$y(x) = B_i\, x + C_i\, x^2 \qquad \text{(II.2)}$$

one can calculate the time each channel corresponded for each streak camera sweeping speed. Here the channel 0 is corresponding to time 0.

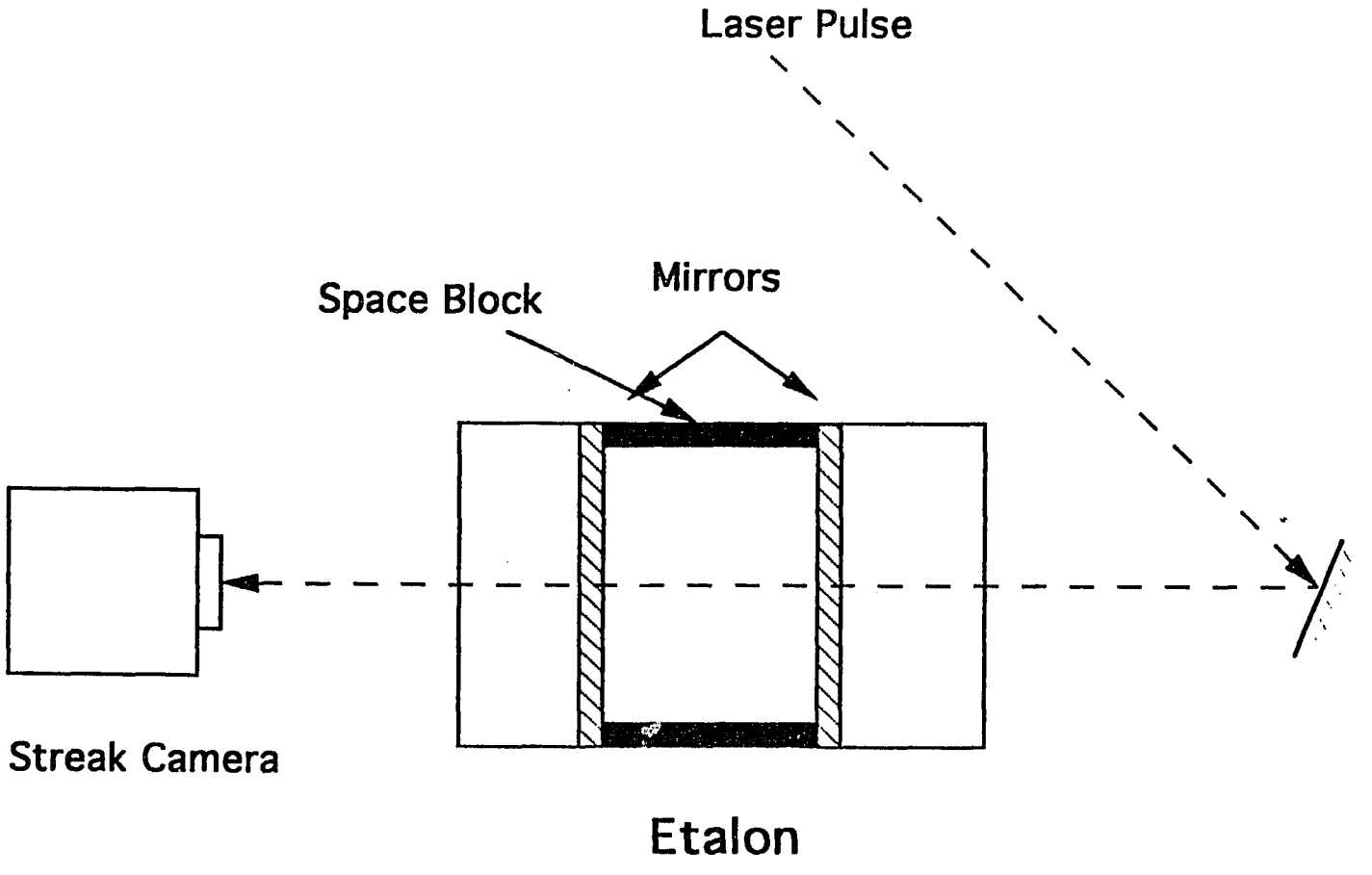

Figure II.1 Optical setup of using Etalon to calibrate the time axis of the streak camera.

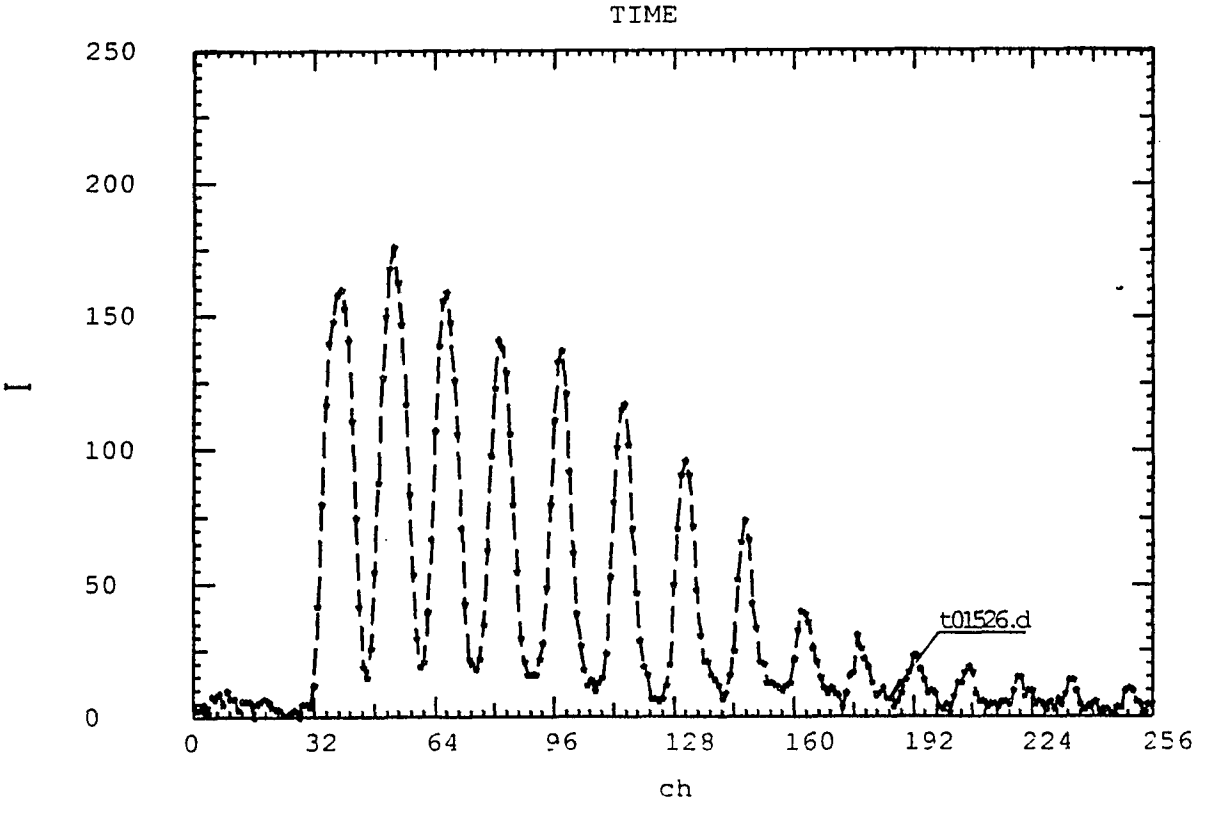

Figure II.2 Temporal profile from Etalon at streak camera sweeping speed 1.5mm/ns.

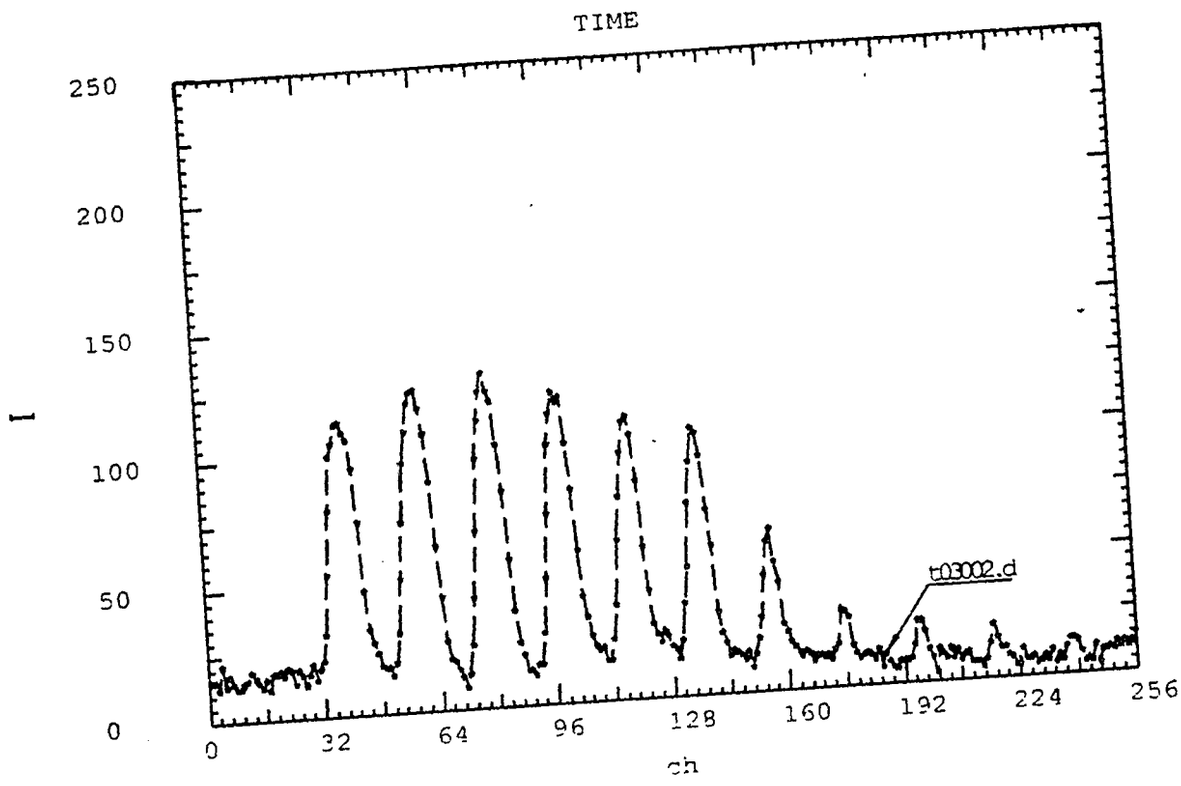

Figure II.3 Temporal profile from Etalon at streak camera sweeping speed 3.0mm/ns.

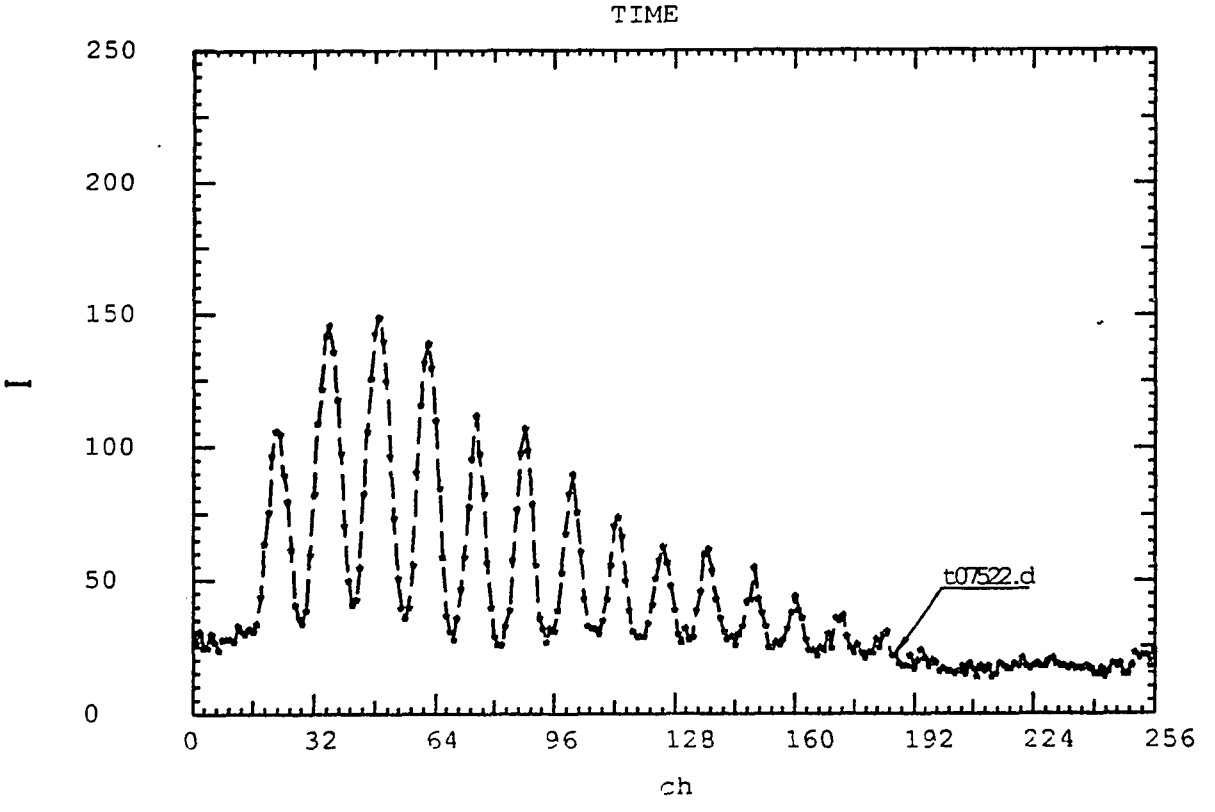

Figure II.4 Temporal profile from Etalon at streak camera sweeping speed 7.5mm/ns.

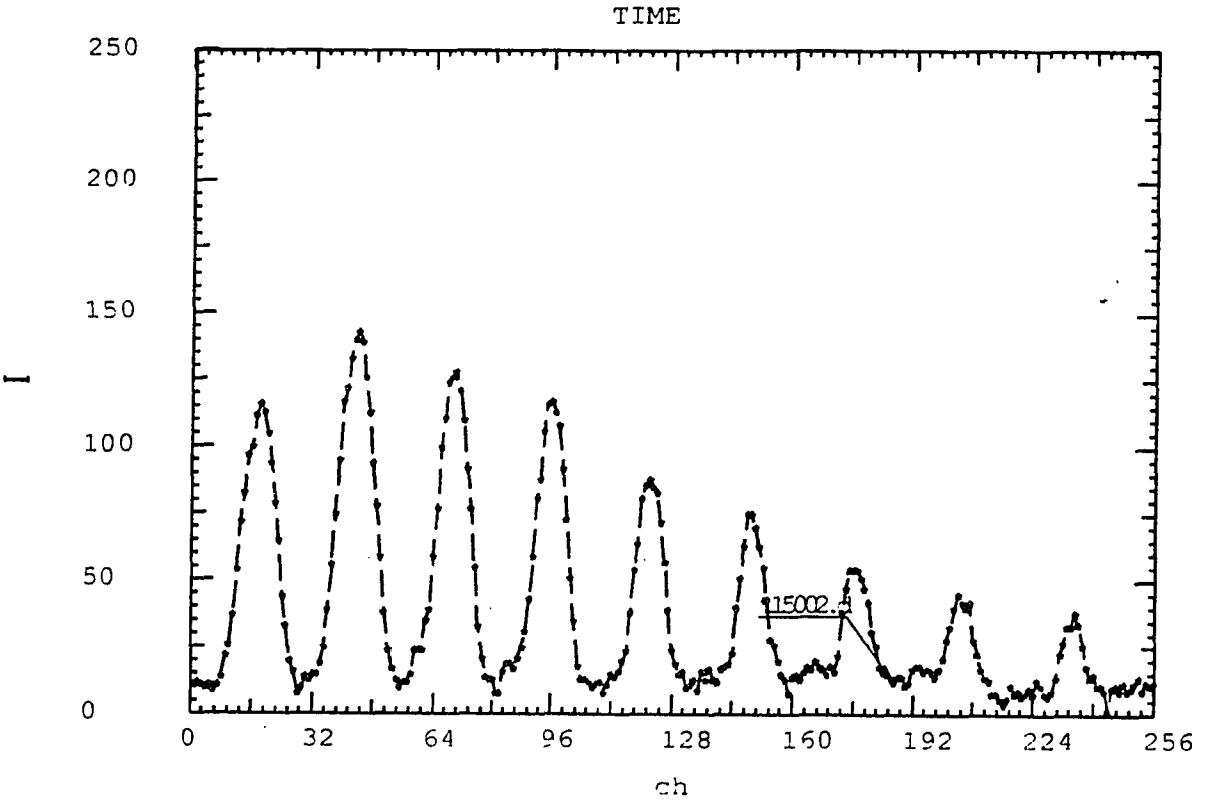

Figure II.5 Temporal profile from Etalon at streak camera sweeping speed 15mm/ns.

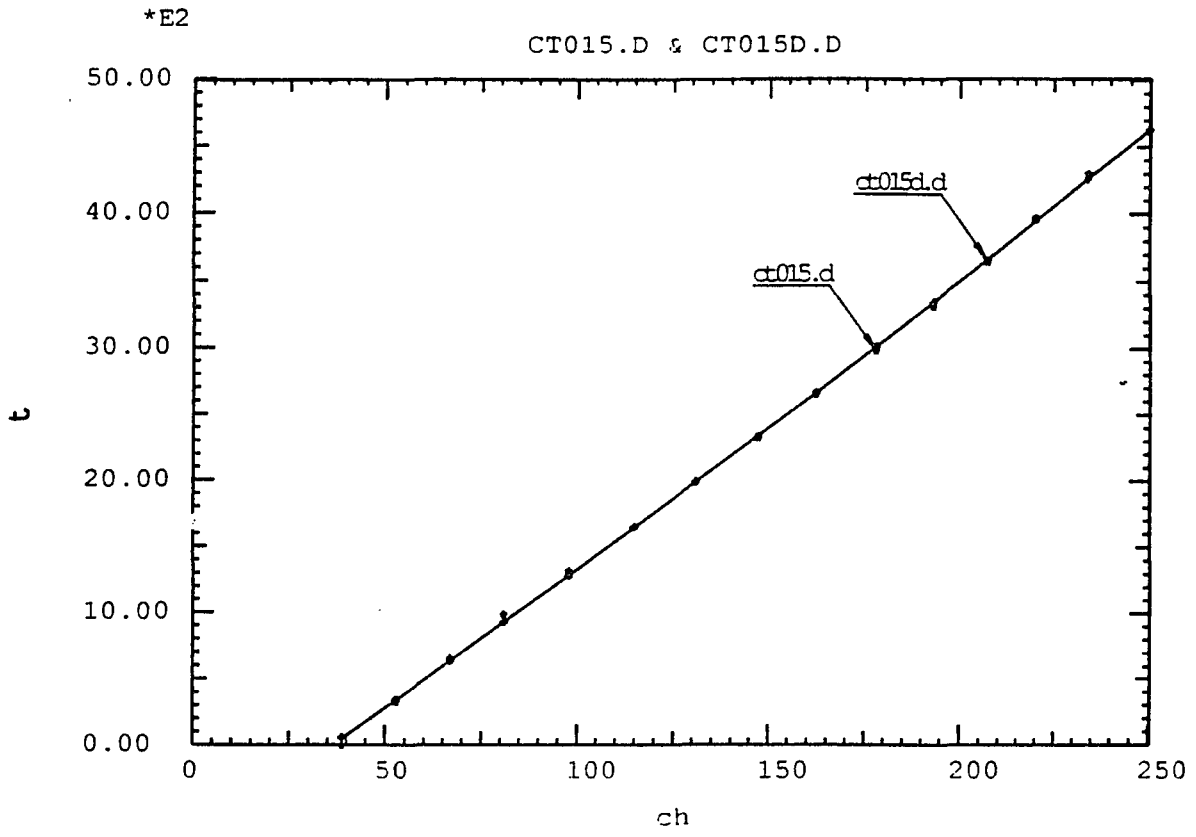

Figure II.6 Goodness of the using the second order function (Eq.II.1) to fit the obtained time vise channel number data at streak camera sweeping speed 1.5mm/ns.

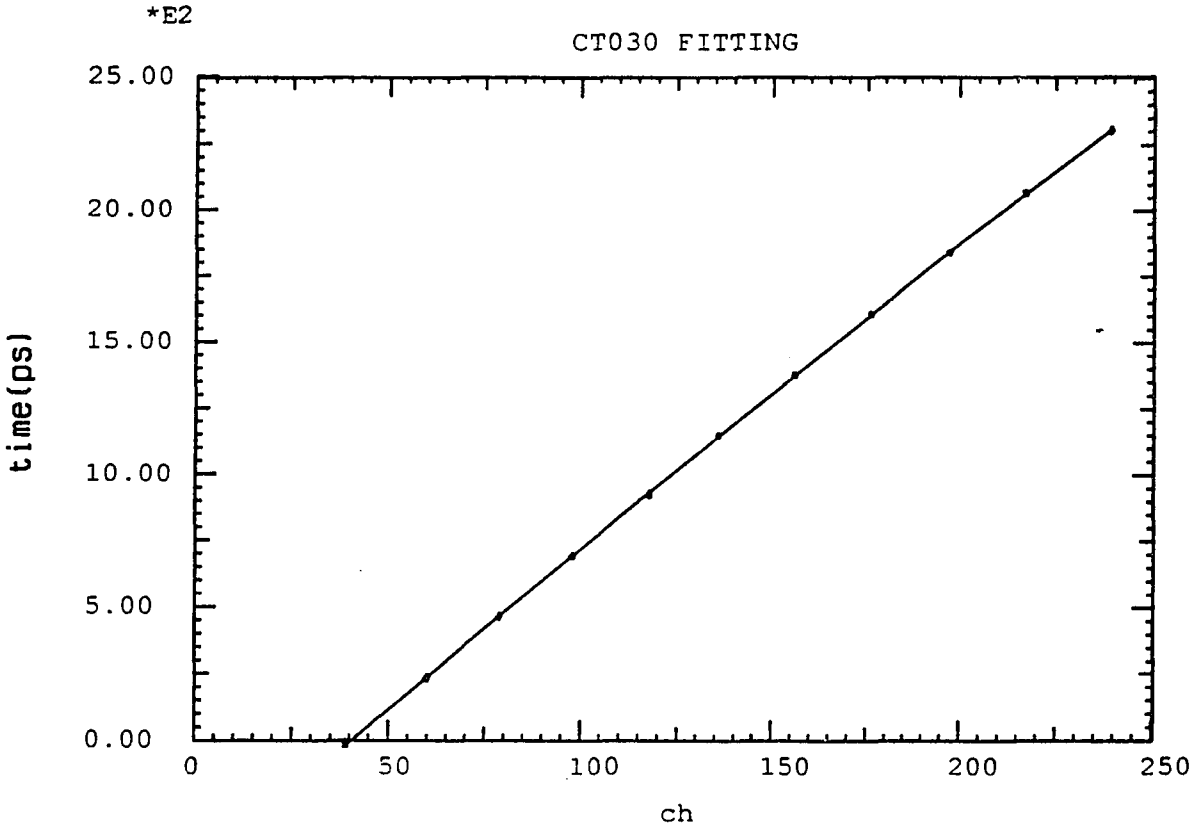

Figure II.7 Goodness of the using the second order function (Eq.II.1) to fit the obtained time vise channel number data at streak camera sweeping speed 3.0mm/ns.

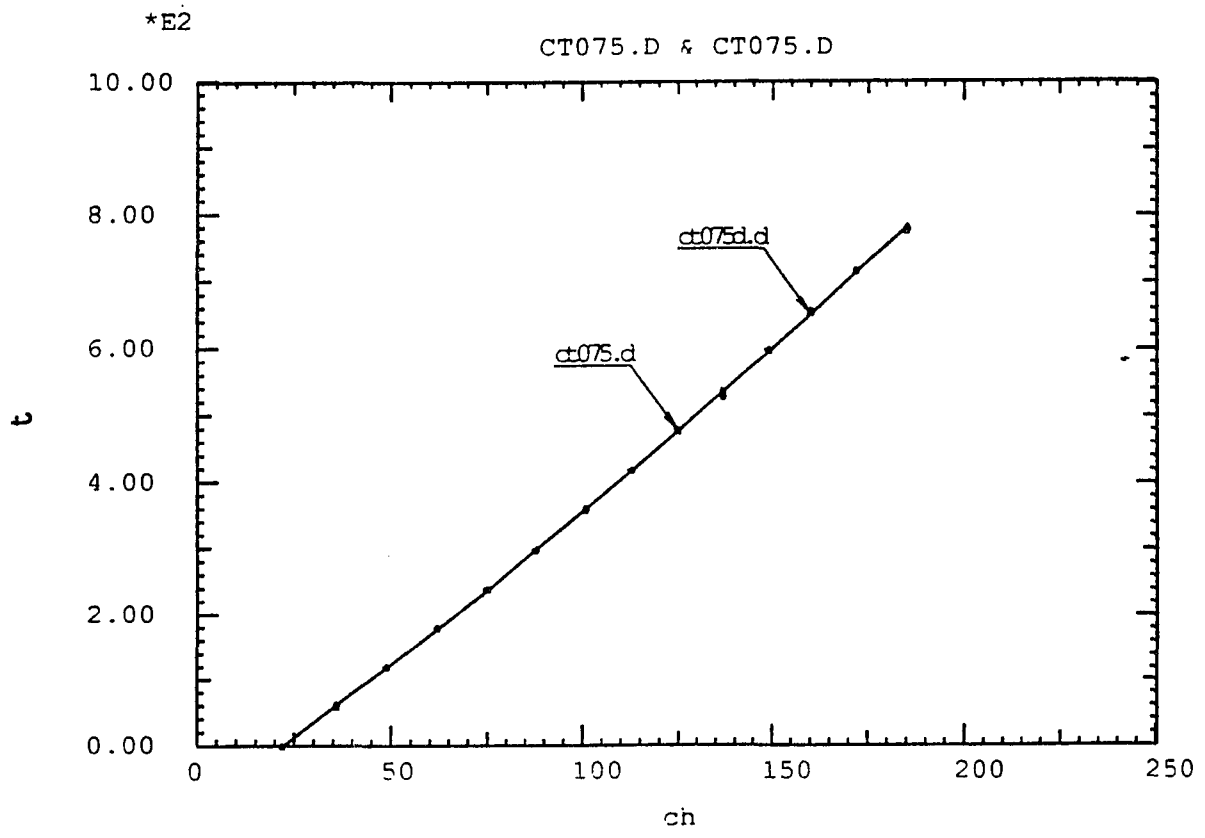

Figure II.8 Goodness of the using the second order function (Eq.II.1) to fit the obtained time vise channel number data at streak camera sweeping speed 7.5mm/ns.

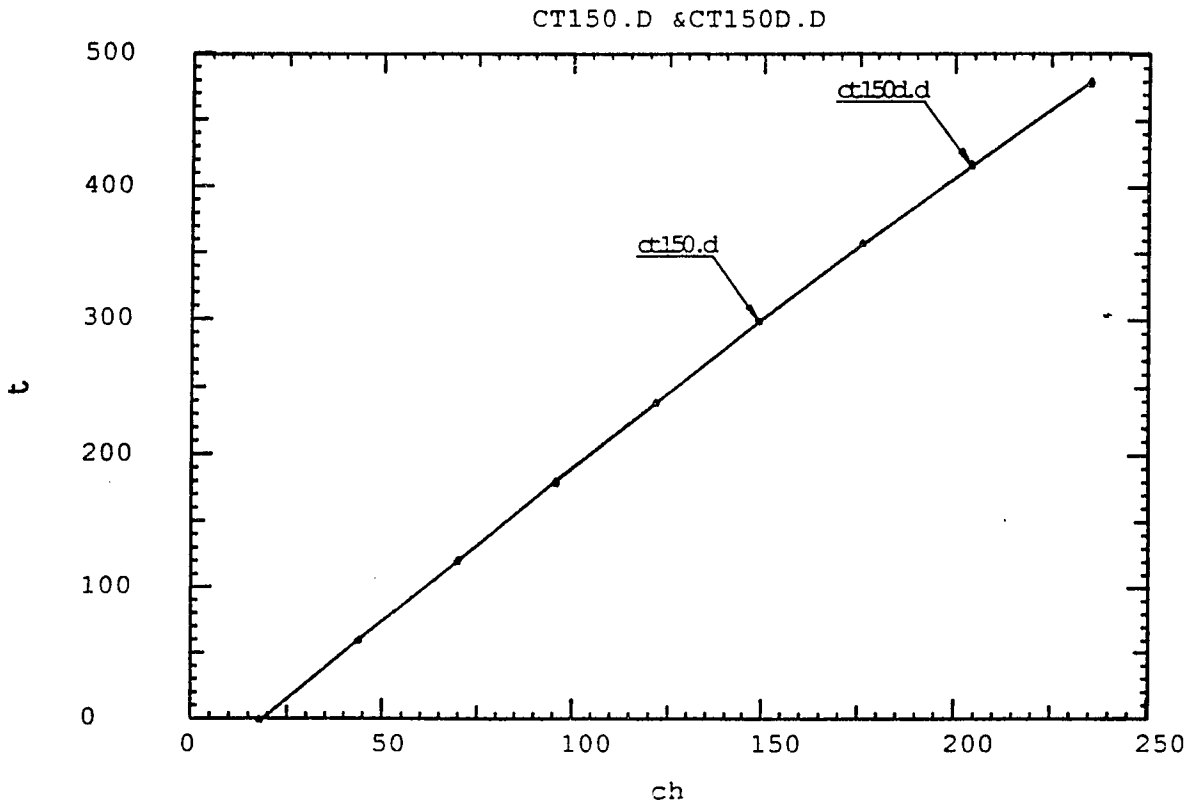

Figure II.9 Goodness of the using the second order fuction (Eq.II.1) to fit the obtained time vise channel number data at streak camera sweeping speed 15mm/ns.

Appendix III Checking the correctness of the measured temporal profile

The fluorescence decay profile from Erythrosin disodium salt dissolved in water (concentration is about 2mM) have been measured in the selected window area for checking the streak camera's working condition. The known decay time of Erythrosin disodium salt in water is around 86ps. The measured fluorescence decay profiles at streak camera sweeping speed 1.5mm/ns and 15mm/ns and the goodness of the exponential function fitting are shown in Figure II.10 and II.11, respectively. The obtained decay time is 96ps and 83ps for 1.5mm/ns and 15mm/ns sweeping speed respectively. They are close to 86ps. Therefore, the measured data from the streak camera are reliable.

One shoule check the system of streak camera by using this dye and obtaining a decay time of 83ps in fluroescence decay profile.

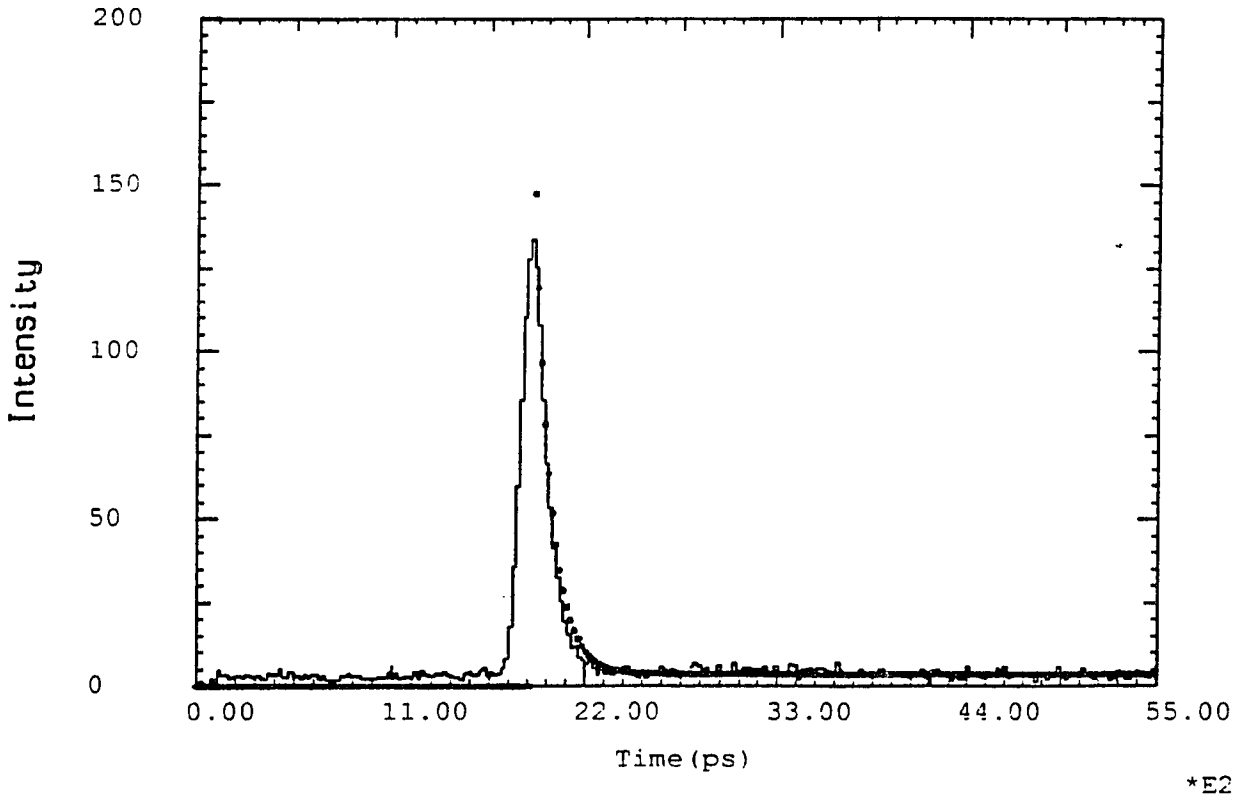

Figure III.1 Measured fluorescence decay profile of Erythrosin disodium salt dissolved in water (concentration is about 2mM) and the goodness of the double exponential function fitting at streak camera sweeping speed 1.5mm/ns. The fast decay time is 96ps.

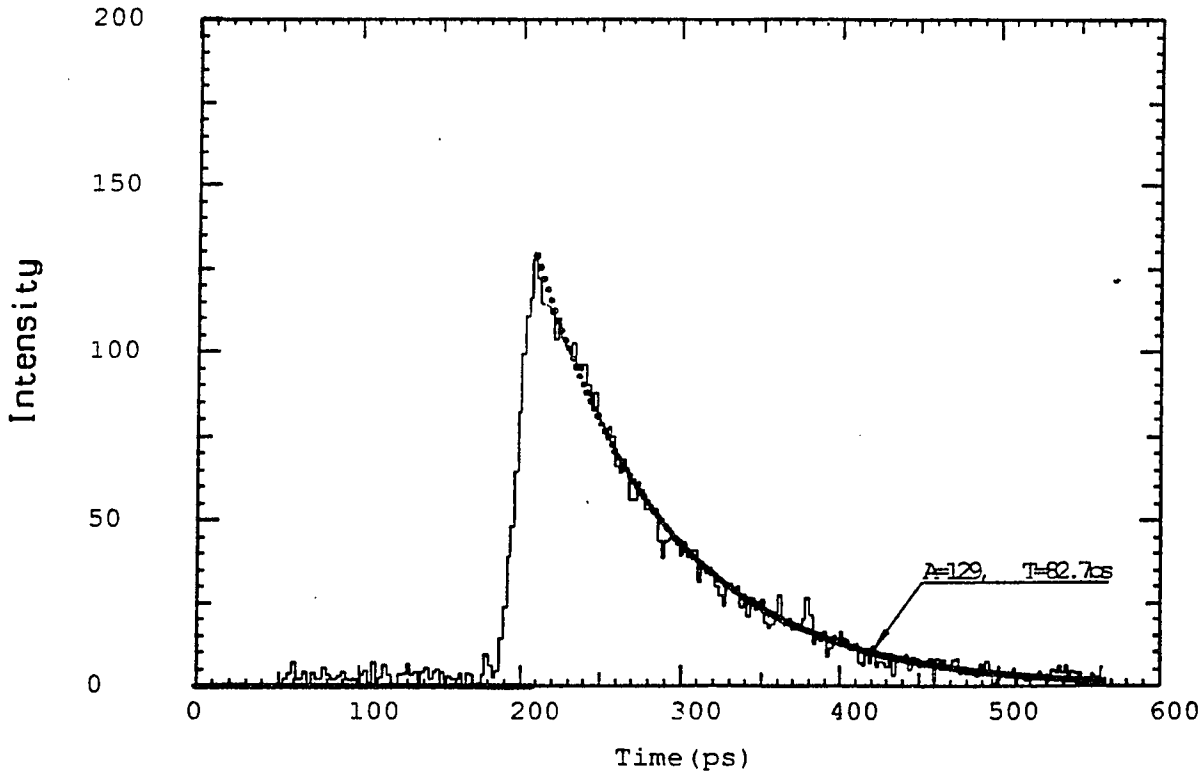

Figure III.2 Measured fluorescence decay profile of Erythrosin disodium salt dissolved in water (concentration is about 2mM) and the goodness of the single exponential function fitting at streak camera sweeping speed 15mm/ns. The fast decay time is 83ps.

Bibliography:

1. Daily News, December 26, (1991)

2. Welsh, Frank A., O'Connor, Michael J., Langfitt, Thomas W., Science, **198**:951, (1977)

3. Andreoni, A., Cubeddu, De Silvestri, S., and Laporta, P. Chem. Phys. Lett **88**, 33-36, (1982).

4. Dougherty, T.J., Kaufman, J.E., Goldfarb, A., Weishaupt, K.R., Boyle, D.G. and Mittelman, A. Cancer Research **38**, 2628, (1978).

5. Kessel, D. Photochem. Photobiol. **38**, 851-859, (1984).

6. Kessel, D., Dougherty, T.J. (Editors) Porphyrin Photosensitization. Plenum Press: New York, (1983).

7. Alfano, R. R. and Yao, S.S. Journ. Dent. Res. **60**, 120-122, (1981).

8. Alfano, R.R., Lam, W., Zarrabi, H.J., Alfano, M.A., Cordero, Tata, B.T. and Swenberg, Charles E. IEEE J. of Quant. Elec. **QE-20**:1512-1516, (1984).

9. R.R. Alfano, D.B. Tata, J. Cordero, P. Tomashefsky, F.W. Longo, and M.A. Alfano, Laser induced fluorescence spectroscopy from native cancerious aqnd normal tissues in IEEE J. quant. Electron. **QE-20**:1507, (1984)

10. Alfano, R.R., Tang, G.C., Pradhan, A., Lam, W., Choy, D.S.J. IEEE J. Quantum Electron. **QE-23**, 1806-1811, (1987).

11. Alfano, R.R., Pradhan, A., Tang, G.C., and Wahl, S.J. Optical sepctroscopic diagnosis of cancer and normal breast tissues in J. Opt. Soc. Am. B, **6**:1015 (1989)

12. Tang, G.C., Pradhan, A., Sha, W.L., Chen, J., Liu, C.H., Wahl, S.J., Alfano, R.R., Pulsed and cw laser fluorescence spectra from cancerous, normal, and chemically treated normal human breast and lung tissues in Appl. Opt. Vol. 28, No. 12, 2337-2342 (1989).

13. Tang, G.C., Pradhan, A., Alfano, R.R., Spectroscopic differences between human cancer and normal lung and breast tissues in Lasers in Surg. and Med., 9, pp. 290-

295 (1989).

14. Alfano, R.R., Das, B.B., Cleary, J., Prudente, R., Celmen, E.J., Bull. N.Y. Acad. Med., second series, **67**(2):143 (1991)

15. Glassman, W. S., Liu, C.H., Tang, G.C., Liubicz, S., Alfano, R.R., Lasers in the Life Science **4(1)**:1 (1991)

16. Pradhan, A., Das, B.B., Yoo, K.M., Cleary, J., , Prudente, R., Celmer, E., and Alfano, R.R. Lasers in the Life Sciences **4(4)**:225 (1992).

17. Alfano, R.R., Liu, C.H., Sha, W.L., Zhu, H.R., Akins, D.L., Cleary, J., Prudente, R., and Cellmer, C. Lasers in the Life Sciences **4(1)**:23 (1991).

18. Liu, C.H., Glassman, W.L.S., Alfano, R.R.Zhu, H.R., Akins, D.L., Deckelbaum, L.I., Stetz, M.L., OBrien, K, and Scott, J. SPIE Proceeding Vol. 1599 **No. 57** (1991).

19. Liu, C.H., Glassman, W.L.S., Zhu, H.R., Akins, D.L., Deckelbaum, L.I., Stetz, M.L., O'Brien, K, Scott, J., and Alfano, R.R. Lasers in the Life Sciences **4(4)**:257 (1992).

20. Liu, C.H., Das, B.B., Glassman, W.L.S., Tang, G.,C. Yoo, K.M., Zhu, H.R., Akins, D.L., Lubicz, S.S., Cleary, J., Prudente, R., Celmer, E., and Alfano, R.R. J. Photochem. Phtobiol. B: Biol. 1-23 (1992).

21. Pradhan, A., Das, B.B., Alfano, R.R., D.L., O'Brien, K, Stetz, M.L., Scott, J., Deckelbaum, L.I. SPIE Proceeding Vol. 1425 (1991).

22. Glassman, W. S., Steinberg, M., Alfano, R.R., Accepted by Lasers in the Life Science. (1993).

23. Kittrel, C., Willet, R.L., de Los Santos Pacheo C., Ratcliff, N.B., Kramer, J.R., Malk, E.G. and Feld, M.S. Appl. Opt. **24**, 2280-2281, (1985).

24. Baraga, J.J., Taroni, P., Park, Y.D., An, K., Maestri, A., Tong, L.L., Rava, R.P., Kittrell, C., Dasari, R.R., and Feld, M.S., Spectrochim. Acta, **45A**:96, (1989).

25. Park, Y.D., Dasari, R.R., Feld, M.S., Time-resolved UV fluorescence spectroscopy of aorta using 320 nm excitation in SPIE Vol. 1204, pp. 499-504 (1990).

26. Cothren, R.D., richards-Kortum, R., Sivak, M.V., Fitzmaurice, M., Rava, R.P., Boyce, G.A., Doxtander, M.,

Blackman, R., Ivanc, T.B., Hayes, G.B., Feld, M.S., Petras, R.E. Gastrointestinal Endoscopy Vol. 36 **2:105** (1990).

27. Richards-Kortum, R., Rava, R.P., Petras, R.E., Fitzmaurice, M., Sivak, M. and Feld, M.S., Photochem. & Photobiol., **53(6)**:777 (1991)

28. Rava, R.P., Richards-Kortum, R., Fitzmaurice, M., Cothren, R., Petras, R., Sivak, M., Levin, H., Feld, M.S., Early detection of dysplasia in colon and bladder tissue using laser induced fluorescence in SPIE Vol 1426, (1991).

29. Deckelbaum, L.I., Jam, J.K., Cabin, H.S., Clubb, K.S., Long, M.B. Lasers Surg. Med. **7:330-335** (1987).

30. Deckelbaum, L.I., Stetz, M.L., O'Brien, Cutruzzola, F.W., Gmitro, A.F., Laifer, L.I., and Gindi, G.R. Lasers in Surgery and Medicine **9**:205-214 (1989).

31. Deckelbaum, L.I., Sarembeck, I.J., Stetz, M.L., O'Brien, Cutruzzola, F.W., Gmitro, A.F., and Ezekowitz, M.D. SPIE Proceeding, **906**:314-319 (1988).

32. Lefell, D.J., Stetz, M.L., Milstone, L.M., Deckelbaum, L.I., In Vivo Fluorescence of Human Skin: A potential marker of Photoaging in Arch Dermatol, **124**:1514-1518 (1988).

33. Kapadia, C.R., Cutruzzola, F.W., O'Brien, K.M., Stetz, M.L., Enriquez, R., Deckelbaum, L.I., Gastroenterology, **99**:150 (1990)

34. Yuanlong, Y., Yanming, Y., Fuming, L. , Yufen, L., and Paozhong, M. Lasers in Surgery and Med. **7**:528-532 (1987).

35. Konig, K., Hibst, R., Flemming, G., Schneckenburger, H., Laser Induced Autofluorescence of Caries, SPIE, 1993.

36. Ankerst, J., Montan, S., and Svanberg, K., Appl. Spectr. **38**:890-6 (1984).

37. Montan, S., Svaberg, K., and Svaberg, S. Opt. Lett. **10**:56-8 (1985).

38. Svanberg, K., Kjellen, E., Ankerst, J., Montan, S., Sjoholm, E., and Svanberg, S. Cancer Res. **46**:3803-8 (1986).

39. Andersson-Engels, J., Ankerst, J., Johansson, K, and Svanberg, K. Lasers Med. Sci. **4**:115-123 (1989).

40. Anderson, P.S., Kjellen, E., Montan, S., Svaberg, K., and Svaberg, S. "Autofluorescence of Various Rodent Tissues and Human Skin Tumor Samples" Unpublished Manuscript, Lund Institute of Technology:Sweden.

41. Anderson, P.S., Gustafson, A., Stenram, U., Svaberg, K., and Svaberg, S. Lasers Med. Sci. , **2**:261-6 (1987).

42. Andersson-Engels, S., Gustafson, A., Stenram, U., Svaberg, K., and Svaberg, S. Lasers in the Life Sciences

43. Lohman, W., Nickel, T., Schmidt, E., and Ibrahim, M. Naturwissenshaften **75**:365-7 (1988).

44. Lohman, W. Mussman, J., Lohman, C. and Konzel, W. Eur. J. Obstet. Gynecol. Reprod. Biol. **31**:249-53 (1989).

45. Lohman, W. Mussman, J., Lohman, C. and Konzel, W. Naturwissenshaften **76**:125-7 (1989).

46. Lohman, W., and Paul, E. Naturwissenshaften **76**:424-6 (1989).

47. Schomacker, Kevin T., Frisoli, J. K., Compton, C. C., Flotte, T.J., Richter, J.M., Nishioka, N.S., and Deutsch, T.F. Lasers in Surgery and Medicine **12**:63-78 (1992)

48. Schomacker, Kevin T., Frisoli, J. K., Compton, C. C., Flotte, T.J., Richter, J.M., Deutsch, T.F. and Nishioka, N.S. Gastroenterology **102**, April,(1992).

49. Biological Sciences Curriculum Study of the American Isntituted of Biological Science, Biological Science -- Molecules to Man, Houghton Mifflin Company, Boston, (1963).

50. Prehn, Richmond T., and Prehn, Lisa M., "pathobiology of neoplasia: a teaching monograph", cancer, ed. by Kruse, louise, Reese, Jean 1., Hart Laura k., The C.V. Mosby Company, (1979).

51. Sugarbaker, Everott V., Ketcham, Alfrad S., "mechanisms and prevention of cancer dissemination: an overview", cancer, ed. by Kruse, louise, Reese, Jean 1., Hart Laura k., The C.V. Mosby Company, (1979).

52. Brachet, J., Sci. Am., **205**:3, (1961)

53. Richands-kortum, R., Thesis, MIT, (1987)

54. Chance, B., Kinetics of Enzyme Reactions Whin Single Cells, Ann. N.Y. Acad. Sci., **97**, (1962).

55. Undenfriend, Sidney. Fluorescence Assay in Biology and Medicine Vol. I. Academic Press: New York. (1962).

56. Freifelder, David, Physical Biochemistry, Second Ed.

57. Cantor, C.R., Schimmel, P.R., Biophysical Chemistry, W.H.Freeman and Company, New York, (1980)

58. Lehninger, Albert L., Principle of Biochemistry third printing, Worth Publishers, Inc., (1984).

59. Longworth, J.W., in Excited States of Proteins and Nucleic Acids, ed. R.F. Steiner and I. Weinryb, New York: Plenum Press, (1971).

60. Hochstrasser, R.M., Nagus, D.K., Proc. Natl. Acad. Sci. USA, **81**:4399, (1984).

61. Fujimoto, D., Akiba, K., Nakamura, N., Isolation and characterization of a fluorescent material in bovine achilles tendon collagen in Biochemical and Biophysical Research Communications, **76(4)**:1124-1129 (1977).

62. Bartley, W., Birt, L.M., Banks, P., The Biochemistry of the Tissues, John Wiley & Sons Ltd, pp730, (1968).

63. Long, Cyril, Biochemists' Handbook, D. Van Nostrand Company Inc., pp229, (1961).

64. Lehninger, Albert L., Principle of Biochemistry second printing, Worth Publishers, Inc., (1978).

65. Eng, John, Lynch, R., and Balaban, R., Nicotinmide Dinucleotide Fluorescence Spectroscopy and Imaging of Isolated Cardiac Myocytes, Biophysical Journal, **55**:621 (1989)

66. Swanson, Carl P., Webster, Peter L., The Cell, 5th ed., Prentice-Hill, Inc., (1985).

67. Visser, A.J.W.G., Kinetics of staking interactions inflavin adenine dinucleotide from time time-resolved flavin fluorescence. photo-chem. photobiol. **40**:703-706, (1984).

68. Wahl, Ph., Auchet, J.C., Visser, A.J.W.G., Muller, F., FEBS Letters, **44(1)**:67, (1974).

69. Aubin, J.E., "Auto-fluorescence of Viable Cultured Mammalian Cells", The Journal of Histochemistry and Cytochemistry, **27**:36, (1979).

70. Lakowicz, Joseph R., Principles of Fluorescence Spectroscopy, 3rd print, Plenum Press, (1986).

71. Benson, R.C., Meyer, R.A., Zaruba, M.E., and McKhann, G.M., Cellular Autofluorescence --Is it due to flavins? The Journal of Histochemistry and Cytochemistry, **27(1)**:44-48, (1979).

72. Liu, C.H., Tang, G.C., Pradhan, A., Sha, W.L., and Alfano, R.R., Lasers in Life Science **3(3)**:167 (1990)

73. Avi-Dor, Y., Olson, J.M., Doherty, M.D., and Kaplan, N.O., J.Biol. Chem., **237**:2377 (1962).

74. Duysens, L.N.M., Amesz, J., J. of Biochem. & Biophys., ACTA, **24**:19, (1957).

75. Boyer, P.D., Theorell, H., Acta chem. Scand., **10**:447 (1956).

76. Chance, B., Baltscheffsky, H., J. Biol. Chem., **233**:736 (1958).

77. Chance, B., Cohen, P., Jobsis, F., Schoener, B., Science **137**:499 (1962).

78. Chance, B., Thorell, B., J.Biol. Chem., **234**:3044 (1959).

79. Schwartz, J.P., Passonneau, J.V., J. Biol. Chem., **249**:4138 (1974).

80. Chance, B., Schoener, B., Oshino, R., Itshak, F., and Nakase, Y., J. Biol. Chem. **254**:4764, (1979).

81. Prodhen, Asima, Ph. D Thesis, (1991).

82. Tata, D.B., Foresti, M., Cordero J., Tomashefsky, P., Alfano, M.A., Alfano, R.R., Biophys. J., **50**:463-469, (1986).

83. Boring, C.C., Squires, T.S., and Tong, T., Cancer Statistics, **41**:18, (1991).

84. Private conversation with Dr. M. Steiberg

85. Fahl, W.E., Rose, D.P., Liskowski, L., and Brown, R.R., "Tryptophan Metabolism and Corticosteroids in th breast cancer", Cancer, **34**:1691-1695, (1974).

86. Cascino A; Cangiano C; Ceci F; Mineot T; Mulieri M; Muscaritoti M; Fanelli FR, Increased Plasma Free Tryptophan Levels in Human Cancer: a Tumor Related Effect?" Anticancer Res, **11(3)**:1313, (1991).

87. Private conversation with Dr. S.P. Schantz